SPECTROSCOPIC STUDIES OF PYRIDINE AND ITS ISOTOPOMER, 2-FLUORO- AND 3-FLUOROPYRIDINE, 1,3-BUTADIENE AND ITS ISOTOPOMERS

A Dissertation

by

PRAVEENKUMAR BOOPALACHANDRAN

Submitted to the Office of Graduate Studies of
Texas A&M University
in partial fulfillment of the requirements for the degree of

DOCTOR OF PHILOSOPHY

December 2011

Major Subject: Chemistry

SPECTROSCOPIC STUDIES OF PYRIDINE AND ITS ISOTOPOMER, 2-FLUORO- AND 3-FLUOROPYRIDINE, 1,3-BUTADIENE AND ITS ISOTOPOMERS

A Dissertation

by

PRAVEENKUMAR BOOPALACHANDRAN

Submitted to the Office of Graduate Studies of
Texas A&M University
in partial fulfillment of the requirements for the degree of

DOCTOR OF PHILOSOPHY

Approved by:

Chair of Committee,	Jaan Laane
Committee Members,	John P. Fackler
	Steven E. Wheeler
	Karl Aufderheide
Head of Department,	David Russell

December 2011

Major Subject: Chemistry

ABSTRACT

Spectroscopic Studies of Pyridine and its Isotopomer, 2-Fluoro- and 3-Fluoropyridine, 1,3-Butadiene and Its Isotopomers. (December 2011)

Praveenkumar Boopalachandran, B.Tech., University of Madras, India;

M.S., Texas A&M University-Commerce; M.S., Texas A&M University

Chair of Advisory Committee: Dr. Jaan Laane

The infrared, Raman and ultraviolet spectra of pyridine-d_0 and pyridine-d_5 were recorded and assigned with a focus on the low-frequency vibrational modes in the $S_1(n,\pi^*)$ electronic excited state. An energy map for the low-frequency modes was constructed and the data for the ν_{18} mode allowed a highly anharmonic one-dimensional potential energy function to be determined for the S_1 excited state. In this $S_1(n,\pi^*)$ state, pyridine is quasi-planar and very floppy with a barrier to planarity of 3 cm^{-1}.

The infrared, Raman and ultraviolet spectra of 2-fluoropyridine (2FPy) and 3-fluoropyridine (3FPy) have been collected and assigned. For 2FPy about 150 bands were observed for the transitions to the vibronic levels of the $S(\pi,\pi^*)$ state at 38,030.4 cm^{-1}. For 3FPy more than a hundred absorption bands associated with the $S(n,\pi^*)$ state at 35,051.7 cm^{-1} and about forty broad bands associated with the $S(\pi,\pi^*)$ state at 37,339 cm^{-1} were observed. The experimental work was complemented by *ab initio* calculations and these also provided calculated structures for 2FPy, 3FPy, and pyridine. They showed that the fluorine atom on the ring participates in the π bonding.

The gas-phase Raman spectra of 1,3-butadiene and its 2,3-d_2, 1,1,4,4-d_4, and d_6 isotopomers have been recorded with high sensitivity in the region below 350 cm^{-1}, in order to investigate the internal rotation (torsional) vibration. The data for all the isotopomers were then fit using a one-dimensional potential energy function of the form $V=½\sum V_n(1-\cos\phi)$. The energy difference between *trans* and *gauche* forms was determined to be about 1030 cm^{-1} (2.94 kcal/mol), and the barrier between the two equivalent *gauche* forms to be about 180 cm^{-1} (0.51 kcal/mol), which agrees well with high-level *ab initio* calculations. The results from an alternative set of assignments also fits the data quite well are also presented. Combination and hot band series involving the ν_{13} torsional vibration of the *trans* rotamer were observed for each of the butadiene isotopomers. In addition, the high signal to noise of the Raman spectra made it possible to detect several dozen bands of the *gauche* rotor which makes up only about 2% of the molecules at ambient temperature.

DEDICATION

To my father, Mr. G. Boopalachandran, and to my mother, Mrs. Vijaya Chandran, for their love and support. Without them, this dissertation would not have seen the light!

ACKNOWLEDGEMENTS

It is a pleasure to thank those who made this doctorate dissertation possible. I owe my deepest gratitude to Dr. Jaan Laane, my research advisor, for his continuous motivation, inspiration and enthusiasm. His guidance has helped me immensely to complete important projects and the writing of this dissertation. I am grateful to my research committee members, Dr. Fackler, Dr. Wheeler and Dr. Aufderheide, for their advice and insightful comments. I would like to thank our collaborator Dr. Norman Craig for providing us butadiene samples for our research and giving us valuable advice in successful completion of our projects. I also would like to thank our other collaborator Dr. Sunghwan Kim for his help in excited state calculations. I deeply appreciate Linda Redd for her kindness and friendship during the time of this research. I am indebted to many of my research group members including Dr. Juan Yang, Dr. Kathleen McCann, Dr. Hee Won Shin and Hye Jin Chun for their help and support. I am grateful to many people in the department of chemistry, Dr. Simon North, the graduate advisor, Sandy Manning and Dr. Lisa Perez for their help and support, as well as the members of the teaching faculty, Dr. Holly Gaede, Dr. Elizabeth Soriaga, and Dr. Vickie Williamson, who have helped me hone my teaching skills. I am forever indebted to my parents for their understanding, endless patience and encouragement. Furthermore, I like to thank Shannon Smith for giving me the moral support and being my best friend during critical times. Finally, I thank God for giving me the confidence and blessings during this research.

TABLE OF CONTENTS

CHAPTER Page

CHAPTER Page

Page

LIST OF TABLES

TABLE Page

TABLE Page

TABLE Page

LIST OF FIGURES

FIGURE Page

FIGURE Page

FIGURE Page

FIGURE Page

FIGURE Page

FIGURE Page

CHAPTER I

INTRODUCTION

Molecular vibrations have been studied by infrared and Raman spectroscopy for nearly a century. These techniques provided insight into molecular bending and enabled scientists to determine the structure and conformations of a wide variety of molecules. Similarly, ultraviolet absorption spectroscopy has contributed a wealth of information on electronic states. Although these techniques have been used for a long time, advances in instrumentation and computer technology in recent years have allowed more extensive investigation to be carried out that heretofore were not possible. In particular, fourier transform spectroscopy for infrared and ultraviolet absorption along with improved lasers and charge coupled device (CCD) detectors for Raman spectroscopy have been critical. The development of computer programs to complement these spectroscopic studies has also been important for this work.

Several spectroscopic investigations were undertaken in this work. First, the vibrational potential energy function (PEF) in the electronic excited state of pyridine and its -d_5 isotopomer was investigated. The vibrational energy states of these molecules both in ground and excited states were studied. Second, the ultraviolet absorption spectra, structure and vibrational assignments in their ground and excited states of 2-fluoro- and 3-fluoropyridine were also studied.

This dissertation follows the style of *The Journal of Physical Chemistry A*.

Ab initio and density functional theory (DFT) calculations were carried out to compute the molecular structures and to support the vibrational assignments of the pyridine and fluoropyridine molecules. In addition, preliminary experimental and theoretical studies of the vibrations, and molecular structures of 2-chloro- and 3-chloropyridine and 2-bromo- and 3-bromopyridine were carried out in their electronic ground states. Third, the gas-phase Raman spectra of 1,3-butadiene and its 2,3-d_2, 1,1,4,4-d_4, and d_6 isotopomers were recorded with high sensitivity. The data in the region below 350 cm^{-1} for all the isotopomers were then fit using a one-dimensional periodic potential energy function. This provided an understanding of the conformational properties of butadiene. Combination and hot band series involving the torsional vibration and other modes of the *trans* rotamer were observed in the Raman spectra. From the high sensitive Raman spectra, the Raman bands from the *gauche* rotor were identified.

PYRIDINE AND ITS ISOTOPOMER

The vibrational spectra of pyridine have been studied in great detail over the past 60 years.[1-31] In particular the ultraviolet absorption spectra of pyridine vapor has previously been extensively studied and assigned by various authors.[1-8] However, most studies did not recognize that the out-of-plane ring-bending mode in its S_1 (n,π*) excited state would be highly anharmonic. In the previous studies, it was reported that pyridine was quasi-planar with a barrier to planarity of about 4 cm^{-1}.[3] However, the results of a potential energy calculation were never presented. None of these studies presented a

ring-bending potential energy function. Moreover, previous investigations only allowed a few of the vibrational fundamentals of the excited electronic state to be assigned.[3]

In this work, the infrared and Raman spectra of liquid and vapor-phase pyridine-d_0 and its -d_5 isotopomer, were recorded and the vibrational frequencies of the electronic ground states were assigned. The ultraviolet absorption spectra of pyridine and its -d_5 isotopomer associated with its $S_1(n,\pi^*)$ electronic excited state were also recorded and analyzed. The one-dimensional ring-puckering potential functions for the excited state of these molecules were determined. *Ab initio* and DFT calculations were carried out to compute the molecular structures and to support the vibrational assignments of the twenty-seven fundamentals in the ground and excited states.

2-FLUORO- AND 3-FLUOROPYRIDINE

As a continuation of investigations on molecules of the pyridine family, the infrared, Raman and uv experiments of 2-fluoropyridine and 3-fluoropyridine (hereafter abbreviated as 2FPy and 3FPy) were carried out. *Ab initio* and DFT calculations were performed to compute the structures of these molecules and to support the vibrational assignments. Both these molecules are planar with C_s symmetry. Previous microwave work showed that the substitution of fluorine atoms affected the geometrical structure of the benzene ring.[32] Similar effects could be expected with the substitution of fluorine atoms in the pyridine ring. J. H. S. Green and co-workers previously reported the infrared and Raman spectra and partial assignments for these molecules in their electronic ground states, but no structural information was reported.[33]

The ultraviolet absorption spectra of 2FPy and 3FPy in the vapor state have been reported in the literature but these spectra were of low quality which limited the extent of the analyses.[34, 35] In 2010 Itoh reported the emission and excitation spectra of both 2FPy and 3FPy vapor.[36] His data were also of low-resolution and provided limited information on the vibronic energy levels since the focus of the work was primarily on fluorescence yields.

In the present work, the infrared and Raman spectra of liquid and vapor-phase 2 FPy and 3FPy were recorded and the vibrational frequencies of the electronic ground states were assigned. The ultraviolet absorption spectra of 2FPy and 3FPy vapors were collected and their vibrational frequencies were assigned in their electronic excited states. The experimental work was complemented by the ground and excited state *ab initio* and DFT calculations. These also provided calculated structures for 2FPy, 3FPy, and pyridine in their ground and excited states.

1,3-BUTADIENE AND ITS ISOTOPOMERS

1,3-Butadiene molecule has been the subject of conformational studies for several decades.[37-56] The internal rotation about the central carbon-carbon bond of 1,3-butadiene can produce *trans*, *cis*, or *gauche* conformations depending on the angle of rotation. The *trans* conformer has long been known to be the predominant one, but whether the higher energy conformer has a *cis* or *gauche* configuration remained a question for many years.

While the early calculations with minimal basis sets predicted the minor conformation to be *cis*, the recent work consistently showed the *gauche* form to have a local energy minimum in the potential energy function.[49] Feller and Craig also reported intensities for infrared and Raman transitions for the *gauche* rotamer computed with high level basis set.[49] A potential energy surface in terms of torsional coordinates through the internal rotation of the C-C group was essential to understand how the molecule changes its conformations and which pathways it followed to interconvert from one structure to another. In the present work, an extensive gas-phase Raman investigation was undertaken, including spectra at high temperatures, of 1,3-butadiene and three of its deuterated isotopomers in order to determine the potential energy function that fit the data for all of the isotopic species. The goal was to accurately determine the energy barriers and the energy differences between the different conformations.

Furthermore, the full Raman spectra of these isotopomers were investigated and in the process, the presence of many combination bands and hot bands involving the ν_{13} torsional vibration of the *trans* conformations were discovered. From such studies it was possible to determine how the torsional frequencies changed in vibrational excited states and thus to evaluate how much interaction there was between the torsional motion and other vibrational modes. From the high quality Raman spectra, numerous Raman bands from the *gauche* rotor which made up only about 2% of the molecular population at ambient temperature were identifed.

In addition, DFT calculations were used to predict the vibrational frequencies of the normal mode assignments of the twenty-four fundamentals in the electronic ground states.

CHLORO AND BROMOPYRIDINE

In order to follow up the work on pyridine and fluoropyridines, chloro- and bromopyridine were also investigated. J. H. S. Green and co-workers have previously reported the infrared and Raman spectra and partial assignments for these molecules in their electronic ground states, but no structural information was reported.[33] In this study, the infrared spectra were recorded and ground state vibrational frequencies of 2-chloro- and 3-chloropyridine, and 2-bromo- and 3-bromopyridine molecules were assigned. DFT calculations were used to predict the vibrational frequencies of the twenty-seven fundamentals.

CHAPTER II

EXPERIMENTAL METHODS

INTRODUCTION

Several experimental spectroscopic techniques were utilized in this work for the vibrational analyses, molecular structure studies and investigation of the vibrational PEFs in the electronic excited states. The spectroscopic techniques used in this research were infrared (IR), Raman and ultraviolet (uv). The different types of transitions are shown in Figure 1. Two of the spectroscopic techniques, IR and Raman, were used for the determination of vibrational energy levels in the electronic ground state. Information on the vibronic energy levels of the electronic excited state was provided by uv spectroscopy. The more specific procedures used for individual molecules will be discussed in the related chapters.

INFRARED SPECTRA

The liquid-phase and vapor-phase mid-infrared spectra were collected on a Bruker Vertex 70 FT spectrometer equipped with a globar light source, a KBr beamsplitter and deuterated lanthanum triglycine sulfate (DLaTGS) detector. The spectra of a capillary film of the liquid were taken by placing a drop of the sample between two polished KBr windows that were 25 mm in diameter and 4 mm in thickness.

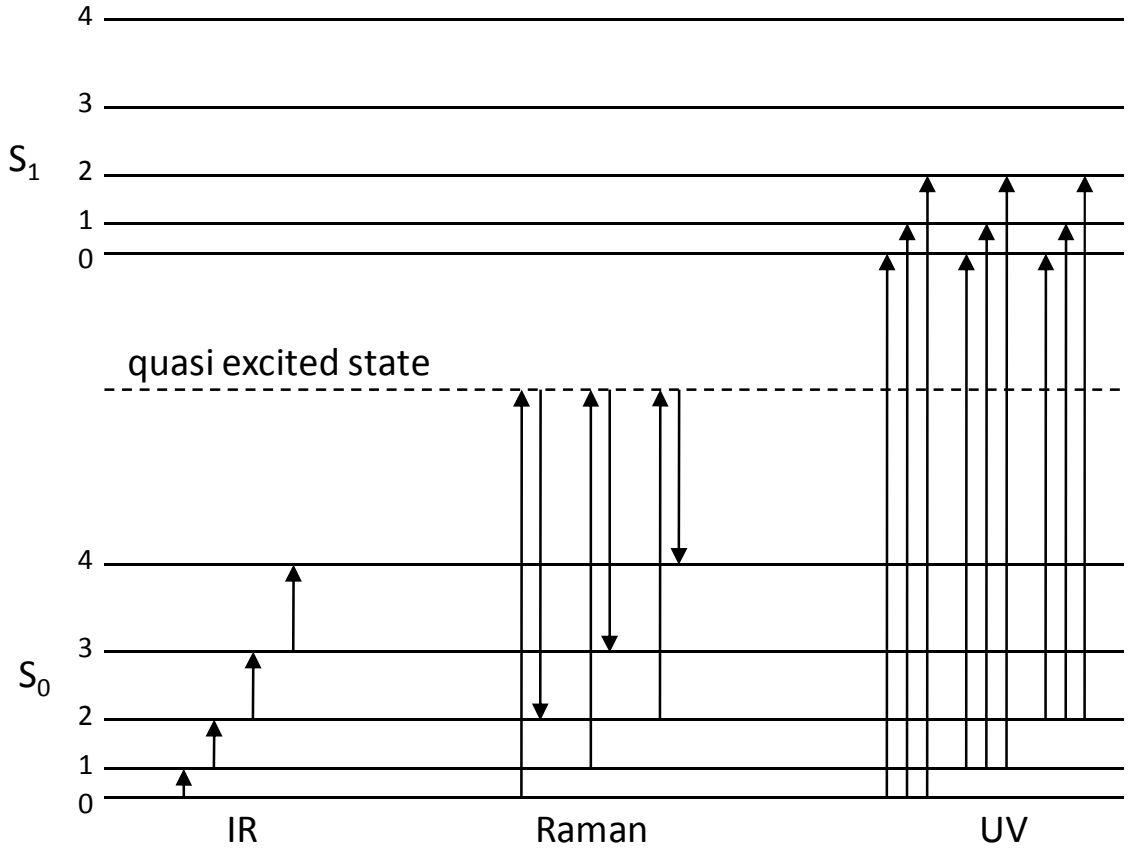

Figure 1. Spectroscopic techniques for the investigation of the vibronic energy levels.

The spectra of the sample and reference background were carried out using the same instrumental parameters. The single-beam spectrum of the sample was then ratioed with the background spectrum to get the transmittance spectrum of the sample in the 400-3400 cm^{-1} spectral region. Typically 512 scans were collected for liquid samples and 1024 scans were collected for vapor samples, and many hundreds of individual spectra were averaged using a resolution of 0.5 cm^{-1}.

The vapor-phase far infrared spectra were also collected on the same instrument, equipped with a mylar beamsplitter, in the 60-600 cm^{-1} spectral region, in 10 cm cells with polyethylene windows, and a mercury cadmium telluride (MCT) detector. The vapor pressures of the samples were in the range of 10-20 Torr for pyridines and halopyridines. Typically 1024 scans were collected and many individual spectra were averaged using a resolution of 0.5 cm^{-1}.

RAMAN SPECTRA

The Raman spectra of the molecules in the vapor-phase were recorded of samples sealed in specially designed, heatable glass Raman cells (80 mm long by 15 mm in diameter).[57] The vapor-phase spectra were acquired at room temperature for pyridine and fluoropyridine samples. Spectral acquisition was mostly carried out at room temperature for butadiene samples but for some cases the samples were heated up to approximately 250° C. A Jobin-Yvon U-1000 spectrometer equipped with a liquid nitrogen-cooled charge-coupled device (CCD) detector was used to collect the spectra. The 532 nm line of a frequency-doubled Nd:YAG Coherent Verdi-10 laser was used and

typically operated at 6 watts of power. Spectral scans spanning 60 cm^{-1} were typically recorded over periods of 4 to 6 hours so that many hundreds of individual spectra could be averaged in the 100 - 3400 cm^{-1} spectral region. The spectral resolution was 0.7 cm^{-1}.

The liquid phase Raman spectra were also collected on the same instrument with samples in glass cuvettes using a laser power of 500 mW. The Raman technique was hindered by colored samples which absorb the excitation frequency and thus produce fluorescence which overwhelmed the Raman signal. Thus, purification using vacuum transfer was normally carried out prior to the experiment to eliminate the presence of colored impurities.

ELECTRONIC ABSORPTION SPECTRA

The ultraviolet absorption spectra of the samples in a 23.5 cm glass cell with quartz windows were recorded at ambient temperature on a Bomem DA8.02 fourier transform spectrometer. A deuterium lamp source, a quartz beamsplitter, and a silicon detector were used. Typically 3000 scans at a resolution of 0.25 cm^{-1} were averaged in the 25000 - 40000 cm^{-1} spectral region. Heating the sample was needed for some pyridine samples. The spectra were collected six times for each molecule utilizing different vapor pressures of the samples. The vapor pressures of the samples at room temperature were in the range of 10-20 Torr for pyridine and halopyridine samples.

CHAPTER III

THEORETICAL AND COMPUTATIONAL METHODS

INTRODUCTION

Theoretical calculations were used to compliment the experimental work. First *ab initio* computations and density-functional theory based on quantum mechanical principles were used to predict molecular structures, energies and vibrational frequencies and intensities. Second, computer programs developed in the Laane laboratories were used to determine one-dimensional potential energy functions which best fit the experimental data for ring puckering and internal rotation vibrations.[58-64]

AB INITIO CALCULATIONS

Ab initio calculations utilized the correct Hamiltonian to determine the properties of the molecule. These calculations were based on theoretical principles and universal physical constants without the implementation of experimental data. Several approximations such as time-independent Schrödinger equation and the the Born-Oppenhimer approximation were implemented in these calculations to be more reliable and efficient. There are several computational methods which were used for molecular structure and conformational studies and determination of Raman and infrared intensities. Computational methods include Harteree-Fock (HF), second-order Møller-Plesset (MP2), coupled cluster (CC) and the density-functional theory (DFT).

In this work, the structures and vibrational frequencies of pyridine -d_0 and its -d_5 isotopomer, 2FPy, 3FPy and *trans* and *gauche* butadiene and its isotopomers for the electronic ground state were calculated using the Gaussian 03 program package.[65] *Ab initio* second order Moller-Plesset (MP2) level of theory with the cc-pVTZ basis set was used to find the optimized geometry. The DFT-B3LYP level of theory with the 6-311++G(d,p) basis set was used to calculate the vibrational frequencies. Based on previous work, a scaling factor of 0.964 was used for the C-H stretching vibrational frequencies and a factor of 0.985 for the lower frequencies.[66-70]

In addition, in collaboration with Sunghwan Kim, the geometries of pyridine -d_0 and its -d_5 isotopomer, 2FPy and 3FPy molecules in the S_0, S(n,π*) and S(π,π*) states were optimized at the CASSCF/6-311++G(d,p) level. Based on previous work, a scaling factor of 0.905 was used for all of the vibrational frequencies in the electronic excited states.[71] All CASSCF computations were performed using the GAMESS package.[72]

PYRIDINE RING BENDING POTENTIAL ENERGY FUNCTION

Low-frequency large-amplitude vibrations such as the out-of-plane ring-bending of pyridine can often be well represented by one-dimensional potential energy functions. The Schrödinger equation

$$H\Psi = E\Psi \tag{3.1}$$

has the Hamiltonian

$$\hat{H}(x) = (-\hbar^2/2)\partial/\partial x(g_{44}(x))\partial/\partial x + V(x) \tag{3.2}$$

In Equation (3.2), x is the out-of-plane ring-bending coordinate, $g_{44}(x)$ is a reciprocal reduced mass expansion and $V(x)$ is the potential function.

R. P. Bell[73] proposed that the ring-puckering vibration of a four-member ring molecule could be represented by a quartic potential energy function of the form

$$V = ax^4 \tag{3.3}$$

The Laane laboratory has a long history[58-63] of studying potential energy functions of large-amplitude vibrations, and the following potential energy function has often been successful in fitting experimental data

$$V = ax^4 + bx^2 \tag{3.4}$$

Equation (3.4), often did a satisfactory job of calculating the vibrational energy levels and the sign of the b determined the conformation of the ring. If b is positive, then the potential function has a single minimum, which indicates a planar conformation. If b is negative, then the potential has a double minimum, indicating a non-planar equilibrium structure. The equilibrium conformation of pyridine is determined by a competition between two opposing forces, ring-angle strain and torsional strain. The ring-angle strain is the restoring force to planarity.

For a molecule that has a non-planar equilibrium conformation, the potential energy parameter b is negative and the barrier to planarity is given by

$$Barrier = \frac{b^2}{4a} \tag{3.5}$$

and the puckering coordinate at the energy minima, is given by

$$x_{\min ima} = \pm\sqrt{\frac{b}{2a}}\,. \tag{3.6}$$

The kinetic energy expansion in this study was computed using computer programs previously described.

POTENTIAL ENERGY FUNCTION FOR INTERNAL ROTATION

The Hamiltonian for the one-dimensional internal rotation is

$$H = -\frac{d}{d\phi}F(\phi)\frac{d}{d\phi} + V(\phi) \tag{3.7}$$

where $F(\phi)$ is the inverse moment of inertia expansion given by

$$F(\phi) = F_0 + \sum_n F_n \cos n\phi\,. \tag{3.8}$$

and $V(\phi)$ is the potential energy of the form

$$V(\phi) = \sum_n \tfrac{1}{2}V_n(1-\cos n\phi) \tag{3.9}$$

The V_n are the potential parameters and ϕ is the angle of internal rotation. In the present work the $F(\phi)$ expansion was calculated by Peter Groner using his Groner FSER program.[74] The V_n values were computed using the VNCOSPX program from the Laane laboratory.[64]

CHAPTER IV

VIBRATIONAL SPECTRA, STRUCTURE, AND THEORETICAL CALCULATIONS OF PYRIDINE-d_0 AND -d_5 IN THEIR GROUND STATES

INTRODUCTION

Pyridine belongs to the C_{2v} point group with one C_2 rotational axis and two reflection planes. It has 27 fundamentals of which 19 are planar modes of A_1 and B_2 symmetry species and 8 are non-planar modes of A_2 and B_1 symmetry species. All the 27 modes are Raman active and all but the A_2 vibrations are IR active.

Pyridine is one of the most important model compounds next to benzene for the study of biomolecular interactions and structures.[10,25] A thorough understanding of the electronic ground and excited states was required along with the knowledge of potential energy function for vibrational and structural analyses. The vibrational spectra and the molecular structure of pyridine have been studied in great detail over the past 60 years.[1-31] A high quality infrared and Raman study of the liquid spectra have been reported by previous researchers.[16] However, there was a lack of high quality vapor Raman and infrared data. In the present work, the infrared and Raman spectra of liquid and vapor-phase pyridine-d_0 and its -d_5 isotopomer were recorded and the vibrational frequencies of the electronic ground states were assigned. *Ab initio* and DFT calculations were carried

out to compute the molecular structures and to verify the vibrational assignments of the twenty-seven fundamentals in the ground states.

EXPERIMENTAL

Pyridine-d_0 and pyridine-d_5 (99% isotopic purity) were purchased from Aldrich and purified by trap to trap distillation.

The Raman spectra of the molecules in the vapor-phase were recorded of samples sealed in specially designed glass cells were previously described in Chapter II. The vapor pressures of the samples at room temperature were about 15 Torr. A Jobin-Yvon U-1000 spectrometer equipped with a liquid nitrogen-cooled CCD detector was used to collect the spectra. The 532 nm line of a frequency-doubled Nd:YAG Coherent Verdi-10 laser was used and typically operated at 6 watts of power. Spectral scans spanning 60 cm^{-1} were typically recorded over periods of 4 to 6 hours so that many hundreds of individual spectra could be averaged. The spectral resolution was 0.7 cm^{-1}. The liquid phase Raman spectra were also collected on the same instrument with samples in glass cuvettes using a laser power of 500 mW.

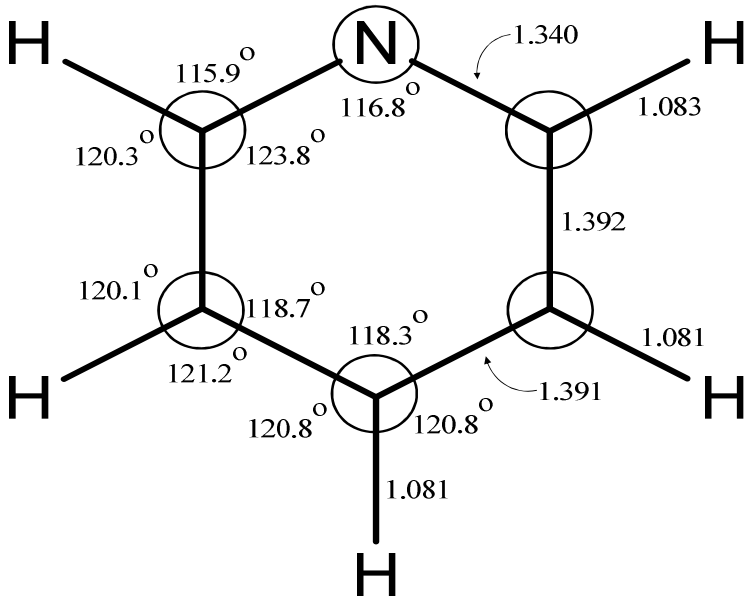

Figure 2. Calculated structures of pyridine-d_0 in its S_0 ground electronic state using MP2/cc-pVTZ level of theory.

The liquid-phase and vapor-phase mid-infrared spectra of these molecules were collected on a Bruker Vertex 70 FT spectrometer equipped with a globar light source, a KBr beamsplitter and deuterated lanthanum triglycine sulfate (DLaTGS) detector. The vapor-phase far infrared spectra (60-600 cm^{-1}) were also collected on the same instrument equipped with a mylar beamsplitter, and a mercury cadmium telluride (MCT) detector. The vapor pressures of the samples were the same as mentioned for the Raman measurements. Typically 1024 scans were collected using a resolution of 0.5 cm^{-1}.

COMPUTATIONS

The structures and vibrational frequencies of pyridine-d_0 and pyridine-d_5 for the electronic ground state were calculated using the Gaussian 03 program package.[65] *Ab initio* second order Moller-Plesset (MP2) level of theory with the cc-pVTZ basis set was used to find the optimized geometry as shown in Figure 2. The DFT-B3LYP level of theory with the 6-311++G(d,p) basis set was used to calculate the vibrational frequencies and the infrared and Raman intensities. Based on previous work,[66-70] a scaling factor of 0.964 was used for the C-H stretching vibrational frequencies and a factor of 0.985 for the lower frequencies.

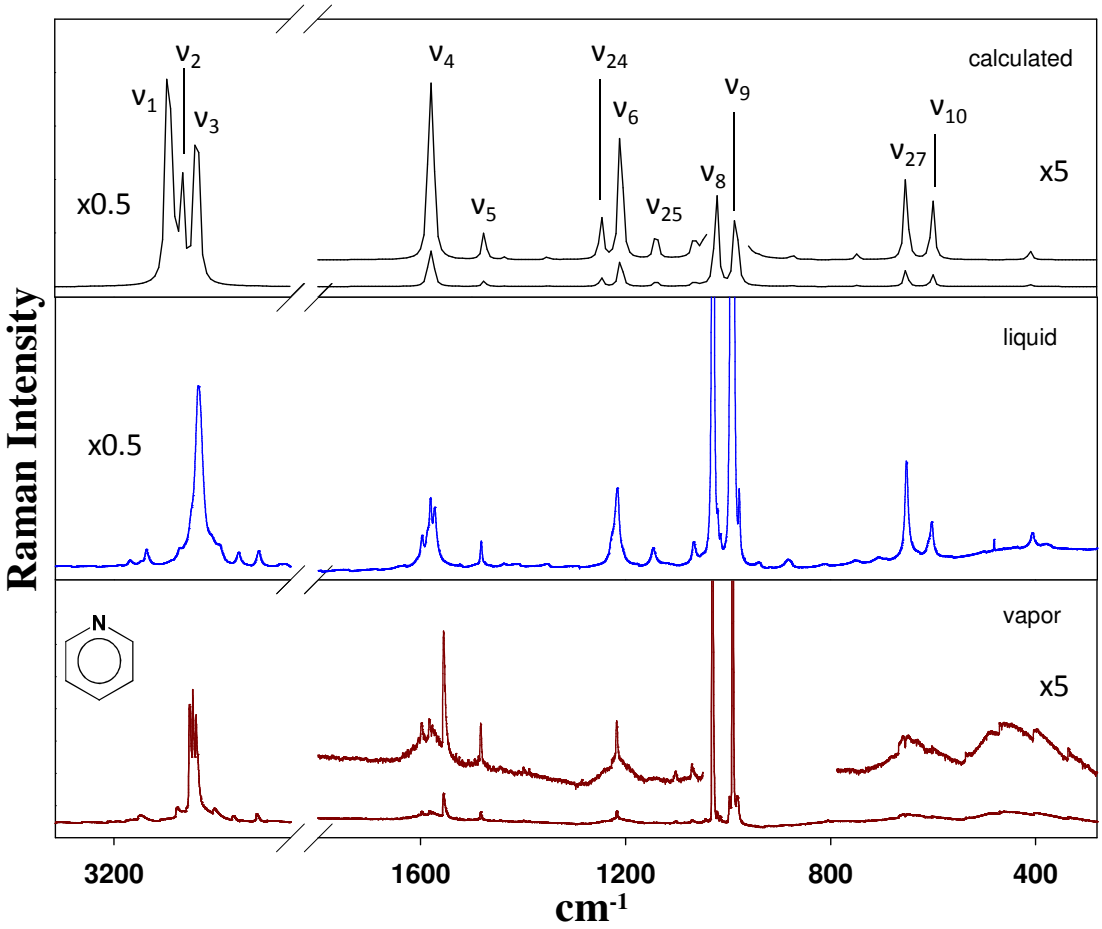

Figure 3. Liquid, vapor, and calculated Raman spectra of pyridine-d_0.

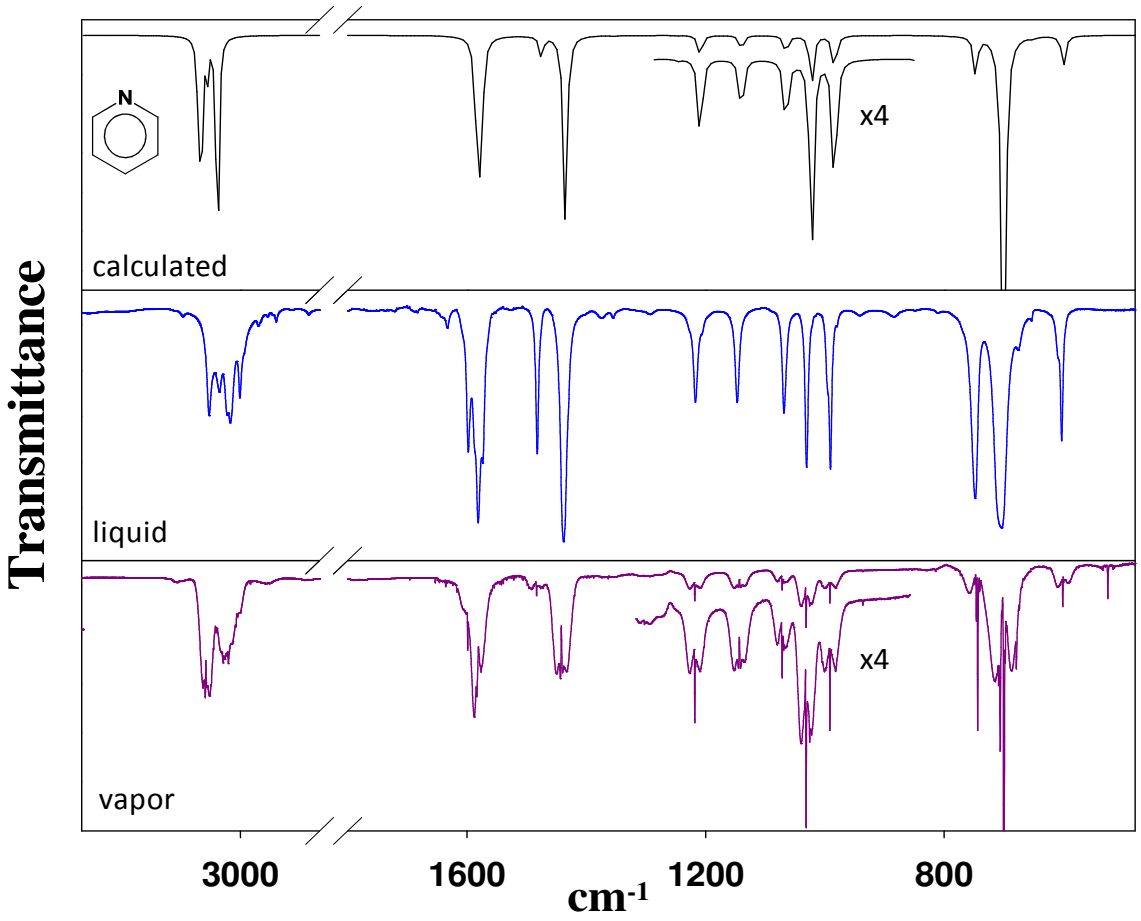

Figure 4. Liquid, vapor, and calculated IR spectra of pyridine-d_0.

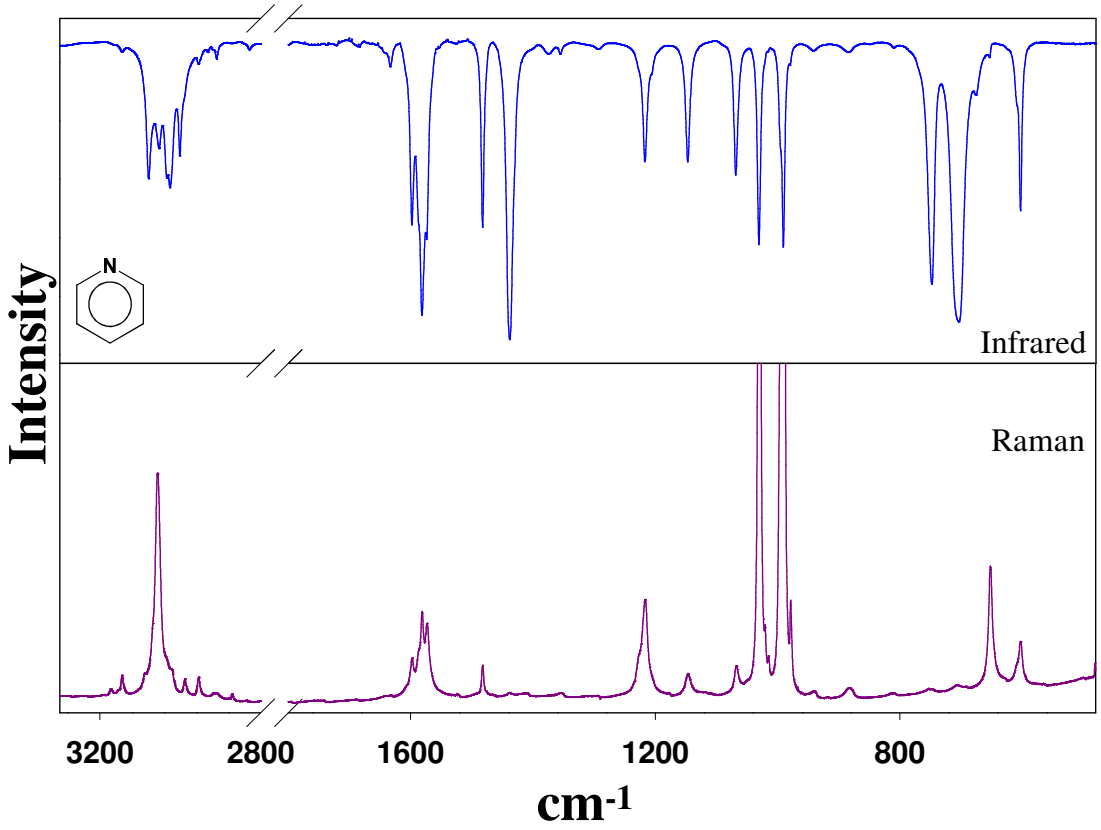

Figure 5. Comparison between IR and Raman spectra of pyridine-d_0.

Table 1: Observed and calculated vibrational frequencies (cm^{-1}) for pyridine-d_0 in the ground state

C_{2v}	ν	Approximate Description	Infrared				Raman[a]				Calculated[b]		OBS
			Liquid		Vapor		Liquid		Vapor		ν	Intensity	Lit[c]
A_1	1	C-H stretch	3079	ms	3073 sh	m	3070 sh	(6.8)	3072	(21.3)	3080	(7, 287)	3094.2
(i.p.)	2	C-H stretch	3052.8	ms	3061	m	3057	(22.7)	3060	(21.3)	3056	(5, 98)	-
	3	C-H stretch	3025.4	ms	-		3021	(2.3)	3030 br	(1.2)	3034	(29, 99)	3030.1
	4	Ring stretch	1581.1	vs	1583.6	ms	1581	(4.4)	1583	(1.0)	1599	(24, 14)	1583.9
	5	Ring stretch	1482.2	s	1483.2	w	1482	(1.6)	1483	(1.7)	1488	(2, 2)	1483.4
	6	C-H wag	1216.8	ms	1217.8	m	1216	(5.2)	1217	(2.7)	1222	(5, 8)	1218.0
	7	C-H wag	1068.5	ms	1071.8	m	1068	(1.2)	1071	(0.3)	1076	(5, 1)	1071.9
	8	Ring bend	1030.5	s	1031.4	m	1030	(83.7)	1031	(100)	1031	(6, 35)	1031.7
	9	Ring breathing	990.6	s	991.3	m	990	(100)	991	(100)	995	(5, 30)	991.4
	10	Ring bend	602.9	s	601.3	m	603	(2.0)	601	(0.3)	607	(4, 4)	601.4
A_2	11	C-H wag	979.9	vw	-	-	979	(4.0)	982 br	(2.3)	981	(0, 0.01)	966
(o.p.)	12	C-H wag	884.2?	vvw	-	-	883	(0.6)	887	(0.2)	879	(0, 0.02)	871
	13	Ring bend	-	-	374.4	w	375 br	(0.2)	-	-	375	(0, 0.04)	373
B_1	14	C-H wag	995.5 sh	m	-	-	995 sh	(23.6)	997	(4.6)	991	(0.02, 0.03)	1007
(o.p.)	15	C-H wag	941.2	vvw	936.2	ms	940 br	(0.3)	-	-	940	(0.02, 0.03)	936.6
	16	C-H wag	747.8	m	743.7	s	748	(0.4)	-	-	746	(12, 0.2)	744.0
	17	Ring bend	704.5	m	699.9	vs	706	(0.4)	-	-	703	(68, 0.03)	700.3
	18	Ring bend	-	-	403.3	m	406	(1.0)	-	-	411	(4, 0.2)	403.3
B_2	19	C-H stretch	3079	ms	3067 sh	m	3070 sh	(6.8)	3066	(21.3)	3072	(25, 36)	3086.9
(i.p.)	20	C-H stretch	3033.6	ms	3031	m	3034	(1.4)	3030 br	(1.2)	3037	(4, 85)	3042.4
	21	Ring stretch	1573.4	s	1575.9	ms	1573	(3.7)	1577	(0.5)	1593	(10, 9)	1580.5
	22	Ring stretch	1437.7	vs	1441.8	m	1438	(0.2)	1443	(0.2)	1448	(27, 0.08)	1441.9
	23	C-H wag	1355.3	w	1363.1	vw	1354	(0.3)	-	-	1363	(0.05, 0.2)	1362.3
	24	Ring stretch*	1227.7 sh	-	1227.4	m	1228 sh	(0.0)	1227 sh	(0.3)	1264	(0.04, 2)	1227
	25	C-H wag	1146.7	ms	1143	mw	1146	(1.2)	-	-	1152	(2, 2)	1143.3
	26	C-H wag	-	-	-	-	-	-	1068?	(0.1)	1060	(0.01, 0.3)	1079
	27	Ring bend	653.2	w	-	-	652	(6.5)	654	(0.7)	659	(0.3, 5)	652

Abbreviations: s, strong; m, medium; w, weak; v, very; sh, shoulder; br, broad; i.p., in-plane; o.p., out-of-plane.

[a] Relative intensities in parenthesis.

[b] B3LYP/6-311++g(d,p); frequencies scaled with a scaling factor of 0.985 for frequencies less than 1800 cm^{-1} and 0.964 for frequencies greater than 1800 cm^{-1}. The calculated relative intensities are shown as (IR, Raman).

[c] Reference 7.

Table 2: Observed vibrational frequencies (cm^{-1}) and assignments for pyridine-d_0

Raman		IR		Assignment	Inferred
3166	mw	-	-	2 υ_4	2x1584 = 3168
3158	m	-	-	-	-
3155	m	-	-	-	-
3152	m	-	-	2 υ_{21}	2x1576 = 3152
3094	m	3094.0	m	-	-
3092	m			3υ_8	3x1031 = 3093
3089	m	3088.3	m	-	-
3072	vvs	3073 sh	m	υ_1	3072
3066	vvs	3066.8sh	m	υ_{19}	3066
3060	vvs	3061	vw	υ_2	3060
-	-	3043.4	m	-	-
3030 br	s	-	-	υ_3/υ_{20}	3030
2998	m	-	-	-	-
2958	s	2958.1	vvw	-	-
-	-	2932.9	m	-	-
2879	mw	-	-	-	-
-	-	2801.8	vvw	$\upsilon_4+\upsilon_6$ $\upsilon_{21}+\upsilon_{24}$	1584+1218 = 2802 1576+1227 = 2803
2798	vw	2797.8	vvw	-	-
2789	vw	2789.9	vvw	-	-
2707	w	-	-	-	-
2696	vw	2696.3	vvw	$\upsilon_5+\upsilon_6$?	1483+1218 = 2701
-	-	2668.2	vvw	$\upsilon_{22}+\upsilon_{24}$	1442+1227 = 2669
2658	vw	-	-	$\upsilon_4+\upsilon_7$	1584+1072 = 2656
-	-	2614.1	w	$\upsilon_4+\upsilon_8$	1584+1031 = 2615
-	-	2590.3	vvw	$\upsilon_{23}+\upsilon_{24}$	1363+1227 = 2590
-	-	2574.2	vw	$\upsilon_4+\upsilon_9$	1584+991 = 2575
2495	w	2496.1	vw	-	-
-	-	2476.3	vw	$\upsilon_5+\upsilon_9$	1483+991 = 2474
2446	mw	2446.3	w		-
2434	w	-	-	2υ_6 $\upsilon_{23}+\upsilon_{26}$?	2x1218 = 2436 1363+1068 = 2431
2369	w	-	-	$\upsilon_{24}+\upsilon_{25}$	1227+1143 = 2370
2329	vs	-	-	-	-
2288	m	2288.5	w	$\upsilon_6+\upsilon_7$	1218+1072 = 2290
2252	w			$\upsilon_6+\upsilon_8$	1218+1031 = 2249
2211	w	-	-	$\upsilon_{25}+\upsilon_{26}$ $\upsilon_6+\upsilon_9$	1143+1068 = 2211 1218+991 = 2209
2198	w			-	-
-	-	2183.2	vvw	$\upsilon_4+\upsilon_{10}$	1584+601 = 2185

Table 2: (Continued)

Raman		IR		Assignment	Inferred
2092	w	2093.0	w	$\upsilon_{22}+\upsilon_{27}$	1442+654 = 2096
2084	w	2084.5	vvw	$\upsilon_5+\upsilon_{10}$	1483+601 = 2084
2062	w	2062.4	w	$2\upsilon_8$ $\upsilon_7+\upsilon_9$	2x1031 = 2062 1072+991 = 2063
-	-	2021.5	w	$\upsilon_8+\upsilon_9$	1031+991 = 2022
2018	vw	2016.8	w	$\upsilon_{23}+\upsilon_{27}$	1363+654 = 2017
-	-	1991.8	w	$2\upsilon_{14}$	2x997 = 1994
1980	vw	1980.8	w	$2\upsilon_9$	2x991 = 1982
-	-	1967.3	w	$2\upsilon_{11}$?	2x982 = 1964
-	-	1942.5	mw	-	-
-	-	1889.4	mw	-	-
1870	vw	1869.2	m	$2\upsilon_{15}$ $\upsilon_{11}+\upsilon_{12}$	2x936 = 1872 982+887 = 1869
-	-	1844.1	m	-	-
1793	vvw	1792.6	m	$\upsilon_{25}+\upsilon_{27}$?	1143+654 = 1797
1725	w	-	-	$\upsilon_{26}+\upsilon_{27}$?	1068+654 = 1722
1599	m	1598.6	m	-	-
-	-	1587.6	vs	-	-
1583	m	1583.6	vvs	υ_4	1584
1577	w	1575.9	vvs	υ_{21}	1576
1555	vs	-	-	-	-
1487	mw	1487.5	vw	$2\upsilon_{16}$	2x744 = 1488
1483	s	1483.2	vw	υ_5	1483
1443	vw	1441.8	m	υ_{22}	1442
1445	w	-	-	$\upsilon_{16}+\upsilon_{17}$	744+700 = 1444
1399	w	1399.1	m	$2\upsilon_{17}$ $\upsilon_{14}+\upsilon_{18}$	2x700 = 1400 997+403 = 1400
1388	w	1387.4	m	-	
-	-	1363.1	m	υ_{23}	1363
1228 sh	mw	1227.4	m	υ_{24}	1227
1217	ms	1217.8	m	υ_6	1218
-	-	1143	mw	υ_{25}	1143
1102	m	-	-	$\upsilon_{17}+\upsilon_{18}$	700+403= 1103
1071	m	1071.8	m	υ_7	1072
1068	mw	-		υ_{26}	1068
1048	w	-	-		
1031	vvs	1031.4	m	υ_8	1031
997	vs	-	-	υ_{14}	997

Table 2: (Continued)

Raman		IR		Assignment	Inferred
991	vvs	991.3	m	υ_9	991
982 br	s	-	-	υ_{11}	982
-	-	936.2	s	υ_{15}	936
887	vw	-	-	υ_{12}	887
806	mw	-	-	2 υ_{18}	2x403 = 806
-	-	743.7	s	υ_{16}	744
-	-	699.9	vvs	υ_{17}	700
654	mw	-	-	υ_{27}	654
601	mw	601.3	vs	υ_{10}	601
-	-	525.7	m	-	-
-	-	403.3	vs	υ_{18}	403
-	-	374.4	w	υ_{13}	374

SPECTROSCOPIC RESULTS

The liquid-phase, vapor-phase, and calculated Raman and infrared spectra of pyridine-d_0 are shown in Figures 3 and 4, and the comparison between infrared and Raman spectra is shown in Figure 5. The liquid-phase, vapor-phase, and calculated Raman and infrared spectra of pyridine-d_5 are shown in Figures 6 and 7, and the comparison between infrared and Raman spectra is shown in Figure 8. The low frequency IR spectra of pyridine-d_0 and pyridine-d_5 are shown in Figure 9. The observed and calculated vibrational frequencies for pyridine-d_0 are summarized in Table 1 and Table 2 presents a tabulation of all the spectral bands including the sum and combination bands. Table 3 summarizes the observed and calculated vibrational frequencies for pyridine-d_5 and Table 4 presents a tabulation of all the spectral bands including the sum and combination bands of the deuterated molecule.

Except for the vapor-phase Raman spectra of the pyridine-d_0 and -d_5 molecules, which is new in this work, similar experimental results and theoretical calculations have been previously presented.[16] However, since the main focus of this work was on the electronic excited states of these molecules, it was desirable to verify the ground state data directly.

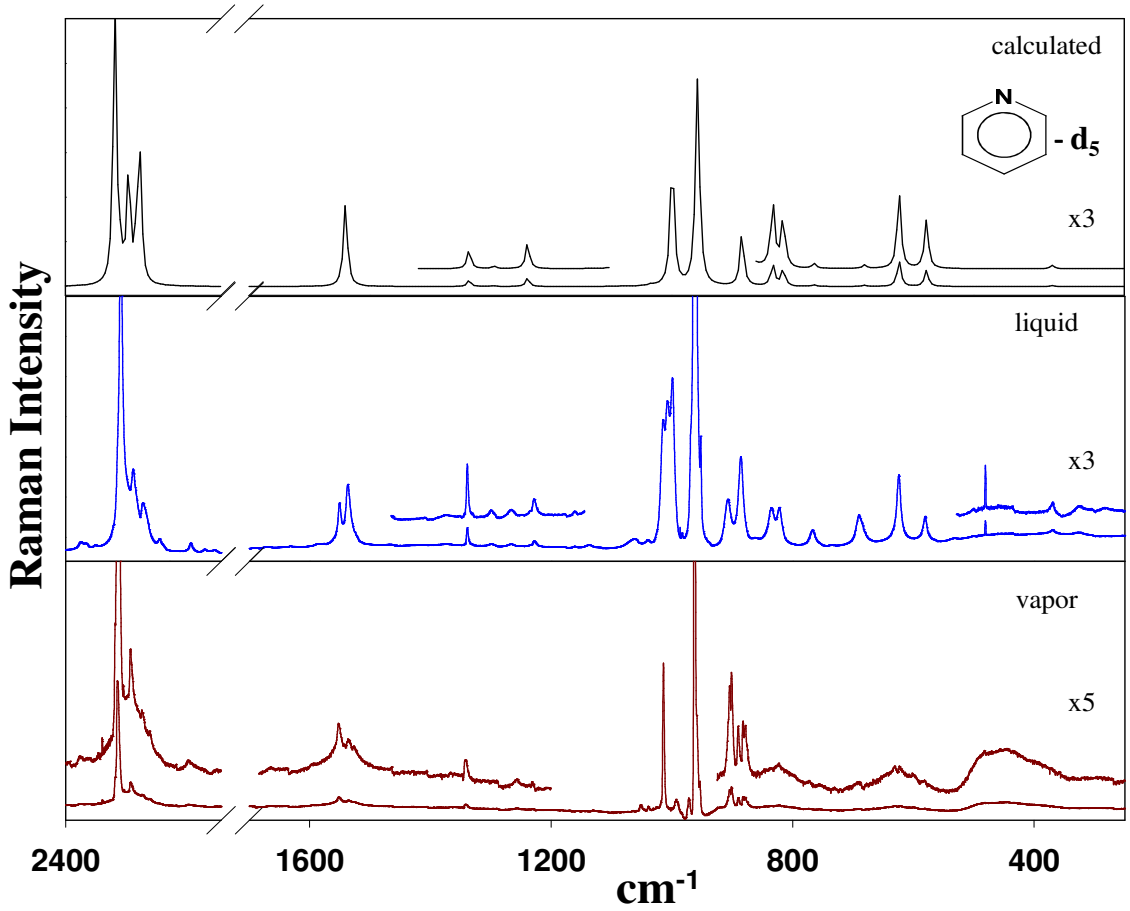

Figure 6. Liquid, vapor, and calculated Raman spectra of pyridine-d_5.

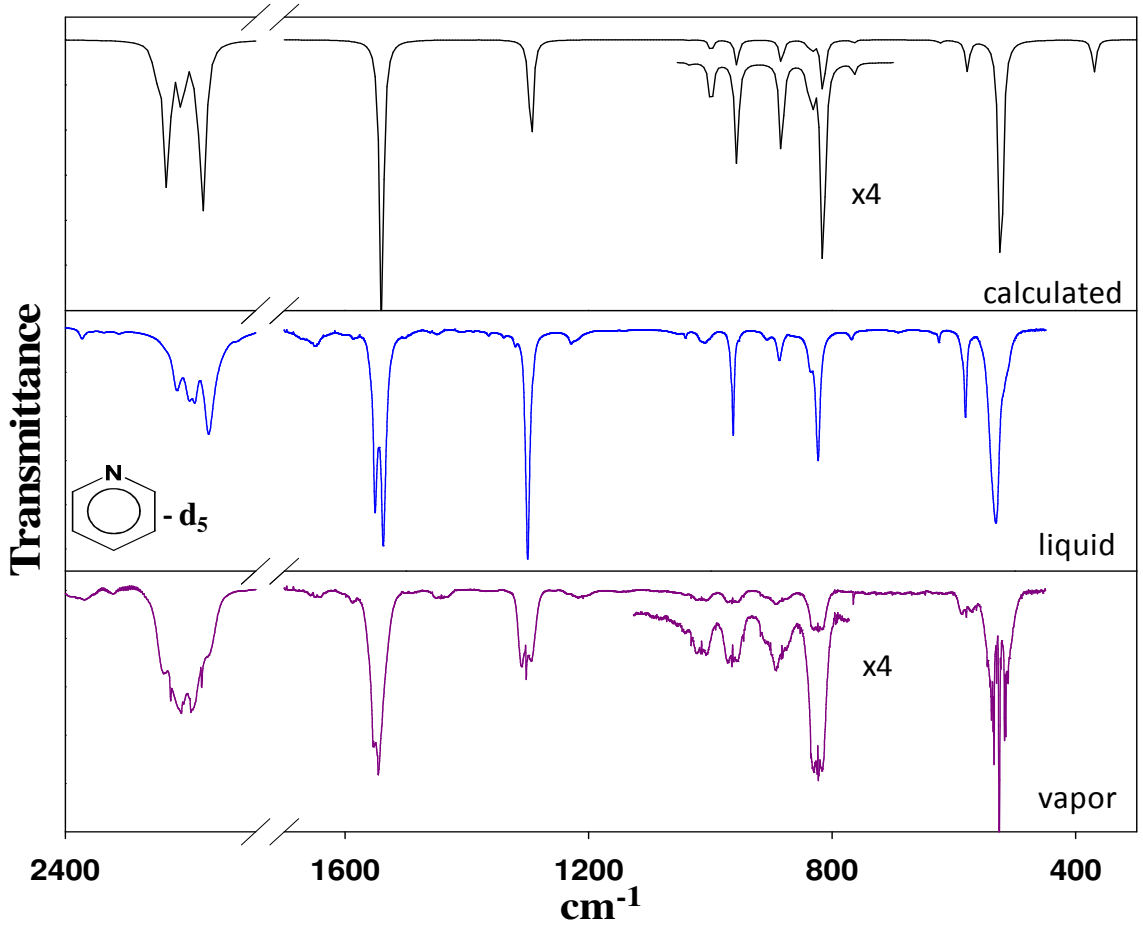

Figure 7. Liquid, vapor, and calculated IR spectra of pyridine-d_5.

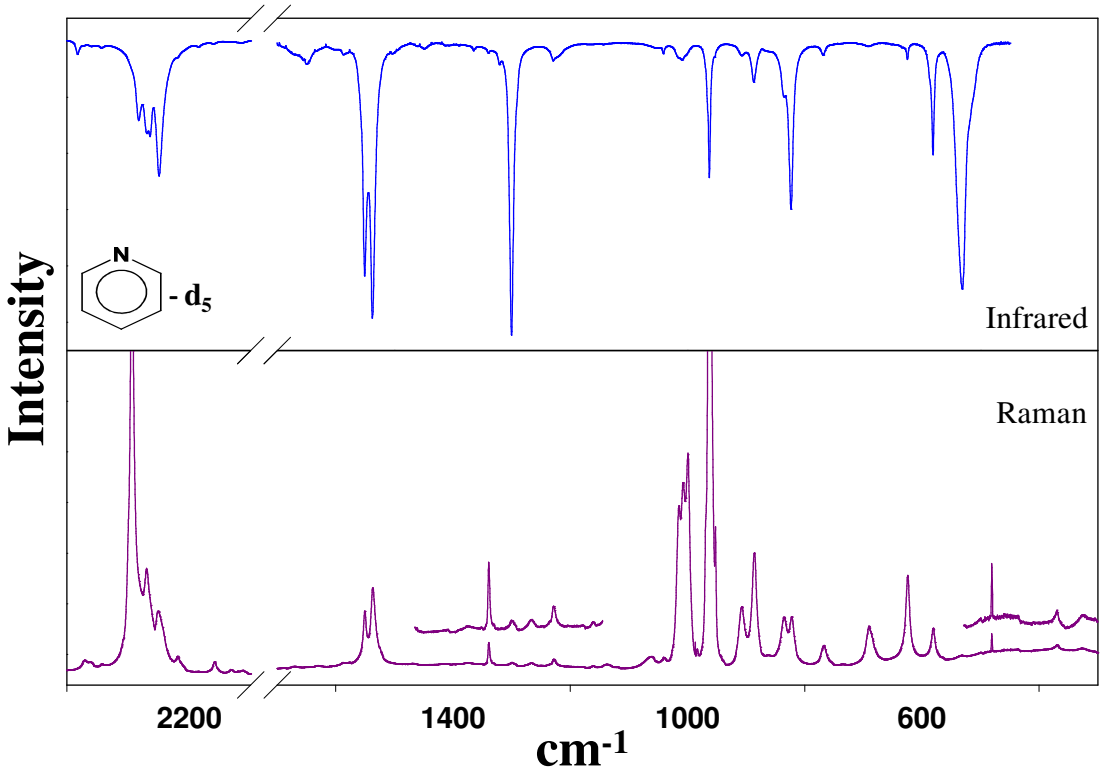

Figure 8. Comparison between IR and Raman spectra of pyridine-d_5.

Table 3: Observed and calculated vibrational frequencies (cm^{-1}) for pyridine-d_5 in the ground state

C_{2v}	ν	Approximate Description	Infrared				Raman[a]				Calculated[b]		OBS
			Liquid		Vapor		Liquid		Vapor		ν	Intensity	Lit[c]
A_1	1	C-H stretch	2294 sh	w	-	-	2294	(10.9)	2299	(642)	2284	(3, 126)	2302
(i.p.)	2	C-H stretch	2269.2	m	2275.6	mw	2270	(1.6)	2275	(55)	2258	(7, 53)	2277
	3	C-H stretch	2263.7	m	2269 sh	w	-	-	2272 sh	(50)	2244	(2, 18)	2269
	4	Ring stretch	1550	vs	1553.9	vs	1550	(1.3)	-	-	1558	(24, 12)	1554
	5	Ring stretch	1340.0	vw	-	-	1339	(0.6)	-	-	1348	(0.2, 1)	1340
	6	C-H wag	886.7	m	882.5	w	886	(3)	-	-	893	(3, 10)	882
	7	C-H wag	823.3	ms	823.6	m	822	(1.2)	824	(101)	823	(8, 2)	824
	8	Ring bend	1009 br		-	-	1007	(4.1)	999	(841)	1007	(0.6, 26)	1014
	9	Ring breathing	962.5	ms	963.4	m	962	(100)	963	(18)	967	(3, 40)	964
	10	Ring bend	581.0	m	579.8	mw	581	(0.7)	-	-	585	(3, 3)	579
A_2	11	C-H wag	-	-	-	-	-	-	816 sh	(41)	813	(0, 0.01)	815
(o.p.)	12	C-H wag	690.9	vw	-	-	690	(0.6)	-	-	684	(0, 0.6)	690
	13	Ring bend	-	-	-	-	326	(0.03)	-	-	320	(0, 0.01)	318
B_1	14	C-H wag	-	-	-	-	-	-	828	(90)	829	(0.4, 0.2)	828
(o.p.)	15	C-H wag	768.1	w	765.2	mw	767	(0.5)	-	-	767	(0.3, 0.4)	765
	16	C-H wag	624.7	w	-	-	624	(2.3)	631 br	(40)	630	(0.4, 5)	631
	17	Ring bend	531.0	vvs	525.6	vvs	532 br	(0.04)	-	-	526	(39, 0.02)	526
	18	Ring bend	-	-	365.5	ms	369	(0.1)	-	-	371	(5, 0.03)	368
B_2	19	C-H stretch	2282.6	m	2289	m	-	-	2288	(15)	2274	(17, 11)	2289
(i.p.)	20	C-H stretch	2249.1	s	2256.5	m	2251 br	(1.5)	2253 br	(20)	2238	(19, 48)	2257
	21	Ring stretch	1550	vs	1545.1	vs	1550	(1.4)	1546	(5)	1558	(24, 12)	1546
	22	Ring stretch	1300.0	vvs	1302.6	vs	1300	(0.1)	1303	(169)	1306	(13, 0.06)	1303
	23	C-H wag	1041.1	vw	-	w	1040	(0.1)	1045	(1653)	1042	(0.07, 0.3)	1046
	24	Ring stretch*	1228.6	mw	1226	vw	1228	(0.2)	1228 sh	(10)	1257	(0.05, 1)	1226
	25	C-H wag	835.6 sh	m	852.5	vw	835	(1.2)	854 br	(10)	841	(1, 3)	856
	26	C-H wag	-	-	-	-	-	-	-	-	823	(0.06, 0.1)	835
	27	Ring bend	624.6	w	625	vvw	-	-	-	-	632	(0.08, 0.08)	626

Abbreviations: s, strong; m, medium; w, weak; v, very; sh, shoulder; br, broad; i.p., in-plane; o.p., out-of-plane.

[a] Relative intensities in parenthesis.

[b] B3LYP/6-311++g(d,p); frequencies scaled with a scaling factor of 0.985 for frequencies less than 1800 cm^{-1} and 0.964 for frequencies greater than 1800 cm^{-1}. The calculated relative intensities are shown as (IR, Raman).

[c] Reference 7.

Table 4: Observed vibrational frequencies (cm^{-1}) and assignments for pyridine-d_5

Raman		IR		Assignment	Inferred
-	-	3108.8	vvw	$2\upsilon_4$	2x1554 = 3108
3063	mw	-	-	-	-
-	-	2878.6	vvw	$\upsilon_1+\upsilon_{10}$ $\upsilon_{20}+\upsilon_{27}$	2299+580 = 2879 2253+625 = 2878
-	-	2852.4	vvw	$\upsilon_2+\upsilon_{10}$	2275+580 = 2855
-	-	2516.1	vvw	$\upsilon_4+\upsilon_9$	1554+963 = 2517
-	-	2476.2	mw	-	-
-	-	2454.1	vw	$2\upsilon_{24}$	2x1226 = 2452
2329	mw	-	-	-	
2299	vvs	-	-	υ_1	2299
2288	w	2289	m	υ_{19}	2288
2275	ms	2275.6	mw	υ_2	2275
2272 sh	m	2269 sh	m	υ_3	2272
2253 br	mw	2256.5	m	υ_{20}	2253
2237	m	-	-	-	-
2164	mw	-	-	$\upsilon_5+\upsilon_7$	1340_{liq}+824 = 2164
-	-	2154.9	vvw	$\upsilon_{22}+\upsilon_{25}$	1303+854 = 2157
-	-	2136.1	vvw	-	
-	-	2089.9	w	$2\upsilon_{23}$	2x1045 = 2090
-	-	2079.1	vw	$\upsilon_{24}+\upsilon_{25}$	1226+854 = 2080
-	-	2065.4	w	-	
-	-	1923.1	mw	$2\upsilon_9$	2x963 = 1926
-	-	1922.3	m	$\upsilon_5+\upsilon_{10}$	1340_{liq}+580 = 1920
-	-	1917.9	m	-	-
-	-	1895.1	w	$\upsilon_{23}+\upsilon_{25}$	1045+854 = 1899
-	-	1844.1	mw	$\upsilon_6+\upsilon_9$	883+963 = 1846
-	-	1837.2	vw	-	-
1595	w	-	-	$\upsilon_{14}+\upsilon_{15}$	828+765 = 1593
		1553.9	vs	υ_4	1554
1546	w	1545.1	vs	υ_{21}	1545
1536	m	-	-	$2\upsilon_{15}$	2x765 = 1530
1527	mw	-	-	-	-
-	-	1480.7	vs	$\upsilon_{25}+\upsilon_{27}$	854+625 = 1479
-	-	1464.8	mw	$\upsilon_6+\upsilon_{10}$	883+580 = 1463
-	-	1458.2	w	$\upsilon_{14}+\upsilon_{16}$	828+631 = 1459
-	-	1401.9	w	$\upsilon_7+\upsilon_{10}$	824+580 = 1404
-	-	1354.7	vw	$\upsilon_{14}+\upsilon_{17}$	828+526 = 1354
1303	w	1302.6	vs	υ_{22}	1303
-	-	1250.7	vs	$2\upsilon_{27}$	2x625 = 1250

Table 4: (Continued)

Raman		IR		Assignment	Inferred
1228 sh	vw	1226	vw	υ_{24}	1226
-	-	1198.6	mw	$\upsilon_{14+}\upsilon_{18}$?	828+366 = 1194
-	-	1187.1	m	-	-
1159	vw	-	-	$2\upsilon_{10}$ $\upsilon_{16+}\upsilon_{17}$	2x580 = 1160 631+526 = 1157
1131	w	-	-	$\upsilon_{15+}\upsilon_{18}$	765+366 = 1131
-	-	1096.1	w	$3\upsilon_{18}$	3x366 = 1098
1052	m	-	-	$2\upsilon_{17}$	2x526 = 1052
		1046.2	w	-	-
1039	m	-	-	-	-
999	vs	-	-	υ_{8}	999
992	s	-	-	$\upsilon_{16+}\upsilon_{18}$?	631+366 = 997
972	s	-	-	-	-
963	ms	963.4	m	υ_{9}	963
959	s	-	-	-	-
954	s	-	-	-	-
904	s	905.2	m	-	-
901	vs	902.8	w	$\upsilon_{17+}\upsilon_{18}$	526+366 = 892
890	m	-	-	-	-
-	-	882.5	w	υ_{6}	883
878	ms	-	-	-	-
854 br	vw	852.5	vw	υ_{25}	854
824	m	823.6	m	υ_{7}	824
-	-	816 sh	m	υ_{11}	816
-	-	800.7	s	-	-
-	-	765.2	mw	υ_{15}	765
-	-	701.6	s	-	-
631 br	mw	-	-	υ_{16}	631
-	-	625	vvw	υ_{27}	625
-	-	579.8	mw	υ_{10}	579.8
-	-	525.6	s	υ_{17}	526
-	-	365.5	ms	υ_{18}	366

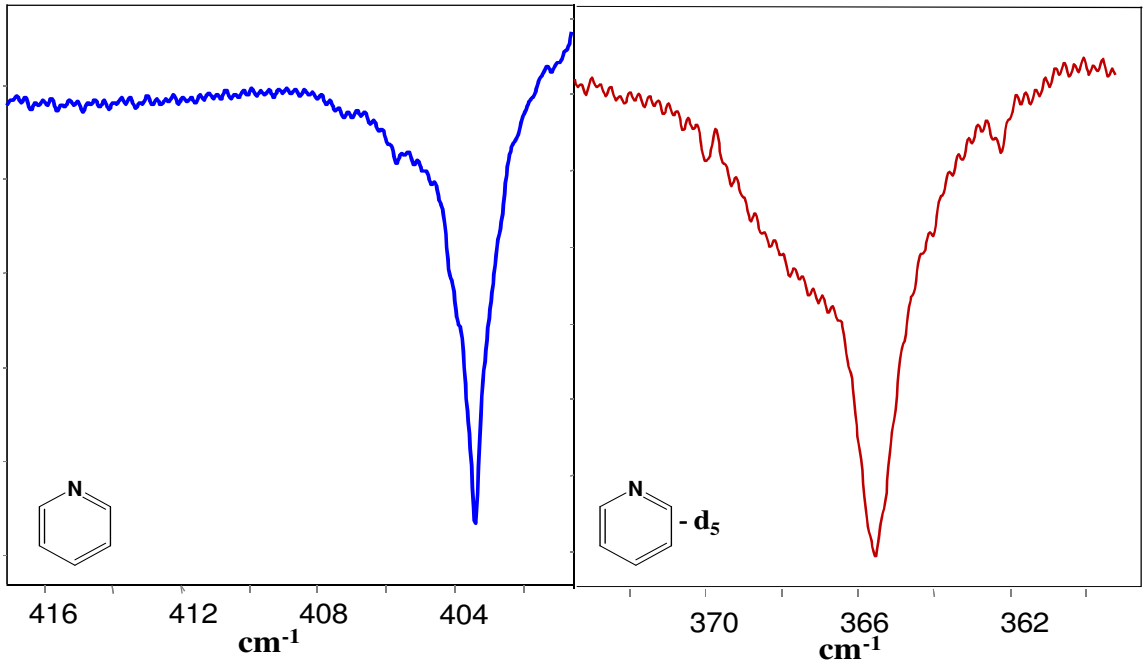

Figure 9. Far IR spectra of pyridine-d_0 and pyridine-d_5.

CHAPTER V

ULTRAVIOLET ABSORPTION SPECTRA OF PYRIDINE-d_0 AND -d_5 AND THEIR RING-BENDING POTENTIAL ENERGY FUNCTION IN THE $S_1(n,\pi^*)$ STATE*

INTRODUCTION

The ultraviolet absorption spectra of pyridine vapor were extensively studied and assigned by Henri and Angenot[1] in 1936 and by Sponer and Stücklen[2] in 1946. The band origin was reported to be 34,769 cm^{-1}. The assignments primarily consisted of identifying the numerical values of quantum states but made few correlations to the actual vibrations involved with these. The studies also did not recognize that the B_1 out-of-plane ring-bending mode in the $S_1(n,\pi^*)$ excited state would be highly anharmonic and of very low-frequency. In 1972 Jessan, Kroto, and Ramsay, in a brief letter to the editor,[3] reinvestigated the pyridine uv spectrum and assigned five transitions to the ν_{18} out-of-plane ring bending mode. In the old traditional literature[4] this is referred to as ν_{16b}. These transitions allowed five quantum states of the bending to be determined in the $S_1(n,\pi^*)$ state, and from these the authors concluded that in this excited state the molecule is quasi-planar with a barrier to planarity of about 4 cm^{-1}.

---

* Reprinted with permission from "Ultraviolet Absorption Spectra of Pyridine-d_0 and -d_5 and their Ring-Bending Potential Energy Fnction in the $S_1(n,\pi^*)$ State" by Boopalachandran, P.; Laane, J., 2008. *Chem. Phys. Lett.*, 462, 178-182, Copyright 2008 by Elsevier.

However, the results of a potential energy calculation were never presented. More recently Villa and co-workers[5] studied the laser induced fluorescence spectra of jet-cooled pyridine and assigned 40 bands up to 2081 cm^{-1} above the electronic band origin. In 2006 Riese and co-workers[6] reported the REMPI spectrum of jet-cooled pyridine and also reported assignments for the $S_1(n,\pi^*)$ state. Neither of these studies examined the nature of the ring-bending potential energy function. Moreover, their investigations only allowed a few of the vibrational fundamentals of the excited electronic state to be assigned.

In the present study the ultraviolet absorption spectra of both pyridine and its d_5 isotopomer recorded under high resolution and with high accuracy were reported. From the data, an energy map for the low-frequency vibrations of the electronic excited state was created and the ring-bending data to calculate the potential energy function for that vibration was utilized. The kinetic energy function for the motion was also computed to provide a meaningful assessment of this large-amplitude vibration.

COMPUTATIONS

The structures and vibrational frequencies of pyridine-d_0 and pyridine-d_5 for the electronic ground state were calculated using the Gaussian 03 program package.[65] *Ab initio* second order Moller-Plesset (MP2) level of theory with the cc-pVTZ basis set was used to find the optimized geometry. The DFT-B3LYP level of theory with the 6-311++G(d,p) basis set was used to calculate the vibrational frequencies. Based on

previous work,[66-70] a scaling factor of 0.964 was used for the C-H stretching vibrational frequencies and a factor of 0.985 for the lower frequencies.

In addition, in collaboration with Sunghwan Kim, the geometries of the two molecules in the S_0, S(n,π*) and S(π,π*) states were also optimized at the CASSCF/6-311++G(d,p) level, using an active space consisting of 8 electrons (2 lone-pair electrons and 6 π electrons) distributed in 7 orbitals (one lone-pair orbital and six π orbitals). The optimized geometries were confirmed to be minima by harmonic vibrational frequency analyses. Based on previous work, a scaling factor of 0.905 was used for all of the vibrational frequencies in the electronic excited states.[71] All CASSCF computations were performed using the GAMESS package.[72] Figure 10 shows the calculated structures of pyridine-d_0 in their ground and electronic excited states.

EXPERIMENTAL

Pyridine and pyridine-d_5 (99% isotopic purity) were purchased from Aldrich and purified by trap to trap distillation. The ultraviolet absorption spectra of the samples in a 23.5 cm glass cell with quartz windows were recorded at ambient temperature on a Bomem DA8.02 fourier transform spectrometer. Typically 3000 scans at a resolution of 0.25 cm^{-1} were averaged. The data were collected six times for each molecule utilizing different vapor pressures of the samples in the 10 to 18 Torr range. The far-infrared spectra of the vapor samples in 10 cm cells with polyethylene windows were also recorded in order to determine the wavenumbers of the ring-bending mode for both isotopomers.

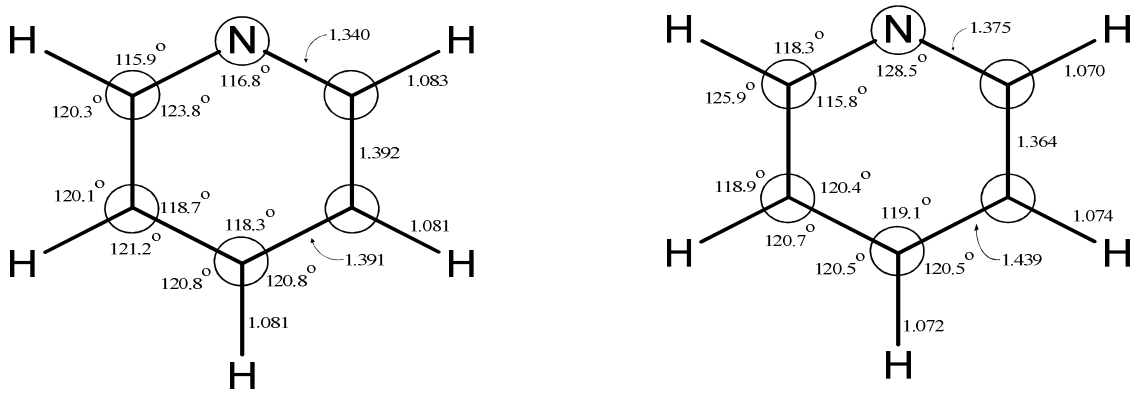

(a) (b)

Figure 10. Calculated structures of pyridine in their (a) S_0 ground electronic state at the MP2/cc-pVTZ level of theory and (b) $S_1(n,\pi^*)$ state at the CASSCF/6-311++G(d,p) level of theory.

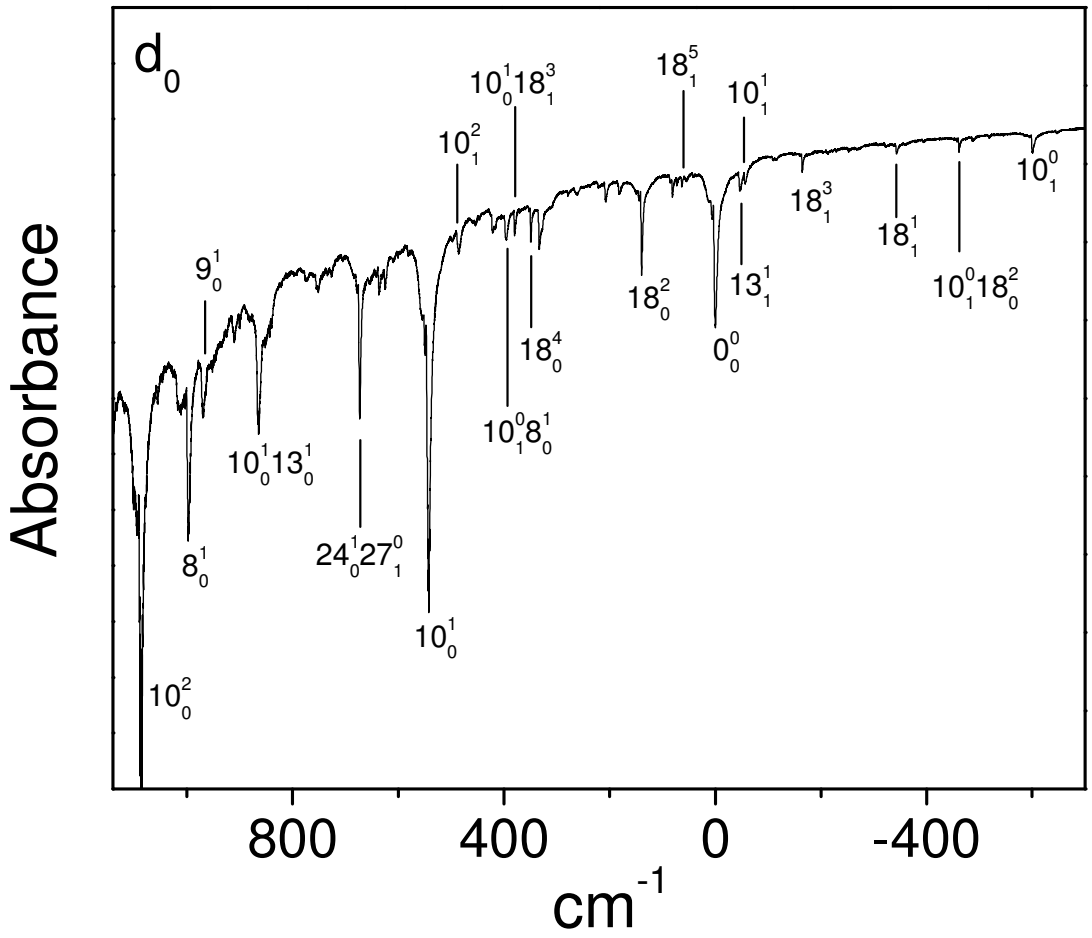

Figure 11a. Ultraviolet absorption spectra of pyridine-d_0 vapors. The wavenumbers shown are relative to the band origins at 34,767.0 cm^{-1}.

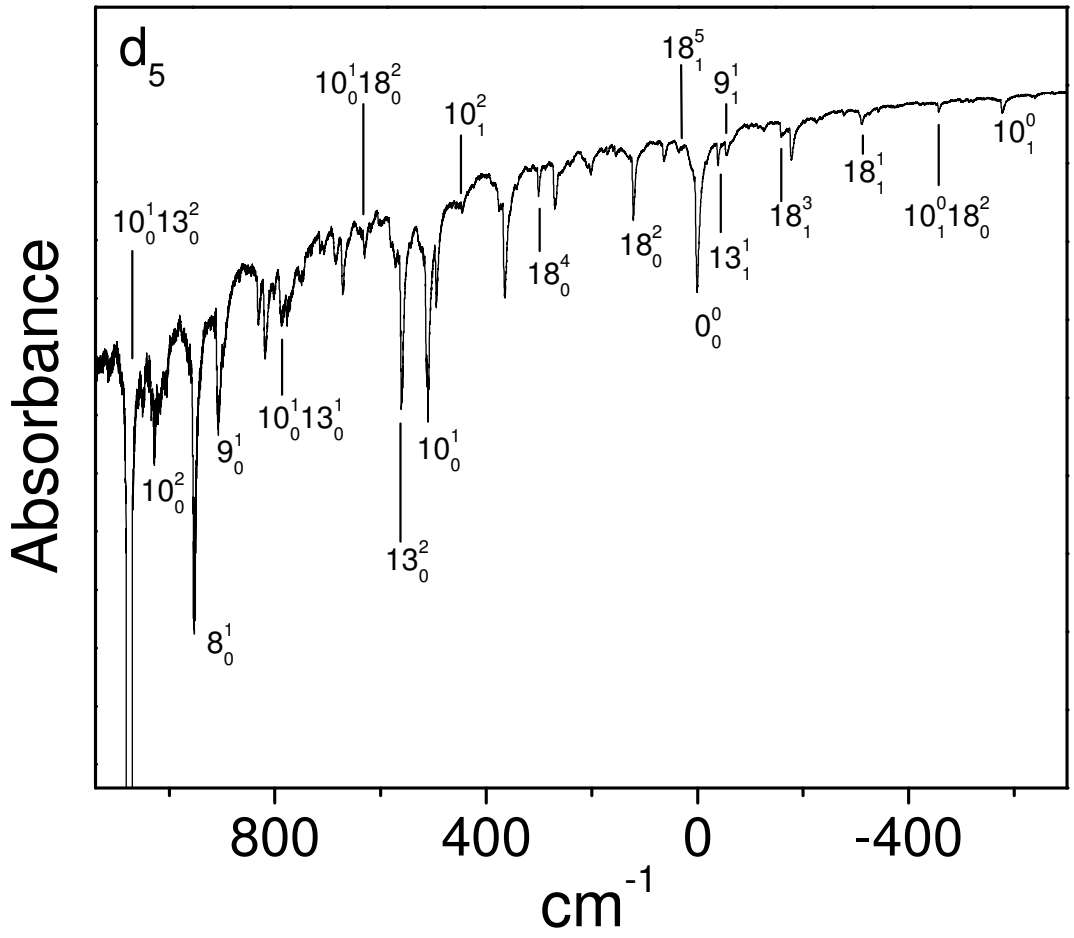

Figure 11b. Ultraviolet absorption spectra of pyridine-d_5 vapors. The wavenumbers shown are relative to the band origins at 34,945.8 cm^{-1}.

Table 5: Observed and calculated vibrational frequencies (cm^{-1}) for pyridine-d_0 in its ground and excited states

C_{2v}	ν	Approximate Description	S_0		S (n,π^*)				S (π,π^*)	
			OBS	CALC[a]	OBS	CALC[b]	OBS RAG[c]	CALC BLPSCK[d]	CALC[b]	CALC BLPSCK[d]
A_1	1	C-H stretch	3072	3080		3074		3100	3055	3079
(i.p.)	2	C-H stretch	3060	3056		3045		3072	3036	3063
	3	C-H stretch	3030	3034		3019		3045	3023	3052
	4	Ring stretch	1584	1599		1507		1532	1499	1700
	5	Ring stretch	1483	1488		1379		1391	1394	1405
	6	C-H wag	1218	1222		1127		1137	1149	1157
	7	C-H wag	1072	1076		987		995	984	988
	8	Ring mode	1031	1031	998	885	995	894	883	891
	9	Ring breathing	991	995	969	857		872	878	885
	10	Ring bend	601	607	542.8	536	542	538	509	511
A_2	11	C-H wag o.p.	982	981		811		816	678	699
(o.p.)	12	C-H wag o.p.	887	879	416	469	411	509	590	601
	13	Ring bend o.p.	374	375	326	348	323	387	260	271
B_1	14	C-H wag o.p.	997	991		810		814	646	662
(o.p.)	15	C-H wag o.p.	936	940		609		623	573	586
	16	C-H wag o.p.	744	746		496		493	470	470
	17	Ring bend o.p.	700	703		476		477	434	439
	18	Ring bend o.p.	403	411	59.5	87	60	72	244	262
B_2	19	C-H stretch	3066	3072		3068		3094	3038	3063
(i.p.)	20	C-H stretch	3030	3037		3021		3046	3024	3051
	21	Ring stretch	1576	1593		1453		1478	1680	1514
	22	Ring stretch	1442	1448		1314		1331	1476	1491
	23	C-H wag i.p.	1363	1363		1271		1285	1337	1348
	24	Ring stretch	1227	1264		1185		1196	1310	1318
	25	C-H wag i.p.	1143	1152		1024		1035	1109	1117
	26	C-H wag i.p.*	1048?	1060		787		821	880	889
	27	Ring bend	654	659	635.7	581	633	587	577	581

Abbreviations: i.p., in-plane; o.p., out-of-plane.

[a] B3LYP/6-311++g(d,p); Frequencies scaled with a scaling factor of 0.985 for frequencies less than 1800 cm^{-1} and 0.964 for frequencies greater than 1800 cm^{-1}.

[b] CASSCF/6-311++G(d,p); scaled with a scaling factor of 0.905.

[c] Reference 6. [d] Reference 12.

Table 6: Ultraviolet absorption spectra for the n→π* transition of pyridine-d_0

Frequency (cm^{-1})						
[a]OBS		SS[b]	VAL[c]	RAG[d]	Assignment	Inferred
-2249.3	vvw				$6_1^0 8_1^0$	-1218-1031 = -2249
-1819.7	vvw				$6_1^0 10_1^0$	-1218-601 = 1819
-1805.5	vvw				10_3^0	3x-601 = -1803
-1632	w				$8_1^0 10_1^0$	-1031-601 = -1632
-1218	w				6_1^0	-1218
-1202	w				10_2^0	2x-601 = -1202
-1140.0	vvw				25_1^0	-1143
-1079	w				$6_1^0 18_0^2$	-1218+139 = -1079
-1061.9	w				$10_2^0 18_0^2$	-1202+139 = -1063
-1030.9	mw	-1031			8_1^0	-1031
-945.1	w				-	
-891.1	w				$8_1^0 18_0^2$	-1031+139 = -892
-866.4	vw				-	
-806.0	vw				18_2^0	2x-403 = -806
-766.3	mw				$10_1^0 18_1^3$	-601-165 = -766
-674.2	w				$6_1^0 10_0^1$	-1218+543 = -675
-646.2	mw				$17_1^0 18_0^1$?	-700+60 = -640
-600.6	vvs	-601			10_1^0	-601
-595	w				$24_1^0 27_0^1$?	-1227+636 = -591
-538.2	vw				-	
-518.6	mw				$10_2^1 18_0^2$?	-1202+543+139 = -520
-487.4	m				$8_1^0 10_0^1$	-1031+543 = -488
-461.8	vs	-464			$10_1^0 18_0^2$	-601+139 = -462
-458	mw				-	
-394.5	mw				-	
-358 br	mw				-	
-343.8	vs	-345			18_1^1	-403+60 = -343
-338	w				-	
-322 br	mw				-	
-308 br	w				-	
-268.1	mw				$18_2^0 10_0^1$?	-2x403+543 = -263
-252.3	mw				$10_1^0 18_0^4$	-601+349 = -252
-228.9	w				-	
-221.6	vvw				$6_1^0 8_0^1$	-1218+998 = -220
-212.8	m				$13_1^1 18_1^3$	-47-165 = -212
-176 sh	w				-	
-165.4	vs	-164			18_1^3	-403+238 = -165
-161 sh	w				-	

Table 6: (Continued)

Frequency (cm^{-1})						
[a]OBS		SS[b]	VAL[c]	RAG[d]	Assignment	Inferred
-133 br	vvw				$6_1^0 10_0^2$	-1218+1086 = -132
-114.6	m				10_2^2	-2x601+2x543 = -116
-109.7	m				-	
-57.2	s	-58			10_1^1	-601+543 = -58
-46.9	vs	-48			13_1^1	-374+326 = -48
-41.4	w				-	
-33.4	vvw				8_1^1	-1031+998 = -33
0	vvs	0	0	0	0_0^0	0
5.7 sh	m				-	
12.2 sh	m				-	
41 br	vw				-	
54.8	mw	53			$8_1^0 10_0^2$	-1031+1086 = 55
63.3	s	62			18_1^5	-403+467 = 64
72.6	m	72	70	71	-	
80.6	vs	80	79	79	$10_1^1 18_0^2$	-59+139 = 80.5
85 sh	w				-	
104 br	vvw				$8_1^1 18_0^2$	-33+139 = 106
139.0	vvs	139	139	139	18_0^2	139
144	m				-	
149 br	w				-	
181.9	vs	181			-	
207.1	vs	206			-	
220.7	m				-	
257	vw				-	
262.0	m				-	
278.9	mw				-	
326sh	vw		325	323	13_0^1	326
332.3	vs	331			-	
348.8	s	348	347	345	18_0^4	349
379.8	s	378			$10_0^1 18_1^3$	543-165 = 378
395.7	s	396	396	394	$10_1^0 8_0^1$	-601+998 = 397
416sh	m			411	12_0^1	416
421.1	s	421			-	
447	w				-	
453.6	w		450		-	
460	w				-	
485.9	s	485	487	487	10_1^2	-601+1086 = 485
497	w				-	
542.8	vvs	542	543	542	10_0^1	543

Table 6: (Continued)

Frequency (cm^{-1})						
[a]OBS		SS[b]	VAL[c]	RAG[d]	Assignment	Inferred
549	w				-	
579	vw				-	
591.7	vw				18_0^6	592
610	vw				-	
624.7	mw		624		$10_1^2 18_0^2$	486+139 = 625
635.7	m	638	635	633	27_0^1	636
652.7	vw				13_0^2	2x326 = 652
672.7	vs	672	672	672	-	
678	w				$10_0^1 18_0^2$	543+139.0 = 682
705	vw				-	
727	vw				-	
753 br	mw		753		-	
774	w	775			$6_1^0 8_0^2$	-1218+2x1997 = 779
795 br	w				-	
864	s	864			-	
899	w				-	
910.8	mw		912		$9_0^1 10_1^1$	969-57 = 912
924.2	vvw				$10_0^2 18_1^3$	1086-165 = 921
951	vvw				-	
968.6	m	968	967		9_0^1	969
997.6	s	995	997	995	8_0^1	998
1010.1	vw				-	
1026.3	vvw				10_1^3	-601+3x543 = 1028
1054	vw				-	
1087.3	vs	1084	1087		10_0^2	2x543 = 1086
1094 sh	w				-	
1102 br	vw		1100		-	
1138.5	mw				-	
1182.3	w				-	
1207	w				-	
1218.8	w				$10_0^1 24_0^1 27_1^0$	542.8+672.7 = 1215.5
1227.1	vw				$10_0^2 18_0^2$	139.0+1085.6 = 1224.6
1367 sh					-	
1392.2	s		1387		$8_0^2 10_1^0$	1997-601 = 1396
1407.7	vw				-	
1451	w		1454		-	
1461.9	vw				$10_0^3 18_1^3$	1627-165 = 1462
1478	vw				-	
1485	vw				-	

Table 6: (Continued)

Frequency (cm^{-1})					
[a]OBS	SS[b]	VAL[c]	RAG[d]	Assignment	Inferred
1511.1	vvw			$9_0^1 10_0^1$	969+543 = 1512
1536.1	s	1535		-	
1539.3	s	1540		$8_0^1 10_0^1$	998+543 = 1541
1549	w			-	
1574	vw			-	
1587	vw			-	
1627	s	1636		10_0^3	3x543 = 1629
1671	mw			-	
1736.3	vvw			$10_0^2 13_0^2$	2x543+2x326 = 1738
1763	vw			-	
1769.3	w			$10_0^3 18_0^2$	3x543+139 = 1768
1797	vw			-	
1852	m	1847		-	
1916	m	1909		$8_0^1 10_0^2 18_1^3$	998+1086-165 = 1919
1927	vvw			-	
1996.8	mw	1997		8_0^2	2x998 = 1996
2080	m	2081		$8_0^1 10_0^2$	998+1086 = 2084
2093	vw			-	
2115	vw			-	
2135.7	vvw			$8_0^2 18_0^2$	1997+139 = 2136
2172	vw			10_0^4	4x543 = 2172
2304	mw			$10_0^4 18_0^2$?	2172+139 = 2311
2382	w			-	
2444	w			-	
2502	vw			-	
2537	vw			$8_0^2 10_0^1$	1997+543 = 2540
2617	vw			-	
2820	vw			-	
2907	vvw			9_0^3	3x969 = 2907
3070	vvw			-	

Abbreviations: s, strong; m, medium; w, weak; v, very; sh, shoulder; br, broad.
[a] Relative to band origin at 34,767.0 cm^{-1}
[b] Reference 2. [c] Reference 5. [d] Reference 6.

ABSORPTION SPECTRA

Figure 11a shows the uv absorption spectrum of pyridine and Figure 11b shows the uv absorption spectrum of pyridine-d_5 relative to the electronic band origins at 34,767.0 and 34,945.8 cm^{-1}, respectively. Some of the more significant transitions were labeled in the figure utilizing the conventional numbering scheme where ν_{27} was the lowest frequency of the B_2 vibrations. The out-of-plane modes were of A_2 and B_1 symmetry so that the out-of-plane ring-bending was ν_{18}. Table 5 summarizes the observed and calculated vibrational frequencies of pyridine-d_0 in its ground and excited states. The more intense absorption bands for pyridine in the -2300 to +3100 cm^{-1} region relative to the 0_0^0 band origin are listed in Table 6 along with their assignments. The frequency values are compared to those reported by Sponer and Stücklen (SS),[2] Villa et al. (VAL),[5] and Riese et al. (RAG).[6] The approximate description for each low-frequency vibration number is given in Table 7 which also lists the generally accepted[7] vibrational frequencies. It was quite remarkable how well SS did in 1946 in not only recording the absorption frequencies, most to ± 1 cm^{-1}, but also in recognizing many of the numerical relationships. For example, the band at 379.8 cm^{-1} assigned to $10_0^1 18_1^3$ (expected near 543 – 165 = 378 cm^{-1}) was reported by SS at 378 and assigned as 542 – 164. Similarly the $8_0^1 10_1^0$ band at 395.7 cm^{-1} (expected near 998 – 601 = 397 cm^{-1}) was reported by SS at 396 cm^{-1} and assigned as 995 – 601. However, in 1946 all of the vibrations of pyridine in its ground state had not been assigned so that SS could not correlate the appropriate descriptions with their observed numbers.

Table 7: Low-frequency vibrations (cm^{-1}) of pyridine-d_0 and -d_5

			Pyridine-d_0			Pyridine-d_5	
		Approximate	S_0	S_1		S_0	S_1
		Description	Lit[a]	Lit[a]	This Work	Obs	This Work
A_1	10	Ring bend	601.4	542	542.8	579.2[a]	510.2
A_2	12	C-H wag (out-of-plane)	871	411	416		
	13	Ring bend (out-of-plane)	373	323	326	318[a]	279
B_1	18	Ring bend (out-of-plane)	403.3	59[b]	59.5	365.5[c]	53.6
B_2	27	Ring bend	652	633	635.7		

[a] Reference 7. [b] Reference 3. [c] This work

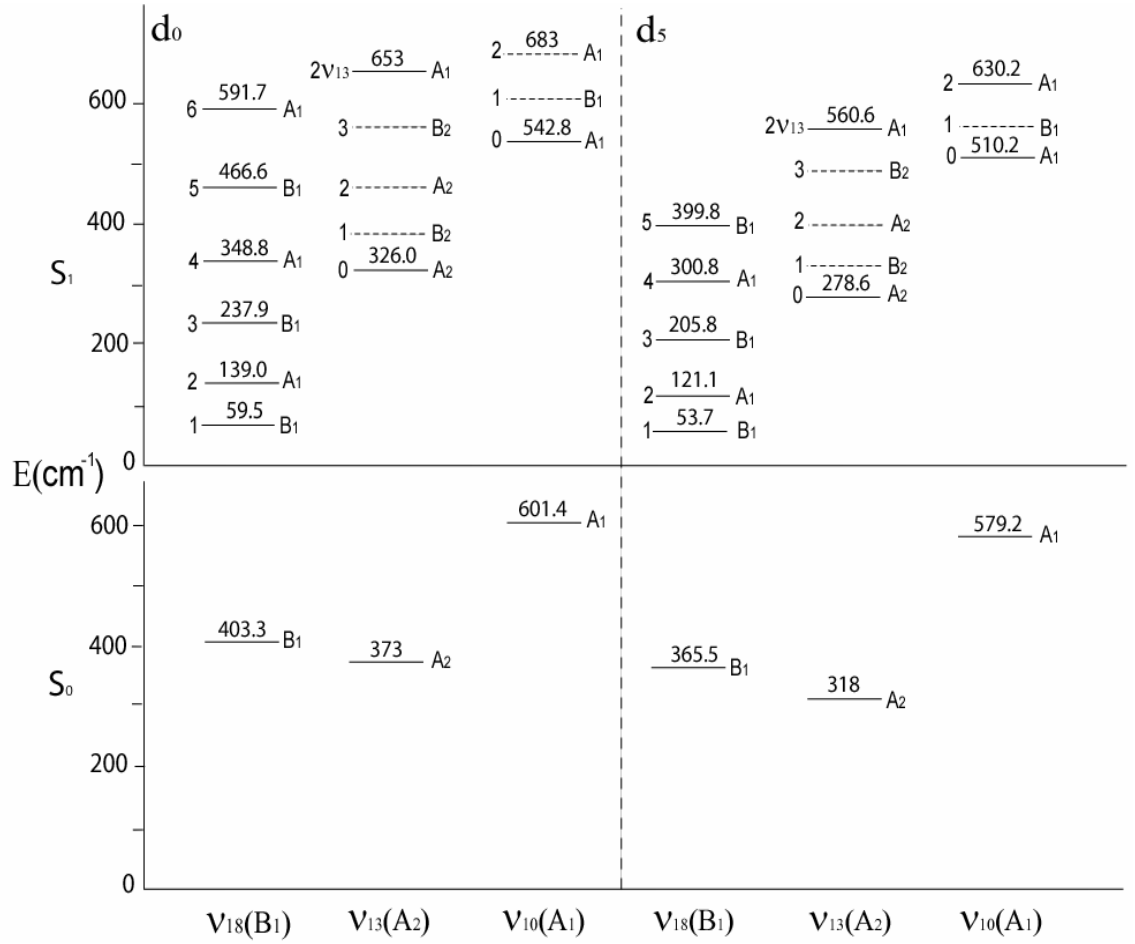

Figure 12. Energy map for the vibrational levels of pyridine (left) and pyridine-d_5 (right) in their ground (bottom) and S_1 excited (top) electronic states.

Moreover, SS did not recognize that ν_{18} (ν_{16b} in older literature) was highly anharmonic in the excited $S_1(n,\pi^*)$ state and that frequencies at -343.8 (18_1^1), -165.4 (18_1^3), 63.3 (18_1^5), 139.0 (18_0^2), and 348.8 (18_0^4) were all associated with just the out-of-plane ring-bending motion. This was later realized by Jessan, Kroto, and Ramsay.[3]

In the present study the focus was on correctly identifying the ν_{18} bending mode levels. Thus it was important to also consider several of the other lower frequency vibrations, namely ν_{13} (A_2 out-of-plane ring-bending), ν_{10} (A_1 in-plane ring-bending), and ν_{27} (B_2 in-plane ring-bending). Figure 12 shows the energy map for these modes in the S_0 and $S_1(n,\pi^*)$ states constructed from the data in Figures 11a, 11b and Tables 5 and 8. Table 7 lists the wavenumbers for these modes. It should be noted that the conventional numbering scheme was utilized with the highest frequency in each symmetry block labeled first rather than the traditional one[7] where ν_1 was the ring-breathing mode. The solid lines indicate observed quantum states whereas the dotted lines represent the expected positions of ν_{18} levels in combination with ν_{10} or ν_{13}. The most dramatic result was for the ν_{18} vibration which had its v = 1 quantum level in S_0 at 403.3 cm^{-1} but declined to 59.5 cm^{-1} in $S_1(n,\pi^*)$. In addition, the energy spacings in S_1 clearly reflected a very non-harmonic pattern. This will be discussed in some detail later. Table 8 summarizes the observed and calculated vibrational frequencies of pyridine-d_5 in its ground and excited states. Table 9 lists the principal absorption bands and assignments in the -1200 to +1900 cm^{-1} region relative to the electronic band origin.

Table 8: Observed and calculated vibrational frequencies (cm^{-1}) for pyridine-d_5 in its ground and excited states

C_{2v}	ν	Approximate Description	S_0		S (n,π*)		S (π,π*)
			OBS	CALC[a]	OBS	CALC[b]	CALC[b]
A_1	1	C-H stretch	2299	2284		2278	2261
(i.p.)	2	C-H stretch	2275	2258		2247	2242
	3	C-H stretch	2272 sh	2244		2229	2231
	4	Ring stretch	1554	1558		1456	1441
	5	Ring stretch	-	1348		1174	1169
	6	C-H wag	883	893		951	951
	7	C-H wag	824	823		871	868
	8	Ring mode	999	1007	953.3	812	832
	9	Ring breathing	963	967	907.6?	714	742
	10	Ring bend	580	585	510.2	518	492
A_2	11	C-H wag o.p.	816 sh	813		628	550
(o.p.)	12	C-H wag o.p.	-	684	389?	409	458
	13	Ring bend o.p.	-	320	279	283	227
B_1	14	C-H wag o.p.	828	829		618	543
(o.p.)	15	C-H wag o.p.	765	767		502	452
	16	C-H wag o.p.	631 br	630		459	379
	17	Ring bend o.p.	526	526		358	346
	18	Ring bend o.p.	366	371	53.6	78	222
B_2	19	C-H stretch	2288	2274		2267	2241
(i.p.)	20	C-H stretch	2253 br	2238		2224	2229
	21	Ring stretch	1545	1558		1388	1680
	22	Ring stretch	1303	1306		1206	1426
	23	C-H wag i.p.	1045	1042		1006	1126
	24	Ring stretch	1226	1257		940	1004
	25	C-H wag i.p.	854 br	841		791	802
	26	C-H wag i.p.*	-	823		711	741
	27	Ring bend	625	632		551	554

Abbreviations: i.p., in-plane; o.p., out-of-plane.
[a] B3LYP/6-311++g(d,p); Frequencies scaled with a scaling factor of 0.985 for frequencies less than 1800 cm^{-1} and 0.964 for frequencies greater than 1800 cm^{-1}.
[b] CASSCF/6-311++G(d,p); scaled with a scaling factor of 0.905.

Table 9: Ultraviolet absorption spectra for the n→π* transition of pyridine-d_5

[a]Frequency (cm^{-1})		Assignment	Inferred
-1210	vvw		
-1158.8	vw	10_2^0	2x-580 = -1160
-1037.1	vvw	$18_0^2 10_2^0$	121-1159 = -1038
-1014	w	-	
-953 br	vvw		
-892.9	w	-	
-879	vw	6_1^0	-883
-824	vw	7_1^0	-824
-779	w	-	
-739	vw	$10_1^0 18_1^3$	-580-160 = -740
-676	vw	-	
-640	w	-	
-635 sh	w	-	
-579	mw	10_1^0	-580
-522	w	-	
515	w	-	
-504	w	-	
-473	vvw	$17_1^0 18_0^1$	-526+54 = -472
-458	m	$10_1^0 18_0^2$	-580+121 = -459
-431	vw	-	
-422	vw	-	
-374	vw	$6_1^0 10_0^1$	-883+510 = -373
-344	mw	-	
-326	vw	-	
-311.8	m	18_1^1	-366+54 = -312
-278	w	$10_1^0 18_0^4$	-580+301 = -279
-264	w	-	
-235	vw	-	
-226	w	-	
-203.9	vvw	$13_1^1 18_1^3$	-160-39 = -199
-179	m	-	
-159.7	m	18_1^3	-366+206 = -160
-144	*vw*	-	
-126.5	w	-	

Table 9: (Continued)

[a]Frequency (cm^{-1})		Assignment	Inferred
-115.2	vw	$27_1^0 10_0^1$?	-625+510 = -115
-107	vvw	-	
-97.4	vw	-	
-67 sh	w	10_1^1	-580+510 = -70
-56	m	9_1^1	-963+908 = -55
-39.4	m	13_1^1	-318+279 = -39
-18	m	-	
0	vvs	0_0^0	0
5.9	w	-	
11 sh	m	-	
35	mw	18_1^5	-366+399.8 = 34
63.3	m	$9_1^1 18_0^2$	-55+121.1 = 66
67.8	w	-	
121.1	s	18_0^2	121.1
126	w	-	
154.6	w	-	
160	vw	-	
170.2	w	-	
177.8	w	-	
201.4	m	$10_0^1 18_1^1$	510-312 = 198
208	w	-	
235	vvw	-	
240.6	mw	13_1^2	-318+559 = 241
269.9	s	-	
300.8	ms	18_0^4	300.8
320 br	w	-	
342	w	-	
364.2	s	-	
374.1	mw	$10_1^0 8_0^1$	-580+953.3 = 373
424	vvw	-	
445.5	mw	10_1^2	1022-580 = 442
458	vvw	-	
494.5	m	-	

Table 9: (Continued)

[a]Frequency (cm^{-1})		Assignment	Inferred
510.2	s	10_0^1	510.2
542	vw	-	
559	s	13_0^2	2x278.6 = 557.2
563.9	w	$10_0^1 18_0^1$?	510+53.7 = 564
572	mw	-	
580	vw	-	
603	vw	-	
618	vw		
630.2	mw	$10_0^1 18_0^2$	510+121.1 = 631
636	vw	-	
671.9	mw	-	
684.7	mw	-	
707.3	w	-	
715.0	w	-	
747	w	-	
777	w	-	
787.8	mw	-	
802	vw	-	
819.0	mw	-	
831.6	mw	-	
867	vvw	-	
907.6	ms	9_0^1	907.6
953.3	ms	8_0^1	953.3
1021.5	w	10_0^2	2x510.2 = 1020.4
1029.3	w	-	
1050	w	-	
1072.5	m	$10_0^1 13_0^2$	510.2+559 = 1069
1079.5	m	$18_0^2 8_0^1$	121.1+953.3 = 1074.4
1115.9	w	13_0^4	4x279 = 1116
1154.4	w	-	
1218	m	-	
1231	mw	-	
1249.6	w	-	
1270	w	-	

Table 9: (Continued)

[a]Frequency (cm^{-1})		Assignment	Inferred
1311	w	-	
1332	vw	-	
1356	w	-	
1380	vvw	-	
1389.6	vvw	-	
1424	w	$9_0^1 10_0^1$?	907.6+510 = 1418
1460 br	m	$10_0^1 8_0^1$	510+953 = 1463
1508 br	mw	$8_0^1 13_0^2$	953+2x279 = 1511
1589 br	w	-	
1654 br	vw	-	
1721 br	vw	-	
1760 br	vw	-	
1898 br	vw	-	

Abbreviations: s, strong; m, medium; w, weak; v, very; sh, shoulder; br, broad.
[a] Relative to band origin at 34945.8 cm^{-1}

The energy levels for ν_{10}, ν_{13}, ν_{18} are also shown in Figure 12. Again the ν_{18} bands were highly anharmonic and at greatly reduced frequencies in the $S_1(n,\pi^*)$ excited state as compared to the ground state.

RING-BENDING POTENTIAL ENERGY FUNCTION

In the S_0 electronic ground state ν_{18} was very nearly harmonic and at a moderately high frequency for a ring-bending mode, 403.3 cm^{-1} for pyridine and 365.5 cm^{-1} for pyridine-d_5. In the $S_1(n,\pi^*)$ excited state, however, as noted by Jessan, Kroto, and Ramsay,[3] its frequency dropped dramatically and the energy spacings were far from harmonic. Because ν_{18} was much lower in frequency than the other modes in the excited state, its potential energy function was approximated quite well with a one-dimensional model. Laane's laboratory has a long history[58-63] of studying potential energy functions of large-amplitude vibrations, and a potential energy function of the form

$$V = ax^4 + bx^2 \tag{5.1}$$

often did a satisfactory job of calculating the vibrational energy levels.

The Hamiltonian

$$\hat{H}(x) = (-\hbar^2/2)\partial/\partial x(g_{44}(x))\partial/\partial x + V(x) \tag{5.2}$$

was utilized, where x is the out-of-plane ring-bending coordinate as previously defined for a six-membered ring.[75] The reciprocal reduced mass expression $g_{44}(x)$ is coordinate dependent and is expressed as an expansion in terms of x:

$$g_{44} = g_{44}^{(0)} + g_{44}^{(2)}x^2 + g_{44}^{(4)}x^4 + g_{44}^{(6)}x^6 \tag{5.3}$$

The coefficients $g_{44}^{(i)}$ in the expansion were calculated using our previously described computer program. For pyridine the expansions are for S_0:

$$g_{44}(S_0) = 0.00924 - 0.04174x^2 - 0.10130x^4 + 0.0100\ x^6 \quad (5.4)$$

and for S_1:

$$g_{44}(S_1) = 0.00962 - 0.04203x^2 - 0.0743x^4 + 0.8262x^6 \quad (5.5)$$

These were used in the Hamiltonian of Equation (5.2) before the potential energy parameters *a* and *b* in Equation (5.1) could be determined.

Utilizing the potential energy programs for calculating the energy levels[58-63] the optimal values of *a* and *b* were determined, which fit the observed ring-bending frequencies for pyridine for its $S_1(n,\pi^*)$ state. The resulting function was

$$V\ (cm^{-1}) = 6.11 \times 10^5\ x^4 - 2.73 \times 10^3\ x^2 \quad (5.6)$$

where x is given in Å. The energy level spacings calculated from this function are given in Table 10 and were compared to the experimental values. While the agreement was not nearly as good as we expected for ground state calculations,[58-63] it showed the one-dimensional approximation was quite reasonable for the electronic excited state. The potential function, quantum states, and energy separations are shown in Figure 13a and Figure 13b for pyridine-d_0 and for pyridine-d_5 respectively. The function had a barrier to planarity of 3 cm^{-1}, but the zero-point energy laid above the barrier, so pyridine is best described as a quasi-planar molecule in its $S_1(n,\pi^*)$ state. The barrier of 3 cm^{-1} was virtually identical to the 4 cm^{-1} value of Jessan, Kroto, and Ramsay,[3] but in their work no parameters for a potential function were presented.

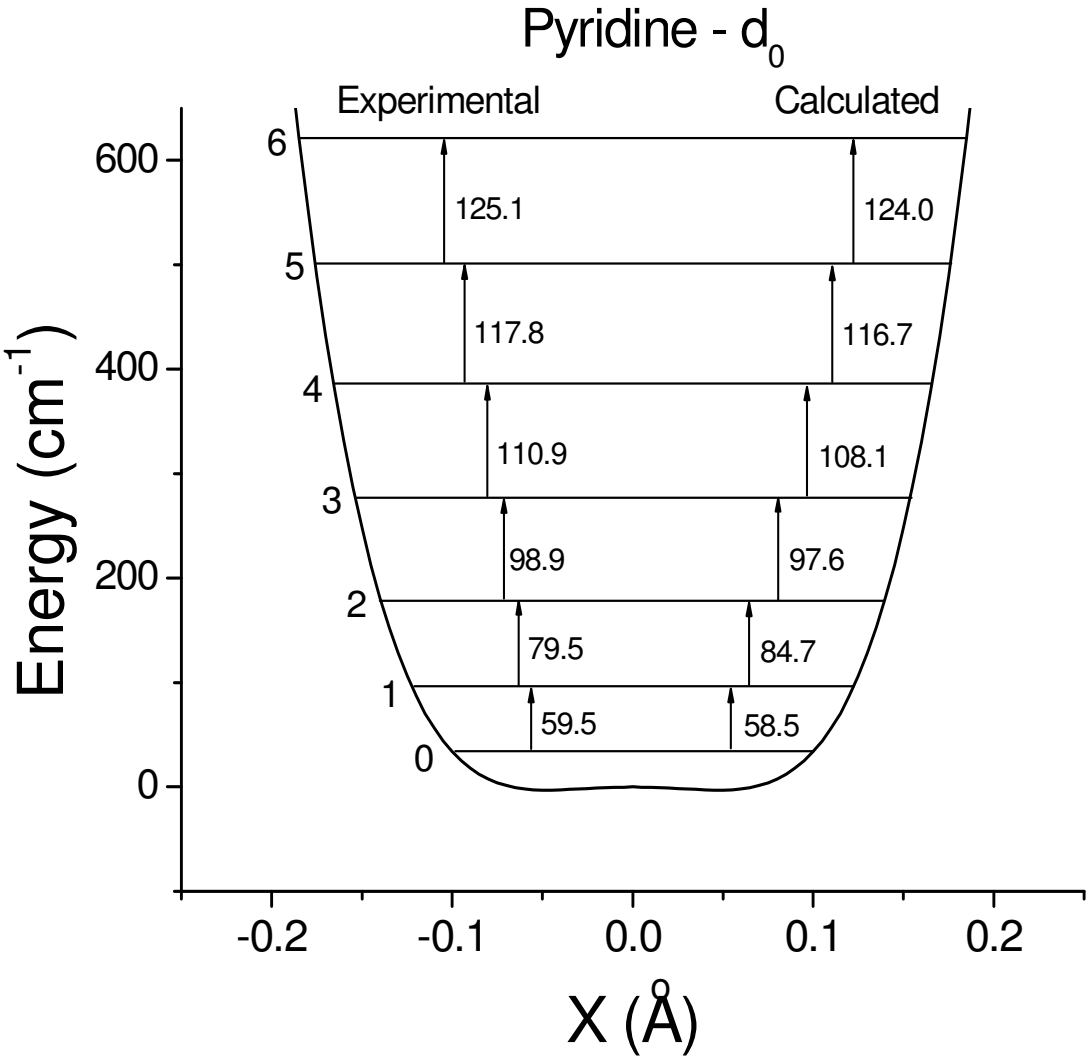

Figure 13a. Ring-bending potential energy functions for pyridine-d_0.

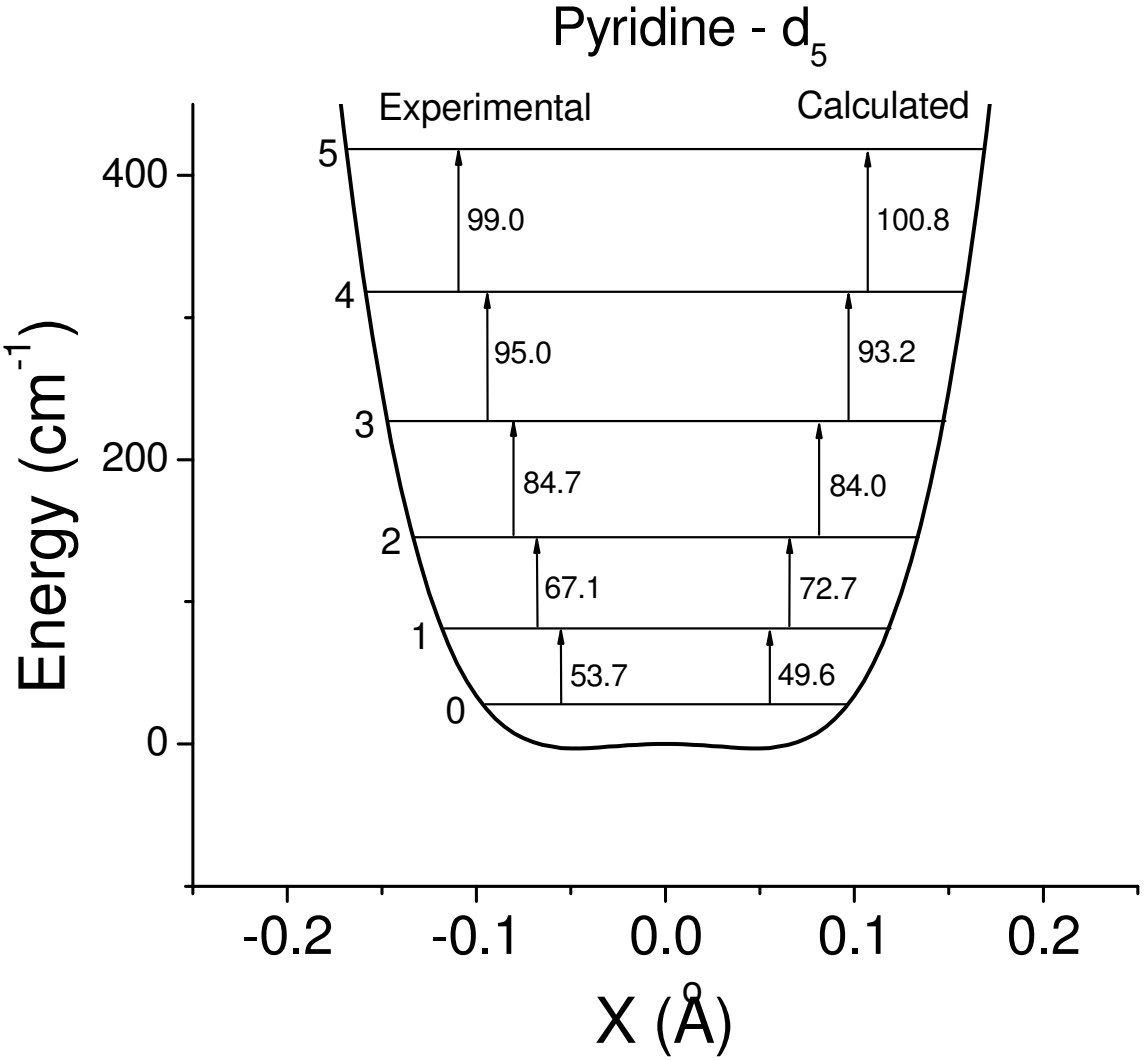

Figure 13b. Ring-bending potential energy functions for pyridine-d_5.

Table 10: Observed and calculated frequencies (cm^{-1}) for the ν_{18} vibration of pyridine-d_0 and pyridine-d_5 in their $S_1(n,\pi^*)$ states

	Pyridine-d_0		Pyridine-d_5	
Separation	Experimental	Calculated[a]	Experimental	Calculated[a]
0-1	59.5	58.5	53.7	49.6
1-2	79.5	84.7	67.1	72.7
2-3	98.9	97.6	84.7	84.0
3-4	110.9	108.1	95.0	93.2
4-5	117.8	116.7	99.0	100.8
5-6	124.6	124.0		

[a] $V\ (cm^{-1}) = (6.11 \times 10^5)\ x^4 - (27.3 \times 10^2)\ x^2$

For comparison purposes, in its S_0 ground state the ring-bending potential energy was calculated to be

$$V = 2.64 \times 10^5 x^2 \qquad (5.7)$$

and the molecule was more rigid.

The calculations for pyridine-d_5 were first carried out using the kinetic energy expansions calculated directly from the reduced mass computer program[75] and the potential energy function of Equation (5.6). When this was used together for S_0, the bending frequency was calculated to be too low, reflecting the fact that the calculated reduced mass ratio μ_{d_5}/μ_{d_0} of 1.36 was too high. This has often been observed for isotopomers of other systems[66-70] and results from the fact that the actual vibration was not purely a ring-bending but had some contribution from other modes which interacted to a small degree. When $\mu_{d_5}/\mu_{d_0} = 1.22$ was used, agreement between observed and calculated bending frequencies was obtained using the potential function of Equation (5.7) for the S_0 state.

For the S_1 state the computed reduced mass ratio of 1.33 was again too high, but not nearly as much as for the electronic ground state. Since the ring-bending frequency was much lower in S_1, it interacted much less with the other vibrational modes and the reduced mass calculation for the pure one-dimensional mode did a much better job of predicting the correct reduced mass ratio. When the μ_{d_5}/μ_{d_0} ratio was reduced to 1.26, the potential energy function in Equation (5.6) for pyridine was effectively used for the d_5 isotopomer. For this ratio, the kinetic energy expansion for pyridine-d_5 in its S_1 state was

$$g_{44}(S_1) = 0.00762 - 0.02111x^2 - 0.17403x^4 + 0.0106x^6 \quad (5.8)$$

The calculated energy separations for the ring-bending of pyridine-d_5 in its S_1 state are given in Table 10.

The results in Figure 14 compared the $S_1(n,\pi^*)$ function to that in S_0 were more dramatic. Not only did pyridine have a tiny barrier in the excited state, but it also became extremely floppy. This was not at all surprising since the $n \rightarrow \pi^*$ transition decreased the degree of π bonding in the electronic excited state.

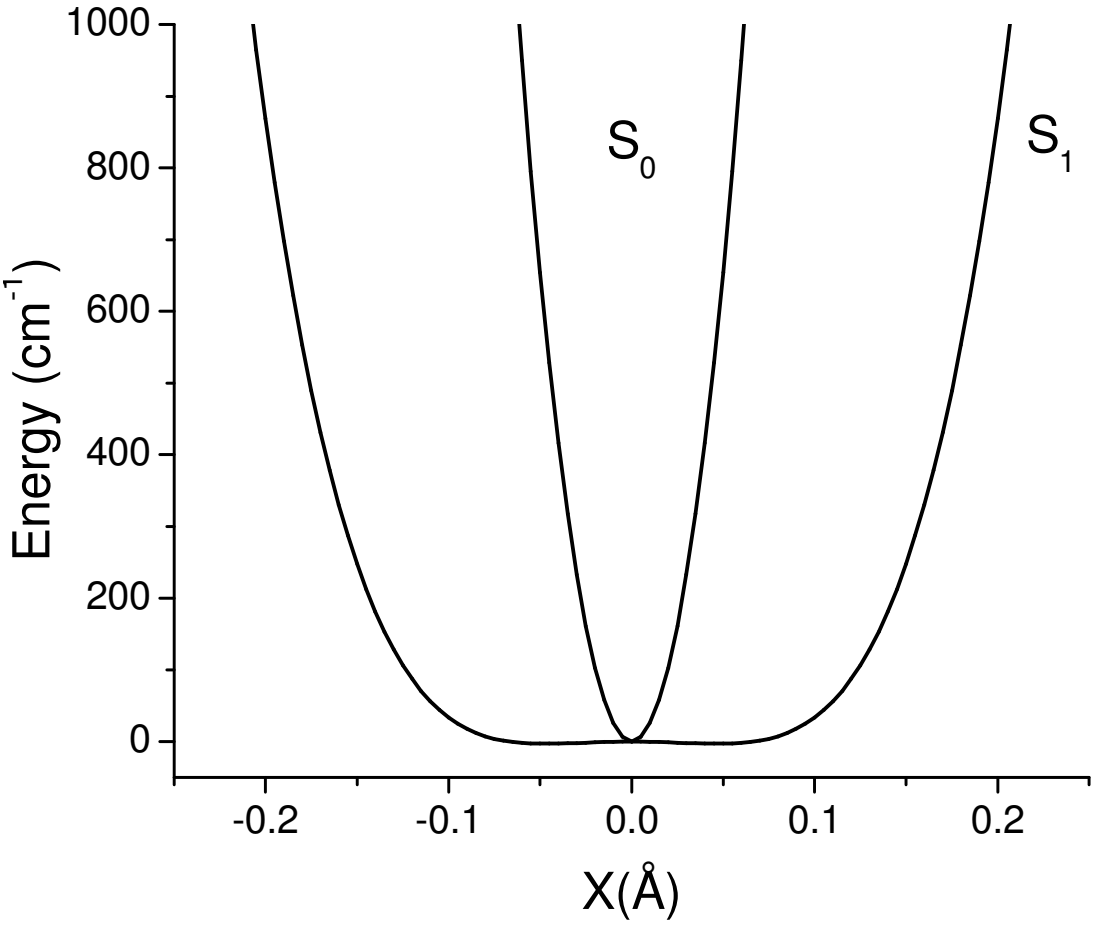

Figure 14. Comparison of the ring-bending potential function of pyridine in its $S_1(n,\pi^*)$ state to that in the S_0 ground state.

CHAPTER VI

VIBRATIONAL SPECTRA, STRUCTURE, AND THEORETICAL CALCULATIONS OF 2-FLUORO- AND 3-FLUOROPYRIDINE IN THEIR GROUND STATES*

INTRODUCTION

In Chapter V, the ultraviolet absorption spectrum of pyridine was reported and it showed that the molecule was very floppy and quasi-planar in its $S_1(n,\pi^*)$ electronic excited state. Determination of the potential energy function for the ring-bending vibration showed the barrier to planarity to be only 3 cm^{-1}. This is in contrast to the S_0 ground state where pyridine is rigidly planar.

In a continuation of the work on the vibrations and structure of pyridine and substituted pyridines in their ground and excited states, this chapter presents the results on two substituted fluoropyridines in their electronic ground states. The infrared and Raman spectra of 2-fluoropyridine (2FPy) and 3-fluoropyridine (3FPy) were analyzed and their vibrational frequencies were determined. *Ab initio* and DFT computations were carried out to compute the structures of these molecules, complement the experimental work and to support the vibrational assignments.

---

* Reprinted with permission from "Vibrational Spectra, Structure, and Theoretical Calculations of 2-Fluoro-and 3-Fluoropyridine in their Ground States" by Boopalachandran, P.; Laane, J., 2011. *Spectrochimica Acta Part A*, 79, 1191-1195,

COMPUTATIONS

The structures and vibrational frequencies of 2FPy and 3FPy for the electronic ground state were calculated using the Gaussian 03 program package.[65] *Ab initio* second order Moller-Plesset (MP2) level of theory with the cc-pVTZ basis set was used to find the optimized geometry. The DFT-B3LYP level of theory with the 6-311++G(d,p) basis set was used to calculate the vibrational frequencies and the infrared and Raman intensities. Based on previous work,[66-70] a scaling factor of 0.964 was used for the C-H stretching vibrational frequencies and a factor of 0.985 for the lower frequencies.

EXPERIMENTAL

2FPy and 3FPy (99% purity) were purchased from Aldrich and purified by trap to trap distillation. The Raman spectra of the molecules in the vapor-phase were recorded of samples sealed in the specially designed glass cells described in Chapter II. The vapor pressures of the samples at room temperature were about 9 Torr for 2FPy and 15 for 3FPy. A Jobin-Yvon U-1000 spectrometer equipped with a liquid nitrogen-cooled CCD detector was used to collect the spectra. The 532 nm line of a frequency-doubled Nd:YAG Coherent Verdi-10 laser was used and typically operated at 6 watts of power. Spectral scans spanning 60 cm^{-1} were typically recorded over periods of 4 to 6 hours so that many hundreds of individual spectra could be averaged. The spectral resolution was 0.7 cm^{-1}. The liquid phase Raman spectra were collected on the same instrument with samples in glass cuvettes using a laser power of 500 mW. The liquid-phase and vapor-phase mid-infrared spectra of 2FPy and 3FPy were collected on a

Bruker Vertex 70 FT spectrometer equipped with a globar light source, a KBr beamsplitter and deuterated lanthanum triglycine sulfate (DLaTGS) detector. The vapor-phase far infrared spectra (60-600 cm^{-1}) were collected on the same instrument equipped with a mylar beamsplitter, and a mercury cadmium telluride (MCT) detector. The vapor pressures of the samples were the same as for the Raman measurements. Typically 1024 scans were collected using a resolution of 0.5 cm^{-1}.

RESULTS AND DISCUSSION

Structures

Figure 15 shows the calculated structures of 2FPy and 3FPy and pyridine in their ground electronic states. The substitution of the fluorine atom on the pyridine ring for the most part had only a minor effect on the ring bond distances and angles. The notable exception was the N-C(F) bond distance for 2FPy which was only 1.313 Å as compared to 1.340 Å for pyridine and 1.344 Å for the other N-C bond of 2FPy. Clearly the substitution of the electronegative fluorine atom resulted in the strengthening of the adjacent N-C bond. There was insignificant effect observed for 3FPy since the fluorine atom was distant from the nitrogen atom. The C-F bond distance was 1.338 Å for 2FPy and 1.340 Å for 3FPy and these values were very similar to the fluorobenzene value of 1.35 Å determined from its microwave spectrum.[76,77]

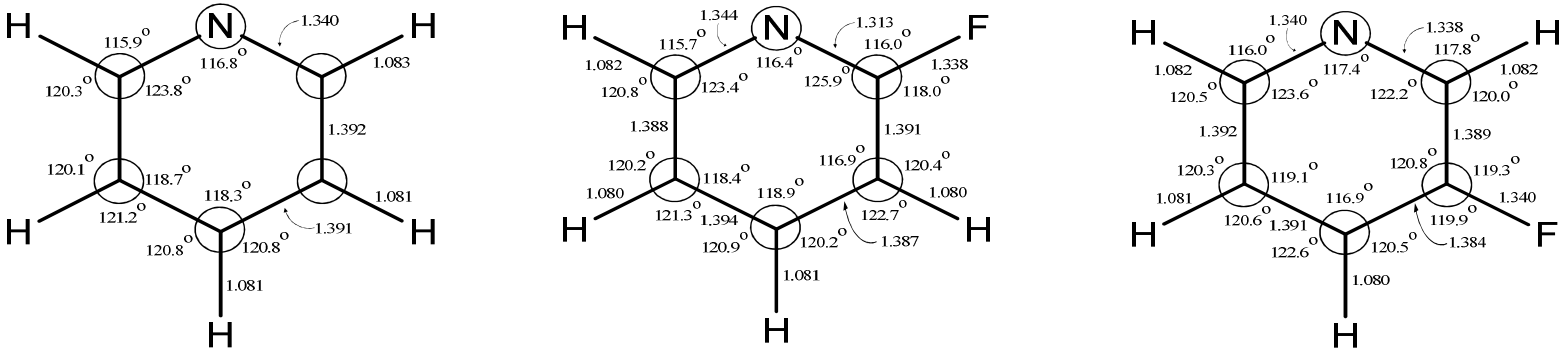

(a) (b) (c)

Figure 15. Calculated structures of (a) pyridine-d_0, (b) 2-fluoropyridine, and (c) 3-fluoropyridine in their S_0 ground electronic state using MP2/cc-pVTZ level of theory.

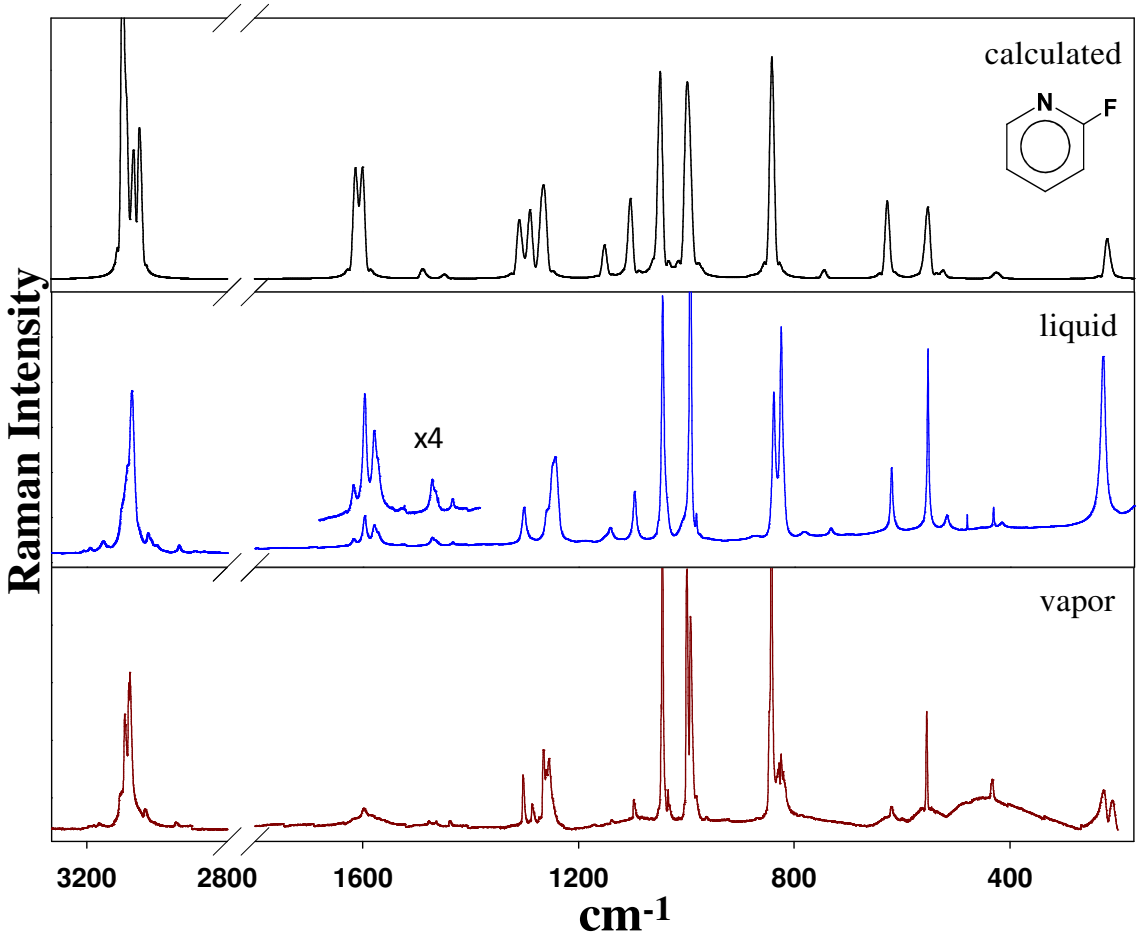

Figure 16. Liquid, vapor, and calculated Raman spectra of 2-fluoropyridine.

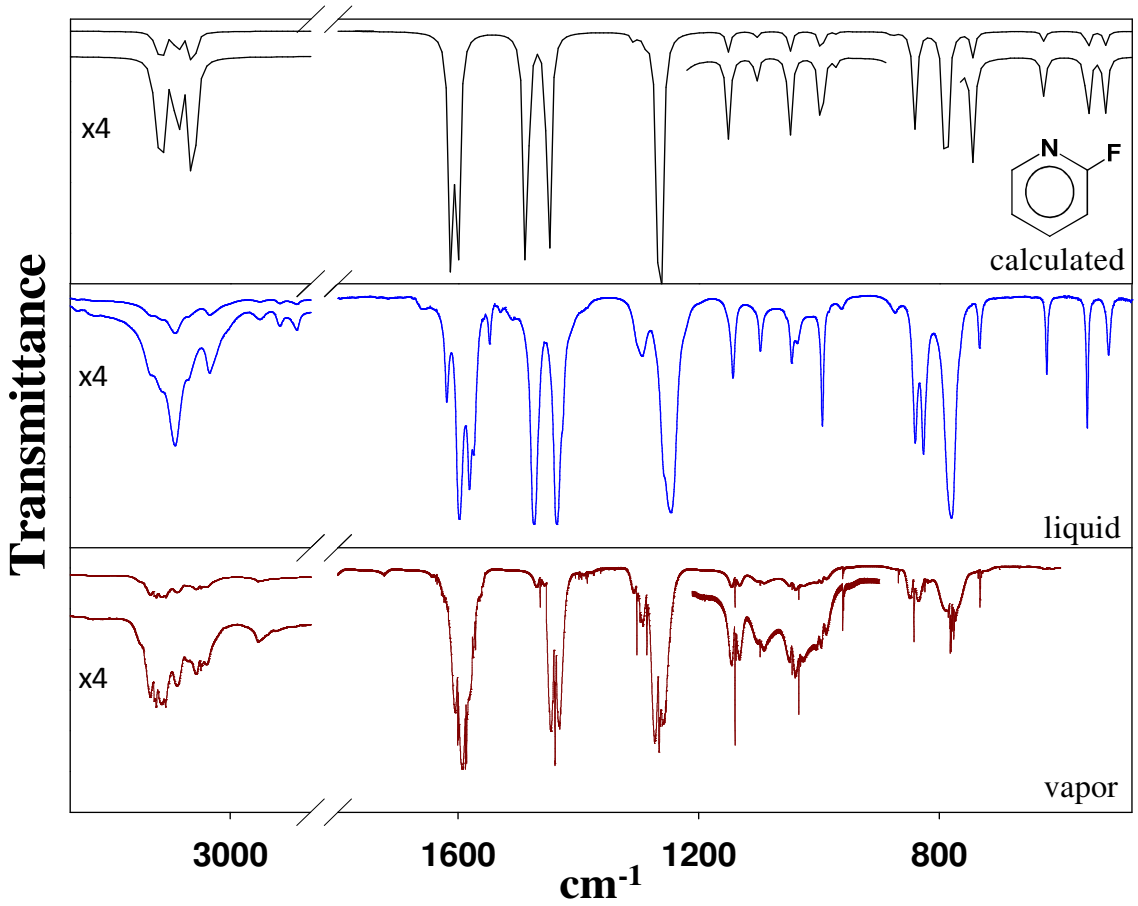

Figure 17. Liquid, vapor, and calculated IR spectra of 2-fluoropyridine.

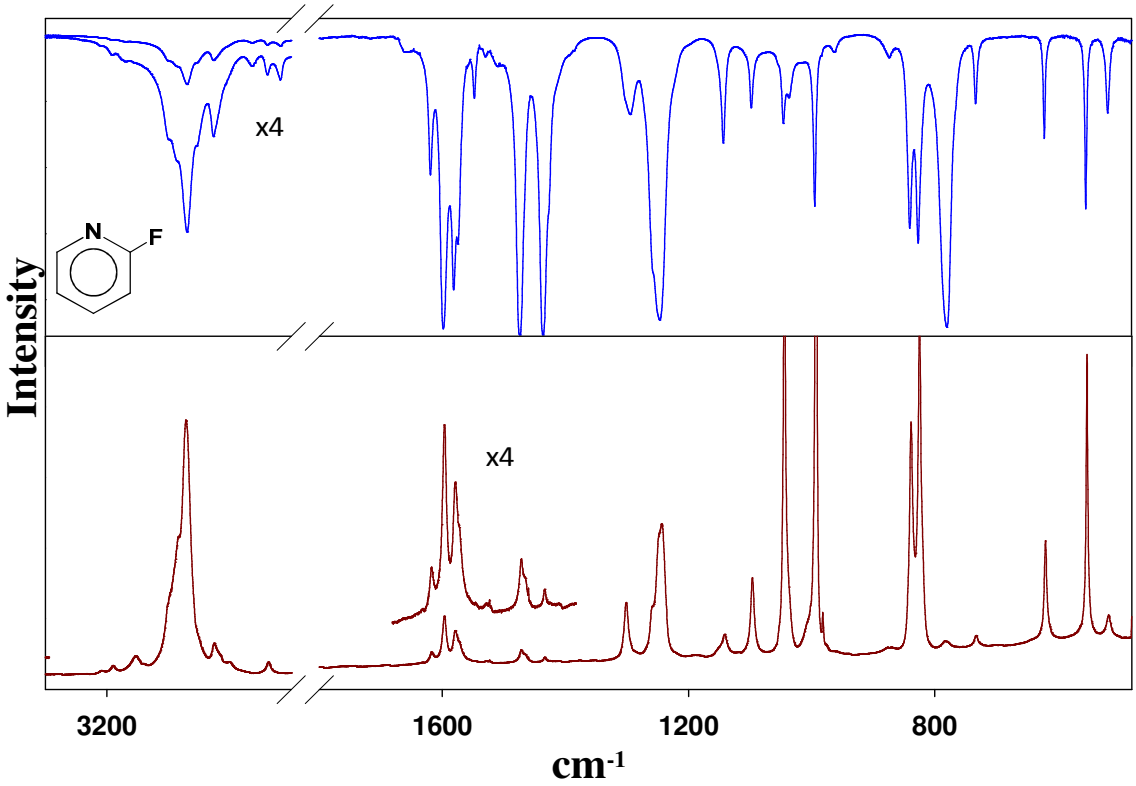

Figure 18. Comparison between IR and Raman spectra of 2-fluoropyridine.

Table 11: Observed and calculated vibrational frequencies (cm^{-1}) for 2-fluoropyridine

Cs	ν	Approximate Description	Infrared				Raman[a]				Calculated[b]		GKP[c]
			Liquid		Vapor		Liquid		Vapor		ν	Intensity	
A'	1	C-H stretch	3100 sh	w	3100.1	s	3101 br	(6)	3100 br	(9)	3096	(0.7, 100)	3097
(i.p.)	2	C-H stretch	3100 sh	w	3092.4	s	3101 br	(6)	3092	(42)	3086	(10, 70)	3094
	3	C-H stretch	3086	mw	3080.9	s	3084	(14)	3080	(56)	3066	(6, 44)	3074
	4	C-H stretch	3069	mw	-	-	3071	(26)	3077	(60)	3050	(10, 55)	3074
	5	Ring stretch	1598	vs	1604.5	s	1596	(5)	-	-	1610	(61, 43)	1598
	6	Ring stretch	1581	vs	1593.0	vs	1579	(4)	-	-	1597	(79, 43)	1580
	7	Ring stretch	1473	vs	1477.6	vvs	1471	(1)	1478	(2)	1480	(78, 5)	-
	8	Ring stretch	1436	vs	1438.7	vvs	1434	(0.5)	1439	(2)	1441	(79, 2)	-
	9	C-H wag	1301	m	1302.9	m	1301	(6)	1303	(18)	1306	(3, 19)	1303
	10	Ring stretch	1295	m	1286.3	m	-	-	1286	(7)	1289	(2, 14)	-
	11	C-F stretch	1258 br	vs	1265.9	vs	1259 br	(6)	1265	(22)	1247	(140, 62)	1249
	12	C-H wag	1143	s	1139.4	vs	1141	(2)	1139	(2)	1148	(6, 10)	1146
	13	C-H wag	1098	m	1097.9	mw	1096	(8)	1098	(7)	1100	(3, 24)	1099
	14	C-H wag	1045	m	1044 sh	m	1044	(41)	1045	(182)	1046	(7, 71)	1045
	15	Ring breathing	994	s	996.6	mw	993	(100)	999	(100)	995	(6, 100)	996
	16	Ring bend	840	vs	842.3	vs	839	(25)	842	(125)	834	(36, 62)	828
	17	Ring bend	621	ms	620.1	w	620	(11)	620	(6)	625	(2, 19)	622
	18	Ring bend	554	s	553.8	m	553	(31)	554	(40)	551	(6, 24)	556
	19	C-F wag	433	w	432.3	vw	431	(3)	433	(7)	427	(0.6, 0.1)	-
A''	20	C-H wag	983	w	-	-	982	(3)	982	(2)	979	(0.1, 0.4)	-
(o.p.)	21	C-H wag	963	w	960.5	mw	962	(0.1)	963	(1)	962	(1, 0.1)	-
	22	C-H wag	873	w	868.2	mw	870	(0.5)	869	(1)	871	(1, 0.1)	-
	23	C-H wag	780	vs	780.4	ms	783	(0.6)	-	-	781	(70, 1)	-
	24	Ring twist	733	m	732.5	m	733	(1)	-	-	732	(6, 1)	-
	25	Ring bend	519	m	517.7	m	517	(2)	-	-	517	(4, 2)	-
	26	Ring bend	417	m	413.8	mw	416	(0.6)	-	-	419	(4, 0.4)	-
	27	C-F wag	-	-	-	-	228	(29)	226	(20)	216	(0, 10)	230

Abbreviations: s, strong; m, medium; w, weak; v, very; sh, shoulder; br, broad; i.p., in-plane; o.p., out-of-plane.[a] Relative intensities in parenthesis.

[b] B3LYP/6-311++g(d,p); frequencies scaled with a scaling factor of 0.985 for frequencies less than 1800 cm^{-1} and 0.964 for frequencies greater than 1800 cm^{-1}. The calculated relative intensities are shown as (IR, Raman).

[c] Reference 33.

Table 12: Observed vibrational frequencies (cm^{-1}) and assignments for 2-fluoropyridine

Infrared		Raman		Assignment	Inferred
3100.1	s	3100 br	m	υ_1	3100
3092.4	s	3092	s	υ_2	3092
-		3089	s	-	-
3080.4	s	3080	s	υ_3	3080
-		3077	s	υ_4	3077
3066.9	s	-		$2\upsilon_{24}+\upsilon_5$	1464+1605 = 3069
3042.8	s	-		$\upsilon_5+\upsilon_8$	1605+1439 = 3044
-		3034	mw	-	-
2965.1	s	-		$2\upsilon_{21}+\upsilon_{14}$	2x961+1045 = 2967
2944.4	vvw	2945	mw	$2\upsilon_{24}+\upsilon_7$	1464+1478 = 2942
2874.5	vw	-		$2\upsilon_{22}+\upsilon_{12}$	2x868+1139 = 2875
2741.1	w	-		$\upsilon_8+\upsilon_9$	1439+1303 = 2742
2567.7	w	-		$\upsilon_9+\upsilon_{11}$ $\upsilon_5+\upsilon_{21}$	1303+1266 = 2569 1605+961 = 2566
2527.6	w	-		$2\upsilon_{11}$	2x1266 = 2532
2434.5	w	-		$\upsilon_6+\upsilon_{16}$ $2\upsilon_{26}+\upsilon_5$	1593+842 = 2435 2x414+1605 = 2433
-		2425	w	$\upsilon_{10}+\upsilon_{12}$	1286+1139 = 2425
2349.0	w	-		$\upsilon_9+\upsilon_{14}$	1303+1045 = 2348
2280.6	vw	-		$2\upsilon_{12}$ $\upsilon_8+\upsilon_{16}$	2x1139 = 2278 1439+842 = 2281
2194.9	w	-		$2\upsilon_{13}$	2x1098 = 2196
2105.6	w	-		$\upsilon_{11}+\upsilon_{16}$	1266+842 = 2108
1947.9	w	-		$\upsilon_{20}+\upsilon_{21}$?	982+961 = 1943
1936.7	w	-		$\upsilon_{13}+\upsilon_{16}$	1098+842 = 1940
-		1682	vvw	$2\upsilon_{16}$	2x842 = 1684
1604.5	s	-		υ_5	1605
1593.0	vs	-		υ_6	1593
-		1571	vvw	$\upsilon_{12}+\upsilon_{19}$	1139+433 = 1572
1504.3	m	-		$\upsilon_{20}+\upsilon_{25}$	982+518 = 1500
1477.6	vvs	1478	w	υ_7	1478
-		1464	w	$2\upsilon_{24}$ $\upsilon_{16}+\upsilon_{17}$	2x733 = 1466 842+620 = 1462
1438.7	vvs	1439	w	υ_8	1439
1302.9	m	1303	m	υ_9	1303
1292.9	ms	-		$2\upsilon_{27}+\upsilon_{16}$	2x226+842 = 1294
1286.3	m	1286	m	υ_{10}	1286
1265.9	vs	1265	ms	υ_{11}	1266
-		1259	s	-	

Table 12: (Continued)

Infrared		Raman		Assignment	Inferred
-		1254	s	$\upsilon_{16}+\upsilon_{26}$ $\upsilon_{24}+\upsilon_{25}$	842+414 = 1256 733+518 = 1251
1189.0	w	-		$\upsilon_{21}+\upsilon_{27}$	961+226 = 1187
1139.4	vs	1139	vw	υ_{12}	1139
1097.9	mw	1098	m	υ_{13}	1098
1091.5	s	-		$\upsilon_{22}+\upsilon_{27}$	868+226 = 1094
1049.2	ms	-		$\upsilon_{17}+\upsilon_{19}$	620+433 = 1053
-		1045	vvs	υ_{14}	1045
1038.9	s	-		$2\upsilon_{25}$	2x518 = 1036
1033.6	m	1034	m	$\upsilon_{17}+\upsilon_{26}$	620+414 = 1034
996.6	mw	999	vs	υ_{15}	997
992	mw	992	s	$\upsilon_{18}+\upsilon_{19}$?	554+433 = 987
-		982	mw	υ_{20}	982
960.5	m	-		υ_{21}	961
868.2	m	869	w	υ_{22}	868
842.3	vs	842	vvs	υ_{16}	842
827.5	m	828	s	$2\upsilon_{26}$	2x414 = 828
824.1	mw	824	s	hot band	824
780.4	ms	-		υ_{23}	780
732.5	m	-		υ_{24}	733
620.1	w	620	mw	υ_{17}	620
553.8	m	554	s	υ_{18}	554
517.7	m	-		υ_{25}	518
432.3	vw	433	m	υ_{19}	433
413.8	mw	-		υ_{26}	414
-		226	m	υ_{27}	226
		210	m	hot band	210

Infrared and Raman Spectra

Figures 16 and 17 show the liquid-phase, vapor-phase, and calculated Raman and infrared spectra of 2FPy, and Figure 18 shows the comparison between infrared and Raman spectrum. Figures 19, 20 and 21 show the spectra for 3FPy. Table 11 summarizes the vibrational data for 2FPy and Table 12 presents a tabulation of all the spectral bands including the sum and combination bands. Table 13 summarizes the data for 3FPy and Table 14 tabulates all of the observed spectral bands for this molecule. Table 15 compares the vibrational frequencies for the ring modes of 2FPy, 3FPy, and the unsubstituted pyridine. Green and coworkers[33] previously made partial assignments for the fluoropyridines and these are also shown in Tables 11 and 13. As expected[66-70] the cc-PVTZ calculation did a remarkably good job of predicting the frequencies. The average difference between experimental and calculated wavenumbers was less than 7 cm^{-1}. From Table 15 it was also clear that most of the pyridine ring vibrational frequencies were not changed much in 2FPy and 3FPy and the highest four ring stretching modes shifted by less than 15 cm^{-1}. The B_2 1227 cm^{-1} band of pyridine shifted to 1286 cm^{-1} in 2FPy and to 1249 cm^{-1} in 3FPy. The two A_1 stretching modes of pyridine at 1031 and 991 cm^{-1} shifted to 994 and 842 cm^{-1} in 2FPy and to 1022 and 816 cm^{-1} in 3FPy. These vibrational shifts for the fluoropyridines reflected interactions with the C-F stretching which occurred at 1266 cm^{-1} for 2FPy and 1228 cm^{-1} for 3FPy. The C-F stretching frequencies were comparable to values of 1238 cm^{-1} for fluorobenzene and 1049 cm^{-1} for methylfluoride.[76-78]

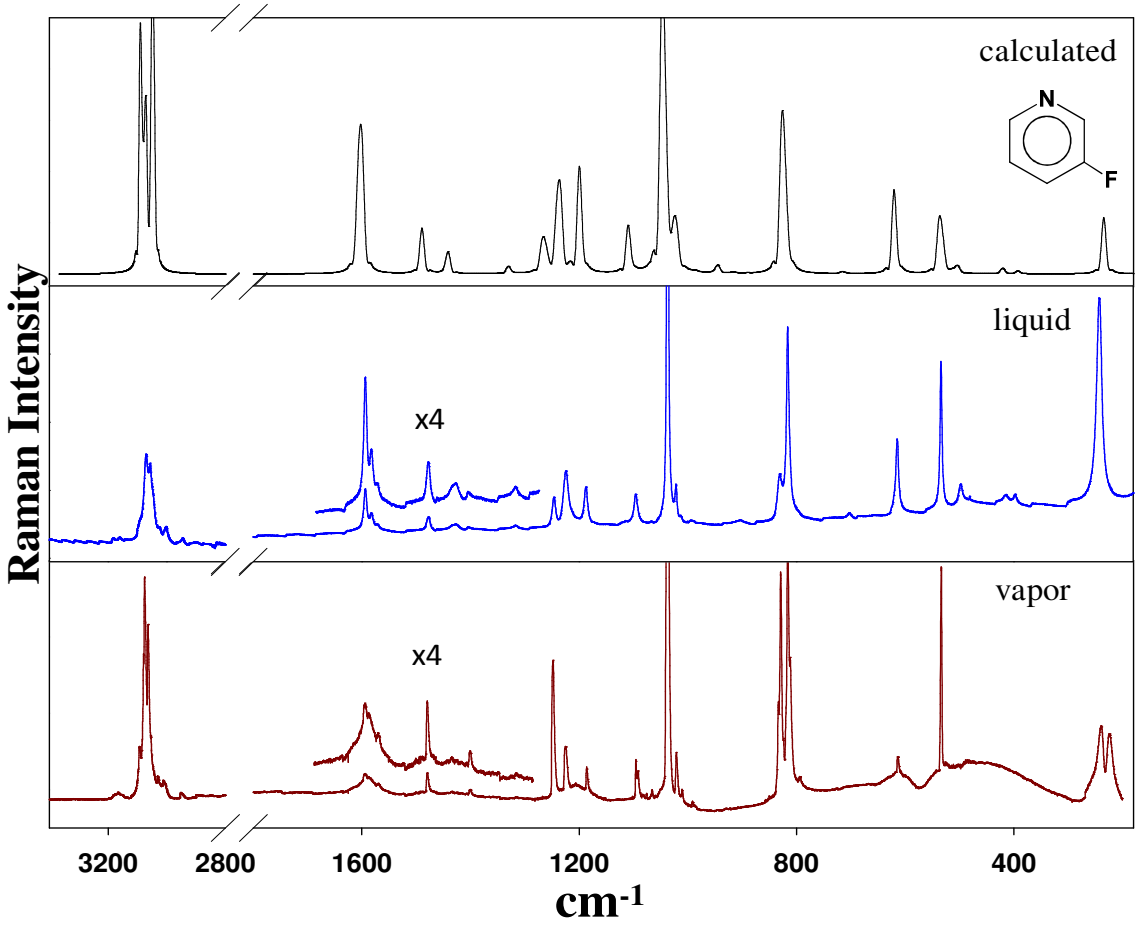

Figure 19. Liquid, vapor, and calculated Raman spectra of 3-fluoropyridine.

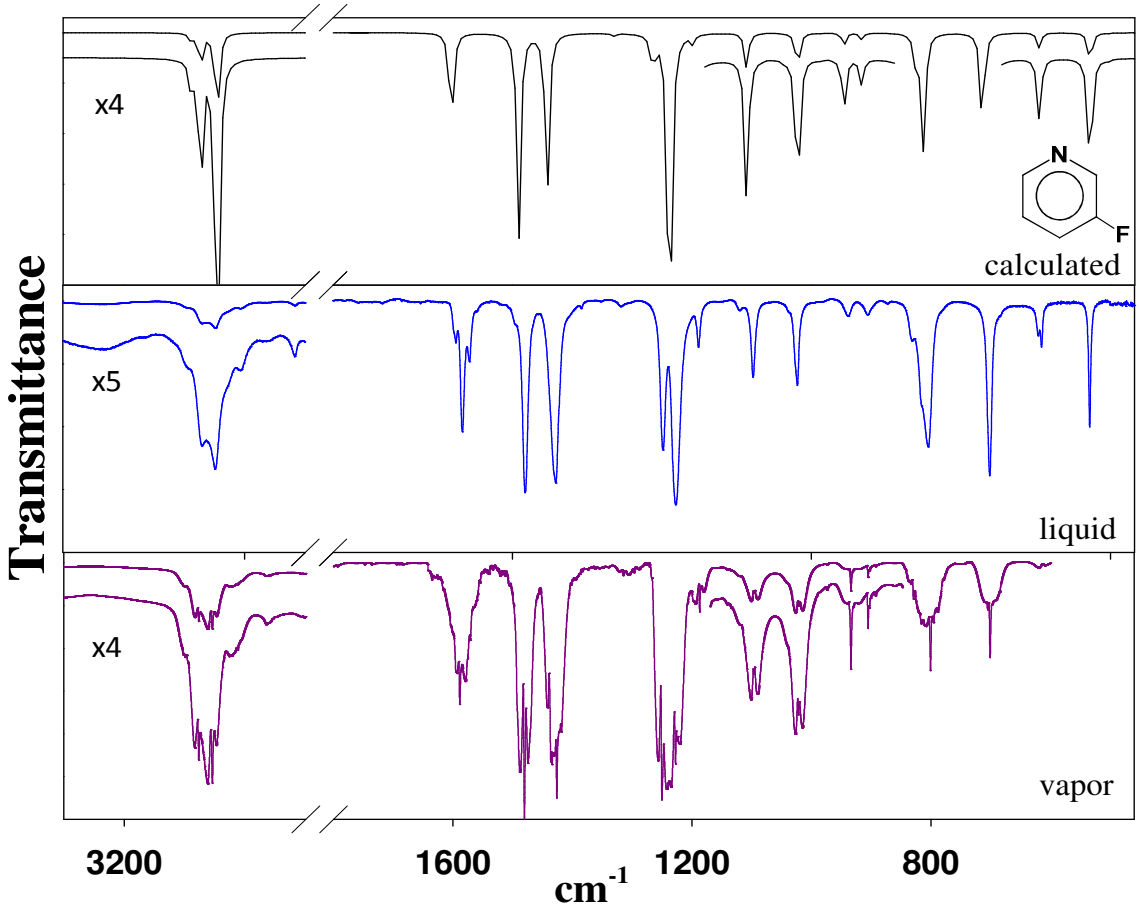

Figure 20. Liquid, vapor, and calculated IR spectra of 3-fluoropyridine.

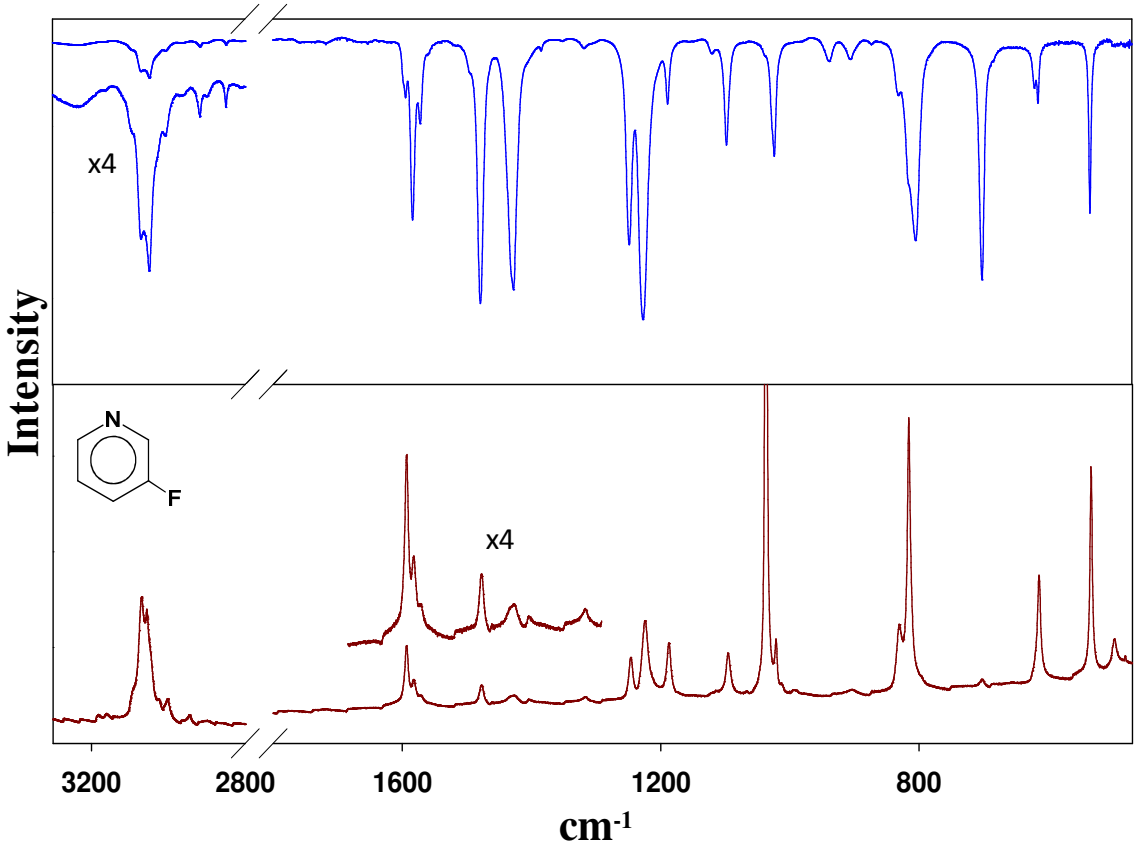

Figure 21. Comparison between IR and Raman spectra of 3-fluoropyridine.

Table 13: Observed and calculated vibrational frequencies (cm^{-1}) for 3-fluoropyridine

Cs	ν	Approximate Description	Infrared				Raman[a]				Calculated[b]		GKP[c]
			Liquid		Vapor		Liquid		Vapor		ν	Intensity	
A'	1	C-H stretch	-	-	-	-	3069	(14)	3079	(10)	3088	(2, 100)	3069
(i.p.)	2	C-H stretch	3070	m	3076.5	m	3069	(14)	3075	(16)	3073	(9, 70)	3058
	3	C-H stretch	-	-	-	-	3056	(12)	3063	(12)	3054	(7, 65)	3069
	4	C-H stretch	3049	m	3054.1	ms	3047 sh	(8)	3054	(5)	3047	(14, 54)	3058
	5	Ring stretch	1594	m	-	-	1593	(7)	1594	(2)	1602	(8, 31)	1594
	6	Ring stretch	1583	s	1588.4	s	1583	(3)	1587 sh	(1)	1596	(20, 28)	1584
	7	Ring stretch	1478	vs	1480.1	vs	1477	(2)	1480	(1)	1482	(60, 10)	1480
	8	Ring stretch	1427	vs	1425.8	vs	1427	(1)	1426	(1)	1438	(52, 7)	1425
	9	C-H wag	1319	w	1315.6	w	1317	(1)	1316	(1)	1323	(1, 2)	1308
	10	Ring stretch	1248	vs	1249.4	vs	1246	(5)	1249	(10)	1265	(3, 10)	1247
	11	C-F stretch	1227	vs	1227.4	vs	1224	(9)	1226	(4)	1223	(131, 41)	-
	12	C-H wag	1189	m	1187.1	m	1187	(6)	1187	(2)	1197	(3, 21)	1187
	13	C-H wag	1098	ms	1096.0	m	1096	(5)	1096	(3)	1107	(12, 10)	1095
	14	C-H wag	1038 sh	w	-	-	1037	(100)	1038	(100)	1041	(0.5, 100)	1038
	15	Ring breathing	1024	ms	1021.8	m	1022	(5)	1022	(4)	1020	(11, 28)	1023
	16	Ring bend	816 sh	ms	816.4	ms	816	(31)	816	(20)	819	(16, 45)	818
	17	Ring bend	615	mw	-	-	614	(12)	613	(2)	619	(4, 17)	616
	18	Ring bend	535	s	533.3	ms	534	(24)	533	(15)	533	(11, 17)	535
	19	C-F wag	-	-	-	-	398	(2)	398	(1)	390	(5, 1)	-
A''	20	C-H wag	981	vw	974.1	vw	-	-	-	-	966	(0.1, 0)	982
(o.p.)	21	C-H wag	938	w	934.0	w	932	(1)	-	-	932	(3, 1)	-
	22	C-H wag	905	w	905.1	w	904	(1)	-	-	905	(2, 1)	-
	23	C-H wag	804	vs	800.7	vs	-	-	-	-	803	(41, 2)	-
	24	Ring twist	702	s	701.0	ms	703	(1)	-	-	702	(29, 1)	702
	25	Ring bend	497	w	506.8	mw	498	(4)	-	-	501	(0.2, 1)	-
	26	Ring bend	415	mw	411.7	m	414	(2)	-	-	414	(3, 1)	410
	27	C-F wag	-	-	-	-	242	(33)	239	(6)	231	(0.6, 7)	244

Abbreviations: s, strong; m, medium; w, weak; v, very; sh, shoulder; br, broad; i.p., in-plane; o.p., out-of-plane.

[a] Relative intensities in parenthesis.

[b] B3LYP/6-311++g(d,p); Frequencies scaled with a scaling factor of 0.985 for frequencies less than 1800 cm^{-1} and 0.964 for frequencies greater than 1800 cm^{-1}. The calculated relative intensities are shown as (IR, Raman).

[c] Reference 33.

Table 14: Observed vibrational frequencies (cm^{-1}) and assignments for 3-fluoropyridine

Infrared		Raman		Assignment	Inferred
-		3079	s	υ_1	3079
3076.5	m	3075	s	υ_2	3075
-		3063	s	υ_3	3063
3054.1	ms	3054	mw	υ_4	3054
-		3031	m	-	-
3012.9	w	3012	m	$\upsilon_6+\upsilon_8$	1588+1426 = 3014
2965.4	vw	-		$2\upsilon_{21}+\upsilon_{13}$	1869+1096 = 2965
-		2953	mw	-	-
2902.3	vw	-		$\upsilon_6+\upsilon_9$	1588+1316 = 2904
2839.6	vw	-		$\upsilon_6+\upsilon_{10}$	1588+1249 = 2837
2819.9	w	-		$\upsilon_5+\upsilon_{11}$	1594+1227 = 2821
2726.9	w	-		$\upsilon_7+\upsilon_{10}$	1480+1249 = 2729
2674.1	w	-		$\upsilon_8+\upsilon_{10}$	1426+1249 = 2675
2573.8	w	-		$\upsilon_7+\upsilon_{13}$	1480+1096 = 2576
2516.4	w	-		$\upsilon_7+\upsilon_{14}$	1480+1038 = 2518
2496.0	vw	-		$2\upsilon_{10}$	2x1249 = 2498
2476.2	m	-		$\upsilon_{10}+\upsilon_{11}$	1249+1227 = 2476
-		2445	w	$\upsilon_8+\upsilon_{15}$	1426+1022 = 2448
-		2435	w	$\upsilon_{10}+\upsilon_{12}$	1249+1187 = 2436
2415.3	w	-		$\upsilon_{11}+\upsilon_{12}$ $\upsilon_7+\upsilon_{21}$	1227+1187 = 2414 1480+934 = 2414
-		2410	w	$\upsilon_5+\upsilon_{16}$ $\upsilon_9+\upsilon_{13}$	1594+816 = 2410 1316+1096 = 2412
2348.1	w	-		$\upsilon_{10}+\upsilon_{13}$	1249+1096 = 2345
2295.9	w	-		$\upsilon_7+\upsilon_{16}$ $\upsilon_5+\upsilon_{24}$	1480+816 = 2296 1594+701 = 2295
2243.8	w	-		$\upsilon_8+\upsilon_{16}$	1426+816 = 2242
2223.8	w	-		$\upsilon_{12}+\upsilon_{14}$ $\upsilon_{10}+\upsilon_{20}$	1187+1038 = 2225 1249+974 = 2223
2078.9	w	-		$2\upsilon_{14}$	2x1038 = 2076
2065.2	mw	-		$\upsilon_{10}+\upsilon_{16}$	1249+816 = 2065
2043.0	w	-		$2\upsilon_{15}$ $\upsilon_{11}+\upsilon_{16}$	2x1022 = 2044 1227+816 = 2043
1877.7	mw	-		$\upsilon_{20}+\upsilon_{22}$	974+905 = 1879
1869.3	mw	1869	vw	$2\upsilon_{21}$	2x934 = 1868
1844.1	m	-		$\upsilon_9+\upsilon_{18}$?	1316+533 = 1849
1829.5	mw	-		$2\upsilon_{25}+\upsilon_{16}$	2x507+816 = 1830
-		1594	m	υ_5	1594
1588.4	s	1587 sh	m	υ_6	1588
1570.6	m	1570	w	$\upsilon_{14}+\upsilon_{18}$	1038+533 = 1571

Table 14: (Continued)

Infrared		Raman		Assignment	Inferred
1480.1	vs	1480	mw	υ_7	1480
1436.4	mw	1436	vw	$\upsilon_{14}+\upsilon_{19}$	1038+398 = 1436
1434.1	m	1435	w	$\upsilon_{15}+\upsilon_{26}$ $2\upsilon_{26}+\upsilon_{17}$	1022+412 = 1434 2x412+613 = 1437
1425.8	vs	1426	w	υ_8	1426
-		1401	mw	$2\upsilon_{24}$	2x701 = 1402
1387.7	w	-		$\upsilon_{20}+\upsilon_{26}$	974+412 = 1386
1349.3	w	-		$\upsilon_{16}+\upsilon_{18}$	816+533 = 1349
1315.6	w	1316	w	υ_9	1316
1249.0	vs	1249	s	υ_{10}	1249
1227.4	vs	1226	m	υ_{11}	1227
1187.1	m	1187	m	υ_{12}	1187
1096.0	m	1096	ms	υ_{13}	1096
-		1091	m	hot band	1091
-		1066	m	$2\upsilon_{18}$	2x533 = 1066
-		1038	vvs	υ_{14}	1038
1021.8	m	1022	m	υ_{15}	1022
-		1011	w	$\upsilon_{17}+\upsilon_{19}$	613+398 = 1011
974.1	vw	-		υ_{20}	974
934.0	m	-		υ_{21}	934
905.1	w	-		υ_{22}	905
829.2	mw	829	s	$2\upsilon_{26}$?	2x412 = 824
816.4	ms	816	s	υ_{16}	816
800.7	vs	-		υ_{23}	801
-		794	mw	-	-
701.0	ms	-		υ_{24}	701
-		613	m	υ_{17}	613
533.3	ms	533	ms	υ_{18}	533
506.8	mw	-		υ_{25}	507
411.7	m	-		υ_{26}	412
-		398	vw	υ_{19}	398
-		239	m	υ_{27}	239
-		224	m	hot band	234

Table 15: Vibrational frequencies (cm^{-1}) of the ring modes of the fluoropyridines compared to pyridine

ν[a]	Approximate Description	2FPy	3FPy	Pyridine
5	Ring stretch	1605	1594	1584
6	Ring stretch	1593	1588	1576
7	Ring stretch	1478	1480	1483
8	Ring stretch	1439	1426	1443
10	Ring stretch	1286	1249	1227
15	Ring breathing	997	1022	1031
16	Ring bend (i.p.)	842	816	991
17	Ring bend (i.p.)	620	613	654
18	Ring bend (i.p.)	554	533	601
24	Ring bend (o.p.)	733	701	700
25	Ring bend (o.p.)	518	507	403
26	Ring bend (o.p.)	414	412	375

Abbreviations: i.p., in-plane; o.p., out-of-plane.
[a] Mode number for 2FPy and 3FPy.

Clearly, in fluorobenzene and the fluoropyridines the higher C-F stretching frequencies reflected interactions with the π bonding within the rings. It was also noteworthy that the two lowest out-of-plane ring vibrations for 2FPy (at 518 and 414 cm^{-1}) were somewhat higher than those for pyridine (403 and 375 cm^{-1}). This indicated that the fluoropyridines were also rigid in their electronic ground state and somewhat more than pyridine itself. As reported in Chapter V, in its $S_1(n,\pi^*)$ excited state pyridine became very floppy.

There was also little difference between the pyridine and fluoropyridine vibrational frequencies for the C-H stretches (3030-3095 cm^{-1}), the in-plane C-H wags (1070-1365 cm^{-1}), and the out-of-plane C-H wags (730-1000 cm^{-1}).

CONCLUSIONS

The structures of 2FPy and 3FPy were calculated and the ring bond distances differed little from those of pyridine. The notable exception was that the N-C(F) bond distance was shortened in 2FPy due to π interactions. The frequencies of the ring modes of the fluoropyridines were also similar to those of pyridine itself. The C-F stretching frequencies at 1266 cm^{-1} for 2FPy and 1228 cm^{-1} for 3FPy reflected bond strengths similar to that in fluorobenzene where ν(C-F) was 1238 cm^{-1}.[76,77]

CHAPTER VII

ULTAVIOLET ABSORPTION SPECTRA AND STRUCTURE, VIBRATIONS, AND THEORETICL CALCULATIONS OF 2-FLUORO- AND 3-FLUOROPYRIDINE IN THEIR ELECTRONIC EXCITED STATES

INTRODUCTION

This work is the continued investigation of the structure and vibrations of pyridine and substituted pyridines in their ground and excited states. In Chapter V, the ultraviolet absorption spectra of the ring-bending vibration of pyridine and its d_5 isotopomer were reported and the potential energy function for this motion was determined. This showed the molecule to be quasi-planar and very floppy with a barrier to planarity of only 3 cm^{-1}. In the ground state, this vibration was rigid and nearly harmonic with a relatively high frequency of 403 cm^{-1}. Recently, the infrared and Raman investigation of the vibrations of 2-fluoropyridine (2FPy) and 3-fluoropyridine (3FPy) in their electronic ground states was successfully completed as reported in Chapter VI. In this study, the ultraviolet absorption spectra of these molecules were reported and the vibronic levels in their electronic excited states were assigned. The experimental work was complemented by theoretical computations which were used to calculate molecular structures and vibrational levels in the excited states.

In 1990 Medhi and Medhi[34,35] reported the electronic absorption spectra of 2FPy and 3FPy under low resolution. They also reported their wavelength accuracy ranged from ±0.5 to ±3 nm (70 to 400 cm^{-1} !) although their data did not seem to be quite as bad as that. For 2FPy they reported a $\pi \rightarrow \pi^*$ transition at 38,047 cm^{-1} and a second one at 49,558 cm^{-1}. For 3FPy they observed an $n \rightarrow \pi^*$ transition at 35,066 cm^{-1}, a $\pi \rightarrow \pi^*$ at 37,355 cm^{-1}, and another $\pi \rightarrow \pi^*$ at 49,674 cm^{-1}. The assignments to $n \rightarrow \pi^*$ or $\pi \rightarrow \pi^*$ were supported by ultraviolet spectra of samples in solution. In 2010 Itoh[36] reported the emission and excitation spectra of both 2FPy and 3FPy vapors. His data was also of low-resolution and provided limited information on the vibronic energy levels since the focus of the work was primarily on fluorescence yields.

EXPERIMENTAL

2FPy and 3FPy (99% purity) were purchased from Aldrich and purified by trap to trap distillation. The ultraviolet absorption spectra of the samples in a 23.5 cm glass cell with quartz windows were recorded at ambient temperature on a Bomem DA8.02 fourier transform spectrometer. Typically 3000 scans at a resolution of 0.25 cm^{-1} were averaged. The data were collected six times for each molecule utilizing different vapor pressures of the samples. The vapor pressures of the samples at room temperature were about 9 Torr for 2FPy and 15 Torr for 3FPy.

COMPUTATIONS

The structures and vibrational frequencies of pyridine, 2FPy and 3FPy for the electronic ground state were calculated using the Gaussian 03 program package.[65] *Ab initio* second order Moller-Plesset (MP2) level of theory with the cc-pVTZ basis set was used to find the optimized geometry. The DFT-B3LYP level of theory with the 6-311++G(d,p) basis set was used to calculate the vibrational frequencies. Based on previous work[66-70], a scaling factor of 0.964 was used for the C-H stretching vibrational frequencies and a factor of 0.985 for the lower frequencies.

In addition, in collaboration with Sunghwan Kim, the geometries of the three molecules in the S_0, S(n,π*) and S(π,π*) states were also optimized at the CASSCF/6-311++G(d,p) level, using an active space consisting of 8 electrons (2 lone-pair electrons and 6 π electrons) distributed in 7 orbitals (one lone-pair orbital and six π orbitals). The optimized geometries were confirmed to be minima by harmonic vibrational frequency analyses. Based on previous work, a scaling factor of 0.905 was used for all of the vibrational frequencies in the electronic excited states.[71] All CASSCF computations were performed using the GAMESS package.[72]

RESULTS AND DISCUSSION

Excited State Structure

Figure 22 shows the ground (S_0) and excited state structures calculated for the S(n,π*) and S(π,π*) states of the two fluoropyridines. The S_0, S_1(n,π*) and S_2(π,π*) structures for pyridine were shown for comparison.

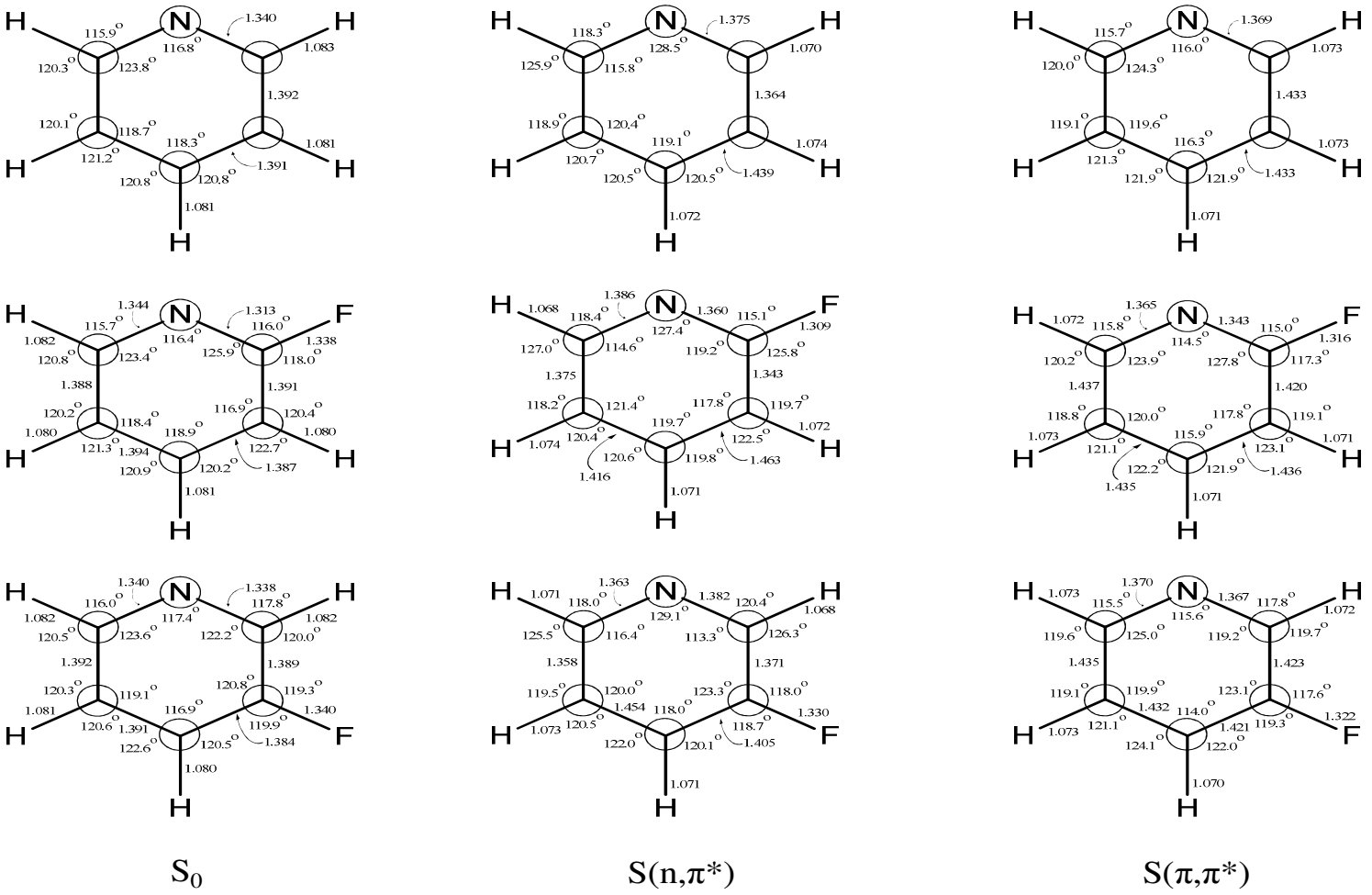

Figure 22. Calculated structures of pyridine, 2FPy, and 3FPy in their S_0, S(n,π*), and S(π,π*) states at the CASSCF/6-311++G(d,p) level of theory for the excited states. Ground state structures are from the MP2/cc-pVTZ computation.

All three molecules were predicted to be planar in both the ground states and excited states with no imaginary frequencies. As expected, in the S(n,π*) states most of the bond distances in the rings were increased due to the increased antibonding character, resulting in a π bonding order of 2.5 versus 3 in the S_0 state. They were further increased in the S(π,π*) states where the π bond order drops to 2. One exception was the C(F)-C bond distance in the S(n,π*) state of 2FPy where this decreased to 1.343 from 1.391 Å. The bond across the ring also slightly decreased to 1.375 from 1.388 Å. At the same time, the C-F bond dropped from 1.338 to 1.309 Å reflecting the redistribution of the π bonding character.

For 3FPy the three similar bonds also decreased in bond length, but not nearly so much. Notably the analogous C-C bonds in pyridine decreased somewhat in the S_1(n,π*) state. The fact that the C-F bond participated in the π bonding system was also evident in the ground state structure of 2FPy where the N-C(F) bond length of 1.313 Å was considerably shorter than the other N-C bond of 1.344 Å. Unlike the S(n,π*) state, the S(π,π*) state did not show these unusual decreases in bond distance. All of the bond distances in the rings increased for both of the fluoropyridines. For 2FPy the average C-C bond distance increased from 1.390 Å in the ground state to 1.432 Å in the S(π,π*) state. 3FPy increased in average value from 1.389 to 1.428 Å. The C-N bond distance for the two molecules each increased by about 0.03 Å.

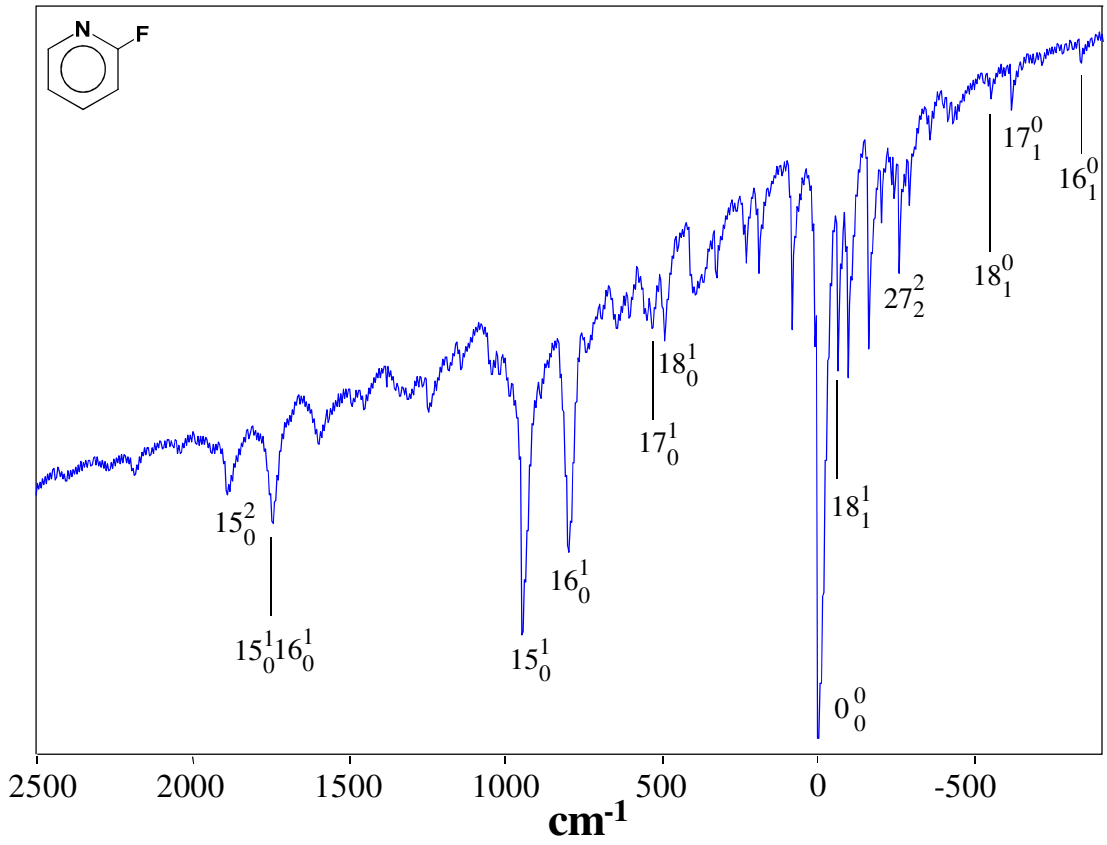

Figure 23. Ultraviolet absorption spectra of 2FPy vapors. Wavenumbers are relative to the π→π* band origin at 38,030.4 cm^{-1}.

Table 16: Observed and calculated electronic transition energies (cm^{-1})

Transition	2FPy		3FPy		Py	
	OBS	CALC[a]	OBS	CALC[a]	OBS	CALC[a]
n→π*	-	39199	35051.7	36617	34767.0	36296
π→π*	38030.4	38796	37339	38311	38350[b]	38312

[a] CASSCF/6-311++G(d,p) level of theory.
[b] Reference 79.

Table 17: Observed and calculated vibrational frequencies (cm^{-1}) for 2-fluoropyridine in its ground and excited states

Sym C_s	ν	Approximate Description	S_0			S (π,π^*)			S (n,π^*)
			OBS	CALC[a]	CALC[b]	OBS	CALC[b]	Lit[c]	CALC[b]
A'	1	C-H stretch	3100	3096	3246		3066		3089
(i.p.)	2	C-H stretch	3092	3086	3235		3053		3055
	3	C-H stretch	3080	3066	3220		3046		3042
	4	C-H stretch	3077	3050	3211		3032		3021
	5	Ring stretch	1605	1610	1709	1690?	1716		1586
	6	Ring stretch	1593	1597	1690	1489	1507		1438
	7	Ring stretch	1478	1480	1595	1453	1475	1454	1381
	8	Ring stretch	1439	1441	1539	1353	1387		1327
	9	C-H wag	1303	1306	1382	1336	1346		1269
	10	Ring stretch	1286	1289	1362	1220	1214		1168
	11	C-F stretch	1266	1247	1263	1243	1236		1210
	12	C-H wag	1139	1148	1161	1045	1106	1045*	1023
	13	C-H wag	1098	1100	1124	934	920	944*	925
	14	C-H wag	1045	1046	1094	887	880	-	879
	15	Ring breathing	997	995	1050	946	960	-	932
	16	Ring bend	842	834	881	797	765	800	789
	17	Ring bend	620	625	659	532	537	526	554
	18	Ring bend	554	551	586	493	492	487	494
	19	C-F wag	433	427	455	396	399	392	380
A''	20	C-H wag	982	979	997	654[d]	661		822
(o.p.)	21	C-H wag	961	962	973	591[d]	585		692
	22	C-H wag	868	871	880	572[d]	555		495
	23	C-H wag	780	781	788	-	457		471
	24	Ring twist	733	732	739	432[d]	404		455
	25	Ring bend	518	517	537	322[d]	338		380
	26	Ring bend	414	419	438	163[d]	235		240
	27	C-F wag	226	216	241	96[d]	167		40

Abbreviations: i.p., in-plane; o.p., out-of-plane.

[a] B3LYP/6-311++g(d,p) level of theory; frequencies scaled with a scaling factor of 0.985 for frequencies less than 1800 cm^{-1} and 0.964 for frequencies greater than 1800 cm^{-1}.

[b] CASSCF/6-311++G(d,p) level of theory; ground state frequencies are scaled with a scaling factor of 0.985 for frequencies less than 1800 cm^{-1} and 0.964 for frequencies greater than 1800 cm^{-1}. Excited state frequencies are scaled with a scaling factor of 0.905.

[c] Reference 34. * Bands have been reassigned.

[d] Values given are one half of the observed double quantum jump transition frequencies.

Ultraviolet Absorption Spectra

Figure 23 shows the ultraviolet absorption spectrum for 2FPy with the wavenumber scale labeled relative to the 0_0^0 band origin for the $\pi \rightarrow \pi^*$ transition at 38,030.4 cm^{-1}. Medhi and Medhi[34] reported this at 38,047 cm^{-1} but also recognized that their wavelength accuracy was poor. Itoh[36] did not report an accurate value. Table 16 shows the calculated value for this transition was in quite good agreement at 38,796 cm^{-1}. The calculated value for the $n \rightarrow \pi^*$ transition was 39,199 cm^{-1}, so it was difficult to know whether the $S(\pi,\pi^*)$ or $S(n,\pi^*)$ was lower in energy. Identification of the observed transitions as $\pi \rightarrow \pi^*$ was confirmed by the reported spectra in solution.[34] Selected absorption bands in Figure 23 were labeled with their assignments, and Table 17 summarizes the assignment of the fundamental vibrational frequencies in the $S(\pi,\pi^*)$ state. The table compares these assignments to the calculated values and to those in the electronic ground state. The calculated values from the B3LYP computation were expected to be more reliable, but the CASSCF values were also shown for comparison. The comparison between observed and calculated values was quite good considering the fact that excited state calculations were less reliable than those for the ground state. Table 17 lists the previously reported values, but several of these were reassigned. In addition, the unconventional vibrational numbering previously used was corrected. In the previous work,[34] the authors only assigned bands to the in-plane A' vibronic levels. However, the double quantum jumps of out-of-plane A" vibrations were expected and most were assigned.

Table 18: Ultraviolet absorption spectra for the π→π* transition of 2FPy

Frequency (cm^{-1})			Assignment	Inferred
OBS[a]		Lit[b]		
-1686	vvw		16_2^0	2x-841 = -1682
-1622	vvw		-	
-1462	vvw		24_2^0	2x-733 = -1466
-1303	vw		9_1^0	-1303
-1265	w		11_1^0	-1266
-1259	vw		-	
-1207	vvw		-	
-1173	vvw		-	
-1139	vw		12_1^0	-1139
-1107	w		18_2^0	2x-553 = -1106
-1087	vw		$10_1^0 27_0^2$?	-1286+191 = -1095
-1053 sh	vw		$17_1^0 19_1^0$	-620-433 = -1053
-1045	mw	-1048	14_1^0	-1045
-1036	vvw		25_2^0	2x-518 = -1036
-1005	mw		-	
-1000	mw	-1002	15_1^0	-997
-992	mw		-	
-984	vvw		-	
-977	vvw		-	
-958	vvw		-	
-938	vw		$11_1^0 26_0^2$	-1266+325 = -941
-910	w	-914	$13_1^0 27_0^2$	-1098+191 = -907
-906	w		27_4^0	4x-226 = -904
-879	vw		$19_1^0 26_1^0 27_1^2$	-433-414-35 = -882
-862 sh	vw		19_2^0	2x-433 = -866
-850 sh	w		$14_1^0 27_0^2$	-1045+191 = -854
-840.9	m	-845	16_1^0	-842
-833	w		26_2^0?	2x-414 = -828
-821	w		$20_1^0 26_0^1$	-982+163 = -819
-812.9	w	-816	$23_1^0 27_1^2$	-780-226+191 = -815
-781	w	-779	$18_2^0 26_0^2$	-(2x554)+325 = -783

Table 18: (Continued)

Frequency (cm^{-1})			Assignment	Inferred
OBS[a]		Lit[b]		
-776	vvw		$13_1^0 26_0^2$	-1098+325 = -773
-770	vvw		$22_1^0 26_0^2 27_1^0$ $24_1^0 27_1^2$	-868+325-226 = -769 -733-35 = -768
-756	w	-752	-	
-725 sh	w		$17_1^0 19_1^0 26_0^2$	-620-433+325 = -728
-715	vw	-715	$14_1^0 26_0^2$	-1045+325 = -720
-698	vvw		$19_0^1 22_1^0 27_1^0$	396-868-226 = -698
-691	vvw	-683	$19_1^0 27_2^2$	-433-259 = -692
-682	vvw		$23_1^0 26_0^2 27_1^0$ $23_1^0 27_0^1$	-780+325-226 = -681 -780+96 = -684
-674	vvw		-	
-649	vvw		$16_1^0 27_0^2$ $15_1^0 26_0^2$	-842+191 = -651 -977+325 = -652
-629 sh	w		$24_1^0 26_0^2 27_1^0$	-733+325-226 = -634
-620	m	-622	17_1^0	-620
-611	vvw		$19_0^1 23_1^0 27_1^0$	396-780-226 = -610
-597	vvw		$15_1^0 19_0^1$ $18_0^1 22_1^0 27_1^0$	-997+396 = -601 493-868-226 = -601
-592	vvw	-594	$18_1^0 19_1^1$	-554+396-433 = -591
-553	mw	-549	18_1^0	-554
-547	vvw		$22_1^0 25_0^1$	-868+322 = -546
-534	vw	-531	$19_0^1 25_1^0 26_1^0$	396-518-414 = -536
-526	vvw		$21_1^0 24_0^1$	-961+432 = -529
-523	vvw		27_4^4	(4x-226)+(2x191) = -522
-509	vvw		$19_0^1 27_4^0$	396-(4x226) = -508
-500	vvw		26_2^2	325-(2x414) = -503
-484	vvw		$18_0^2 24_2^0$	(2x493)-(2x733) = -480
-467	vvw		19_2^1 $18_0^1 24_1^0 27_1^0$	396-(2x433) = -470 493-733-226 = -466
-453 sh	vvw		$13_1^0 25_0^2$ $23_1^0 25_0^1$	-1098+2x322 = -454 -780+322 = -458
-442	w		$18_0^1 25_1^0 26_1^0$	493-518-414 = -439

Table 18: (Continued)

Frequency (cm^{-1})			Assignment	Inferred
OBS[a]		Lit[b]		
-434	w	-432	19_1^0	-433
-431	w		$19_0^1 26_2^0$	396-2x414 = -432
-415.2	w	-412	$18_0^1 27_4^0$ $25_1^0 26_0^2 27_1^0$	493-(4x226) = -411 -518+325-226 = -419
-401.1	w		$14_1^0 25_0^2$	-1045+644 = -401
-388	vvw		$16_0^1 21_1^0 27_1^0$	797-961-226 = -390
-374 sh	vvw		$17_0^1 27_4^0$	532-(4x226) = -372
-358.1	mw	-359	$18_1^0 27_0^2$	-554+191 = -363
-349	vw		$19_0^1 25_1^0 27_1^0$ $15_1^0 25_0^2$	396-518-226 = -348 -997+644 = -353
-345	vvw		$23_1^0 24_0^1$	-780+432 = -348
-309 br	w		$16_0^1 18_2^0$	797-(2x554) = -311
-290.8	m	-288	$17_1^0 26_0^2$ 22_1^1	-620+325 = -295 -868+572 = -296
-287	vw		$25_1^2 26_1^0$	2x322-518-414 = -288
-278	vw		$21_0^1 22_1^0$	591-868 = -277
-259.0	ms	-260	27_2^2	-(2x226)+191 = -261
-243.8	m	-248	$19_0^1 26_1^0 27_1^0$ $19_1^0 27_0^2$	396-414-226 = -244 -433+191 = -242
-232	mw	-237	$18_1^0 26_0^2$	-554+325 = -229
-200.3	m	-203	$11_1^0 17_0^2$ $16_1^0 25_0^2$	-1266+(2x532) = -202 -842+644 = -198
-161.6	s	-168	$16_0^1 24_1^0 27_1^0$ $15_0^1 18_2^0$	797-733-226 = -162 946-1107 = -161
-157	mw		$19_0^1 18_1^0$	396-554 = -158
-94.6	s	-98	$19_1^2 27_2^0$ $24_1^2 27_1^0$	2x396-433-(2x226) = -93 -733+863-226 = -96
-91.1	m		17_1^1	532-620 = -88
-63.1	s	-65	18_1^1	493-554 = -61
-61	mw		$12_0^1 18_2^0$	1045-1107 = -62
-8	m		$12_0^1 17_1^0 19_1^0$	1045-620-433 = -8

Table 18: (Continued)

Frequency (cm^{-1})			Assignment	Inferred
OBS[a]		Lit[b]		
0	vvvs	0	0_0^0	0
9	mw		$12_0^1 25_2^0$	1045-2x518 = 9
44	vw		$17_0^1 19_1^1 27_2^0$ $16_1^0 14_0^1$	532+396-433-(2x226) = 43 -842+887 = 45
59	w		$18_0^1 19_1^0$	493-433 = 60
87.1	s	83	$18_1^0 25_0^2$?	-554+644 = 90
91	vw		$19_0^3 13_1^0$	(3x396)-1098 = 90
116	vvw		$15_0^1 26_2^0$	946-(2x414) = 118
157	vvw		$16_0^1 26_1^0 27_1^0$	797-414-226 = 157
181 sh	w		$17_0^1 18_0^1 16_1^0$ $22_0^2 24_1^0 27_1^0$	532+493-842 = 183 1144-733-226 = 185
191.4	ms	188	27_0^2	191
202	vvw		$15_0^1 25_1^0 27_1^0$	946-518-226 = 202
232.5	m	229	$19_0^3 24_1^0 27_1^0$	(3x396)-733-226 = 229
239.7	mw		$19_0^2 18_1^0$ $22_0^2 27_4^0$	(2x396)-554 = 238 1144-(4x226) = 240
270	vvw	264	$18_0^1 19_0^1 17_1^0$	493+396-620 = 269
324.6	m	325	26_0^2	325
340	vvw		$16_0^1 27_2^0$	797-(2x226) = 345
366	mw		$16_0^1 19_1^0$	797-433 = 364
379	mw		27_0^4	2x191 = 382
396	mw	392	19_0^1	396
400	mw		$17_1^1 18_0^1$ $22_0^2 25_1^0 27_1^0$	-91+493 = 402 1144-518-226 = 400
450	w	447	$14_0^1 19_1^0$	887-433 = 454
492.9	m	487	18_0^1	493
532	m	526	17_0^1	532
548	mw	551	$16_0^2 14_1^0$ $19_0^3 26_1^0 27_1^0$	(2x797)-1045 = 549 (3x396)-414-226 = 548
566	vvw		27_0^6? $17_1^0 19_0^3$	3x191 = 573 -620+3x396 = 568
605	m	603	$16_0^2 18_1^0 19_1^0$	(2x797)-554-433 = 607

Table 18: (Continued)

Frequency (cm^{-1})			Assignment	Inferred
OBS[a]		Lit[b]		
644	m	642	25_0^2	644
692	w	695	$22_0^2 27_2^0$	1144-2x226 = 692
736	mw		$19_0^3 27_2^0$	(3x396)-(2x226) = 736
743	mw		$16_0^1 19_0^1 27_2^0$	797+396-(2x226) = 741
797	vs	800	16_0^1	797
863	vvw		24_0^2	863
887	w	889	14_0^1	887
934	m		13_0^1	934
945.5	vs	944	15_0^1	946
972	vw		$16_0^2 17_1^0$	(2x797)-620 = 974
988	w	984	18_0^2	2x493 = 986
1018	w	1017	$17_0^1 18_0^1$?	532+493 = 1025
1045	mw	1045	12_0^1	1045
1144	mw	1143	22_0^2	1144
1182	w	1181	21_0^2	1182
1220	vvw		10_0^1	1220
1243	mw		11_0^1	1243
1307	mw	1309	20_0^2	1307
1336	vw		9_0^1	1336
1353	vw		8_0^1	1353
1453	w	1454	7_0^1	1453
1489	vw	1488	6_0^1	1489
1597	m	1598	16_0^2	2x797 = 1594
1690	vw		5_0^1?	1690
1744.2	m	1745	$15_0^1 16_0^1$	946+797 = 1743
1889	mw	1892	15_0^2	2x946 = 1892
1939	vw		-	
2042	vw	2051	-	
2099	vvw		-	
2131	vvw		-	
2187	w		-	
2267	vw	2269	-	
2406	vw		-	

Table 18: (Continued)

Frequency (cm^{-1})		Assignment	Inferred
OBS[a]	Lit[b]		
2544	vw	-	
2592	vvw	-	
2686	w	-	
2833	vw	-	
2989	w	-	

Abbreviations: s, strong; m, medium; w, weak; v, very; sh, shoulder; br, broad.
[a] Relative to band origin at 38,030.4 cm^{-1}
[b] Reference 34.

The lower wavenumber transitions of both A' and A" vibrations generally corresponded to the strongest absorption bands and agreed reasonably well with the computed values. However, assignments in the table above about 1200 cm^{-1} were less certain. Assignments of the C-H stretching modes were not attempted. The calculations predicted that the highest wavenumber ring stretching mode would occur near 1700 cm^{-1} as compared to 1605 cm^{-1} for the S_0 electronic ground state. The computed structure for the S(π,π*) state did not elucidate this increased value. An observed very weak band at 1690 cm^{-1} was tentatively assigned to this vibration. Numerous combinations and overtones were observed in addition to the fundamentals. Table 18 summarizes the assignments for the 150 observed absorption bands for 2FPy.

Although spectra for the n$\rightarrow\pi$* transition were not observed, the calculated wavenumbers for the vibronic levels in the S(n,π*) state are given in Table 17. As noted previously, this state was calculated to be slightly higher in energy than the S(π,π*) state. Since it is not known for certain which was S_1 or S_2, the subscript designations for the states were not included.

Figures 24a and 24b show the ultraviolet absorption spectrum of 3FPy, which has its n$\rightarrow\pi$* band origin at 35,051.7 cm^{-1} (35,066 cm^{-1} reported previously). The $\pi\rightarrow\pi$* band origin is at 37,339 cm^{-1} (37,355 cm^{-1} reported previously). The bands for the n$\rightarrow\pi$* were generally sharp and the wavenumber accuracy ranged from $\pm$0.2 cm^{-1} to $\pm$2 cm^{-1} in most cases.

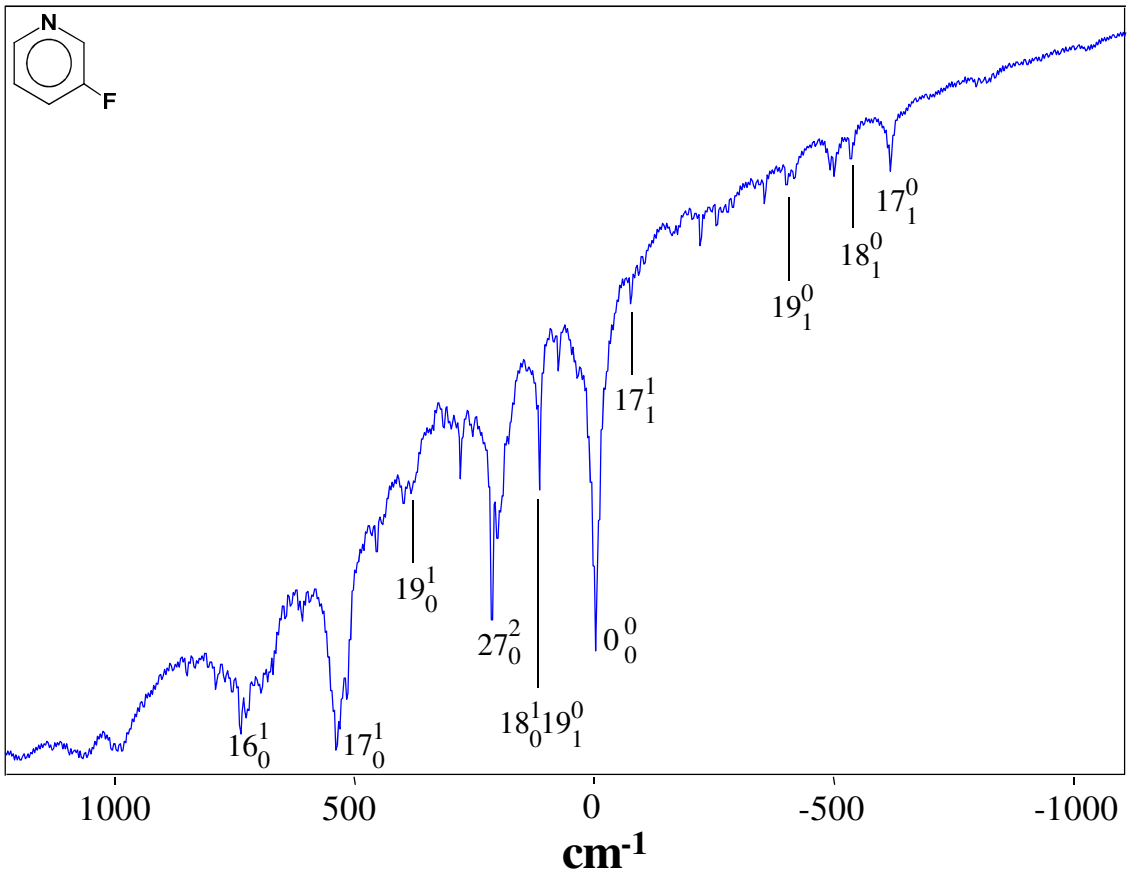

Figure 24a. Ultraviolet absorption spectra of 3FPy vapors. The spectrum is of approximately 15 Torr of sample. The wavenumber scale is relative to the n→π* band origin at 35,051.7 cm^{-1}.

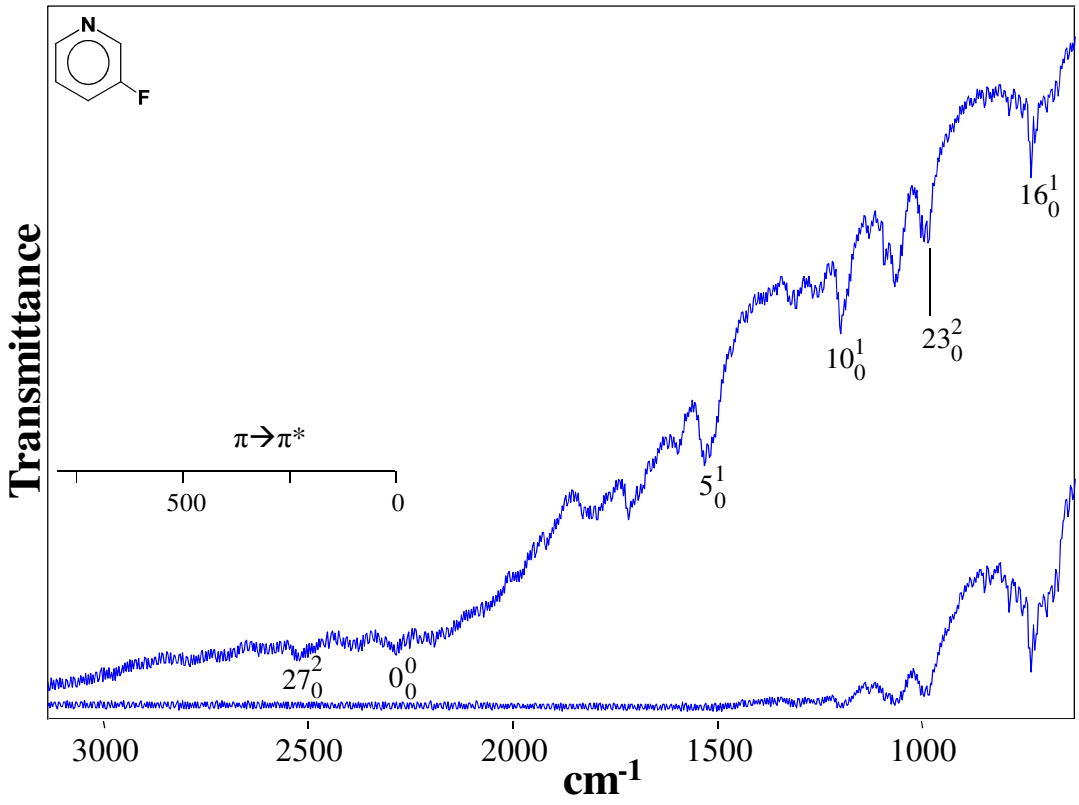

Figure 24b. Ultraviolet absorption spectra of 3FPy vapors. The spectrum is of approximately 6 Torr of sample. The wavenumber scale is relative to the π→π* band origin at 37,339 cm^{-1}.

The $\pi \rightarrow \pi^*$ bands were much broader and the band maxima were accurate to about ±5 cm^{-1}. Table 19 summarizes the assignments for the fundamental frequencies of 3 FPy and compares these to the ground state and to previously reported values.[35] Again, as for 2FPy, double quantum jumps for the out-of-plane A" vibrations were assigned and found in reasonably good agreement with the computed values. Tables 20 and 21 list the assignments for the large number of observed values for the $n \rightarrow \pi^*$ and $\pi \rightarrow \pi^*$, respectively. Table 22 summarizes the data for the twelve ring vibrations of 2FPy and 3FPy in their S_0, $S(n,\pi^*)$, and $S(\pi,\pi^*)$ states and compares these to the pyridine values (from Chapters IV and V). The C-F stretching and bending frequencies were also shown. Observed values were shown without parentheses, while computed (scaled) values were given in parentheses. As always, vibrational descriptions were approximate as vibrational coupling was common, especially for the less symmetrical fluoropyridines. Notably the out-of-plane C-F wagging motion mixed heavily with the out-of-plane ring modes.

Table 19: Observed and calculated vibrational frequencies (cm^{-1}) for 3-fluoropyridine in its ground and excited states

Sym C_s	ν	Approximate Description	S_0			S (n,π^*)			S (π,π^*)		
			OBS	CALC[a]	CALC[b]	OBS	CALC[b]	Lit[c]	OBS	CALC[b]	Lit[c]
A'	1	C-H stretch	3079	3088	3238	-	3095			3071	
(i.p.)	2	C-H stretch	3075	3073	3226	-	3069			3048	
	3	C-H stretch	3063	3054	3222	-	3059			3044	
	4	C-H stretch	3054	3047	3208	-	3035			3030	
	5	Ring stretch	1594	1602	1709	1532	1510			1699	
	6	Ring stretch	1588	1596	1696	1519	1488			1512	
	7	Ring stretch	1480	1482	1588	1320	1361		1488	1496	
	8	Ring stretch	1426	1438	1524	1309	1299			1385	
	9	C-H wag	1316	1323	1418	-	1227		1324	1311	
	10	Ring stretch	1249	1265	1340	1199	1185	1204		1265	
	11	C-F stretch	1227	1223	1272	1132	1119		1206	1217	
	12	C-H wag	1187	1197	1181	1005	1037			1122	
	13	C-H wag	1096	1107	1103	997	971			977	
	14	C-H wag	1038	1041	1085	939	935		~ 900	931	923
	15	Ring stretch	1022	1020	1082	790	850			874	
	16	Ring bend	816	819	867	737	768	737	690	751	
	17	Ring bend	613	619	655	540	548	535	500	534	501
	18	Ring bend	533	533	563	517	488		426	467	438
	19	C-F wag	398	390	419	383	384		316	373	
A''	20	C-H wag	974	966	981	799[d]	790			666	
(o.p.)	21	C-H wag	934	932	947	628[d]	614			605	
	22	C-H wag	905	905	923	547[d]	545			577	
	23	C-H wag	801	803	811	493[d]	480			439	
	24	Ring twist	701	702	712	425[d]	465			387	
	25	Ring bend	507	501	510	305[d]	277		298[d]	314	
	26	Ring bend	412	414	436	227[d]	246	452*	272[d]	243	
	27	C-F wag	231	231	253	107[d]	84	211*	118[d]	166	238*

Abbreviations: i.p., in-plane; o.p., out-of-plane.

[a] B3LYP/6-311++g(d,p) level of theory; frequencies scaled with a scaling factor of 0.985 for frequencies less than 1800 cm^{-1} and 0.964 for frequencies greater than 1800 cm^{-1}.

[b] CASSCF/6-311++G(d,p) level of theory; ground state frequencies are scaled with a scaling factor of 0.985 for frequencies less than 1800 cm^{-1} and 0.964 for frequencies greater than 1800 cm^{-1}. Excited state frequencies are scaled with a scaling factor of 0.905.

[c] Ref erence 35.* Bands reassigned; double quantum jumps value given in table.

[d] Values given are one half of the observed double quantum jump transition frequencies.

Table 20: Ultraviolet absorption spectra for the n→π* transition of 3FPy

Frequency (cm^{-1})			Assignment	Inferred
OBS[a]		Lit[b]		
-1228	vw		11_1^0	-1227
-1187	vvw		12_1^0	-1187
-1149	vvw		-	
-1104	vvw		-	
-1071	vvw		18_2^0	2x-533 = -1066
-1038	vw		14_1^0	-1038
-1023	mw	-1029	15_1^0	-1022
-967	vw		$12_1^0 27_0^2$	-1187+214 = -973
-928	w		27_4^0?	2x-231 = -924
-887	vvw		$13_1^0 27_0^2$?	-1096+214 = -882
-834	w		-	
-819	vw	-821	26_2^0	2x-412 = -824
-816	vw		16_1^0	-816
-807 br	vw		$15_1^0 27_0^2$	-1022+214 = -808
-795	mw	-799	$22_1^0 27_0^1$	-905+107 = -798
-752	vvw		$19_0^1 22_1^0 27_1^0$	383-905-231 = -753
-698	vvw	-701	$22_1^0 27_0^1$?	-801+107 = -694
-644 br	vw	-654	$12_1^0 17_0^1$	-1187+540 = -647
-614	ms	-618	17_1^0	-613
-594 sh	w		$24_1^0 27_0^1$	-701+107 = -594
-540 sh	w		$19_0^1 25_1^0 26_1^0$	383-507-412 = -536
-533	m	-534	18_1^0	-533
-498	m	-501	-	
-490	m		$25_1^0 26_1^0 27_0^4$ $17_0^1 23_1^0 27_1^0$	-507-412+(2x214) = -491 540-801-231 = -492
-482	w		$20_1^0 23_0^1$	-974+493 = -481
-457	w		$17_2^0 19_0^2$	2x-613+2x383 = -460
-416 br	mw		$12_1^0 19_0^2$	-1187+2x383 = -421
-413	w	-411	$15_1^0 25_0^2$	-1022+609 = -413
-409	w		$22_1^0 23_0^1$	-905+493 = -412
-399	m		19_1^0	-398
-384	w		$21_1^0 22_0^1$ $17_0^1 27_4^0$	-934+547 = -387 540-928 = -388

Table 20: (Continued)

Frequency (cm^{-1})			Assignment	Inferred
OBS[a]		Lit[b]		
-374	vw		$17_0^1 25_1^0 26_1^0$	540-507-412 = -379
-353	m	-358	-	
-335	w	-339	-	
-330 sh	vvw		$16_0^1 18_2^0$	737+(2x-533) = -329
-318	vw		$18_1^0 27_0^2$ $17_0^1 19_1^0 27_2^0$	-533+214 = -319 540-398+(2x-231) = -320
-300	vw		$26_1^0 27_0^1$	-412+107 = -305
-287	w		$15_1^0 16_0^1$ $17_0^1 26_2^0$	-1022+737 = -285 540-2x412 = -284
-255	m	-260	$15_1^0 19_0^2$ $22_0^1 23_1^0$	-1022+(2x383) = -256 547-801 = -254
-240 br	vw		$17_1^0 19_1^2$	-613+2x383-398 = -245
-220	m	-226	$18_0^1 25_1^0 27_1^0$	517-507-231 = -221
-204	mw		$23_0^1 24_1^0$	493-701 = -208
-174	mw		$21_0^1 23_1^0$	628-801 = -173
-162 br	mw	-157	$19_0^2 24_1^0 27_1^0$ $19_1^2 18_1^0$	2x383-701-231 = -166 2x383-398-533 = -165
-146	vvw		$15_0^1 24_1^0 27_1^0$? $18_1^0 19_0^1$	790-701-231 = -142 -533+383 = -150
-127	vvw		$15_0^1 25_1^0 26_1^0$	790-507-412 = -129
-120	vvw		$15_1^0 18_0^1 19_0^1$	-1022+517+383 = -122
-103 br	mw		$18_1^0 27_0^4$	-533+(2x214) = -105
-92	mw		-	
-82 sh	vw		16_1^1	737-816 = -79
-75	m	-78	17_1^1 $19_0^1 27_2^0$	-613+540 = -73 383+(2x-231) = -79
0	vvs	0	0_0^0	0
25 sh	w		$19_0^2 25_1^0 27_1^0$	2x383-507-231 = 28
36 sh	mw		$15_1^0 17_0^1 18_0^1$	-1022+540+517 = 35
50 sh	mw		$19_1^0 26_0^2$	-398+454 = 56
76	m	74	$18_1^0 25_0^2$	-533+609 = 76

Table 20: (Continued)

Frequency (cm^{-1})			Assignment	Inferred
OBS[a]		Lit[b]		
84	vw		$16_1^0 18_0^1 19_0^1$	-816+517+383 = 84
117	ms	114	$18_0^1 19_1^0$	517-398 = 119
123 sh	vw		$16_0^1 17_1^0$	737-613 = 124
134	vvw		$22_0^1 26_1^0$	547-412 = 135
143	vvw		$15_0^1 26_1^0 27_1^0$ $17_0^1 19_1^0$	790-412-231 = 147 540-398 = 142
180 sh	mw		-	
194	w		$24_0^1 27_1^0$	425-231 = 194
202 br	m		$16_0^1 18_1^0$	737-533 = 204
214	vs	211	27_0^2	214
256	mw	248	$17_0^2 26_2^0$	(2x540)+(2x-412) = 256
279	m	272	$17_0^2 19_2^0$	(2x540)-(2x398) = 284
288 br	w		$20_0^1 25_1^0$	799-507 = 292
301	mw	303	$16_1^1 19_0^1$ $19_0^2 27_2^0$	-82+383 = 301 (2x383)+(2x-231) = 304
314	mw		$17_0^1 18_0^1 25_1^0 27_1^0$	540+517-507-231 = 319
383	m		19_0^1	383
398	m		$15_0^1 19_1^0$?	790-398 = 392
440 br	mw		$17_1^1 18_0^1$	-75+517 = 442
454	m	452	26_0^2	454
464 br	vw		17_1^2	(2x540)-613 = 467
517	ms		18_0^1	517
531 sh	mw		$17_1^0 19_0^3$	-613+3x383 = 536
539.5	vs	535	17_0^1	540
593 br	vvw		$19_0^1 27_0^2$	383+214 = 597
609	mw	605	25_0^2	609
616	mw		$18_1^0 19_0^3$	-533 + (3x383) = 616
633 br	mw		$18_0^2 19_1^0$	(2x517)-398 = 636
645	w		27_0^6	3x214 = 642
670	mw		-	
681	mw	683	$17_0^2 19_1^0$	(2x540)-398 = 682
695	w	697	-	
704	vw		-	

Table 20: (Continued)

Frequency (cm^{-1})			Assignment	Inferred
OBS[a]		Lit[b]		
724	m		$16_0^1 19_1^1$	737+383-398 = 722
737	ms	737	16_0^1	737
755	mw	753	$17_0^1 27_0^2$	540+214 = 754
769	mw		19_0^2	2x383 = 766
785 sh	vvw		-	
790	mw	789	15_0^1	790
799	w		$23_0^1 25_0^1$	493+305 = 798
806	vw		-	
832 br	vw	833	-	
849	mw		24_0^2	850
913	w		-	
921	w		$17_0^1 19_0^1$	540+383 = 923
939	vw		14_0^1	939
985 br	m		23_0^2	985
997	m		13_0^1	997
1005	m	1001	12_0^1	1005
1050	w		$21_0^1 24_0^1$	628+425 = 1053
1059	w		$17_0^1 18_0^1$	540+517 = 1057
1067	m	1065	-	
1076 sh	vw		17_0^2	2x540 = 1080
1087 sh	w		-	
1093	m	1091	22_0^2	1093
1110	w		$18_0^1 19_0^1 27_0^2$	517+383+214 = 1114
1132.	mw		11_0^1	1132
1151	w		19_0^3	3x383 = 1149
1188 sh	vvw		-	
1199	m	1204	10_0^1	1199
1208 sh	w		$13_0^1 27_0^2$	997+214 = 1211
1225	vw		-	
1256 br	mw		21_0^2	1256
1309	mw		8_0^1	1309
1320	mw		7_0^1	1320
1417	vw		$18_0^2 19_0^1$	2x517+383 = 1417
1508 sh	w		$13_0^1 18_0^1$	997+517 = 1514

Table 20: (Continued)

Frequency (cm^{-1})			Assignment	Inferred
OBS[a]		Lit[b]		
1519	mw		6_0^1	1519
1532	m	1532	5_0^1	1532
1539	w		$13_0^1 17_0^1$	997+540 = 1537
1597	m		20_0^2	1597
1662	vw		$18_0^1 19_0^3$	517+1151 = 1668
1684	w		$17_0^1 19_0^3$	540+1151 = 1691
1794	mw		$16_0^1 17_0^1 18_0^1$	737+540+517 = 1794
1918	m		$13_0^1 17_0^1 19_0^1$	997+540+383 = 1920

Abbreviations: s, strong; m, medium; w, weak; v, very; sh, shoulder; br, broad.
[a] Relative to band origin at 35,051.7 cm^{-1}.
[b] Reference 35.

Table 21: Ultraviolet absorption spectra for the $\pi \rightarrow \pi^*$ transition of 3FPy

Frequency (cm^{-1})			Assignment	Inferred
OBS[a]		Lit[b]		
-1019	m	-1023	15_1^0	-1022
-932	w		$18_1^0 19_1^0$	-533-398 = -931
-569	m	-573	$18_1^1 27_2^0$	-533+426-2x231 = -569
-530	w	-527	18_1^0	-533
-494	m	-491	$14_1^0 26_0^2$	-1038+543 = -495
-460	m	-461	27_2^0	2x-231 = -462
-393	w		$18_0^1 26_2^0$	426-2x412 = -398
-344	vw		$14_1^0 16_0^1$	-1038+690 = -348
-304 br	mw	-304	$14_1^0 17_0^1 27_0^2$	-1038+500+236 = -302
-283	vvw	-288	$15_1^0 17_0^1 27_0^2$	-1022+500+236 = -286
-230	w	-230	$16_0^1 27_4^0$	690-4x231 = -234
-155	w		$17_1^0 18_0^2 19_1^0$	-613+2x426-398 = -159
-121	mw	-122	$14_0^1 15_1^0$	900-1022 = -122
-94	mw	-96	$15_1^0 17_0^1 18_0^1$	-1022+500+426 = -96
-64	mw	-64	$18_0^2 25_1^0 26_1^0$	2x426-507-412 = -67
-32 sh	vvw		$17_0^1 18_1^0$	500-533 = -33
-9 sh	m		$19_0^2 26_1^0 27_1^0$	2x316-412-231 = -11
0	ms		0_0^0	0
29 sh	vw	30	$18_0^1 19_1^0$	426-398 = 28
88	mw		$14_0^1 16_1^0$?	900-816 = 84
107	w	108	$16_1^0 17_0^1 18_0^1$	-816+500+426 = 110
123	mw		$17_1^1 27_0^2$	500-613+236 = 123
173	vw		$17_0^2 26_2^0$	2x500-2x412 = 176
202	vw	204	$17_0^1 18_1^0 27_0^2$	500-533+236 = 203
236	s	238	27_0^2	236
316	mw	318	19_0^1	316
410	w	416	$18_1^0 19_0^3$	-533+3x316 = 415
426	w	438	18_0^1	426
500	ms	501	17_0^1	500
543	mw	544	26_0^2	543
596	w		25_0^2	596
690	m		16_0^1	690
~ 900	s	923	14_0^1	900

Table 21: (Continued)

Frequency (cm^{-1})			Assignment	Inferred
OBS[a]		Lit[b]		
1206	w		11_0^1	1206
1324	w		9_0^1	1324
1488	ms	1489	7_0^1	1488
~ 1830	ms	1841	15_0^2?	2x~900 = ~1800
2428	mw		-	
2789	mw		-	
2978	vw		7_0^2	2x1488 = 2976

Abbreviations: s, strong; m, medium; w, weak; v, very; sh, shoulder; br, broad.
[a] Relative to band origin at 37,338.9 cm^{-1}.
[b] Reference 35.

Table 22: Vibrational frequencies (cm^{-1}) comparisons for selected vibrations of the fluoropyridines and pyridine

ν^b	Approximate Description	S_0			S (n,π^*)			S (π,π^*)		
		2FPy	3FPy	Py[c]	2FPy	3FPy	Py[c]	2FPy	3FPy	Py[c]
5	Ring stretch	1605	1594	1584	(1586)	1532	(1507)	1690	(1699)	(1499)
6	Ring stretch	1593	1588	1576	(1438)	1519	(1453)	1489	(1512)	(1680)
7	Ring stretch	1478	1480	1483	(1381)	1320	(1379)	1453	1488	(1394)
8	Ring stretch	1439	1426	1442	(1327)	1309	(1314)	1353	(1385)	(1476)
10	Ring stretch	1286	1249	1227	(1210)	1199	(1185)	1220	(1265)	(1310)
15	Ring breathing	997	1022	1031	(879)	790	(857)	946	(874)	(878)
16	Ring bend (i.p.)	842	816	991	(789)	737	(885)	797	690	(883)
17	Ring bend (i.p.)	620	613	654	(554)	540	636	532	500	(577)
18	Ring bend (i.p.)	554	533	601	(494)	517	543	493	426	(509)
24	Ring twist (o.p.)	733	701	700	(454)	425	(476)	432	(387)	(434)
25	Ring bend (o.p.)	518	507	403	(380)	305	326	322	298	(260)
26	Ring bend (o.p.)	414	412	375	(240)	227	60	163	272	(244)
11	C-F stretch	1266	1227	-	(1168)	1132	-	1243	1206	-
19	C-F wag (i.p.)	433	398	-	(380)	383	-	396	316	-
27	C-F wag (o.p.)	226	231	-	(40)	107	-	96	118	-

Abbreviations: i.p., in-plane; o.p., out-of-plane.

[a] Values in parentheses are calculated values. CASSCF/6-311++G(d,p) level of theory; scaled with a scaling factor of 0.905.

[b] Mode number for 2FPy and 3FPy.

[c] Values taken from Chapter IV and V.

CONCLUSION

Both the structures and vibronic levels of 2FPy and 3FPy were investigated in their electronic excited states and compared these to those of pyridine. In the S(n,π*) states the N-C bond distances and the C(3)-C(4) and C(4)-C(5) all increased, reflecting decreased π bonding. However, the C(2)-C(3) and C(5)-C(6) bonds decreased in all cases, suggesting an approximate structure. The decrease in the C(2)-C(3) bond was especially pronounced for 2FPy where the fluorine was attached to the C(2) atom. Notably the C-F bond itself decreased from 1.391 Å in the S_0 state to 1.343 Å in the S(n,π*) state. In the study of the 2FPy ground state (Chapter VI), the fluorine atom clearly had significant π bonding interactions with the ring. For 3FPy there was considerably less of this effect. The S(π,π*) state structures showed little surprise as all of the N-C and C-C bond distances increased due to the decrease in π bond character.

Although the computation of excited state energy levels was considerably less reliable than for the ground states, the computed electronic transition frequencies agree quite well (±2%) with those observed. Moreover, the calculated vibrational frequencies agreed in the most part to about 5%. For the lower frequency large-amplitude, anharmonic modes the agreement was poorer but still provided guidance. In the previous work on pyridine (Chapter V), analysis of its ν_{18} ring bending mode at 403 cm^{-1} in the ground state and 59.5 cm^{-1} in its S_1(n,π*) state showed that the rigid pyridine ring in the S_0 state became very floppy in the excited state. In fact, a tiny barrier to planarity of 3 cm^{-1} was determined.

For 2FPy and 3FPy the rings remained more rigid in their excited states than pyridine, as the bending frequencies were in the 163 to 272 cm^{-1} range compared to their ground state. This out-of-plane ring mode was strongly coupled to the out-of-plane C-F wagging motion, which decreased from about 230 cm^{-1} in the S_0 states to about 100 cm^{-1} for the observed excited states. The 2FPy and 3FPy ring rigidity and the strong vibrational coupling reflect the significant role of the fluorine atom in the π bonding in the excited states as well as the ground states.

CHAPTER VIII

GAS-PHASE RAMAN SPECTRA AND THE POTENTIAL ENERGY FUNCTION FOR THE INTERNAL ROTATION OF 1,3-BUTADIENE AND ITS ISOTOPOMERS*

INTRODUCTION

The internal rotation about the central carbon-carbon bond of 1,3-butadiene can produce *trans*, *cis*, or *gauche* conformations depending on the angle of rotation, as shown in Figure 25. The *trans* conformer has long been known to be the predominant one[37-39], but whether the higher energy conformer has a *cis* or *gauche* configuration remained a question for many years. Aston and co-workers[40] found evidence that a second conformer was present 2.3 kcal/mol higher in energy from a calorimetric study, but they could not determine its structure. Lipnick and Garbisch[41] carried out NMR studies at various temperatures and determined the energy difference to be 2.1 kcal/mol. These workers favored the *gauche* structure for the higher energy form, but their data were not sufficient to rule out the planar *cis* form. Cole and co-workers[42] reported the far-infrared spectrum of 1,3-butadiene, and its 1,1,4,4-d_4 and -d_6 isotopomers and observed a series of bands for the ν_{13} internal rotation (torsion) for each molecule.

---

* Reprinted with permission from "Gas-Phase Raman Spectra and the Potential Energy Function for the Internal Rotation of 1,3-Butadiene and its Isotopomers" by Boopalachandran, P.; Craig, N.; Groner, P.; Laane, J., 2011. *J. Phys. Chem. A*, In press, by American Chemical Society.

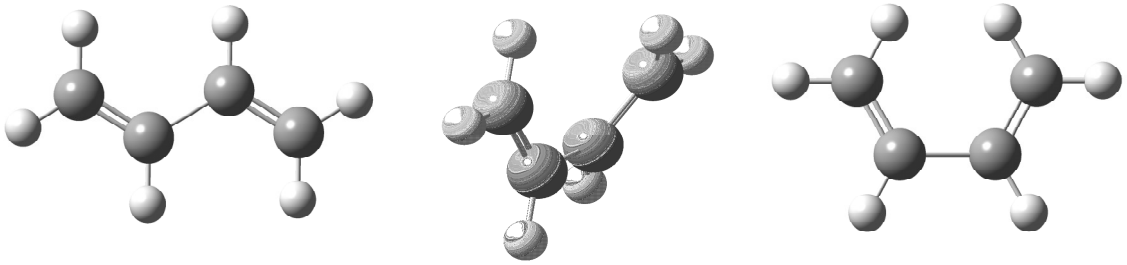

(a) (b) (c)

Figure 25. The (a) *trans*, (b) *gauche, and* (c) *cis* forms of 1,3-butadiene.

The 0→1 transitions were observed at 162.5, 149.2, and 141.7 cm^{-1} for the d_0, d_4, and d_6 molecules, respectively. These workers calculated a potential energy barrier of 1900 ± 800 cm^{-1} using a quadratic/quartic potential function, but provided no data for a second conformer.

In 1974, Carreira[43] reported the gas-phase Raman spectrum of 1,3-butadiene and observed seven sub-bands, which were assigned to double quantum jumps of the ν_{13} vibration of the *trans* conformer. He also observed three other features, which he assigned to a *cis* structure. The data were then used to calculate a periodic potential energy function, which had a barrier of 2504 cm^{-1} (7.15 kcal/mol) at 90° rotation where 0° corresponded to the planar *trans* structure. The energy for the *cis* form at 180° was calculated to be 873 cm^{-1} (2.49 kcal/mol) in reasonable agreement with the earlier studies.[40,41] Infrared, Raman, and ultraviolet spectroscopy studies of matrix isolated 1,3-butadiene[44-46] also supported the idea that the *cis* structure was the minor conformer. A 1983 Raman study by Panchenko and co-workers[47] reported gas-phase Raman spectra for the $2\nu_{13}$ regions of 1,3-butadiene and its *cis*, *cis*-1,4-d_2 and -d_6 isotopomers. They again assumed the minor conformer to have the *cis* structure.

In 1991 Engeln and co-workers[48], referred to as ECR, reported new gas-phase Raman data for 1,3-butadiene and observed new features, which were assigned to the *gauche* conformer. Notably, they observed a band at 214.9 cm^{-1}, which was attributed to one of the transitions arising from a lower quantum state of the *gauche* conformer. ECR also calculated a periodic potential function based on $\cos n\varphi$ terms[64] using n = 1 to 6. Although exact values were not reported, the reported V_n values correspond to a barrier

between *trans* and *gauche* forms of 2075 cm^{-1}, and the *gauche* form at 138° lies 989 cm^{-1} higher than the *trans* structure. The barrier between the two equivalent *gauche* forms (corresponding to the *cis* structure) was 408 cm^{-1}.

A number of theoretical calculations have been carried out to determine the energy differences between the 1,3-butadiene conformations beginning as early as 1970. These were summarized in a recent high level *ab initio* study by Feller and Craig.[49] While the early calculations with minimal basis sets predicted the minor conformation to be *cis*, the recent work has consistently shown the *gauche* form to have a local energy minimum in the potential energy function. Feller and Craig also reported intensities for infrared and Raman transitions for the *gauche* rotamer computed with the B3LYP/aug-cc-pVTZ model.[49]

In the present work, an extensive gas-phase Raman investigation was undertaken, including spectra at high temperatures, of 1,3-butadiene and three of its deuterated isotopomers and determined the potential energy function that fit the data for all of the isotopic species. To the best of our knowledge, these spectra have the best signal to noise ratios and have the highest sensitivity of any that have been recorded of these molecules. Improved F-term expansions for each isotopomer were calculated by making use of the calculated structures from the high level *ab initio* calculations.[49] The goal was to accurately determine the energy barriers and the energy differences between the different conformations. Numerous Raman bands attributable to the *gauche* conformation were also observed throughout the entire Raman spectra of all of the isotopomers. These results will be reported in Chapter X.

EXPERIMENTAL

Butadiene was supplied by Aldrich, the 2,3-d_2 species was supplied by CDN Isotopes (99% D, Quebec, Canada), and the 1,1,4,4-d_4 and d_6 species were supplied by Cambridge Isotope Laboratories (98% D). Purity of the samples was confirmed by infrared spectroscopy prior to sealing the samples in the cells.

Raman spectra of gas-phase 1,3-butadiene and its isotopomers were recorded for samples with simplified optics at various temperatures sealed in specially designed glass cells which were previously described in Chapter II. A Jobin-Yvon U-1000 spectrometer equipped with a liquid nitrogen-cooled CCD detector was used to collect the spectra. The 532 nm line of a frequency-doubled Nd:YAG Coherent Verdi-10 laser was used and generally operated at 6 watts of power. Spectral regions spanning 60 cm^{-1} were typically collected over periods of 4 to 6 hours so that many hundreds of individual spectra could be averaged. Spectral acquisition was mostly carried out at room temperature for these samples but for some cases the samples were heated up to approximately 250° C. The resolution of the spectra was 0.7 cm^{-1}.

CALCULATIONS

Potential Energy Function

Computer program previously described[64] was utilized to calculate the energy levels and to fit the observed data. The Hamiltonian for the internal rotation is

$$H = -\frac{d}{d\phi}F(\phi)\frac{d}{d\phi} + V(\phi) \qquad (8.1)$$

and the potential energy function and F value expansion (inverse moment of inertia) are given by

$$V(\phi) = \sum_n \tfrac{1}{2} V_n (1 - \cos n\phi) \tag{8.2}$$

and

$$F(\phi) = F_0 + \sum_n F_n \cos n\phi \tag{8.3}$$

In his calculation, Carreira[43] utilized n = 1 to 4 for $V(\phi)$ while ECR used n = 1 to 6. In the present work, the terms up to n = 6 was used. For the kinematic F expansion, Carreira had terms up to n = 4 whereas ECR[48] also included the small F_5 term. In the present work, the F_n terms up to n = 6 was used. Recent high level *ab initio* calculations[49] provided the structural data for this molecule at different angles of internal rotation. These data are shown in Table 23 and were used with the Groner FSER program[74] to calculate the F-term value for different ϕ values (Table 24). In this program, it is assumed that all structural parameters $R(\phi)$ are functions of ϕ defined by

$$R(\phi) = R(0) + B\cos\phi \tag{8.4}$$

$R(0)$ is the value of the coordinate for the *trans* conformation at $\phi = 0^o$ and coefficient B is determined from the structures obtained from the *ab initio* calculations for the gauche conformation at $\phi = 144.5^o$. From the F-term values, the parameters F_i in Equation (8.3) were calculated. These results are given in Table 25 for each of the isotopomers. It is interesting to note in Table 23 that the C-C bond length increased and the C=C bond length decreased slightly as the molecule rotated away from the *trans* structure reflecting the decrease in conjugation associated with the π orbitals.

Table 23: Calculated[a] 1,3-butadiene energy and structural parameters as a function of internal rotation angle

Angle(φ)	Energy (cm^{-1})	Bond distances (Å)		CCC Bond angle α(123)
		r(C=C)	r(C-C)	
0° *(trans)*	0	1.3377	1.4548	123.5°
40°	1021.2	1.3365	1.4672	123.5°
78°[b]	2236.4	1.3327	1.4824	123.8°
90°	2157.6	1.3329	1.4818	123.8°
110°	1645.6	1.3322	1.4730	123.8°
144.5° *(gauche)*	1053.8	1.3362	1.4682	124.4°
180°[b] *(cis)*	1221.3	1.3371	1.4696	126.3°

[a] Reference 49.
[b] Transition state.

Table 24: Calculated F values (cm^{-1}) for 1,3-butadiene and its isotopomers as a function of internal rotation angle

Angle (degrees)	d_0	2,3-d_2	1,1,4,4-d_4	d_6
0	2.7090	2.2834	2.2688	1.9376
22.5	2.7151	2.2887	2.2665	1.9375
45.0	2.7429	2.3103	2.2694	1.9435
67.5	2.8184	2.3636	2.3017	1.9709
90.0	2.9757	2.4677	2.3935	2.0382
112.5	3.2448	2.6357	2.5691	2.1586
135.0	3.6216	2.8563	2.8255	2.3247
157.5	4.0054	3.0663	3.0901	2.4872
180.0	4.1787	3.1569	3.2099	2.5581
202.5	4.0054	3.0663	3.0901	2.4872
225.0	3.6216	2.8563	2.8255	2.3247
247.5	3.2448	2.6357	2.5691	2.1586
270.0	2.9757	2.4677	2.3935	2.0382
292.5	2.8184	2.3636	2.3017	1.9709
315.0	2.7429	2.3103	2.2694	1.9435
337.5	2.7151	2.2887	2.2665	1.9375

Table 25: Coefficients (cm^{-1}) of the F(φ) expansion

Isotopomer	F_0	F_1	F_2	F_3	F_4	F_5	F_6
d_0 calculated	3.1960	-0.6779	0.2333	-0.0534	0.0137	-0.0035	0.0009
d_2 calculated	2.5886	-0.4113	0.1261	-0.0243	0.0054	-0.0010	0.0000
d_2 adjusted	2.7040	-0.4297	0.1317	-0.0254	0.0056	-0.0011	0.0000
d_4 calculated	2.5560	-0.4317	0.1723	-0.0363	0.0095	-0.0023	0.0005
d_4 adjusted	2.5630	-0.4329	0.1727	-0.0364	0.0095	-0.0023	0.0005
d_6 calculated	2.1386	-0.2898	0.1045	-0.0195	0.0045	-0.0009	0.0000
d_6 adjusted	2.2690	-0.3074	0.1109	-0.0206	0.0048	-0.0009	0.0000

Ab initio and DFT Calculations

Previous calculations by Feller and Craig were taken to very high levels.[49] In the present study, computations to include the deuterated isotopomers were performed so that frequency values for both *trans* and *gauche* conformations were predicted. In particular, DFT calculations with the B3LYP model and the cc-pVTZ basis set were utilized to provide the theoretical harmonic vibrational frequencies. Based on previous work,[66-70] a scaling factor of 0.985 was used.

Analysis of Data

In order to assign the spectra of 1,3-butadiene and its three deuterated isotopomers, the following approach was used. First the computed energy values in Table 23 were utilized to calculate the V_n terms of Equation (8.2) that best fit these. These V_n terms, as well as other values to be discussed below, are given in Table 26. Table 27 shows the calculated Raman wavenumbers (cm^{-1}) for the d_0 molecule based on the theoretical potential function from the *ab initio* calculation and on the calculated F_n terms in Table 25. The table also shows the observed transitions, which will be discussed later. As can be seen, the agreement was remarkably good considering that no adjustments were made on the potential energy terms or the F_n values. In Table 27 the single quantum jump transitions from the far-infrared[42,50] and the double quantum jump transitions from the Raman spectrum in this work for the *trans* potential well are shown without a + or – sign since these levels are not degenerate.

Table 26: Potential energy function parameters

Calculation	Parameters (cm^{-1})						Energies[a] (cm^{-1})		
	V_1	V_2	V_3	V_4	V_5	V_6	E_{gauche}	E_{cis}	$E_{barrier}$
Theoretical[b]	507.0	1550.0	739.0	-213.0	-24.8	-3.2	1054	1221	2236
d_0	463.6	1551.2	771.0	-225.1	-21.5	17.0	1032	1213	2258
d_2	463.6	1541.7	772.6	-228.3	-15.9	16.4	1026	1220	2250
d_4	463.6	1535.5	782.6	-217.9	-18.3	12.8	1035	1223	2233
d_6	463.6	1557.8	745.3	-215.3	-2.3	0.7	1020	1207	2236
Alternate model									
d_0	620.0	1072.2	925.2	-99.2	-57.6	-10.6	1081	1488	1988
d_2	620.0	1064.6	916.8	-96.9	-53.0	-9.3	1080	1484	1975
d_4	620.0	1134.7	911.0	-123.6	-53.9	-4.6	1093	1477	2032
d_6	620.0	1073.1	925.8	-96.7	-60.8	-12.6	1083	1485	1989

[a] Energies relative to *trans* conformation.
[b] Parameters based on energy values in Table 23.

Table 27: Calculated and observed Raman transitions (cm^{-1}) for the internal rotation of 1,3-butadiene-d_0

Transition	Calculated		Observed
	Theory[a]	Adjusted[b]	
trans			
0-1	157.0	162.7	162.42[c]
1-2	155.8	160.0	159.91[c]
2-3	154.2	157.3	157.25[c]
0-2	312.7	322.7	322.4
1-3	310.0	317.3	317.3
2-4	306.6	311.7	311.9
3-5	302.5	305.9	306.4
4-6	297.9	299.9	300.4
5-7	292.7	293.4	293.6
6-8	286.8	286.6	286.3
7-9	280.1	279.3	279.0
gauche			
(0^+-2^+)	215.5	213.6	214.9
(0^--2^-)	286.5	283.7	282.0
(1^+-3^+)	268.8	261.2	261.9
(1^--3^-)	317.0	314.2	obsc[d]

[a] Calculated using the theoretical V_n values in Table 26.
[b] Calculated using the V_n values for d_0 in Table 26.
[c] Reference 50.
[d] Obscured by stronger *trans* band.

In the IR spectrum, the transitions are $A_g \leftrightarrow A_u$. In the Raman spectrum, they correspond to either $A_g \rightarrow A_g$ or $A_u \rightarrow A_u$ transitions of the C_{2h} conformation. The single jump $A_g \leftrightarrow A_u$ transitions are symmetry forbidden in the Raman-spectra. There are two equivalent *gauche* conformations so that the levels for this structure below the barrier at the *cis* configuration are doubly near-degenerate. These are labeled, following the convention of ECR,[48] with + or – signs to indicate the lower and higher energy states of the near-degenerate levels. The *gauche* conformation has C_2 symmetry so the + states have symmetry species A while the – states are of B symmetry. In principle, the single quantum jumps of the *gauche* conformer are symmetry allowed for Raman, which have a predicted activity of 2.9 $Å^4$ amu^{-1}. Despite heroic efforts, these quantum jumps were not observed in the expected 100 to 200 cm^{-1} region, where the shoulder of the exciting line interferes. Instead, the observed transitions again correspond to double quantum jumps n^+ to $n^+ + 2$ or n^- to $n^- + 2$.

Utilizing the theoretical V_n values as a starting point, they were then adjusted in the VNCOSPX program[64] to obtain the best frequency fit with the observed data. These calculated values are shown in Table 27 in the "Adjusted" column. For the deuterated isotopomers, the same potential function was then used along with the calculated F_n terms in Table 25 to predict the torsional frequencies. In each case, the calculated isotopic shift was greater than that observed. This outcome was not unexpected, since a one-dimensional approximation for the internal rotation was utilized, and this vibration mixed with other motions and to a different degree for each of the isotopomers.

To correct for this effect, the F_n values for each isotopomer were adjusted by a ratio that matched the observed isotopic shift for the *trans* conformer. These values are shown as the "adjusted" terms in Table 25. For the d_2 and d_6 isotopomers the F_n values were increased about 5% while for the d_4 there was little change. In general, this adjustment provided fairly good agreement with the observed values. However, in addition to the vibrational mixing producing a decreased isotopic shift, this mixing was expected to alter somewhat the potential energy parameters V_n. Hence, after adjusting the F_n terms with a fixed ratio, the V_n terms were then adjusted to produce the best fit with the experimental data. These adjustments corresponded to only about 1% changes in the energies calculated for different angles of internal rotation. In the discussion below, the results of both the "unadjusted" (Calc I) and "adjusted" (Calc II) calculations for the deuterated isotopomers will be presented.

It should also be noted that the spectral region investigation includes not only the transitions from the *trans* and *gauche* wells, but also hot bands from other low-lying vibrations. Notably, the ν_{24} (B_u) angle bending vibrational excited state at 299 cm^{-1} for the *trans* d_0 molecule has a population of about 24% of the ground state population and thus a shifted torsional series can arise from this state. Laane's group have observed such "side bands" often in their previous investigation of molecules such as cyclopentane[80,81] and the *trans* rotamer of butadiene. Such hot bands can account for several of the unassigned bands in the spectra. In addition, and very importantly, theoretical calculations in this and previous work predict that the *gauche* rotamer will have its ν_{12} (A) angle bending vibration in this region with a predicted activity of 9.3 $Å^4$

amu^{-1}.[49] For each of the isotopomers, this band has been observed close to the value predicted and with higher intensity than that expected for the torsional series. Notably, in the ECR study,[48] these workers assigned the ν_{12} *gauche* band to be the $0^- \rightarrow 2^-$ band of the torsional motion.

One other factor to consider during assignments is that the d_4 and d_6 isotopomers were stated to be 98% isotopically pure. This composition means that the d_4 sample would contain about 8% 1,1,4-d_3 molecules and the d_6 would contain about 12% of the three types of d_5 molecules. These species were expected to give rise to Raman bands from their *trans* states that are comparable in intensity to those from the *gauche* states of the primary isotopomers.

While the assignments for the *gauche* well that best correspond to the theoretically predicted ones was favored, different set of assignments that are similar to those proposed by ECR for the d_0 molecule were tested. These assignments placed the $1^+ \rightarrow 3^+$ band at 214.9 cm^{-1} rather than the $0^+ \rightarrow 2^+$ band. In addition, for this alternative assignment the $0^- \rightarrow 2^-$ transition was ascribed to a band at 275.1 cm^{-1}, whereas ECR had assigned it to 270.8 cm^{-1}, which was the ν_{12} band of the *gauche* form from this study. Also, the band at 261.9 cm^{-1}, which was assigned to $1^+ \rightarrow 3^+$ for the first model, was chosen to be $0^+ \rightarrow 2^+$ for the alternative model. In addition, the previously unassigned band at 255.3 cm^{-1} was ascribed to $1^- \rightarrow 3^-$. With this second set of assignments, the same procedure was followed in order to fit the data for the deuterated isotopomers. Calculations based on both of these assignments will be discussed below.

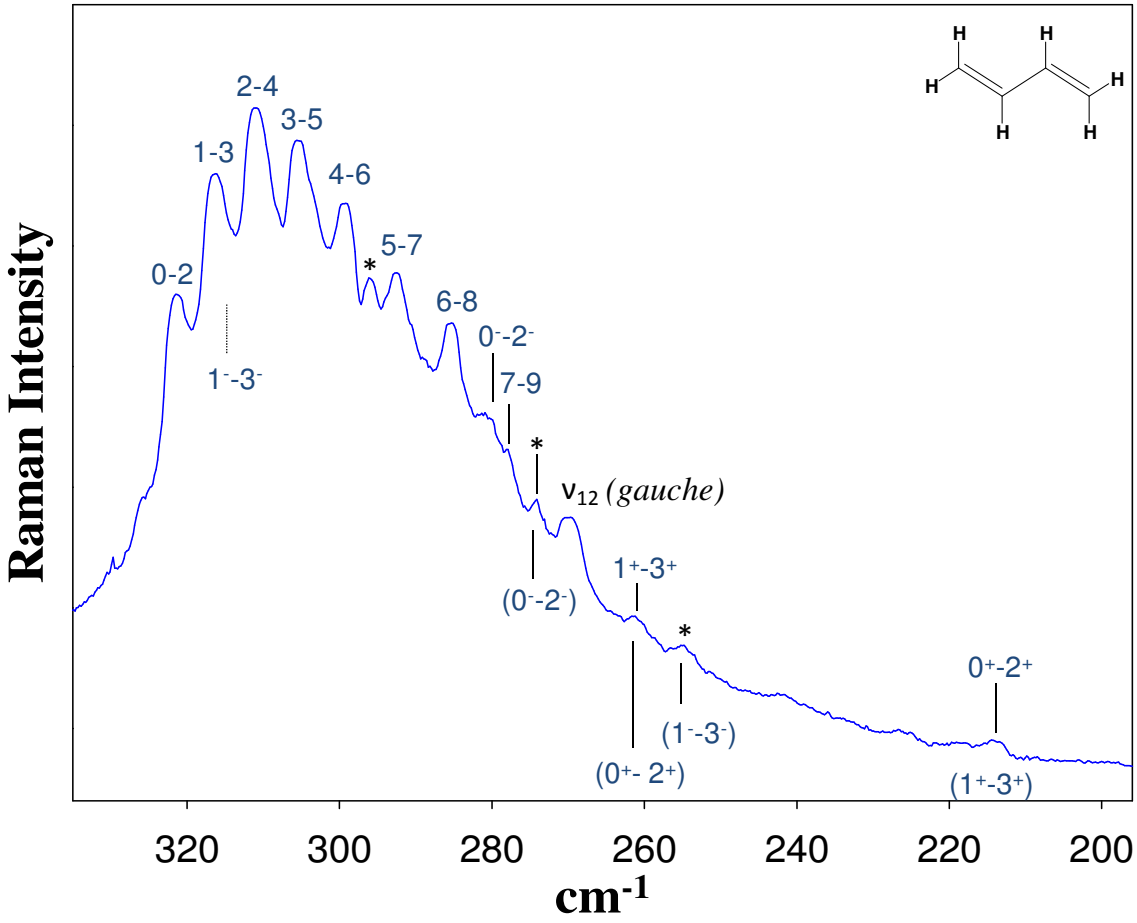

Figure 26. Gas-phase Raman spectrum of the torsional vibration of 1,3-butadiene. * for unassigned bands.

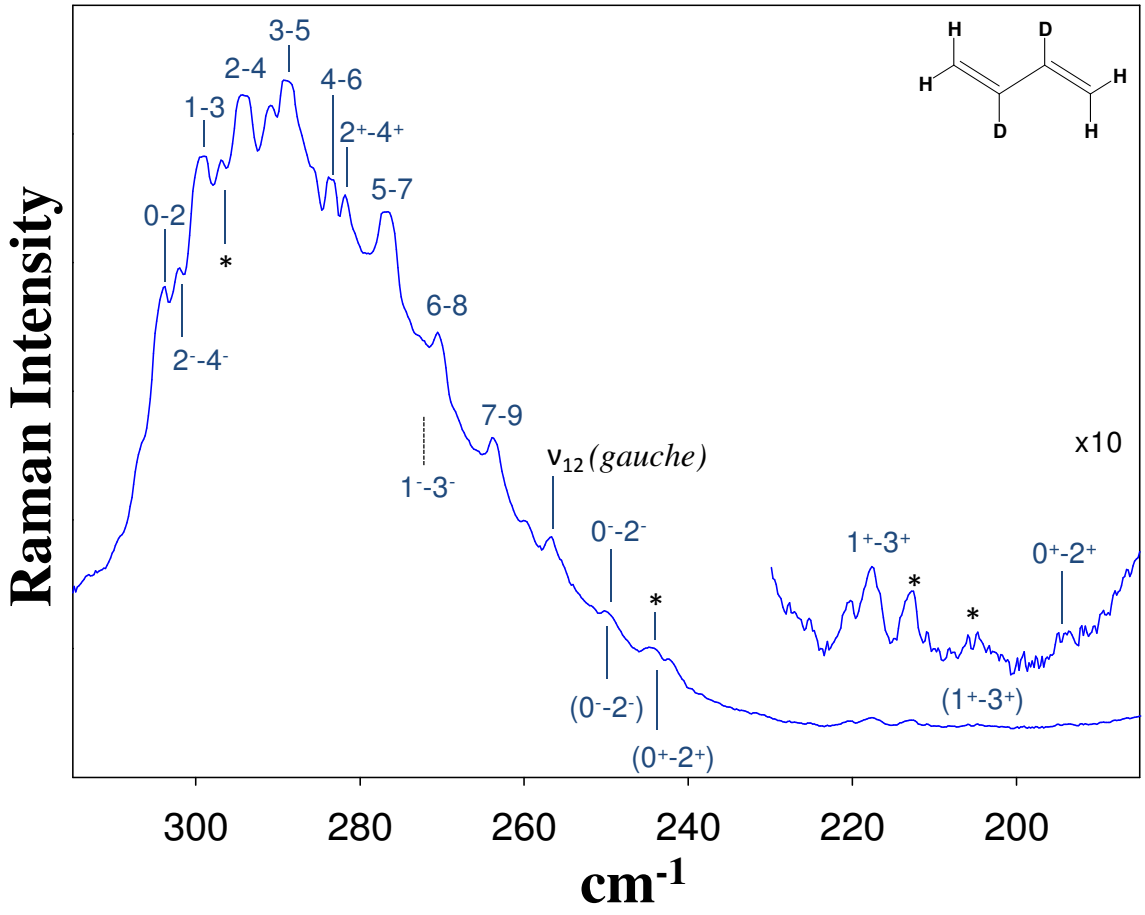

Figure 27. Gas-phase Raman spectrum of the torsional vibration of 1,3-butadiene-2,3-d_2. * for unassigned bands.

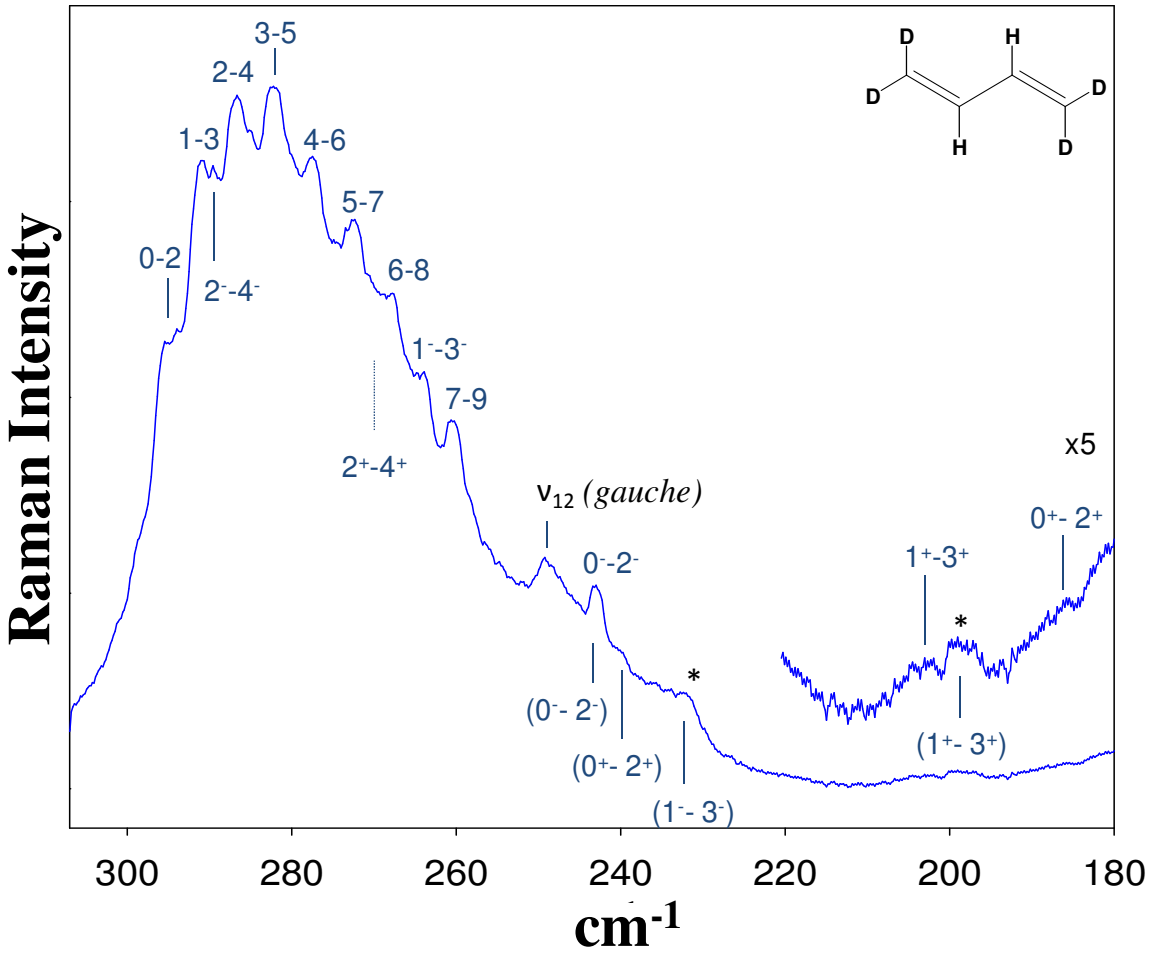

Figure 28. Gas-phase Raman spectrum of the torsional vibration of 1,3-butadiene-1,1,4,4-d_4. * for unassigned bands.

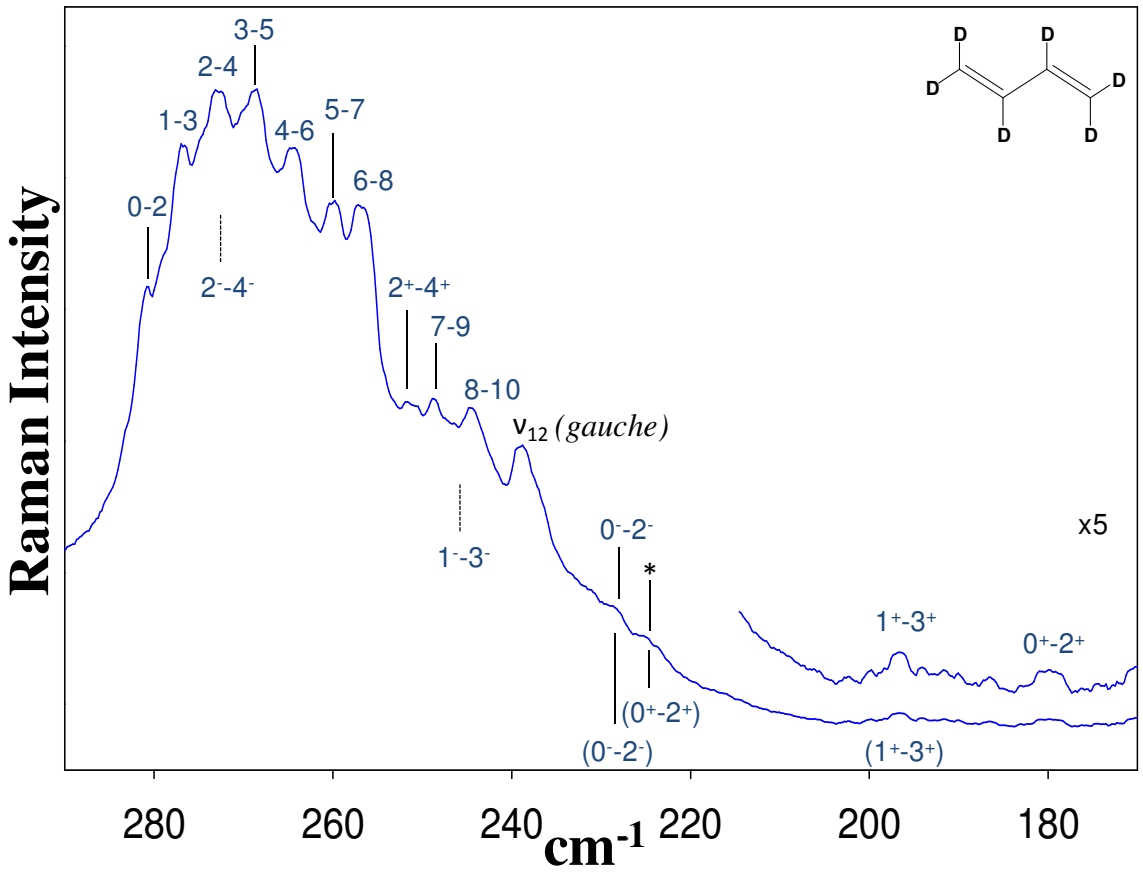

Figure 29. Gas-phase Raman spectrum of the torsional vibration of 1,3-butadiene-d_6. * for unassigned bands.

RESULTS AND DISCUSSION

Figures 26 to 29 show the low-frequency spectra for 1,3-butadiene, and its 2,3-d_2, 1,1,4,4-d_4, and d_6 isotopomers. The assignments for the torsional vibrations are shown in each case.

The primary set of assignments based on the theoretical model is shown without parentheses, while the alternative assignments are shown in parentheses. The *trans* conformation has C_{2h} symmetry, and the torsion about the double bond (ν_{13}) is of symmetry species A_u, for which single quantum transitions are forbidden in the Raman spectrum. However, the allowed double quantum jumps were clearly observed. For the d_0 molecule Figure 26 shows eight transitions for the *trans* conformer, which has non-degenerate quantum states. Also prominent is the ν_{12} angle bending band for the *gauche* conformer at 270.8 cm^{-1}. As Table 28 shows, this frequency is in excellent agreement with the DFT calculated value of 269 cm^{-1}. Moreover, shown in the table, this band is also clearly evident in the Raman spectra of the other isotopomers, and in reasonable agreement with the calculated values, although for the d_4 isotopomer the agreement (249 cm^{-1} observed vs. 231 cm^{-1} calculated) was the poorest. ECR[48] had assigned this band for the d_0 to the $0^-\rightarrow2^-$ (they reported it to be 269.9 cm^{-1}) and the 214.9 cm^{-1} band to $1^+\rightarrow3^+$. In this work, the latter was assigned to the $0^+\rightarrow2^+$ and a band at 282.0 cm^{-1} to the $0^-\rightarrow2^-$ (Figure 26).

Table 28: Calculated and observed ν_{12} bands (cm^{-1}) for *gauche* 1,3-butadiene and its isotopomers

Isotopomer	Observed	Calculated[a]	Lit[b]	Lit[c]
d_0	270.8	269	274	275
d_2	257.4	266	-	-
d_4	249.1	231	236	-
d_6	238.5	230	234	-

[a] B3LYP/6-311++g(d,p); frequencies scaled with a scaling factor of 0.985; this work.
[b] Reference 51.
[c] Reference 49.

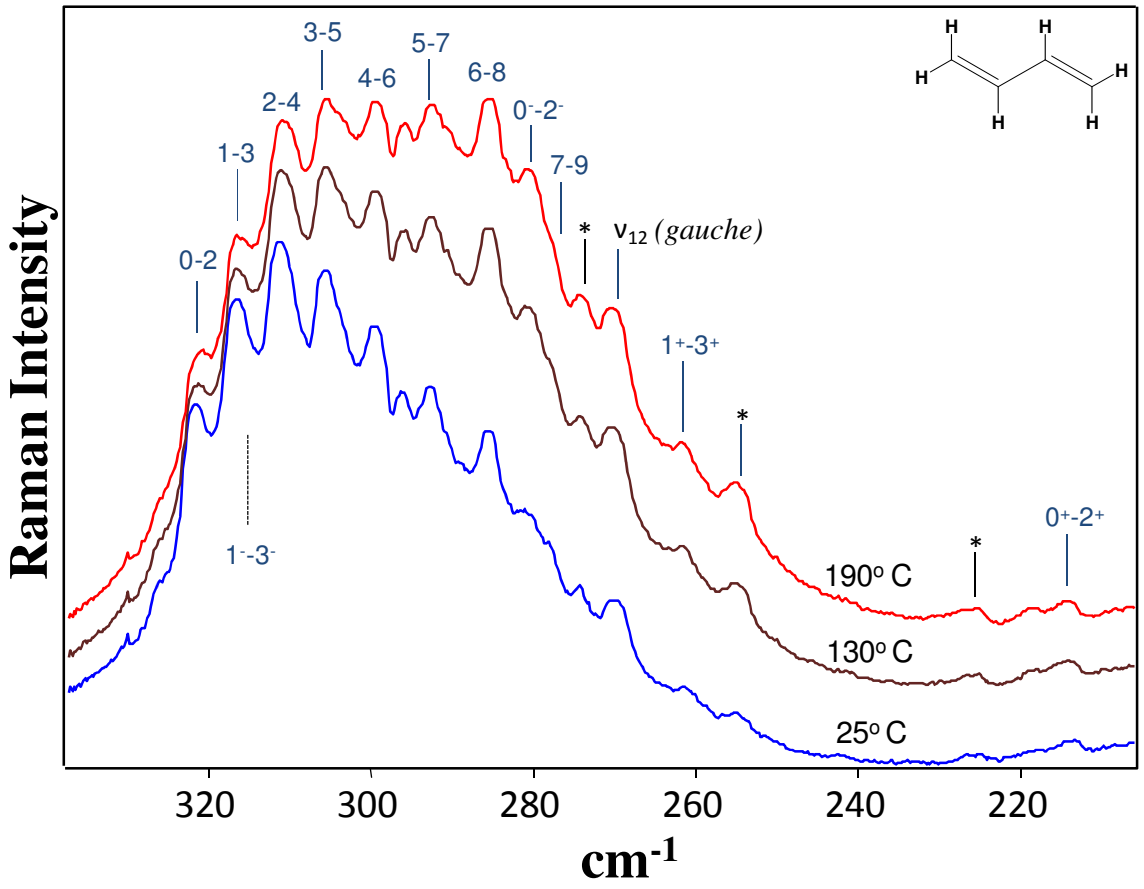

Figure 30. Gas-phase Raman spectrum of the torsional vibration of 1,3-butadiene at different temperatures. * for unassigned bands.

The calculated potential energy function has a considerably lower energy barrier than ECR between the two equivalent *gauche* conformations in agreement with the theoretical potential function. This lower transition state energy primarily accounts for the difference in the consequences of the two assignments. The $1^- \rightarrow 3^-$ transition was calculated by the potential to be at 314.2 cm^{-1}, but this region is obscured by the much stronger bands from the *trans* well. Several bands in the spectra marked by asterisks were not specifically assigned. As discussed above, bands arising from torsional transitions coupled to the excited states of other low-frequency vibrations such as ν_{24} were expected and observed.

Raman spectra at elevated temperatures were collected, and two of these are shown in Figure 30 for the d_0 molecule. It was hoped deconvoluting the spectra would provide accurate intensity measurements, but the broadening of the bands precluded accuracy. Nonetheless, the spectra show that the bands from the higher quantum levels of the *trans* conformer as well as levels of the *gauche* rotamer do increase in relative intensity as expected.

After the adjusted potential energy function for the d_0 molecule was obtained, the function was used as a starting point with the F_n parameters to calculate the frequencies for the isotopomers. As discussed above, the computed F_n values predicted isotopic shifts that were too large. These values were scaled up to best fit the transition frequencies for the *trans* conformer (Table 25).

The results from these calculations are shown as Calc I in Table 29 for the d_2, d_4, and d_6 molecules. As can be seen, the agreement between observed and calculated values is reasonably good, but differences up to several cm^{-1} are present for the *gauche* transitions. Recognizing that vibrational mixing with other modes makes the one-dimensional approximation imperfect, further small refinements were made to the potential energy parameters. These are shown in Table 26. Table 29 (Calc II) then shows the very good agreement between observed and calculated frequencies for the isotopomers after refinement. All values agree within 2 cm^{-1}. What made this investigation particularly difficult was that only about 2% of the molecules[81] were in the *gauche* form at room temperature, so that its Raman bands were very weak. The observation of numerous *gauche* bands throughout the higher frequency Raman spectrum will be reported in Chapter X, which increased in relative intensity as the temperature rose. Thus, the presence of this *gauche* form is evident.

Table 29: Observed and calculated[a] torsional transitions (cm^{-1}) for the isotopomers of 1,3-butadiene

Transition	d_2			d_4			d_6		
	OBS	Calc I	Calc II	OBS	Calc I	Calc II	OBS	Calc I	Calc II
trans-well									
0-1	-	-	-	149.2[b]	148.7	148.7	141.7[b]	137.9	141.2
1-2	-	-	-	146.9[b]	146.6	146.7	-	-	-
0-2	303.8	296.8	303.6	295.3	295.3	295.3	280.9	273.8	280.7
1-3	299.1	292.3	298.7	290.9	291.1	291.3	276.9	270.0	277.1
2-4	294.1	287.7	293.7	286.6	286.7	286.9	273.1	266.0	273.3
3-5	288.9	282.8	288.5	282.1	282.1	282.3	268.9	261.9	269.3
4-6	283.4	277.8	283.1	277.2	277.2	277.4	264.7	257.7	264.9
5-7	276.7	272.6	277.4	272.2	271.9	272.2	260.1	253.3	260.3
6-8	270.4	267.1	271.4	267.5	266.4	266.5	257.2	248.7	255.3
7-9	263.7	261.1	265.1	260.1	260.5	260.5	248.9	243.8	250.0
8-10	-	-	-	-	-	-	244.4	238.7	244.4
gauche-well									
(0^+-2^+)	194	184.8	193.4	186?	184.9	187.4	180	166.9	178.6
(0^--2^-)	250.1	241.6	251.2	243.3	241.8	241.9	228.8	213.0	229.4
(1^+-3^+)	217.7	211.6	217.3	204	212.2	207.1	196.7	178.3	195.1
(1^--3^-)	-	264.1	272.4	263.8	264.3	261.1	obsc[c]	228.5	246.5
(2^+-4^+)	281.7	274.7	281.6	270.0	274.7	268.7	251.3	234.3	252.4
(2^--4^-)	302.0	295.3	303.3	289.2	295.0	290.5	obsc[c]	256.6	273.5

[a] Calculated frequencies based on F_n values from Table 25 and V_n values from Table 26. Cal I is from the V_n values for d_0 without refinement and Cal II is from the adjusted V_n terms for the individual isotopomers.
[b] Reference 42.
[c] Obscured by stronger *trans* band.

Nonetheless, as can be seen in Figures 26 to 29, a few bands (marked by *) that have not been specifically assigned and could have conceivably come from the *gauche* transitions. There are three of these in Figure 26 for the d_0 molecule, including a band of moderate intensity at 296.9 cm^{-1}. This could be a hot band, as discussed, or a difference band such as ν_{22}-ν_{23}. Similarly, the other isotopomers also show such bands, some of which could be from isotopic impurities. This complication is mentioned because an alternative assignment similar to that proposed by ECR cannot be dismissed. In order to evaluate the ECR model, numerous potential energy calculations were carried out starting from their assignments. Observed frequencies and F values were utilized for this purpose, and the 270.8 cm^{-1} band for the d_0 molecule as the $0^- \rightarrow 2^-$ transition were no longer used, since this band is clearly ν_{12} for the *gauche* form. After determining the best set of V_n values for these assignments, the same potential energy function were utilized for the deuterated isotopomers and the F values were adjusted as before to correct for the isotopic shift. As before, the V_n slightly was slightly refined for each of the isotopomers to obtain the best frequency fit. These values are shown in Table 26 for the "Alternative model." The F_n values are the same as for the previous assignment (Table 25).

Table 30: Observed and calculated[a] torsional transitions (cm^{-1}) for the *gauche* conformers of 1,3-butadiene isotopomers (alternate assignments)

Transition	d_0		d_2		d_4		d_6	
	OBS	CALC	OBS	CALC	OBS	CALC	OBS	CALC
0^+-2^+	261.9	263.6	244.4	245.2	240.2	240.2	225.1	227.0
0^--2^-	275.1	273.0	250.1	249.4	243.3	245.6	228.8	228.5
1^+-3^+	214.9	214.2	204	203.6	198	196.8	196.7	196.0
1^--3^-	255.3	255.9	-	231.0	232.2	228.7	-	211.3
2^+-4^+	-	201.9	177	176.9	-	176.8	-	161.6
2^--4^-	(255.3)[b]	256.3	-	226.3	-	227.0	-	202.6

[a] Calculated frequencies based on F_n values from Table 25 and V_n values from Table 26.
[b] Used twice.

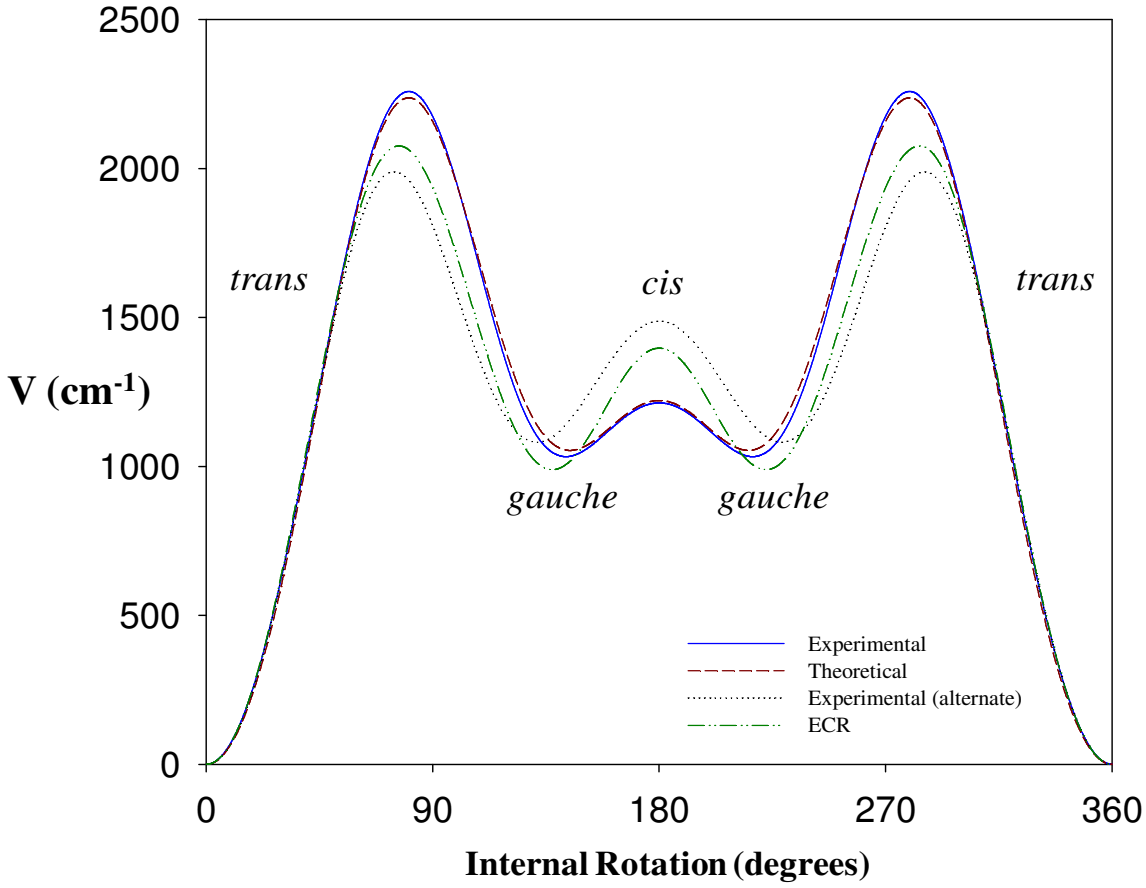

Figure 31. Theoretical and experimental potential energy functions for the internal rotation of 1,3-butadiene. The literature ECR[48] function is also shown.

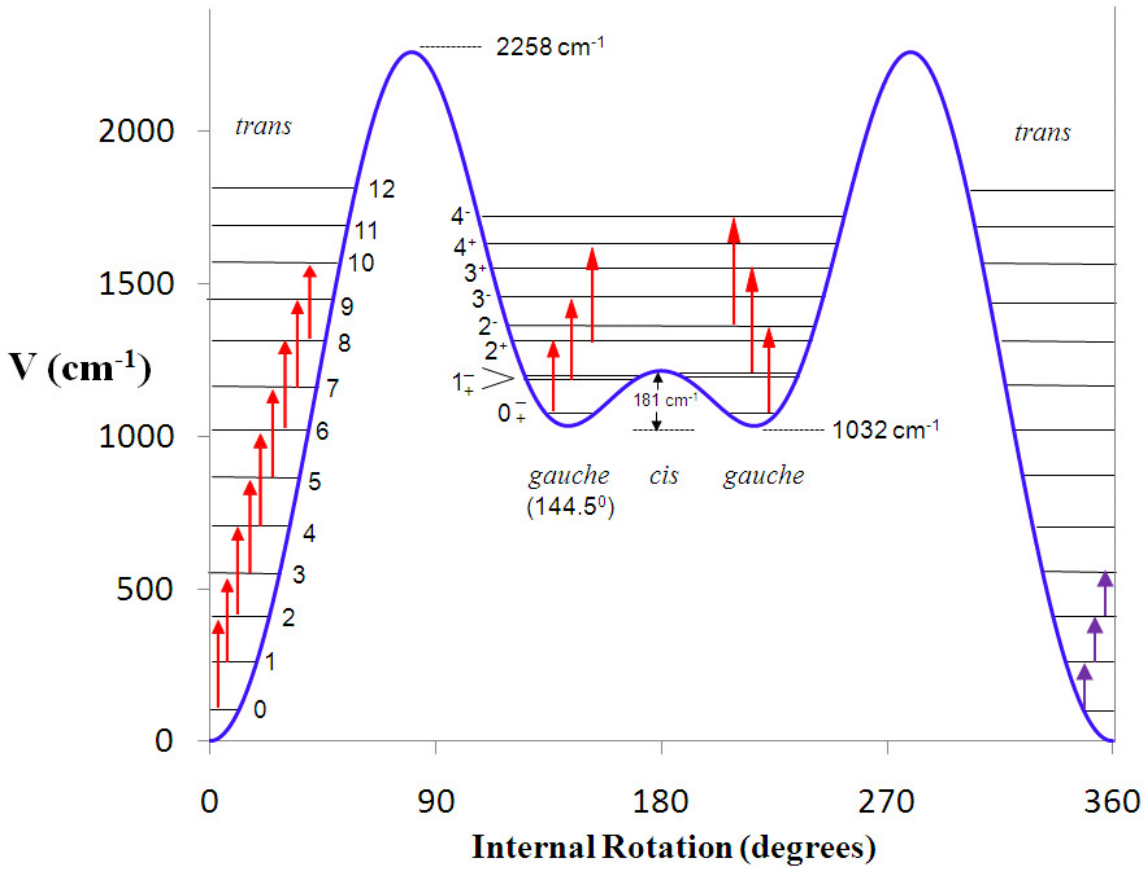

Figure 32. Potential energy function and observed Raman transitions for the internal rotation of 1,3-butadiene. Observed infrared transitions are shown as purple lines.

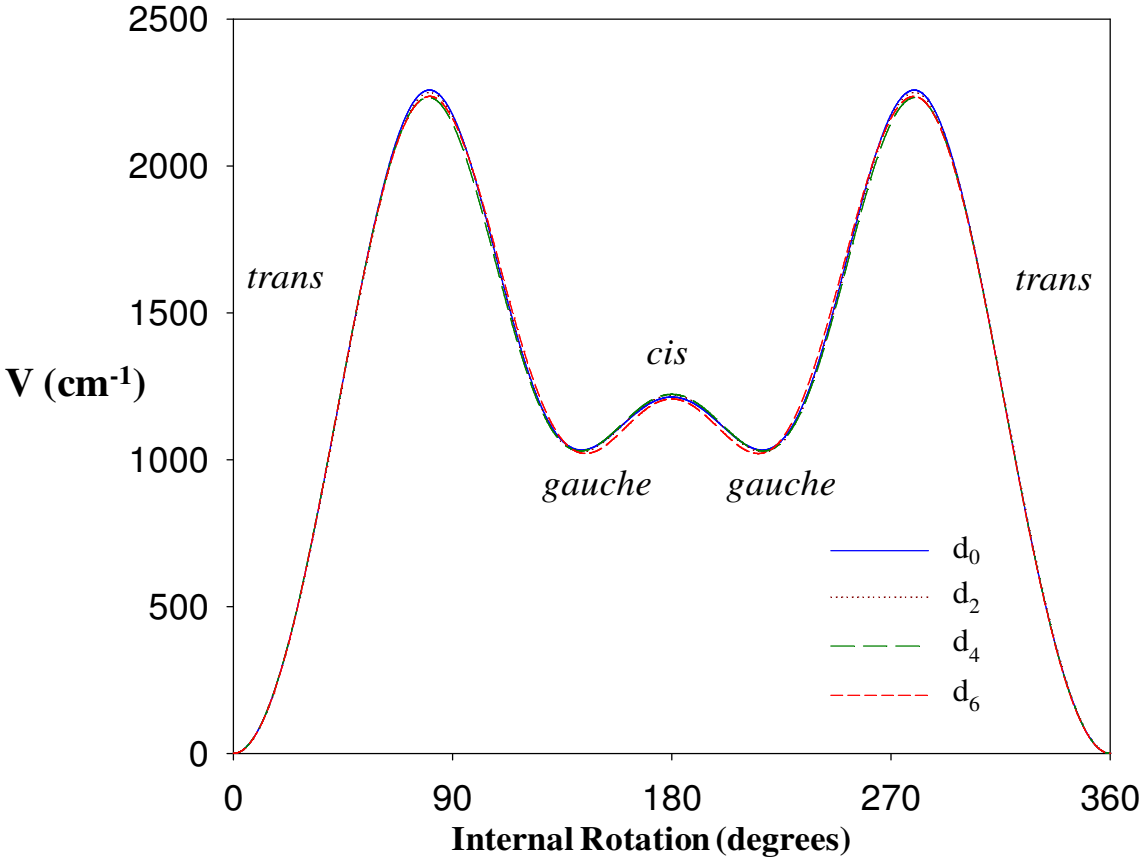

Figure 33. Comparison of potential energy functions determined for 1,3-butadiene isotopomers.

Figures 26 to 29 show the assignments for all of the isotopomers for this alternative model within parentheses. These are summarized in Table 30 for all of the isotopic species. Since the *trans* frequencies, both calculated and observed, were essentially unchanged from those shown in Tables 27 and 29, these are not shown in Table 30. This alternative calculation did just about as well for frequencies as the one described previously. This result was especially true for the d_0 isotopomer. However, what is not evident in the table is that other significant bands in the spectra such as 180 cm^{-1} for the d_6 and 217.7 cm^{-1} for the d_2 are not accounted for, and these are transitions involving the lower energy *gauche* quantum states. On the other hand, this alternative assignment did account for different bands that were not assigned in the other model. Moreover, this model did a somewhat better job of fitting the data for the d_4 isotopomer. What is evident is that the spectra themselves show extra bands, for reasons discussed above, that do not arise from the principal *trans* and *gauche* structures, and this complication makes a definitive choice between these two models difficult.

Figure 31 compares the calculated potential energy curves for the primary and alternative models for the d_0 molecule to the theoretically predicted one.[49] The potential function reported by ECR[48] is also shown. Figure 32 shows the energy levels and observed transitions for the primary model, and Figure 33 compares the very slightly different potential functions for the four isotopomers.

As can be seen in Table 26, which lists the calculated and experimental energy differences between the *trans*, *gauche*, and *cis* forms along with the energy barrier, the *gauche* form is about 1030 cm^{-1} (2.94 kcal/mol) higher in energy than the *trans*

conformer and the *cis* saddle point is about 180 cm^{-1} (0.51 kcal/mol) higher. The corresponding theoretically calculated values are 1054 cm^{-1} (3.01 kcal/mol) and 167 cm^{-1} (0.48 kcal/mol). The agreement is remarkably good. The *trans* to *gauche* barrier is about 2250 cm^{-1} (6.43 kcal/mol) as compared to the *ab initio* value of 2236 cm^{-1} (6.39 kcal/mol).

Table 26 also presents the data for the alternative model, and Figure 34 shows the potential function and transitions for this case. As is evident, the primary difference between these assignments is that for this alternative model the barrier of about 405 cm^{-1} (1.16 kcal/mol) at the *cis* configuration is considerably higher. For this model the *gauche* form is calculated to be about 1080 cm^{-1} (3.09 kcal/mol) higher in energy than the *trans* form in agreement with high level theoretical calculations. However, the disagreement with the theoretical calculations in the height of the *cis* barrier leads to a preference for the first model.

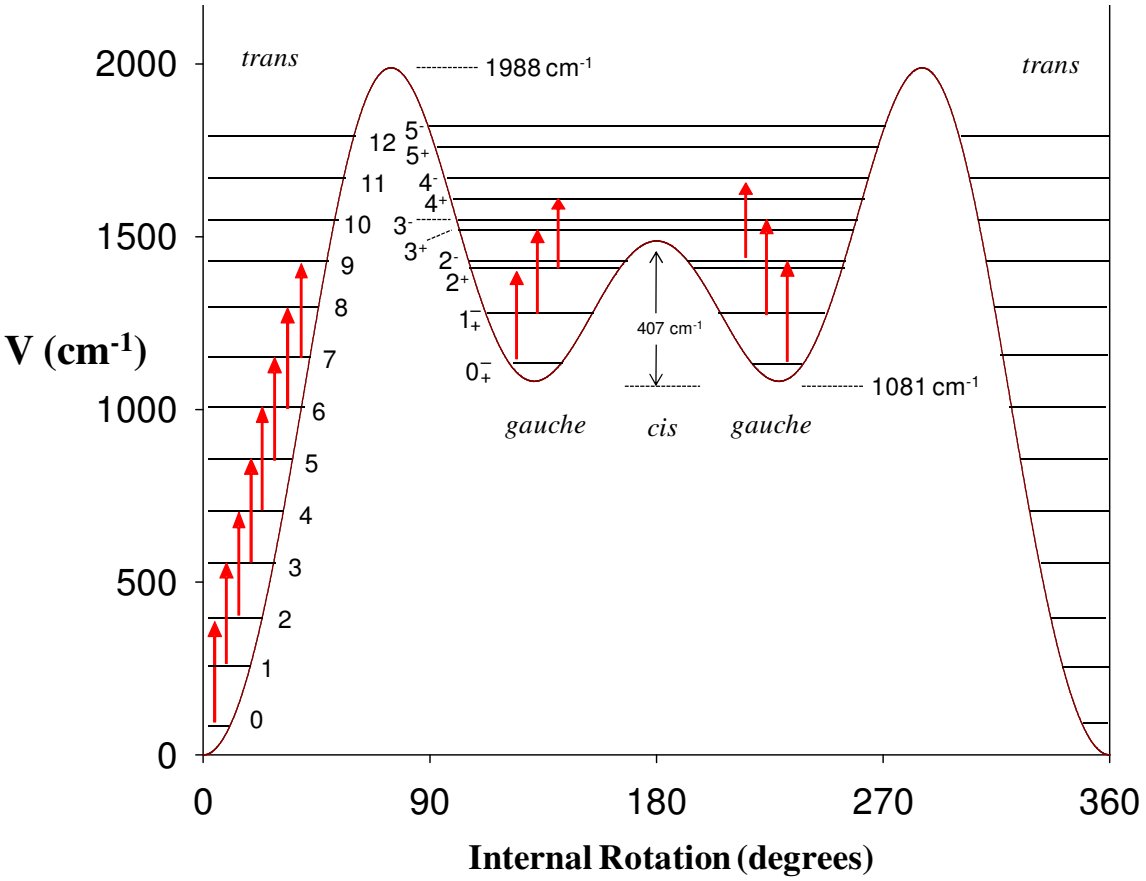

Figure 34. Potential energy function and observed Raman transitions for the internal rotation of 1,3-butadiene (alternate model).

CONCLUSION

Because of the low abundance at room temperature of *gauche*-1,3-butadiene (~2%), it was difficult to obtain gas-phase Raman spectra good enough to accurately determine the internal rotation potential energy function in the vicinity of the *gauche* rotamer. In this work, the results from hundreds of hours of Raman scans in the low-frequency region were presented for 1,3-butadiene-d_0, and its 2,3-d_2, 1,1,4,4-d_4, and d_6 isotopomers. Structural results from high level *ab initio* calculations were used to obtain reliable internal rotor constants F_n. *Ab initio* calculations were used to obtain a starting point for the calculation of the one-dimensional potential energy function for internal rotation. The experimental results agreed remarkably well with the theoretical calculations, but less well with earlier calorimetric[40] and NMR studies,[41] which reported lower energy differences between the two conformations. Nonetheless, the alternative assignment presented in this study cannot be dismissed. This alternative agrees less well with the theoretical computations, but it is not significantly worse in accounting for the observed spectra. The abundance of bands not directly associated with transitions within the one-dimensional potential energy function and from sources such as isotopic impurities and hot bands greatly complicated the analyses and thus has made a clear choice of the correct assignment difficult.

CHAPTER IX

GAS-PHASE SPECTRA OF COMBINATION AND HOT BANDS ASSOCIATED WITH THE TORSIONAL VIBRATION OF *TRANS*-1,3-BUTADIENE AND ITS DEUTERATED ISOTOPOMERS*

INTRODUCTION

An extensive analysis of the low-frequency, gas-phase Raman spectra for the torsional (internal rotation) vibration of 1,3-butadiene and its 2,3-d_2, 1,1,4,4-d_4, and d_6 isotopomers was reported in Chapter VIII. From the data, a one-dimensional periodic potential energy function governing the internal rotation vibration between the *trans* and *gauche* rotamers was determined. The *trans* conformation was the dominant species, whereas the *gauche* conformation lied 1030 cm^{-1} higher in energy and was present in about 2% abundance at room temperature. The full gas-phase Raman spectra of these isotopomers were also investigated in search of additional evidence for the elusive *gauche* rotamer. In the process, the presence of many combination bands and hot bands were discovered involving the torsional vibration, all of which were analyzed to rule out additional evidence for the torsional mode of the *gauche* rotamer. Torsional hot bands previously have been observed in infrared spectra of 1,3-butadiene.[50]

---

* Reprinted with permission from "Gas-Phase Raman Spectra of Combination and Hot Bands Associated with the Torsional Vibrations of *Trans*- 1,3-Butadiene and its Duterated Isotopomers" by Boopalachandran, P.; Craig, N.; Laane, J., 2011. *J. Mol. Spectrosc. A*, In press, by Elsevier.

From hot bands in infrared and Raman spectra, it is possible to determine how the torsional frequencies change in vibrational excited states and thus to evaluate how much interaction occurs between the torsional motion and other vibrational modes. The results for the Raman spectra are presented here. Because vapor-phase Raman spectra are inherently weak, and because the combination bands and hot bands are much weaker still, the observations presented here are quite unusual. However, Laane's group previously reported Raman combination bands involving the ring-puckering motion for cyclopentene,[82] silacyclobutane,[83] and 1,3-disilacyclobutane.[84] In none of the cases they observed nearly as many combinations and hot band series as reported here. Much of the new detail can be attributed to improved instrumentation, including a 6 watt laser and a CCD detector cooled with liquid nitrogen. In previous work, combination band series were observed in the infrared spectra of molecules with internal rotations[85] or out-of plane ring vibrations.[85-90]

EXPERIMENTAL

Samples of 1,3-butadiene-d_0, and its 2,3-d_2, 1,1,4,4-d_4, and d_6 isotopomers were flame-sealed at a pressure of 1 atm. Butadiene was supplied by Aldrich, the 2,3-d_2 species was supplied by CDN Isotopes (99% D, Quebec, Canada), and the 1,1,4,4-d_4 and d_6 species were supplied by Cambridge Isotope Laboratories (98% D). Purity of the samples was confirmed by infrared spectroscopy prior to sealing the samples in the cells.

Raman spectra of gas-phase 1,3-butadiene and its isotopomers were recorded for samples with simplified optics at various temperatures sealed in specially designed glass

cells which were previously described in Chapter II.[91] A Jobin-Yvon U-1000 spectrometer equipped with a liquid nitrogen-cooled CCD detector was used to collect the spectra. The 532 nm line of a frequency-doubled Nd:YAG Coherent Verdi-10 laser was used and generally operated at 6 watts of power. Spectral regions spanning 60 cm^{-1} were typically collected over periods of 4 to 6 hours so that many hundreds of individual spectra could be averaged. The resolution of the spectra was 0.7 cm^{-1}.

SPECTROSCOPIC RESULTS

Table 31 lists the vibrations of the *trans* rotamer of 1,3-butadiene-d_0, and its 2,3-d_2, 1,1,4,4-d_4, and d_6 isotopomers that are relevant to the investigation of the combination bands and hot bands. The Raman values for the Raman active B_g modes are from this work while the infrared active A_u and B_u wavenumbers are from the literature.[42,51-53] The torsional levels in the excited states of ν_{10}, ν_{12}, $2\nu_{12}$, $\nu_{10} + \nu_{12}$, $\nu_{15} + \nu_{16}$, and $\nu_{23} + \nu_{24}$ among the four isotopomers were observed. (The $\nu_{23} + \nu_{24}$ state is in Fermi resonance with ν_6 for the d_0 species.) It was quite remarkable to get observable transitions to the overtone state of ν_{12} and the $\nu_{10} + \nu_{12}$ and $\nu_{15} + \nu_{16}$ combination states. Since the ν_{10} and ν_{12} states were of A_u symmetry, the observed combination bands also involved single quantum changes of ν_{13}, which was also of A_u symmetry, so the transitions were $A_g \rightarrow A_g$ or $A_u \rightarrow A_u$. Because of this symmetry requirement, hot bands appeared in the Raman spectrum without an accompanying fundamental transition, which appeared in the infrared spectrum.

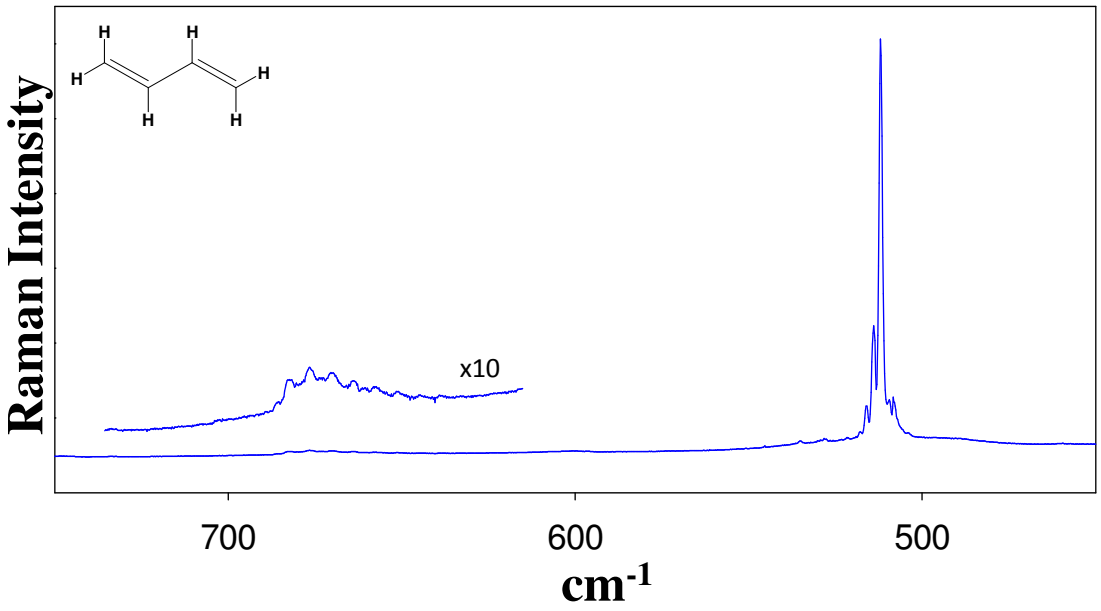

Figure 35. Raman spectrum showing the relative intensity of the $\nu_{12} + \nu_{13}$ sum bands as compared to the ν_9 fundamental band.

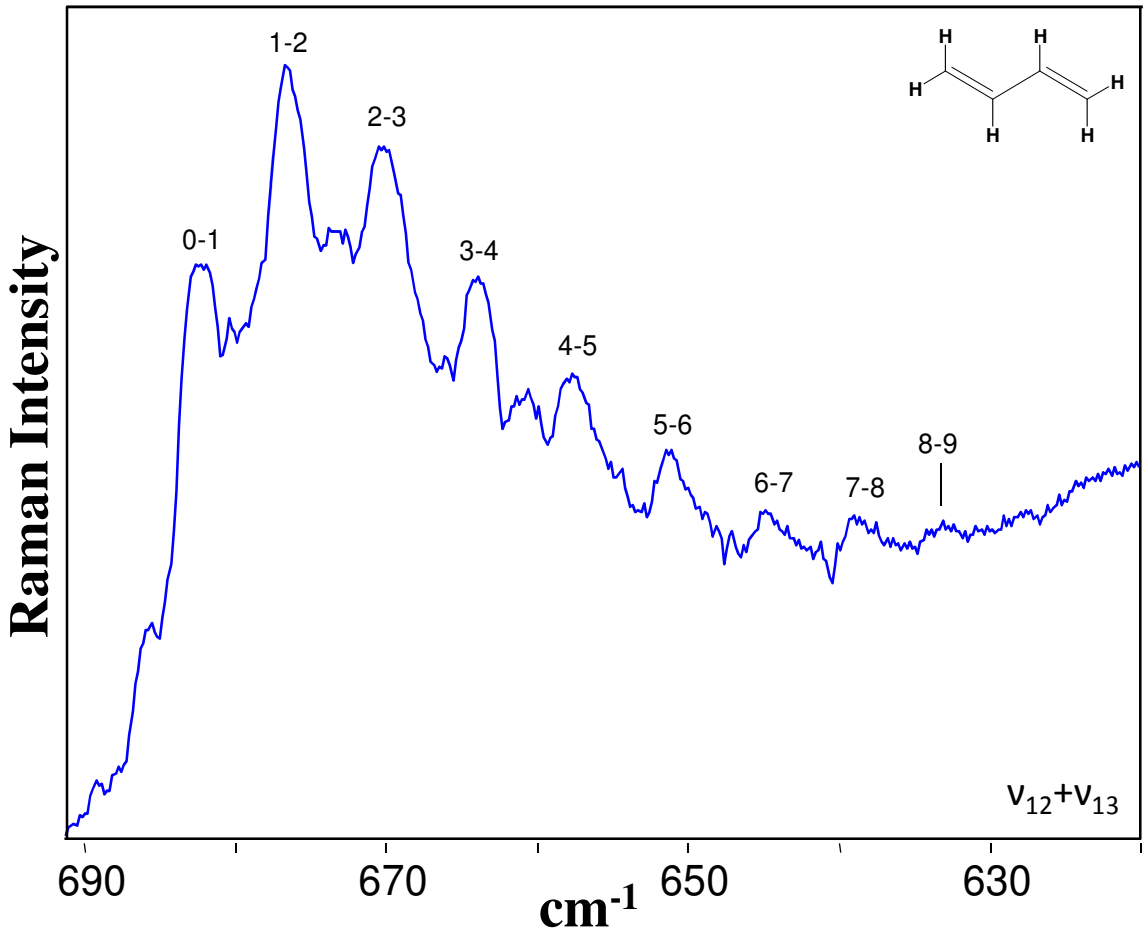

Figure 36. Raman spectrum of the 1,3-butadiene $\nu_{12} + \nu_{13}$ sum bands originating from ν_{12} = 524.6 cm^{-1}. The quantum numbers for the ν_{13} mode in the lower and upper states are shown.

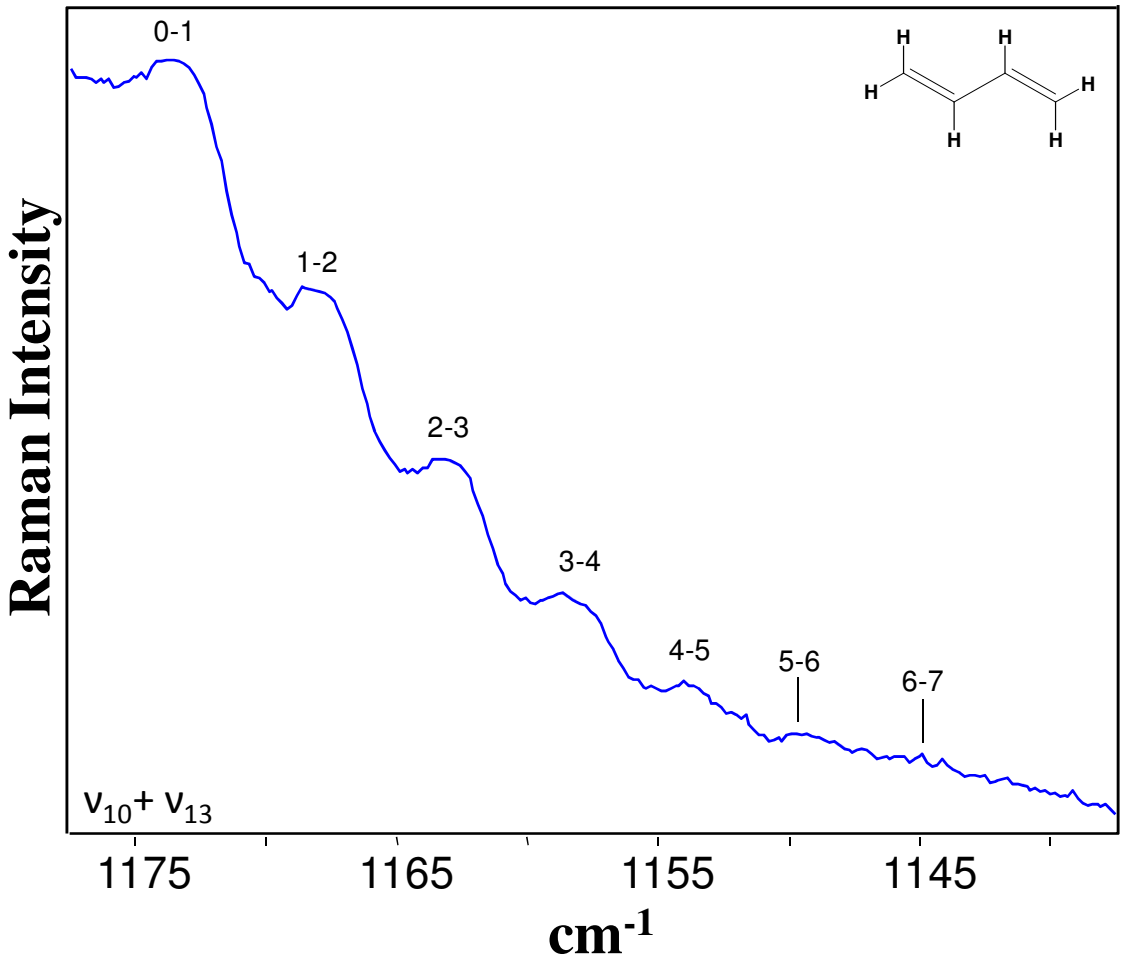

Figure 37. Raman spectrum of the 1,3-butadiene ν_{10} + ν_{13} sum bands originating from ν_{10} = 1013.8 cm^{-1}.

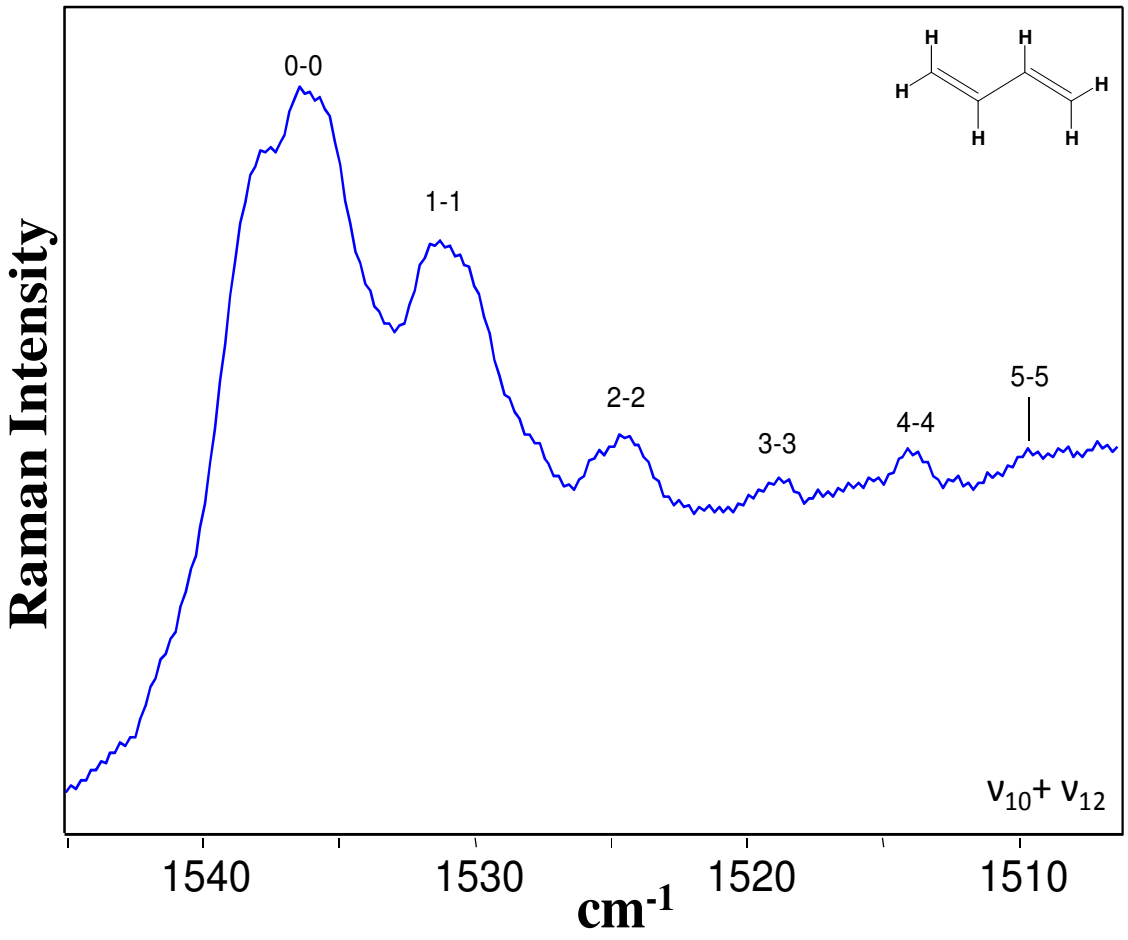

Figure 38. Raman spectrum of the 1,3-butadiene hot band transitions to the $\nu_{10} + \nu_{12}$ vibrational excited state.

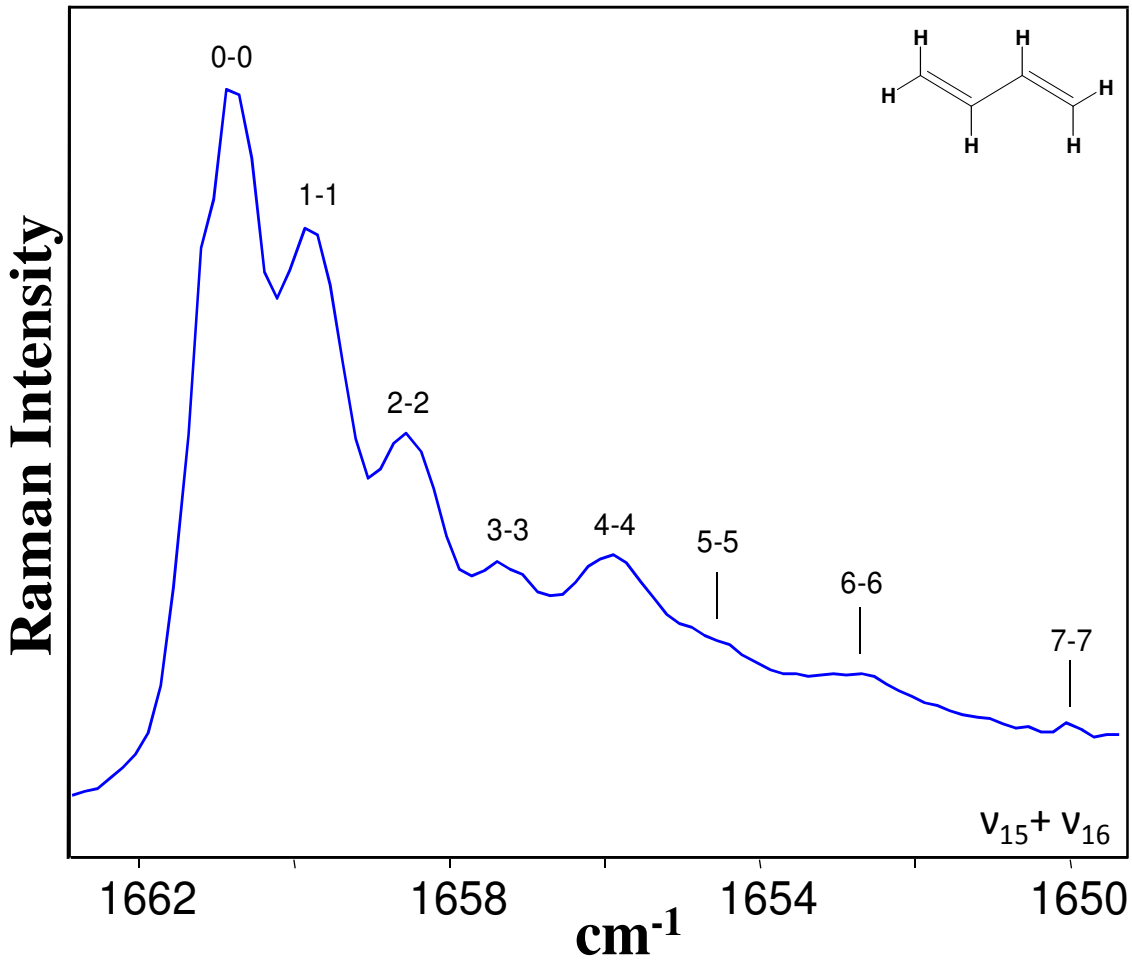

Figure 39. Raman spectrum of the 1,3-butadiene hot band transitions to the $\nu_{15} + \nu_{16}$ vibrational excited state.

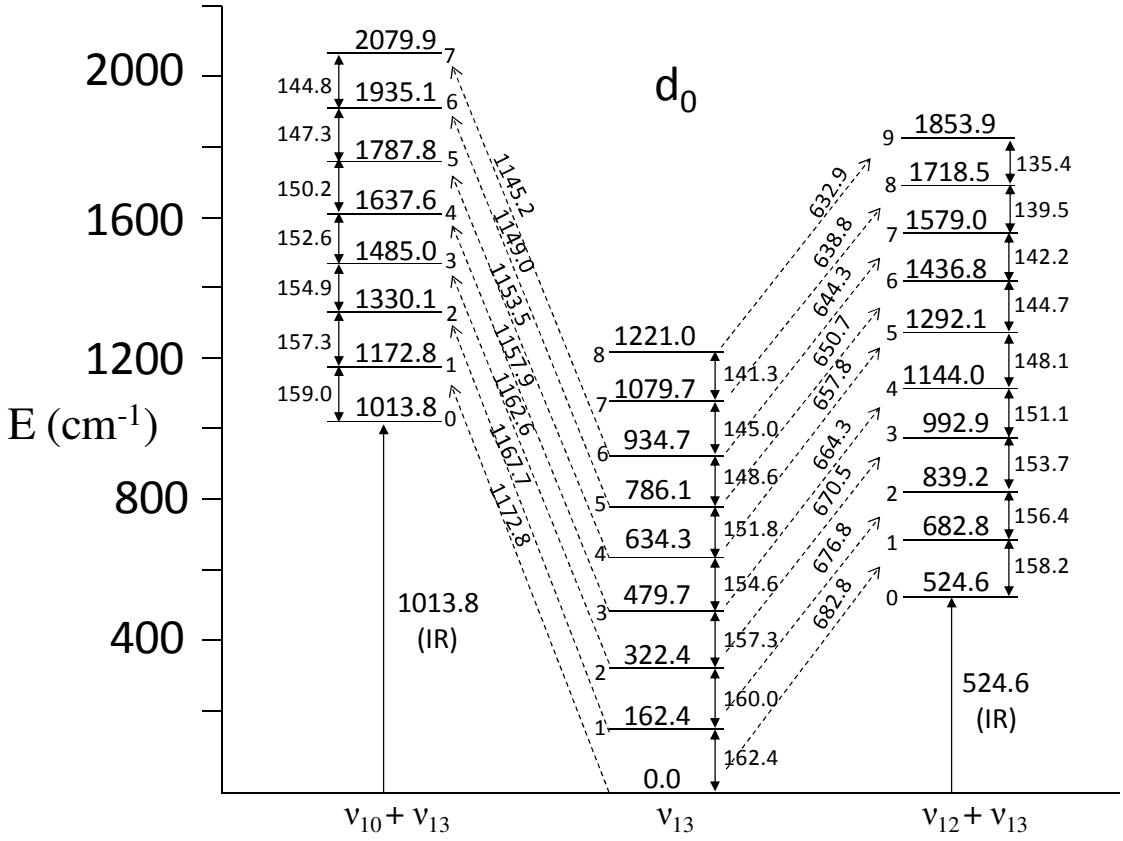

Figure 40. Energy level diagram for 1,3-butadiene showing transitions to the $\nu_{10} + n\nu_{13}$ and $\nu_{12} + n\nu_{13}$ excited states.

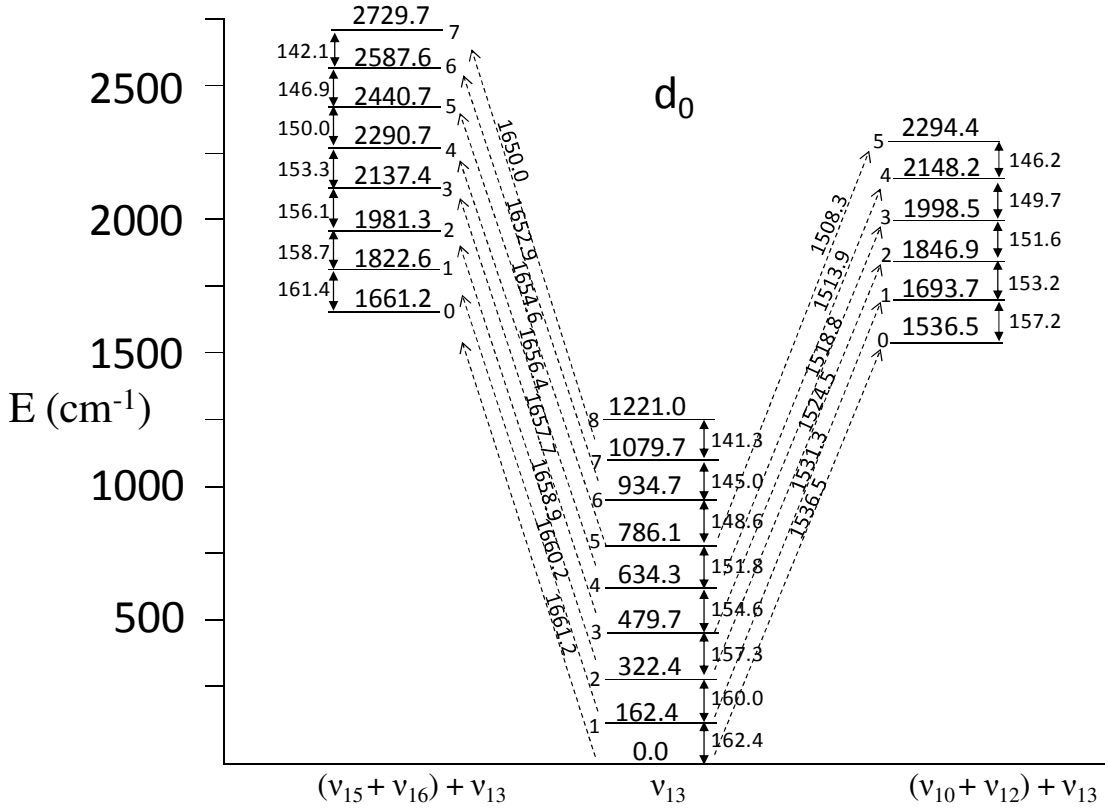

Figure 41. Energy level diagram for 1,3-butadiene showing transitions to the $\nu_{15} + \nu_{16}$ and the $\nu_{10} + \nu_{12}$ excited states.

Table 31: Vibrations[a] of *trans*-1,3-butadiene-d_0 and its isotopomers associated with hot bands and combinations

C_{2h}	Approximate Description	d_0	d_2	d_4	d_6
A_u	υ_{10} C-H (C-D) wag	1013.8	852.0	955.4	736
	υ_{12} CH_2 (CD_2) twist	524.6	480.3	396.8	381
	υ_{13} torsion	162.4	152.6	149.2	141.7
B_g	υ_{15} CH_2 (CD_2) wag	918	913	726.1	702
	υ_{16} CH_2 (CD_2) twist	748	742	606.1	603
B_u	υ_{23} CH_2 (CD_2) rock	990	840	813	730
	υ_{24} C=C-C def	299	287	258	252

[a] Vibrational frequencies of A_u and B_u are taken from References 42, 51-53.

Table 32: Analysis of hot bands (cm^{-1}) of *trans*-1,3-butadiene-d_0 for transitions involving the torsional vibration (υ_{13})

		υ_{12}		υ_{10}			$\upsilon_{23} + \upsilon_{24}$
Transition[a]	υ_{13}[b]	ν_{obs}[c]	υ_{obs}[c] - υ_{12}	ν_{obs}[d]	ν_{obs}[d] - υ_{10}	Transition[a]	ν_{obs}[e]
0-1	162.4	682.8	158.2	1172.8	159.0	0-0	1298
1-2	160.0	676.8	152.2	1167.7	153.9	1-1	1301
2-3	157.3	670.5	145.9	1162.6	148.8	2-2	1307
3-4	154.6	664.3	139.7	1157.9	144.1	3-3	1311
4-5	151.8	657.8	133,2	1153.5	139.7	-	-
5-6	148.6	650.7	126.1	1149.0	135.2	-	-
6-7	145.0	644.3	119.7	1145.2	131.4	-	-
7-8	141.3	638.8	114.2	-	-	-	-

[a] Quantum numbers for the υ_{13} torsional vibrational states.
[b] Reference 92.
[c] $\nu_{obs} = \nu_{12} + (n+1)\nu_{13} - n\nu_{13}$.
[d] $\nu_{obs} = \nu_{10} + (n+1)\nu_{13} - n\nu_{13}$.
[e] $\nu_{obs} = \nu_{23} + \nu_{24} + (n+1)\nu_{13} - n\nu_{13}$.

Table 33: Energy level spacings (cm^{-1}) of υ_{13} of *trans*-1,3-butadiene-d_0 in vibrational excited states

Spacing	υ_{13} [a]	Vibrationally Excited States				
		υ_{12}	υ_{10}	$\upsilon_{10} + \upsilon_{12}$	$\upsilon_{15} + \upsilon_{16}$	$\upsilon_{23} + \upsilon_{24}$
0-1	162.4	158.2	159.0	157.2	161.4	165
1-2	160.0	156.4	157.3	153.2	158.7	166
2-3	157.3	153.7	154.9	151.6	156.1	162
3-4	154.6	151.1	152.6	149.7	153.3	-
4-5	151.8	148.1	150.2	146.2	150.0	-
5-6	148.6	144.7	147.3	-	146.9	-
6-7	145.0	142.2	144.8	-	142.1	-

[a] Reference 92.

Torsional combination bands in the infrared involving ν_{12} and ν_{15} have previously been studied,[50] but here the observed transitions were g↔u and Δv was only 1 for a single mode. Fifteen combination band or hot band series involving the ν_{13} torsional mode were observed for butadiene and three of its isotopomers.

1,3-Butadiene-d_0

Figures 35 and 36 show the Raman sum bands for the $\nu_{12} + \nu_{13}$ series for 1,3-butadiene-d_0. Figure 35 displays the huge intensity difference between the sum bands near 680 cm^{-1} as compared to the band for the ν_9 (A_g) angle bending mode at 512 cm^{-1}. Figure 36 displays these bands on an expanded scale. The $\nu_{10} + \nu_{13}$ sum band series is shown in Figure 37. Figures 38 and 39 show the hot band series to the $\nu_{10} + \nu_{12}$ and $\nu_{15} + \nu_{16}$ combination states, respectively. Figures 40 and 41 show the energy level diagrams and the observed transitions for the four bands. As noted above, the quantum number of ν_{13} must change along with the quantum number of ν_{10} or ν_{12} in Figure 40. Because the $\nu_{10} + \nu_{12}$ and $\nu_{15} + \nu_{16}$ combinations have A_g symmetry, the quantum number of ν_{13} does not change in the hot band transitions in Figure 41. A stack of ν_{13} levels adds to a single excitation of ν_{10}, ν_{12}, $\nu_{10} + \nu_{12}$, and $\nu_{15} + \nu_{16}$.

Table 32 gives the frequencies of the bands and the frequency separations from the band origins for $\nu_{12} + \nu_{13}$ and $\nu_{10} + \nu_{13}$. Table 33 uses this data as well as other hot band data to present the ν_{13} energy spacings for the ν_{10}, ν_{12}, $\nu_{10} + \nu_{12}$, $\nu_{15} + \nu_{16}$, and $\nu_{23} + \nu_{24}$ vibrationally excited states. As can be seen, the differences between ν_{13} levels in the excited states are smaller than for the corresponding differences in the torsion itself,

indicating that the torsional potential becomes somewhat less stiff in the excited states. An exception is the $\nu_{23} + \nu_{24}$ excited state where the energy spacings for ν_{13} were slightly larger. Differences in the magnitudes of the spacings (about 1 cm^{-1} for $\nu_{15} + \nu_{16}$ up to 7 cm^{-1} for $\nu_{10} + \nu_{12}$) reflect the degree of interaction between the ν_{13} torsion and these excited vibrational states.

A particularly interesting case for 1,3-butadiene-d_0 is that for the Fermi doublet near 1290 cm^{-1}, as shown in Figure 42. *Ab initio* calculations predicted ν_6, the A_g C-H wag, to be in the 1285-1291 cm^{-1} range.[54] The $\nu_{23} + \nu_{24}$ sum band, also of A_g symmetry, was expected near 990+299 = 1289 cm^{-1}. Fermi resonance pushed the levels apart to 1278 and 1298 cm^{-1}. Furthermore, hot bands arising from excited ν_{13} torsional levels can be seen in Figure 42 for the higher frequency component of the resonance pair. This component, which is an approximately equal mixture of ν_6 and $\nu_{23} + \nu_{24}$, has been arbitrarily labeled $\nu_{23} + \nu_{24}$. The wavenumbers of the hot bands and the differences are listed in Tables 32 and 33, respectively. The 1278 cm^{-1} band also seems to show some hot band structure, but the spacing seems too tight as compared to the higher frequency component of the Fermi resonance.

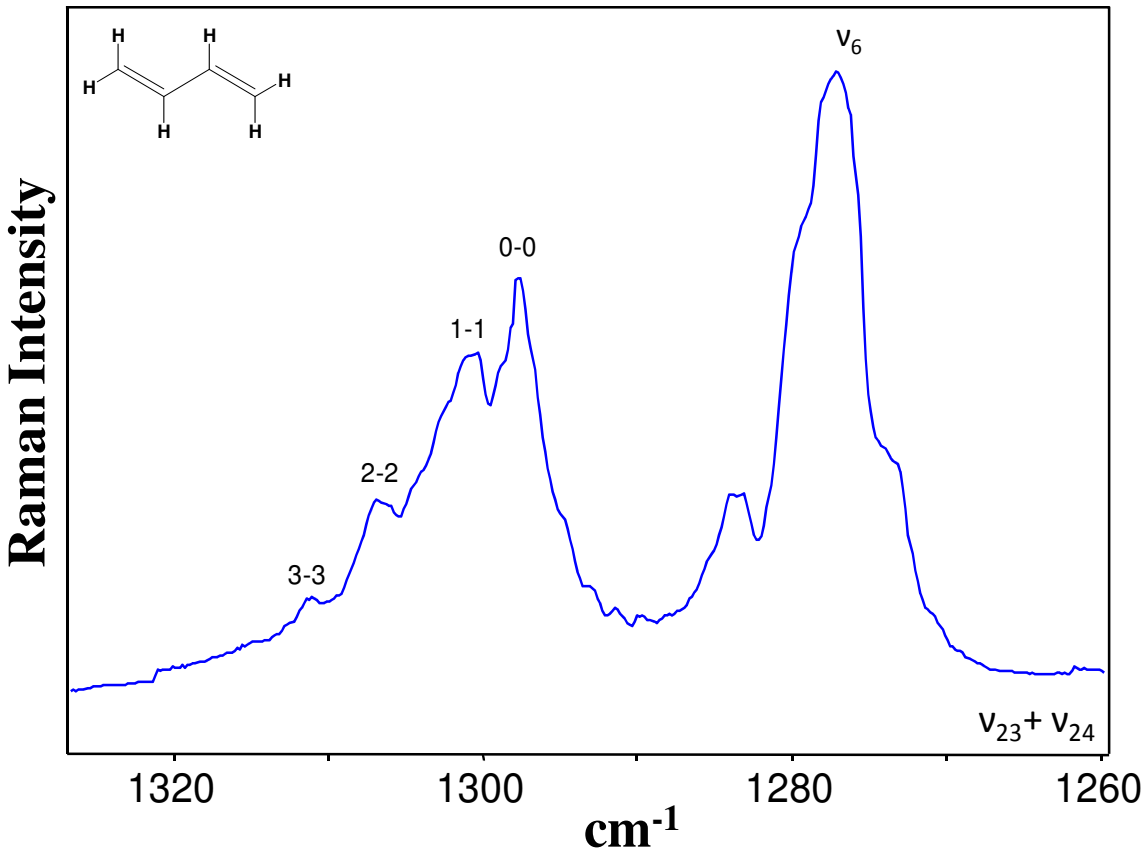

Figure 42. Raman spectrum of the Fermi doublet and hot bands for 1,3-butadiene.

1,3-Butadiene-2,3-d_2

For the d_2 species, as for the d_0 species, sum bands to the ν_{12} and ν_{10} excited states are observed (Figures 43 and 44, respectively), in which the quantum number changes for ν_{13} as well as for ν_{12} and ν_{10}. The energy diagram in Figure 45 shows the levels and the connecting transitions for these two instances. Figure 46 displays the hot band series associated with the $2\nu_{12}$ overtone. The corresponding transitions were not observed for the d_0 species. Because $2\nu_{12}$ has A_g symmetry, the quantum number of ν_{13} did not change in this hot band series. Figure 47 shows the corresponding energy scheme and transitions. The other hot band series observed for the d_2 species were for $\nu_{10} + \nu_{12}$ and $\nu_{15} + \nu_{16}$ combinations, which have A_g symmetry. Figures 48 and 49 present the observed spectra. The energy level diagram is in Figure 50. As can be seen, the ν_{13} quantum number did not change for the $A_g \rightarrow A_g$ or $A_u \rightarrow A_u$ transitions. Tables 34 and 35 summarize the data.

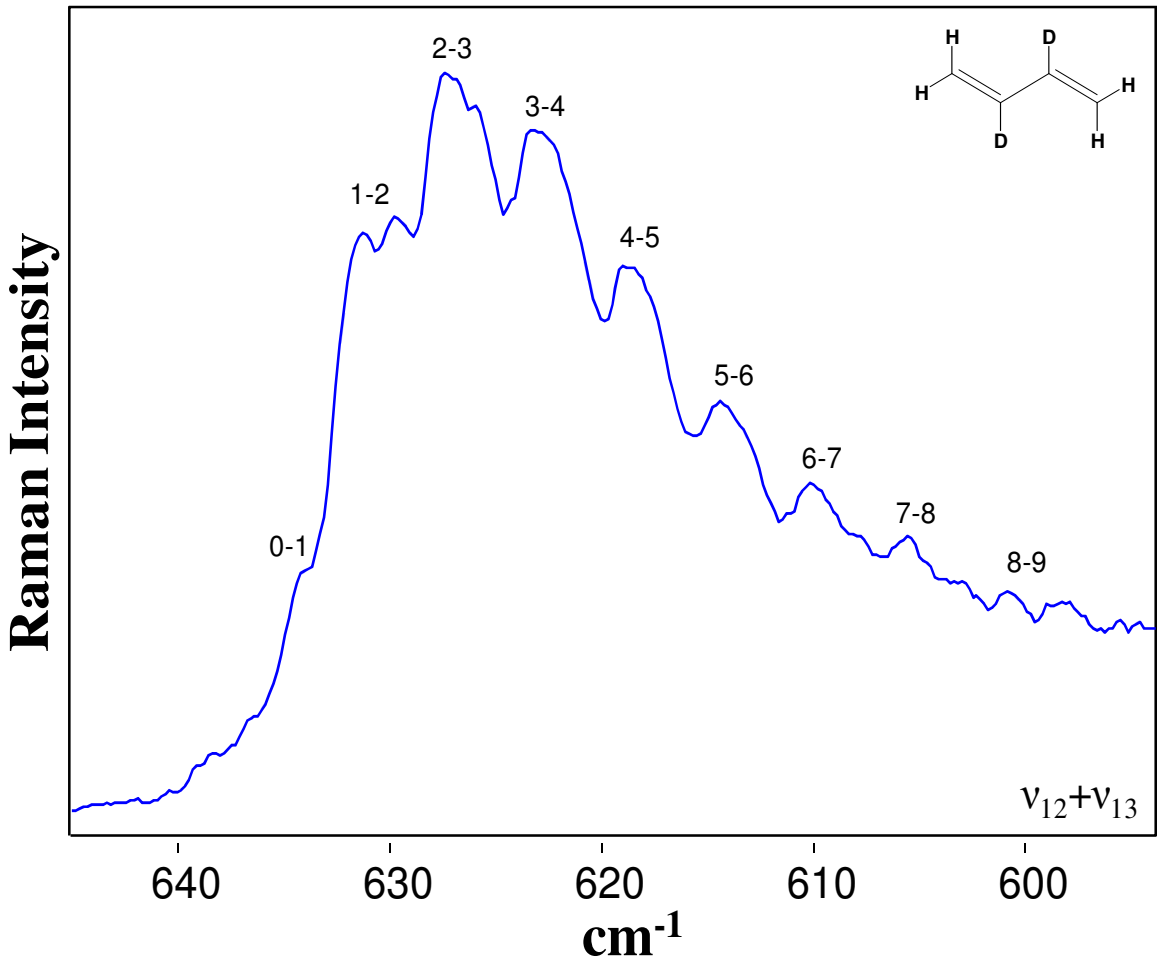

Figure 43. Raman spectrum of the 1,3-butadiene-2,3-d_2 ν_{12} + ν_{13} sum bands originating from ν_{12} = 480.3 cm^{-1}.

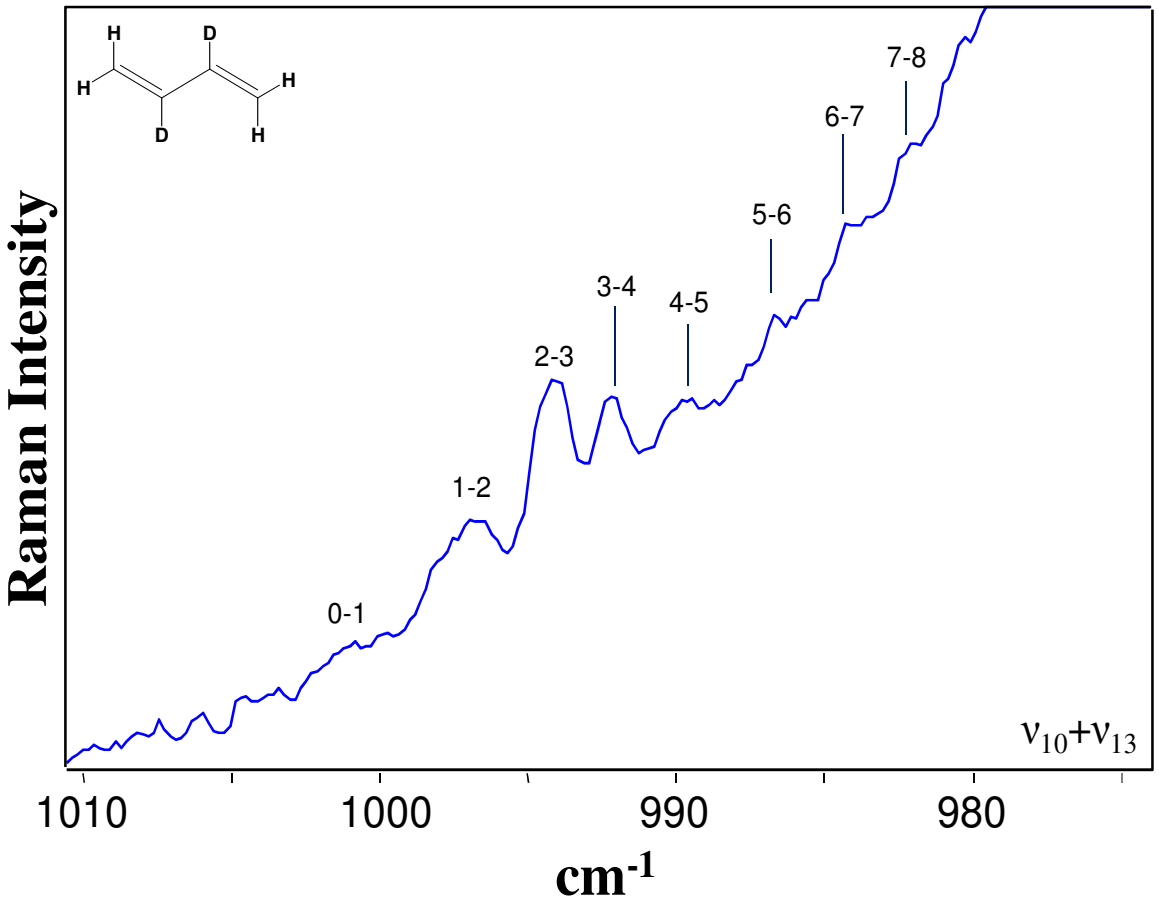

Figure 44. Raman spectrum of the 1,3-butadiene-2,3-d_2 $\nu_{10} + \nu_{13}$ sum bands originating from ν_{10} = 852.0 cm^{-1}.

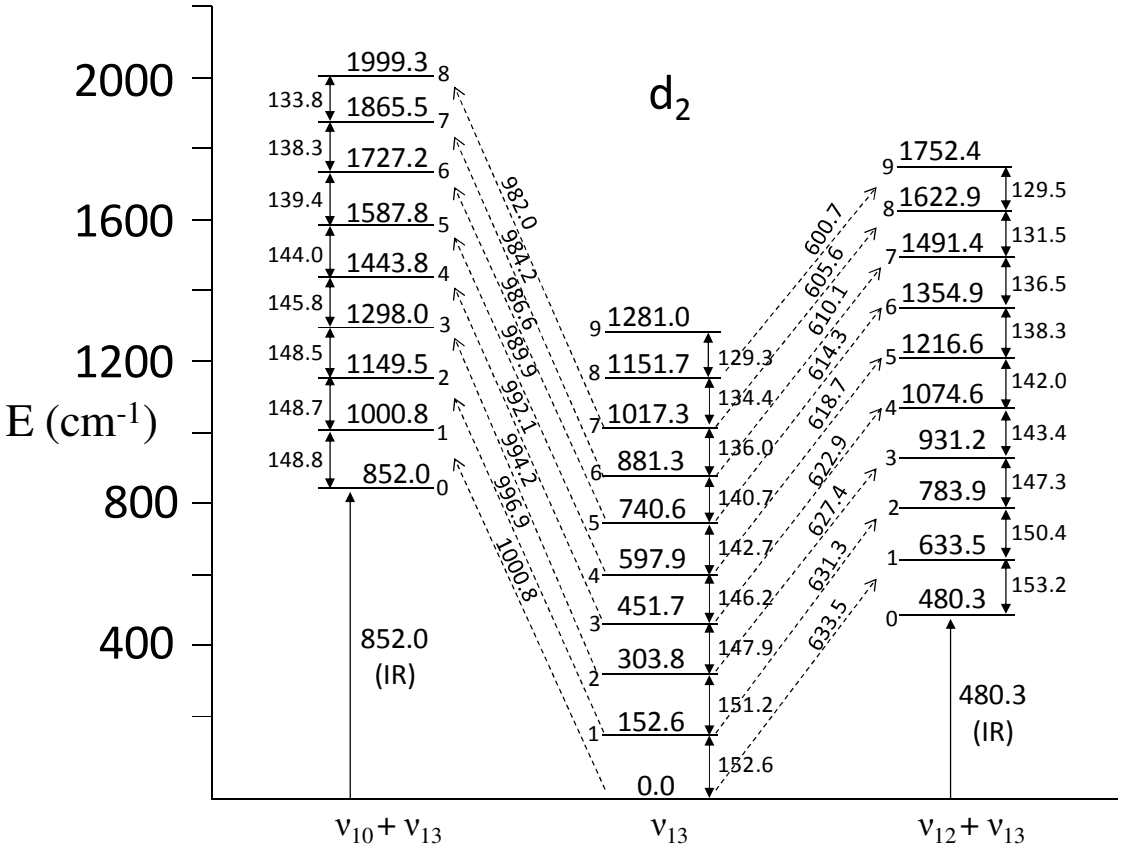

Figure 45. Energy level diagram for 1,3-butadiene-2,3-d_2 showing transitions to the ν_{10} and ν_{12} excited states.

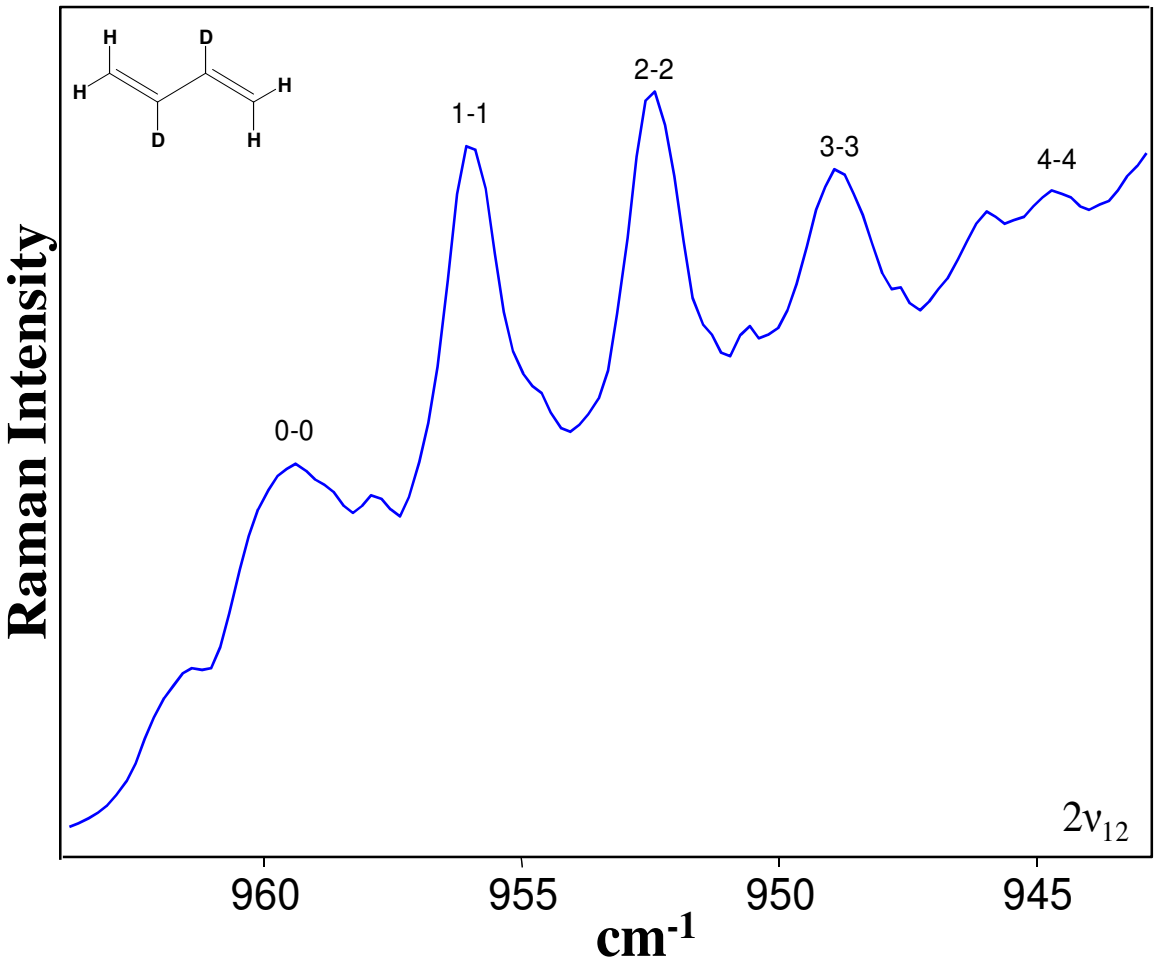

Figure 46. Raman spectrum of the 1,3-butadiene-2,3-d_2 hot band transitions to the $2\nu_{12}$ excited state.

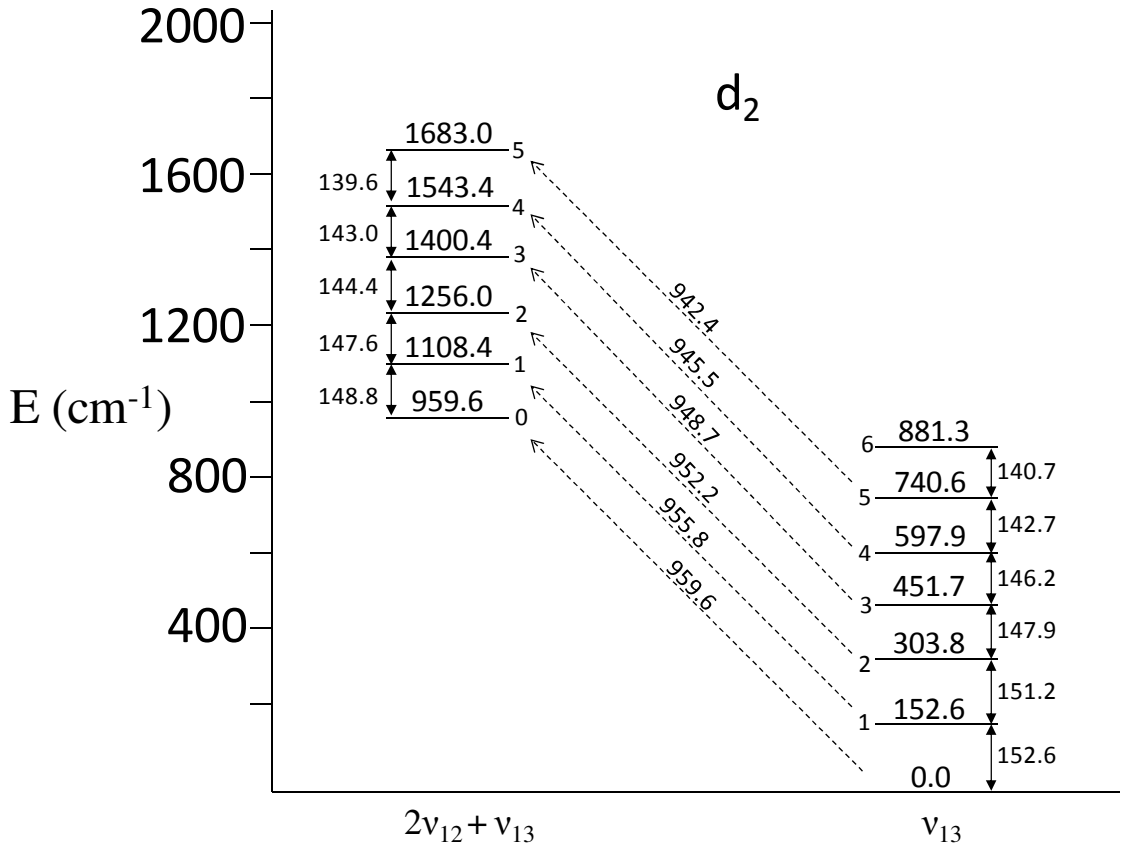

Figure 47. Energy level diagram for 1,3-butadiene-2,3-d_2 showing hot band transitions to the $2\nu_{12}$ excited states.

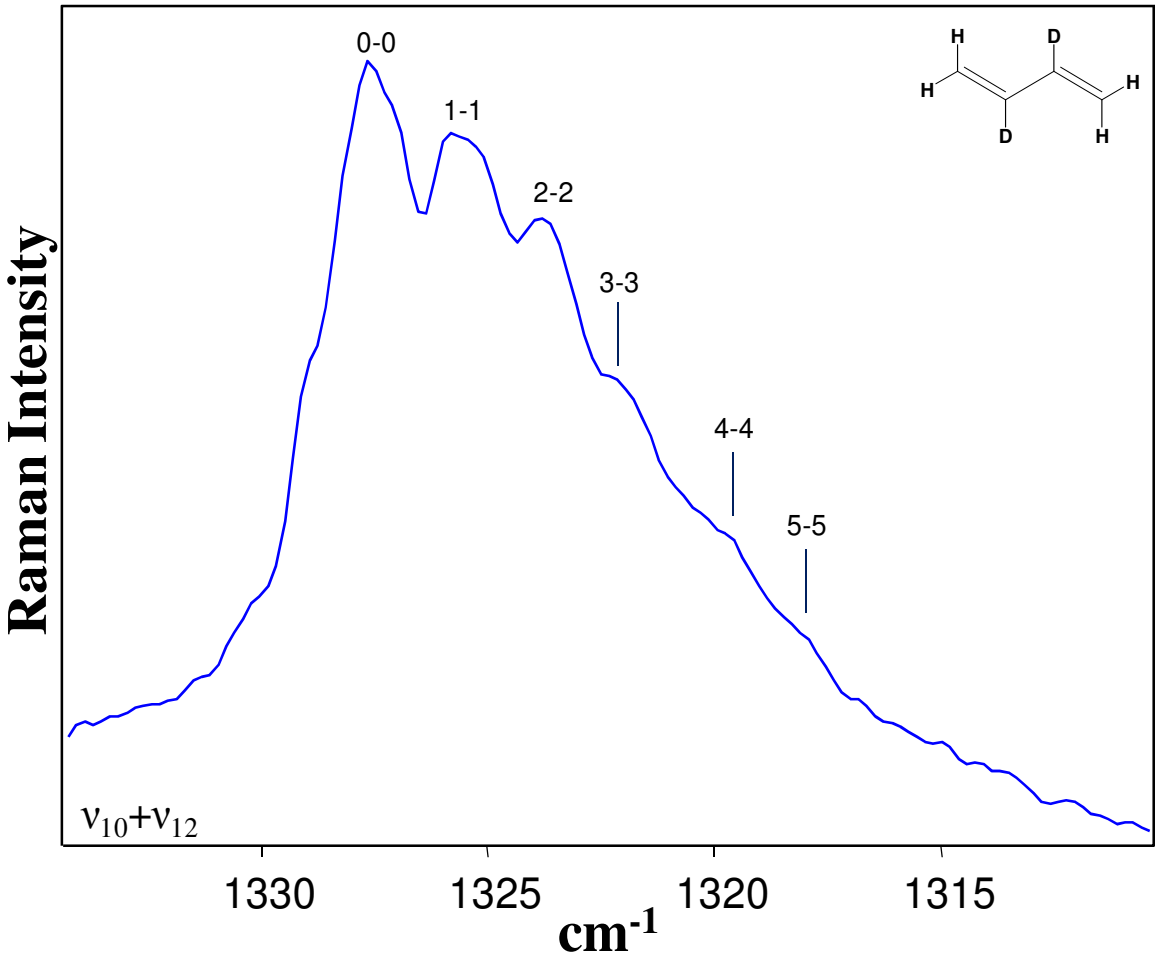

Figure 48. Raman spectrum of the 1,3-butadiene-2,3-d_2 hot band transitions to the ν_{10} + ν_{12} vibrational excited state.

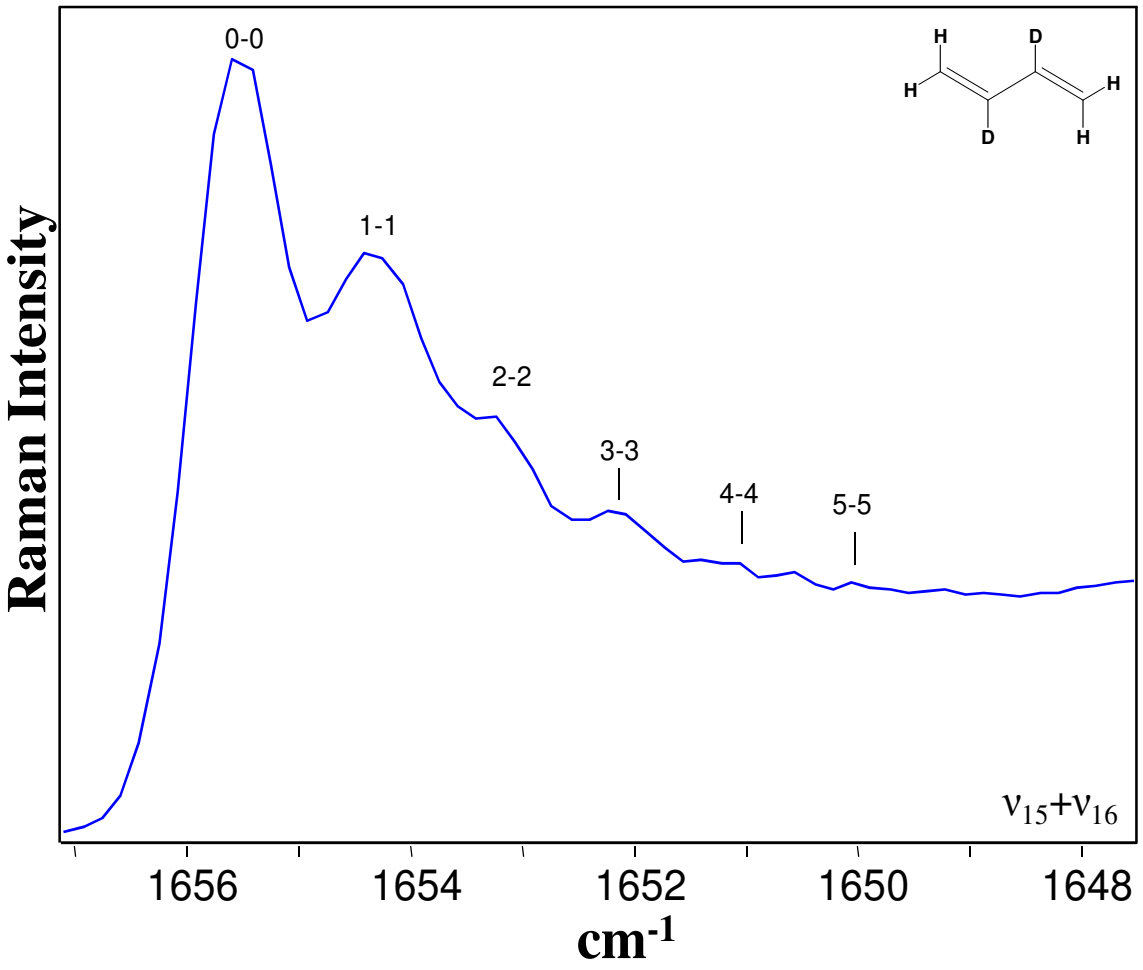

Figure 49. Raman spectrum of the 1,3-butadiene-2,3-d_2 hot band transitions to the ν_{15} + ν_{16} vibrational excited state.

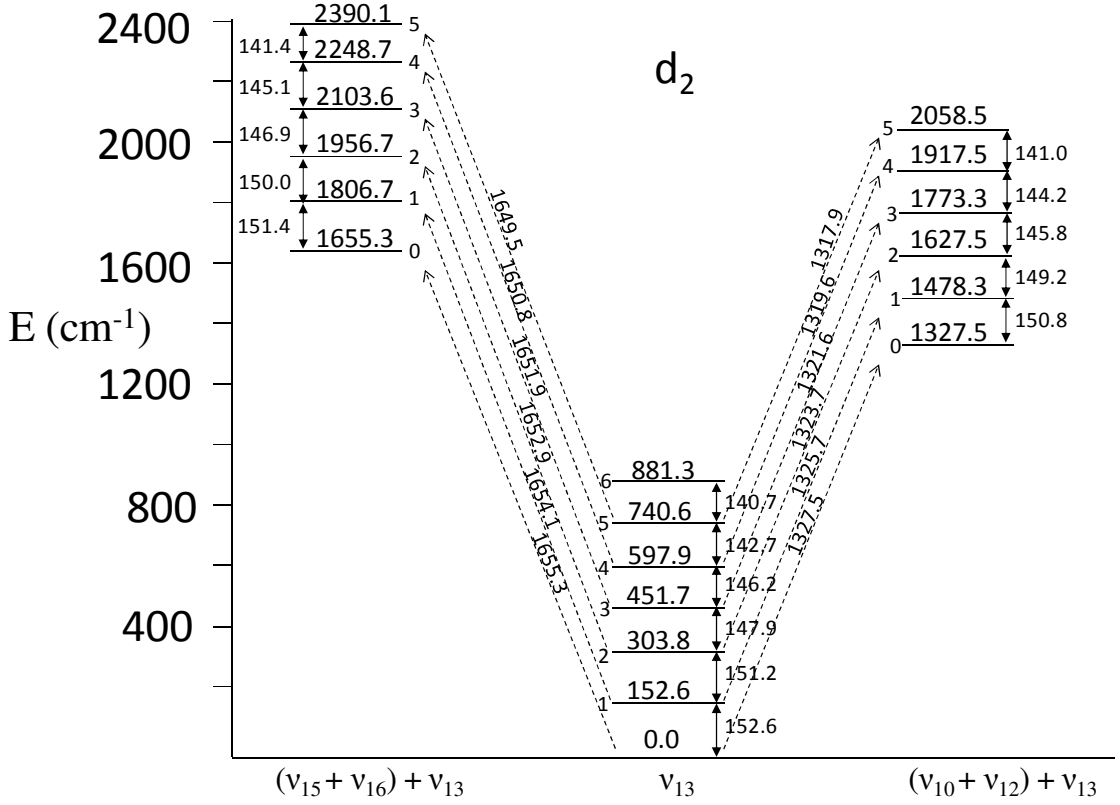

Figure 50. Energy level diagram for 1,3-butadiene-2,3-d_2 showing transitions to the $\nu_{15} + \nu_{16}$ and the $\nu_{10} + \nu_{12}$ excited states.

Table 34: Analysis of hot bands (cm^{-1}) of *trans*-1,3-butadiene-2,3-d_2 involving the torsional vibration (υ_{13})

		υ_{12}		υ_{10}			$2\upsilon_{12}$
Transition[a]	υ_{13}[b]	ν_{obs}[c]	ν_{obs}[c] - υ_{12}	ν_{obs}[d]	ν_{obs}[d] - υ_{10}	Transition[a]	ν_{obs}[e]
0-1	152.6	633.5	153.2	1000.8	148.8	0-0	959.6
1-2	151.2	631.3	151.0	996.9	144.9	1-1	955.8
2-3	147.9	627.4	147.1	994.2	142.2	2-2	952.2
3-4	146.2	622.9	142.6	992.1	140.1	3-3	948.7
4-5	142.7	618.7	138.4	989.9	137.9	4-4	945.5
5-6	140.7	614.3	134.0	986.6	134.6	5-5	942.4
6-7	136.0	610.1	129.8	984.2	132.2		
7-8	134.4	605.6	125.3	982.0	130.0		
8-9	129.3	600.7	120.4	-	-		

[a] Quantum numbers for the υ_{13} torsional vibrational states.
[b] Reference 92.
[c] $\nu_{obs} = \nu_{12} + (n+1)\nu_{13} - n\nu_{13}$.
[d] $\nu_{obs} = \nu_{10} + (n+1)\nu_{13} - n\nu_{13}$.
[e] $\nu_{obs} = 2\nu_{12} + (n+1)\nu_{13} - n\nu_{13}$.

Table 35: Energy level spacings (cm^{-1}) of υ_{13} of *trans*-1,3-butadiene-2,3-d_2 in vibrational excited states

Spacing	υ_{13}[a]	Vibrationally Excited States				
		υ_{12}	υ_{10}	$\upsilon_{10} + \upsilon_{12}$	$\upsilon_{15} + \upsilon_{16}$	$2\upsilon_{12}$
0-1	152.6	153.2	148.8	150.8	151.4	148.8
1-2	151.2	150.4	148.7	149.2	150.0	147.6
2-3	147.9	147.3	148.5	145.8	146.9	144.4
3-4	146.2	143.4	145.8	144.2	145.1	143.0
4-5	142.7	142.0	144.0	141.0	141.4	139.6
5-6	140.7	138.3	139.4	-	-	-
6-7	136.0	136.5	138.3	-	-	-
7-8	134.4	131.5	133.8	-	-	-
8-9	129.3	129.5	-	-	-	-

[a] Reference 92.

1,3-Butadiene-1,1,4,4-d_4

For the d_4, as for the d_0 and d_2 species, sum bands to the ν_{12} and ν_{10} excited states are observed as shown in Figures 51 and 52, respectively. The energy diagram in Figure 53 shows the levels and the connecting transitions for these two instances. The hot band series observed for the d_4 species was for $\nu_{10} + \nu_{12}$ combination, which has A_g symmetry. Figure 54 presents the observed spectra. The energy level diagram is shown in Figure 55. Tables 36 and 37 tabulate the data.

1,3-Butadiene-d_6

Figure 56 shows the sum band to the ν_{12} excited states for the d_6 species. Figure 57 displays the hot band series associated with the $2\nu_{12}$ overtone. The corresponding hot band transitions were not observed for the d_0 and d_4 species. Figure 58 presents the corresponding energy diagram. Tables 38 and 39 show the data numerically.

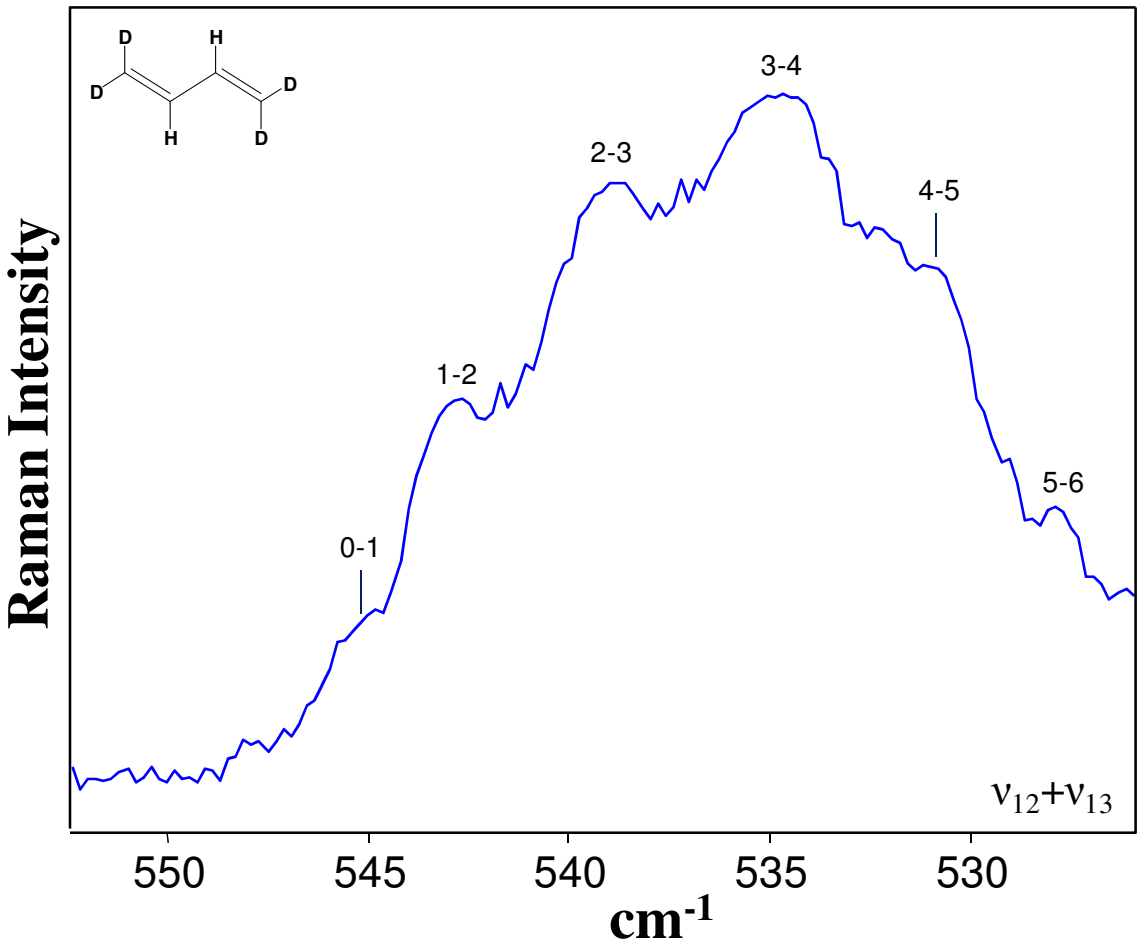

Figure 51. Raman spectrum of the 1,3-butadiene-1,1,4,4-d_4 $\nu_{12} + \nu_{13}$ sum bands originating from ν_{12} = 396.8 cm^{-1}.

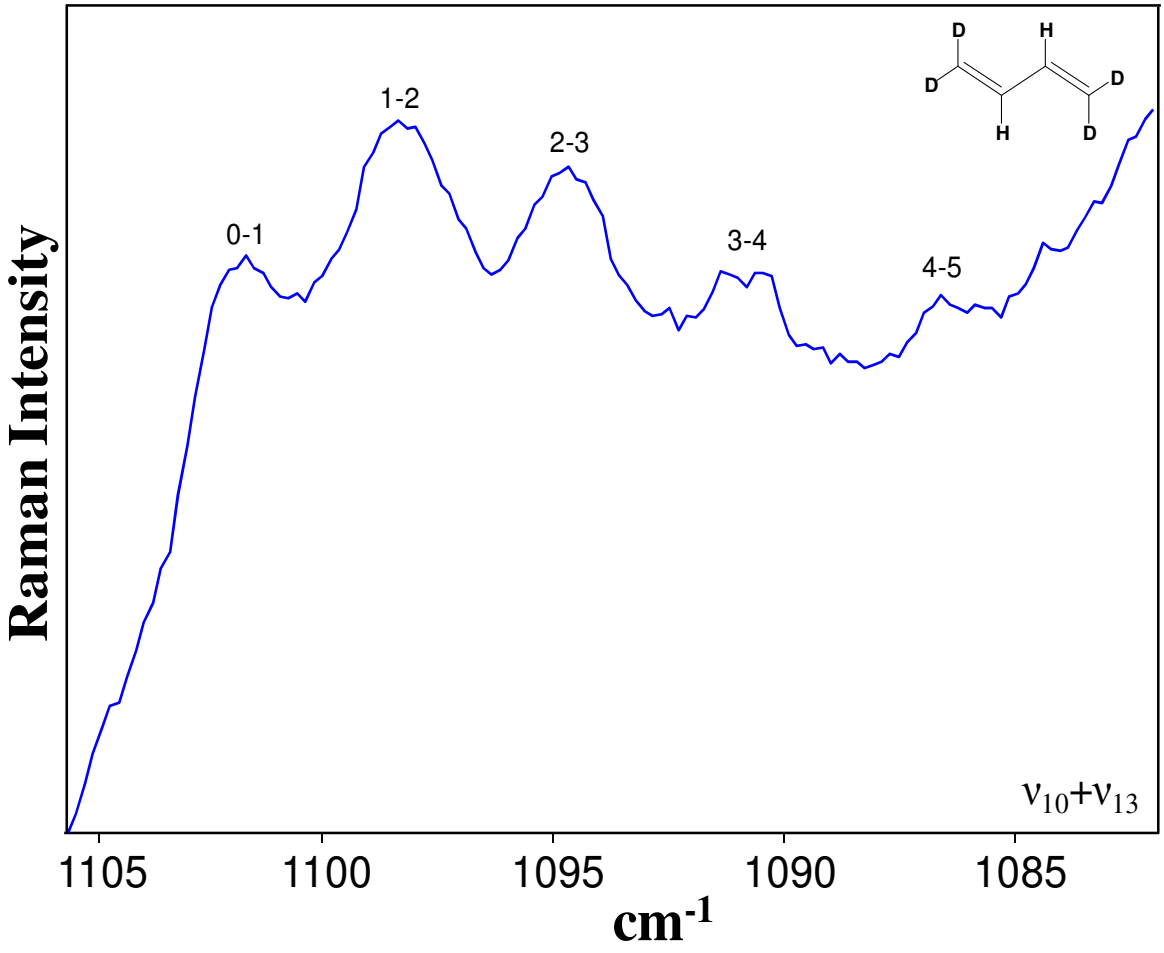

Figure 52. Raman spectrum of the 1,3-butadiene-1,1,4,4-d_4 $\nu_{10} + \nu_{13}$ sum bands originating from ν_{10} = 955.4 cm^{-1}.

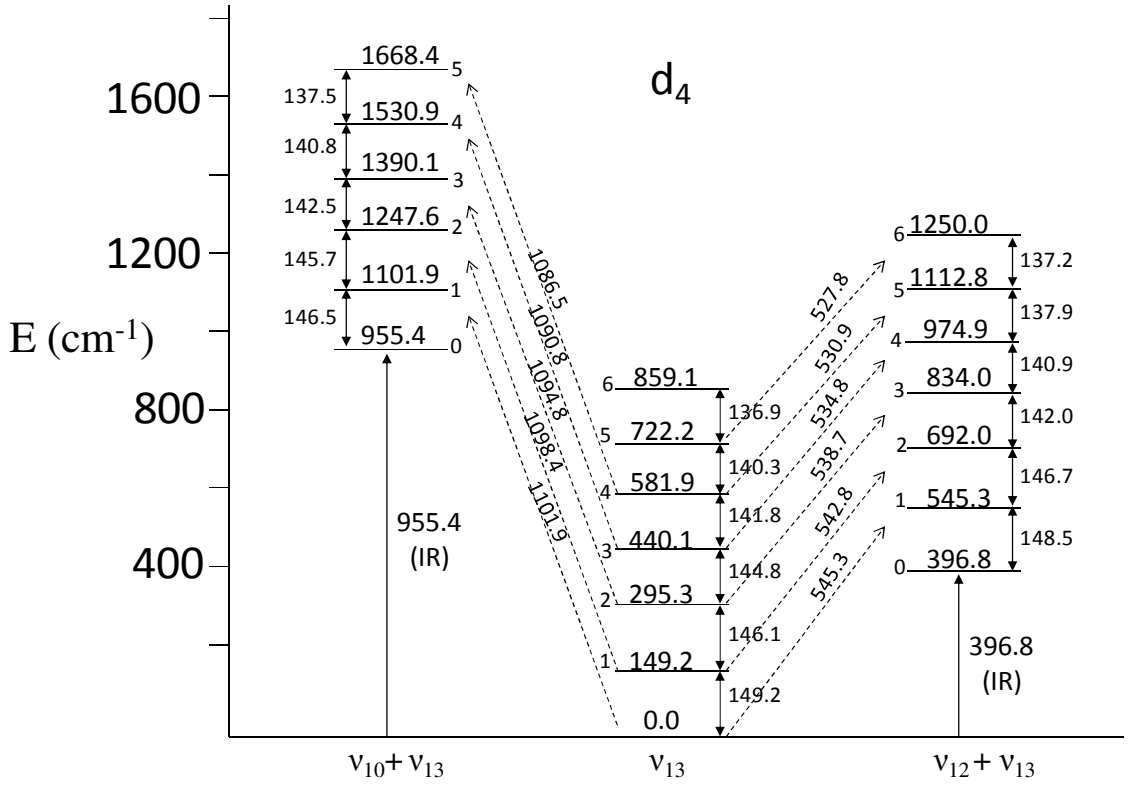

Figure 53. Energy level diagram for 1,3-butadiene-1,1,4,4-d_4 showing transitions to the ν_{10} and ν_{12} excited states.

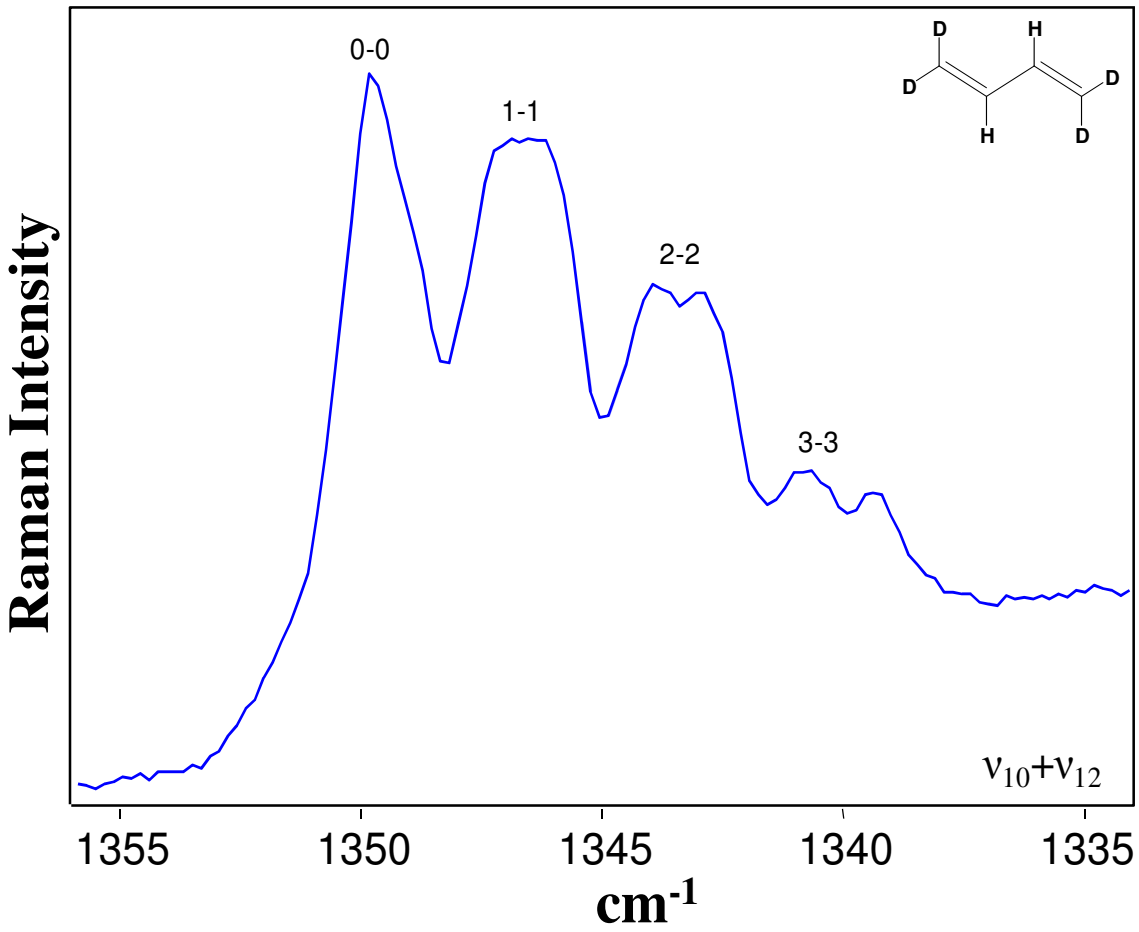

Figure 54. Raman spectrum of the 1,3-butadiene-1,1,4,4-d_4 hot band transitions to the $\nu_{10} + \nu_{12}$ vibrational excited state.

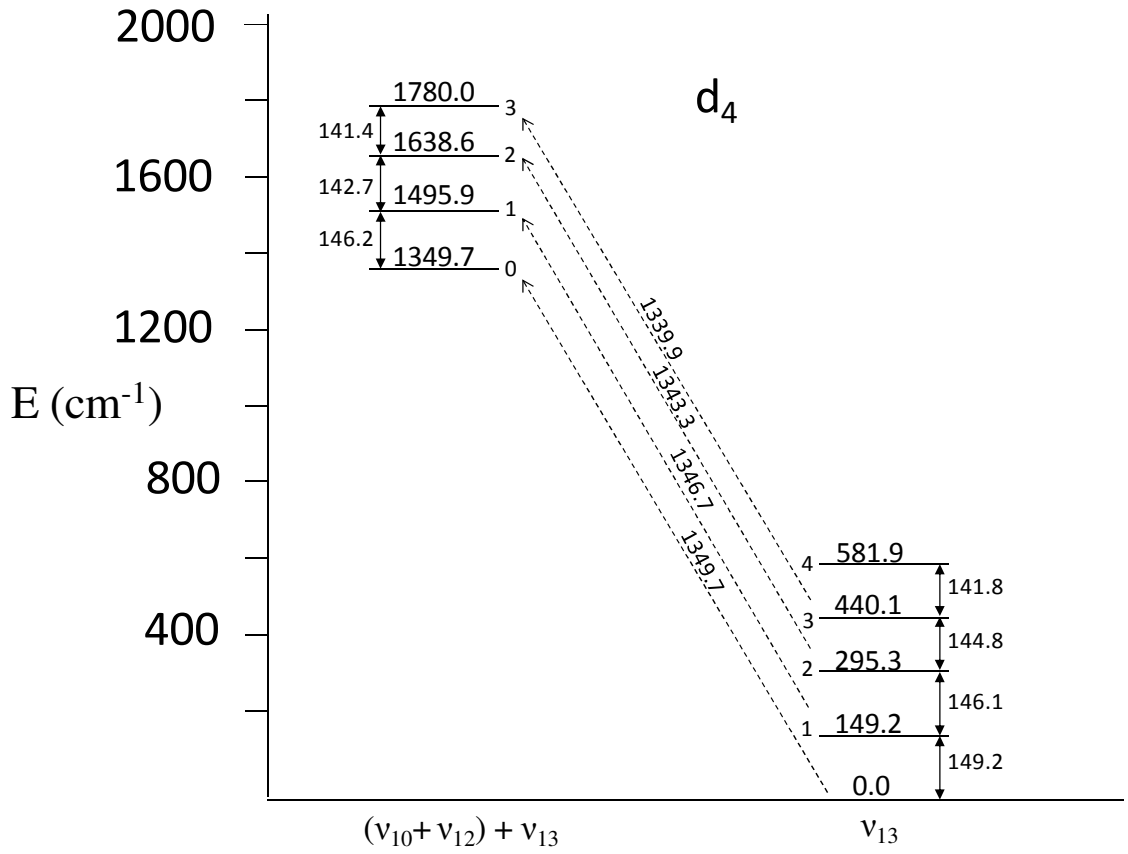

Figure 55. Energy level diagram for 1,3-butadiene-1,1,4,4-d_4 showing transitions to the $\nu_{10} + \nu_{12}$ excited states.

Table 36: Analysis of hot bands (cm^{-1}) of *trans*-1,3-butadiene-1,1,4,4-d_4 involving the torsional vibration (υ_{13})

		υ_{12}		υ_{10}	
Transition[a]	υ_{13}[b]	ν_{obs}[c]	ν_{obs}[c] - υ_{12}	ν_{obs}[d]	ν_{obs}[d] - υ_{10}
0-1	149.2	545.3	148.5	1101.9	146.5
1-2	146.1	542.8	146.0	1098.4	143.0
2-3	144.8	538.7	141.9	1094.8	139.4
3-4	141.8	534.8	138.0	1090.8	135.4
4-5	140.3	530.9	134.1	1086.5	131.1
5-6	136.9	527.8	131.0	-	-

[a] Quantum numbers for the υ_{13} torsional vibrational states.
[b] Reference 92.
[c] $\nu_{obs} = \nu_{12} + (n+1)\nu_{13} - n\nu_{13}$.
[d] $\nu_{obs} = \nu_{10} + (n+1)\nu_{13} - n\nu_{13}$.

Table 37: Energy level spacings (cm^{-1}) of υ_{13} of *trans*-1,3-butadiene -1,1,4,4-d_4 in vibrational excited states

Spacing	υ_{13}[a]	Vibrationally Excited States		
		υ_{12}	υ_{10}	$\upsilon_{10} + \upsilon_{12}$
0-1	149.2	148.5	146.5	146.2
1-2	146.1	146.7	145.7	142.7
2-3	144.8	142.0	142.5	141.4
3-4	141.8	140.9	140.8	-
4-5	140.3	137.9	137.5	-
5-6	136.9	137.2	-	-

[a] Reference 92.

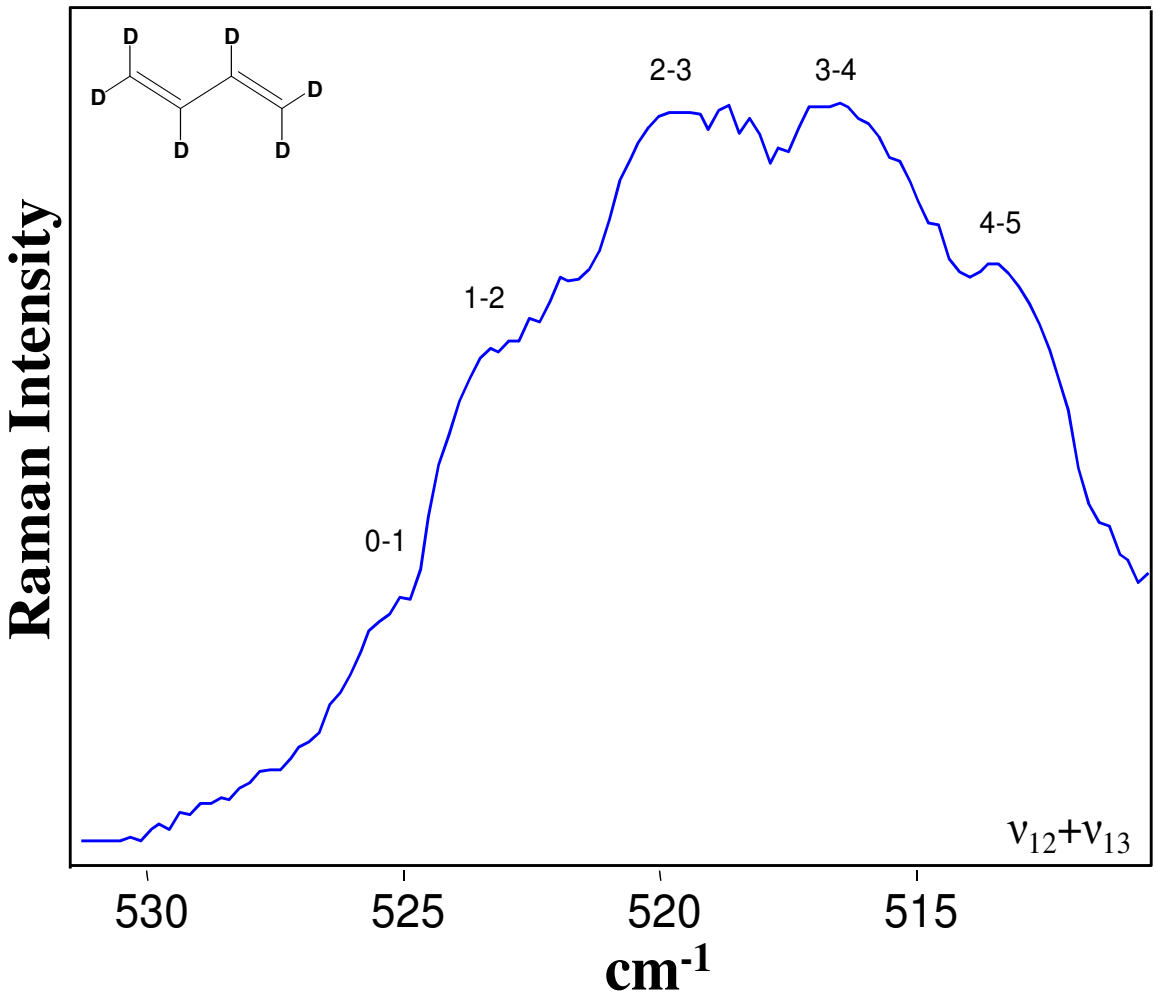

Figure 56. Raman spectrum of the 1,3-butadiene-d_6 $\nu_{12} + \nu_{13}$ sum bands originating from ν_{12} = 381 cm^{-1}.

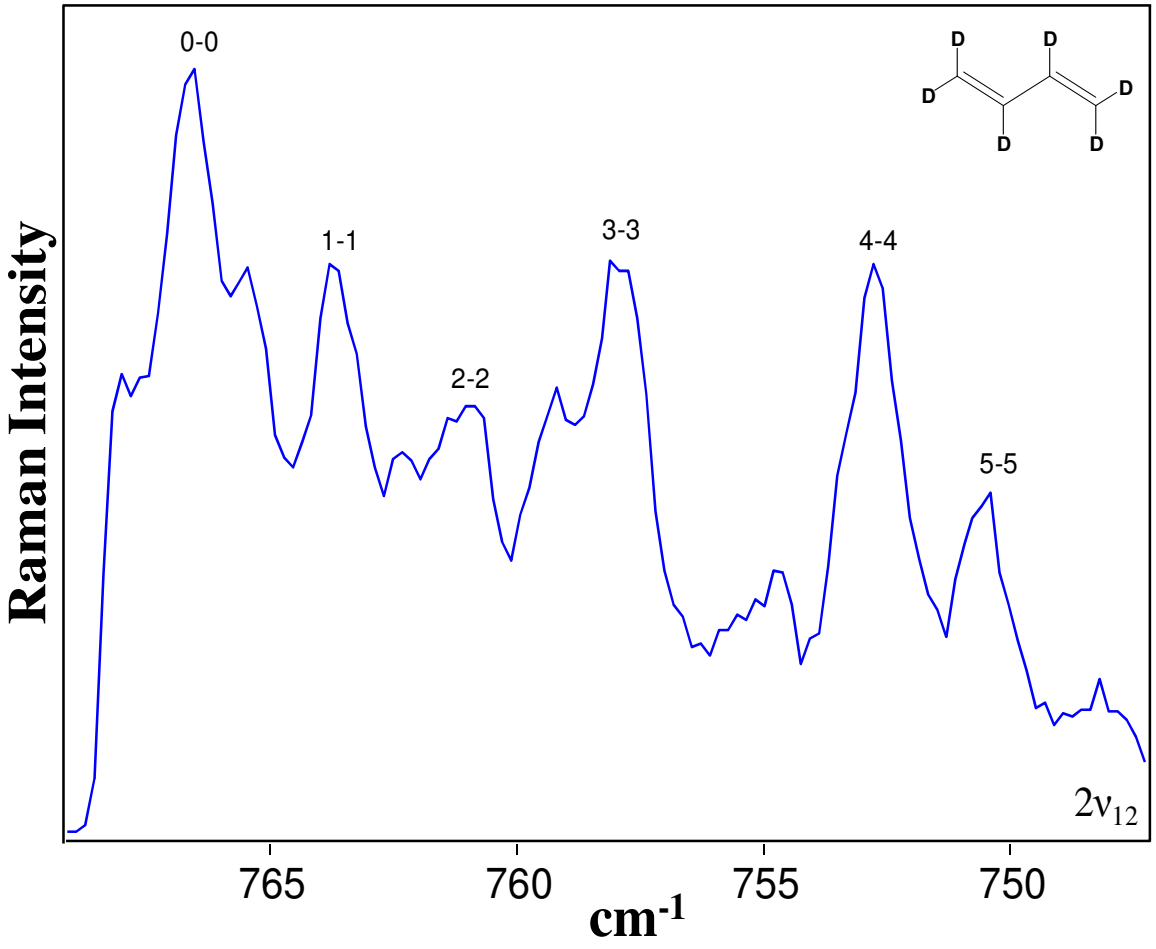

Figure 57. Raman spectrum of the 1,3-butadiene-d_6 hot bands to $2\nu_{12}$ excited state.

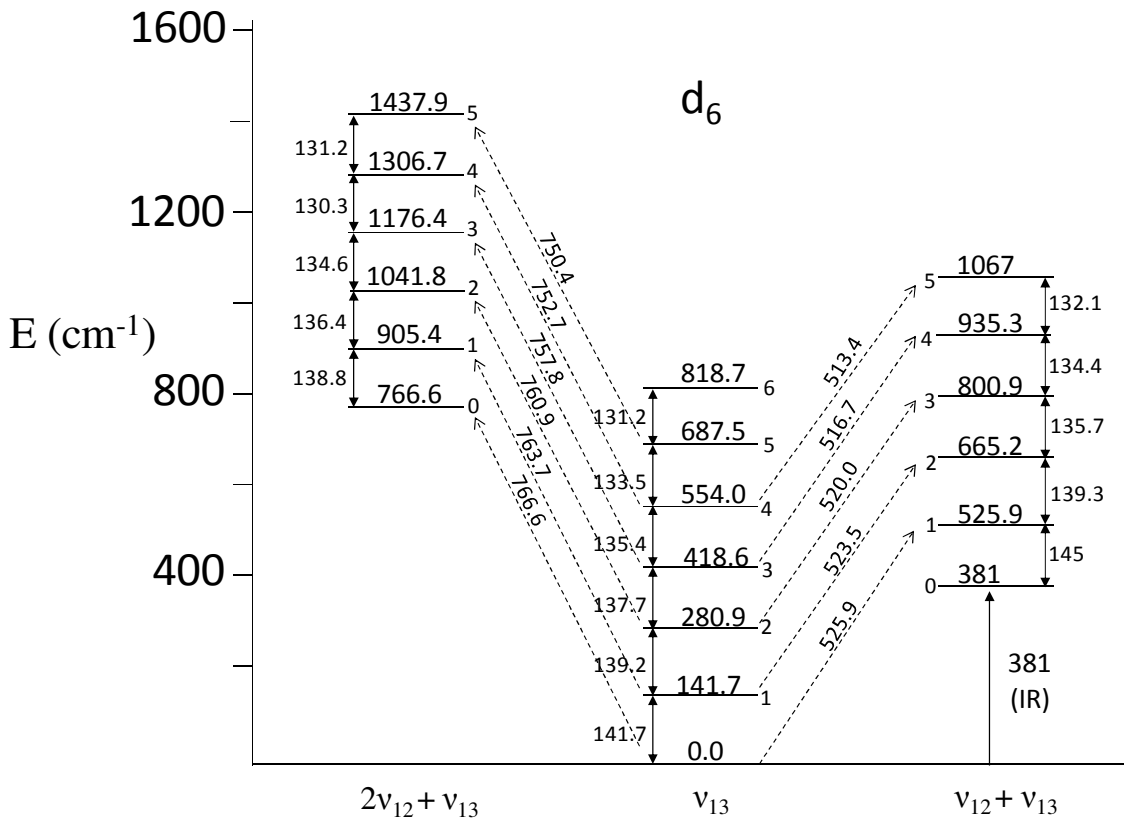

Figure 58. Energy level diagram for 1,3-butadiene-d_6 showing transitions to the ν_{12} and $2\nu_{12}$ vibrational excited states.

Table 38: Analysis of hot bands (cm^{-1}) of *trans*-1,3-butadiene-d_6 involving the torsional vibration (υ_{13})

		υ_{12}			$2\upsilon_{12}$
Transition[a]	υ_{13}[b]	ν_{obs}[c]	ν_{obs}[c] - υ_{12}	Transition[a]	ν_{obs}[d]
0-1	141.7	525.9	145	0-0	766.6
1-2	139.2	523.5	139.3	1-1	763.7
2-3	137.7	520.0	135.7	2-2	760.9
3-4	135.4	516.7	134.4	3-3	757.8
4-5	133.5	513.4	132.1	4-4	752.7
5-6	131.2	-	-	5-5	750.4

[a] Quantum numbers for the υ_{13} torsional vibrational states.
[b] Reference 92.
[c] $\nu_{obs} = \nu_{12} + (n+1)\nu_{13} - n\nu_{13}$.
[d] $\nu_{obs} = 2\nu_{12} + (n+1)\nu_{13} - n\nu_{13}$.

Table 39: Energy level spacings of υ_{13} of (cm^{-1}) of *trans*-1,3-butadiene-d_6 in vibrational excited states

Spacing	υ_{13}[a]	Vibrational Excited States	
		υ_{12}	$2\upsilon_{12}$
0-1	141.7	145	138.8
1-2	139.2	139.3	136.4
2-3	137.7	135.7	134.6
3-4	135.4	134.4	130.3
4-5	133.5	132.1	131.2

[a] Reference 92.

CONCLUSION

Several aspects are noteworthy about these results. First, is that all the combinations except for those with the Fermi doublet were with out-of-plane vibrations of the *trans*-1,3-butadiene, and these modes were the ones expected to couple most strongly to the out-of-plane torsional motion. Despite diligent searching, no combination or hot bands for the *gauche* conformer were observed. Only about 2% of the molecules at ambient temperature were in the *gauche* quantum state. Second, transitions to the ν_{13} torsional states in vibrational states that were already combinations were observed, namely $\nu_{10} + \nu_{12}$, $2\nu_{12}$, $\nu_{15} + \nu_{16}$, and $\nu_{23}+ \nu_{24}$. These observations were most unusual. The third result was that the torsional energy spacings were not the same in vibrational excited states as in the ground state, a simple subtraction of the vibrational frequency of the other mode did not yield an accurate determination of what the actual levels for ν_{13} were in the ground state of the other vibrations. This effect is evident in Tables 32, 34, 36, and 38. Also, as Tables 33, 35, 37, and 39 show, the torsional energy spacings are generally smaller in the vibrational excited states than the ground state with the largest effect for the $\nu_{10} + \nu_{12}$ combination state. These smaller energy spacings reflect the fact that the vibrations ν_{10} and ν_{12}, in particular, can be thought of as being cooperative with the torsional motion in that the internal rotation barrier between the *trans* and *gauche* conformations is decreased in these excited states.

The full Raman spectra of 1,3-butadiene-d_0, and its 2,3-d_2, 1,1,4,4-d_4, and d_6 isotopomers will be presented in Chapter X. These will show bands from not only the *trans* conformer but also the *gauche* conformer.

CHAPTER X

GAS-PHASE RAMAN SPECTRA OF *TRANS*- AND *GAUCHE*- 1,3-BUTADIENE AND THEIR DEUTERATED ISOTOPOMERS

INTRODUCTION

An extensive investigation of the Raman spectra of the internal rotation vibration (torsion) of 1,3-butadiene and its 2,3-d_2, 1,1,4,4-d_2, and d_6 isotopomers was reported in Chapter VIII. The one-dimensional potential energy function determined for this vibration confirmed that the *trans* rotamer of the molecule is the predominant form (~98%) and that the *gauche* rotamer constitutes the remainder of the molecules. This is in accord with recent *ab initio* calculations.[49] In addition, the observation of numerous combination and hot band series involving the torsional vibration was reported in Chapter IX. The vibrational spectra of 1,3-butadiene and its isotopomers have been studied many dozens of times (refer to citations in references 1 and 2), but high quality Raman studies of the gas phase have been lacking. Only the 1990 investigation by Wiberg and Rosenberg[53] is comprehensive. Their spectra were recorded with 2 cm^{-1} resolution, but additional details were not given and only wavenumber listings for assigned fundamentals were presented. Presumably charge coupled device (CCD) detection, which allows prolonged averaging, was not used and there was no indication that high laser power was available. Consequently, a reinvestigation of the gas-phase Raman spectra of this molecule and its isotopomers was undertaken using high (6W) laser power and CCD detection. This allowed very good signal to noise ratios and very

weak signals detection. Spectra at 260° C were also collected. In 2003, the authors published a detailed review describing the methodology for collecting vapor-phase spectra at elevated temperatures.[91] One of the goals of this study was to identify Raman bands from the *gauche* rotamer which makes up about 2% of the molecular population at ambient temperature. Previous matrix isolation studies using infrared and Raman spectroscopy have reported the presence of bands due to the *gauche* form.[44,55]

1,3-Butadiene has 24 vibrations which for the *trans* rotamer are distributed as

$$\Gamma_{trans} = 9A_g + 4A_u + 3B_g + 8B_u \quad (10.1)$$

The A_g vibrations are expected to produce polarized Raman bands which are sharp and with significant intensity. The B_g vibrations are also Raman active but are expected to be weaker and broader. The A_u and B_u vibrations are infrared active but Raman forbidden. Numerous high quality infrared investigations of 1,3-butadiene and its isotopomers have been published.[49] The *gauche* rotamer has C_2 symmetry and its vibrational symmetry species are

$$\Gamma_{gauche} = 13A + 11B \quad (10.2)$$

and all of the vibrations are symmetry allowed for both infrared and Raman spectra. Again, the totally symmetric vibrations are generally expected to produce the strongest Raman bands.

EXPERIMENTAL

Butadiene was supplied by Aldrich, the 2,3-d_2 species was supplied by CDN Isotopes (99% D, Quebec, Canada), and the 1,1,4,4-d_4 and d_6 species were supplied by Cambridge Isotope Laboratories (98% D). Purity of the samples was confirmed by infrared spectroscopy prior to sealing the samples in the cells.

Raman spectra of gas-phase 1,3-butadiene-d_0, and its 2,3-d_2, 1,1,4,4-d_4, and d_6 isotopomers were recorded for samples with simplified optics at various temperatures sealed in specially designed glass cells which was previously described in Chapter II. A Jobin-Yvon U-1000 spectrometer equipped with a liquid nitrogen-cooled CCD detector was used to collect the spectra. The 532 nm line of a frequency-doubled Nd:YAG Coherent Verdi-10 laser was used and generally operated at 6 watts of power. Spectral regions spanning 60 cm^{-1} were typically collected over periods of 4 to 6 hours so that many hundreds of individual spectra could be averaged. The resolution of the spectra was 0.7 cm^{-1}.

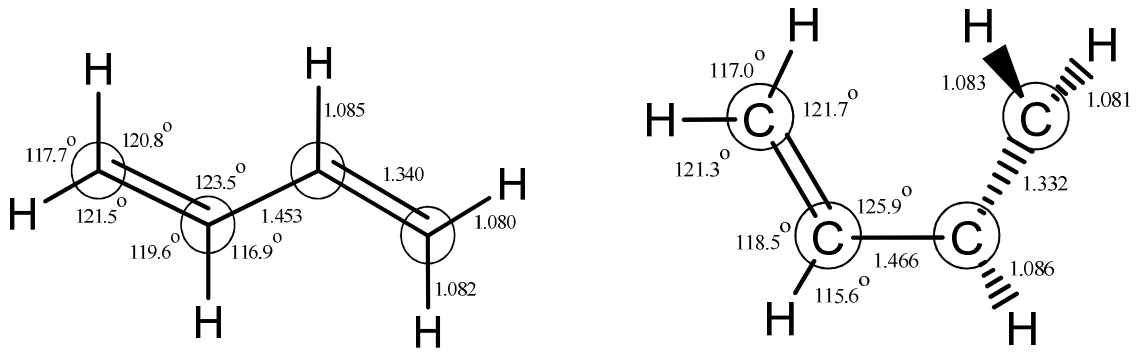

Figure 59. Calculated structures of 1,3-butadiene (a) *trans*, (b) *gauche* in their S_0 ground electronic state using MP2/cc-pVTZ level of theory.

THEORETICAL CALCULATIONS

The structures and vibrational frequencies of 1,3-butadiene-d_0, and its 2,3-d_2, 1,1,4,4-d_4, and d_6 isotopomers for the electronic ground state were calculated using the Gaussian 03 program package.[65] *Ab initio* second order Moller-Plesset (MP2) level of theory with the cc-pVTZ basis set was used to find the optimized geometry for *trans* and *gauche* rotors as shown in Figure 59. The DFT-B3LYP level of theory with the 6-311++G(d,p) basis set was used to calculate the vibrational frequencies and the Raman intensities. Based on previous work,[66-70] a scaling factor of 0.964 was used for the C-H stretching vibrational frequencies and a factor of 0.985 for the lower frequencies. The calculated results here will be compared to those of Feller and Craig,[49] and reference will be made to the potential energy distributions calculated by McKean and co-workers.[54]

RESULTS AND DISCUSSION

Although the Raman spectra of 1,3-butadiene-d_0, and its 2,3-d_2, 1,1,4,4-d_4, and d_6 isotopomers has been studied previously, there are no high quality figures to show these in the literature.

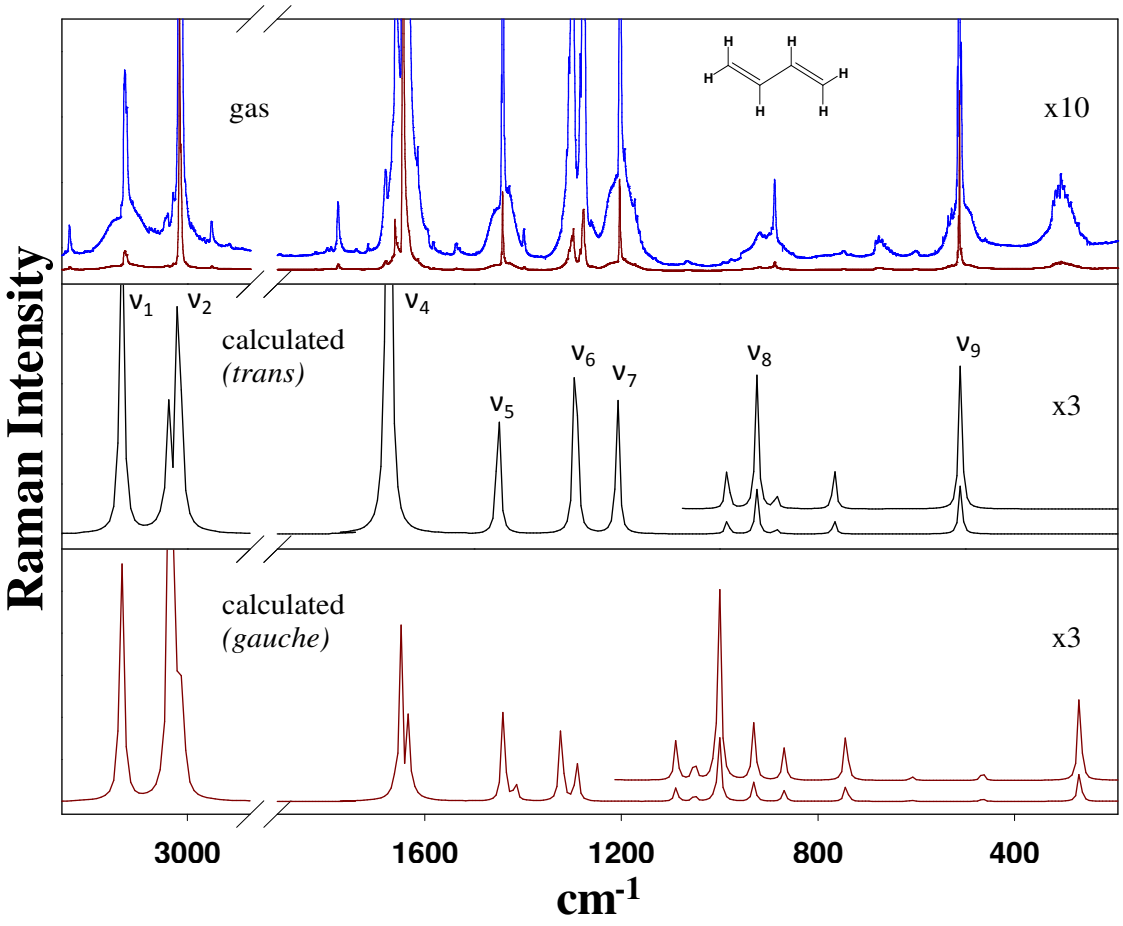

Figure 60. Gas-phase and calculated Raman spectra of 1,3-butadiene-d_0.

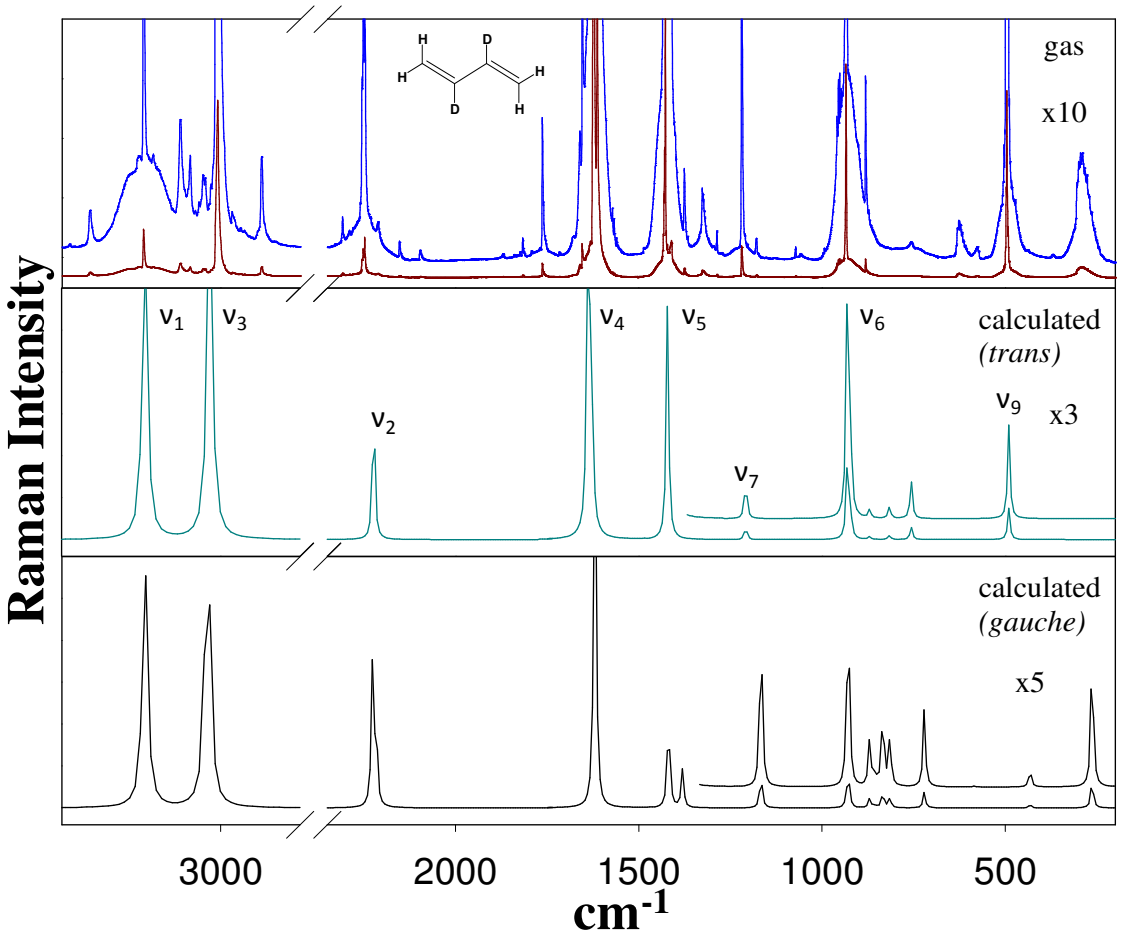

Figure 61. Gas-phase and calculated Raman spectra of 1,3-butadiene-2,3-d_2.

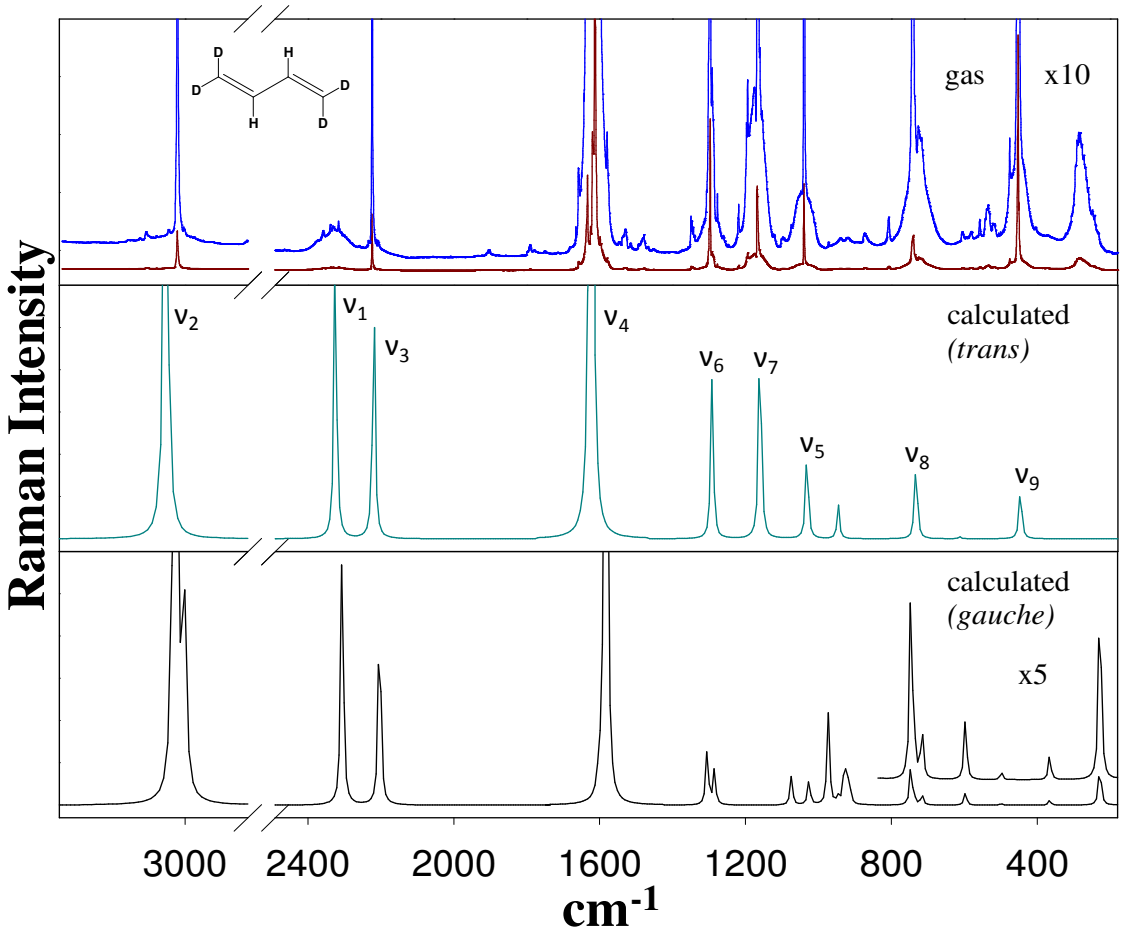

Figure 62. Gas-phase and calculated Raman spectra of 1,3-butadiene-1,1,4,4-d_4.

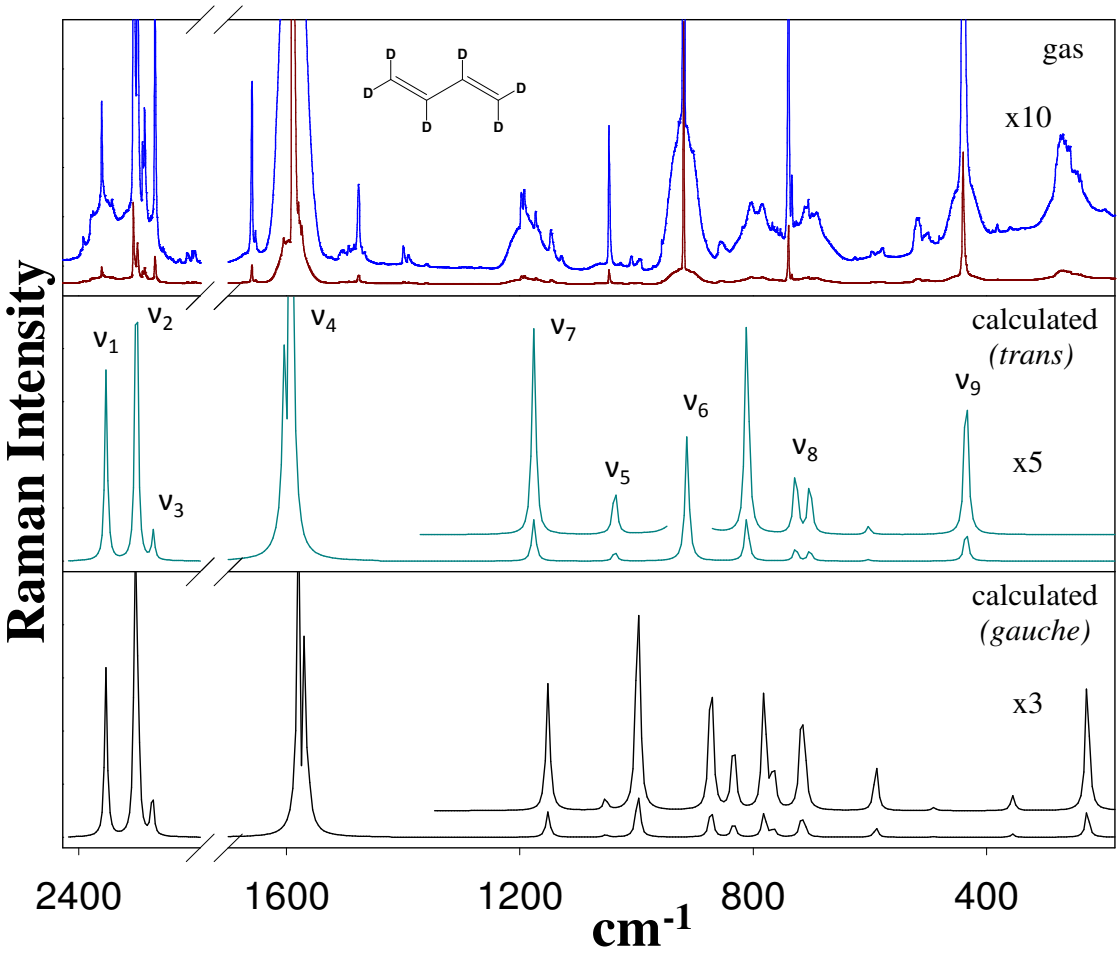

Figure 63. Gas-phase and calculated Raman spectra of 1,3-butadiene-d_6.

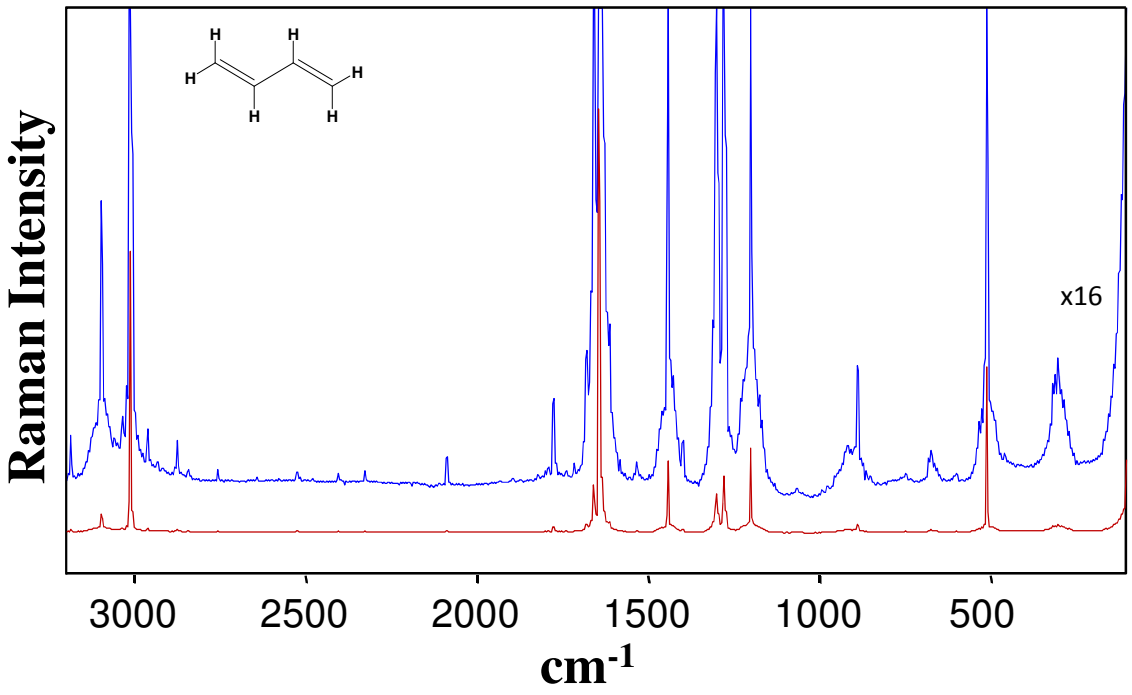

Figure 64. Gas-phase Raman spectrum of 1,3-butadiene in the 200-3200 cm^{-1} region.

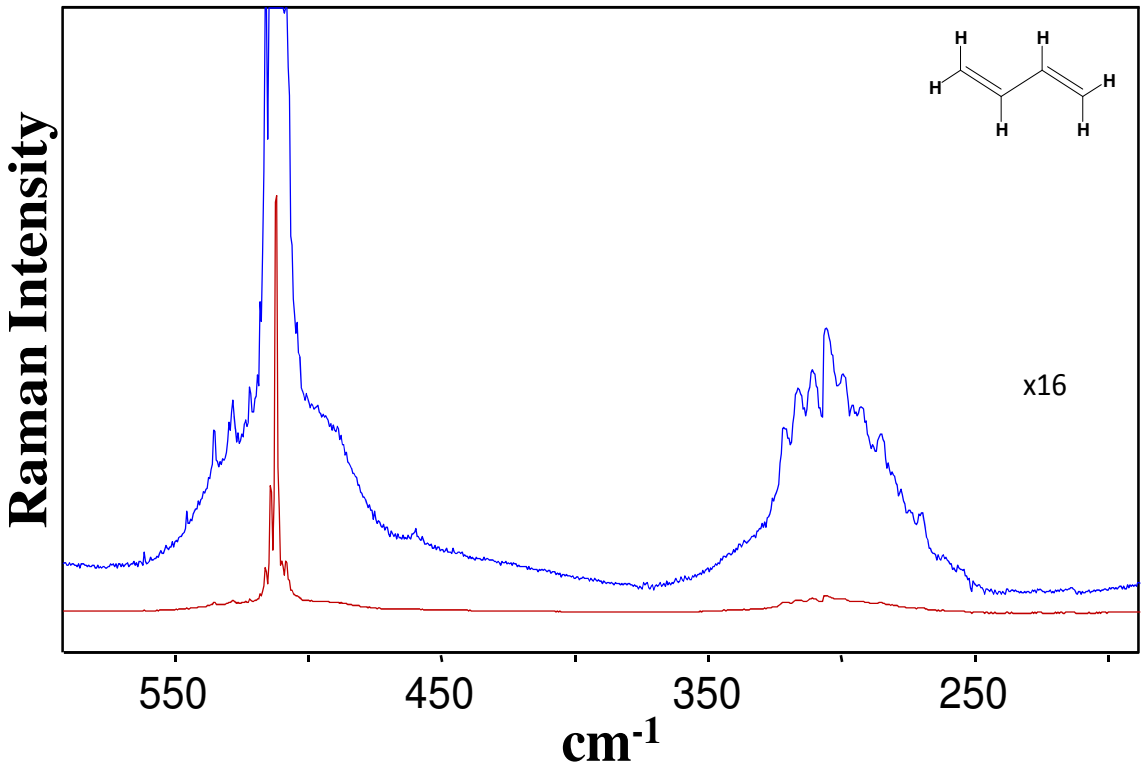

Figure 65. Gas-phase Raman spectrum of 1,3-butadiene in the 200-600 cm^{-1} region.

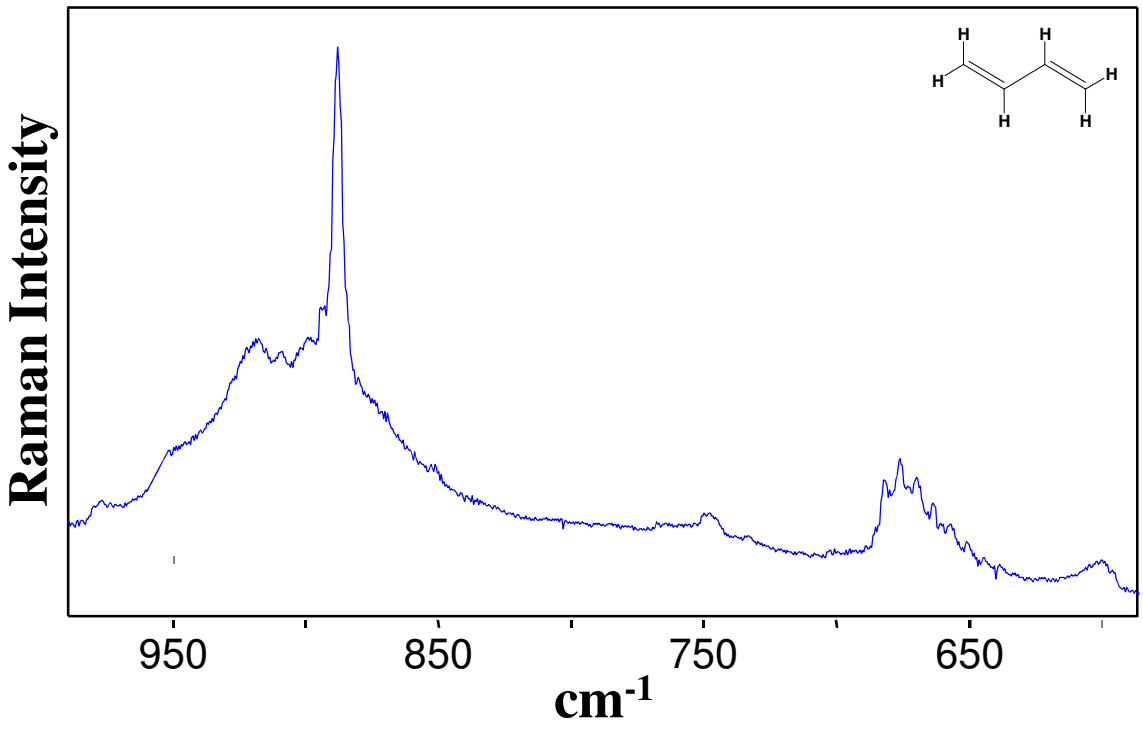

Figure 66. Gas-phase Raman spectrum of 1,3-butadiene in the 600-1000 cm^{-1} region.

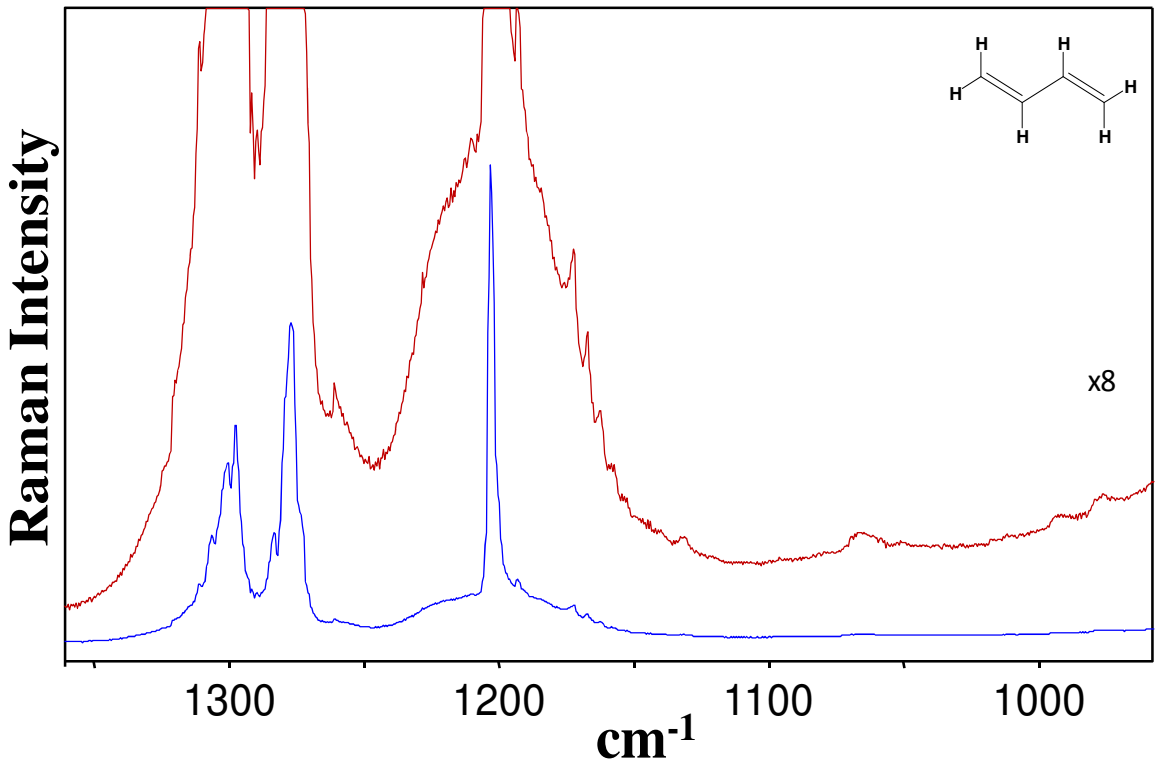

Figure 67. Gas-phase Raman spectrum of 1,3-butadiene in the 950-1350 cm^{-1} region.

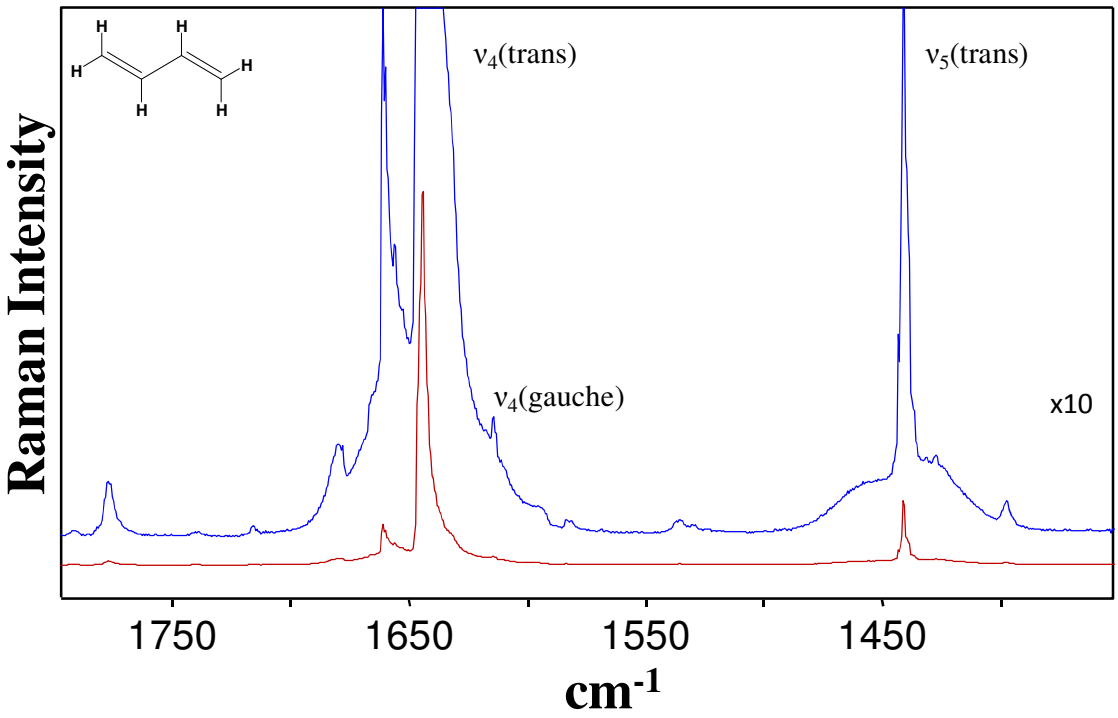

Figure 68. Gas-phase Raman spectrum of 1,3-butadiene in the 1350-1800 cm^{-1} region.

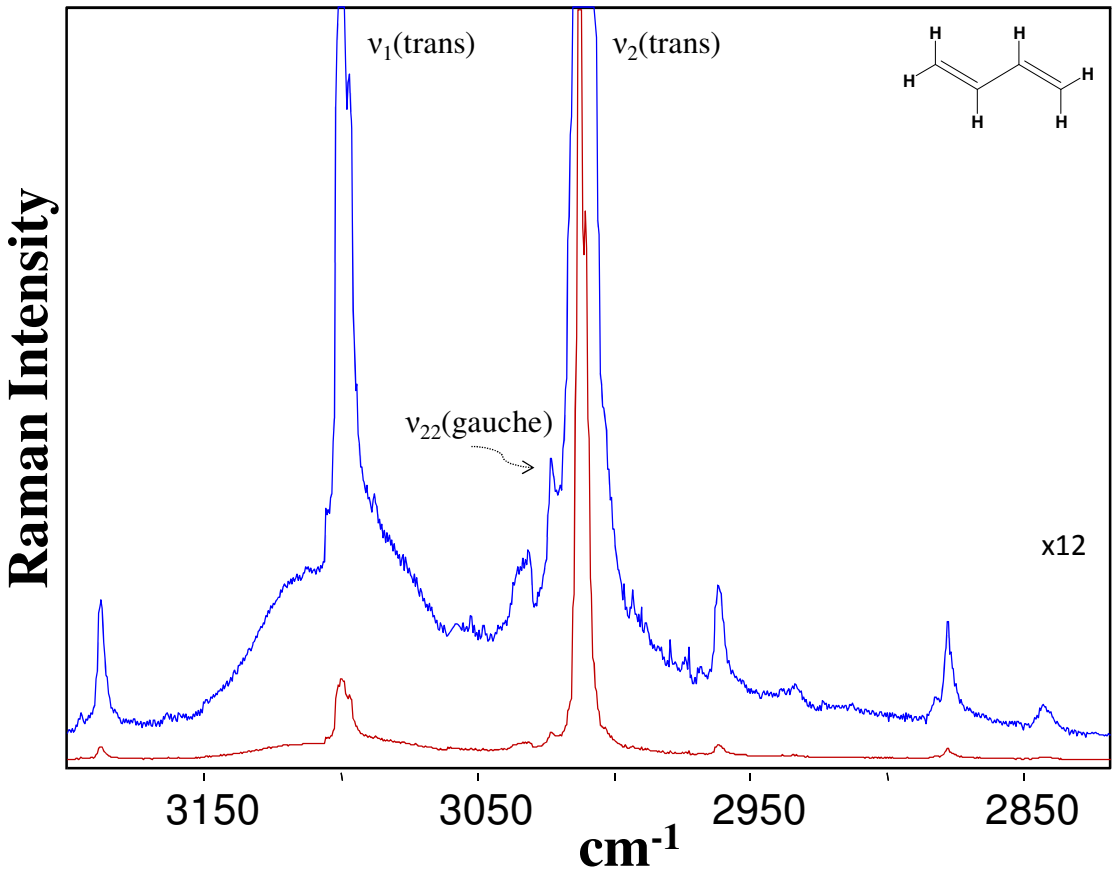

Figure 69. Gas-phase Raman spectrum of 1,3-butadiene in the 2800-3200 cm^{-1} region.

Table 40: Observed and calculated vibrational frequencies (cm^{-1}) and intensities for *trans* 1,3-butadiene-d_0

C_{2h}		Approximate Description	OBS		Calculated[b]		OBS / Lit[c]
A_g	υ_1	CH_2 antisym str	3099	(3)	3105	(42)	3100
	υ_2	CH_2 sym str	3012.5	(66)	3022	(81)	3013
	υ_3	C-H sym str	3010 sh	(20)	3010	(12)	3013
	υ_4	C=C sym str	1644.3	(100)	1674	(100)	1644
	υ_5	CH_2 def	1442.2	(18)	1450	(12)	1441
	υ_6	C-H wag (i.p.)	1277.8	(13)	1293	(20)	1277
	υ_7	C-C str[f]	1204.2	(19)	1208	(11)	1203
	υ_8	CH_2 rock[f]	888.8	(2)	885	(0.5)	888
	υ_9	C=C-C def	512.2	(39)	510	(3)	512
A_u	υ_{10}	C-H wag (o.p.)[g]	-	-	1039	(0)	1014
	υ_{11}	CH_2 wag	-	-	925	(0)	908
	υ_{12}	CH_2 twist[g]	-	-	531	(0)	525
	υ_{13}	C-C tors	322.4 (0-2)[d]	-	173	(0)	162.4[e]
B_g	υ_{14}	C-H wag (o.p.)	977	(0.1)	984	(4)	965
	υ_{15}	CH_2 wag	909.5	(0.1)	924	(3)	908
	υ_{16}	CH_2 twist	748	(0.1)	766	(1)	752
B_u	υ_{17}	CH_2 antisym str	-	-	3105	(0)	3101
	υ_{18}	C-H str	-	-	3023	(0)	3055
	υ_{19}	CH_2 sym str	-	-	3019	(0)	2984
	υ_{20}	C=C antisym str	-	-	1620	(0)	1597
	υ_{21}	CH_2 def	-	-	1392	(0)	1381
	υ_{22}	C-H wag (i.p.)	-	-	1299	(0)	1294
	υ_{23}	CH_2 rock	-	-	988	(0)	990
	υ_{24}	C=C-C def	-	-	292	(0)	299[e]

[a] Relative intensities in parenthesis. Observed intensities indicate peak height.
[b] B3LYP/6-311++g(d,p); frequencies scaled with a scaling factor of 0.985 for frequencies less than 1800 cm^{-1} and 0.964 for frequencies greater than 1800 cm^{-1}.
[c] Reference 53. [d] Reference 92. [e] Reference 56.
[f] The C-C stretch and CH_2 rock are strongly coupled.
[g] The CH wag and CH_2 twist are strongly coupled.

Table 41: Observed and calculated vibrational frequencies (cm^{-1}) and intensities for *trans* 1,3-butadiene-2,3-d_2

C_{2h}		Approximate Description	OBS		Calculated[b]		OBS Lit[c]	CALC Lit[d]
A_g	υ_1	CH_2 antisym str	3097.6	(10)	3104	(41)	3099	3110
	υ_2	CH_2 sym str	3004.0	(42)	3020	(50)	3005	3022
	υ_3	C-D sym str	2248.5	(9)	2230	(18)	2249	2232
	υ_4	C=C sym str	1623.6	(100)	1651	(100)	1613	1629
	υ_5	CH_2 def	1427.8	(65)	1434	(26)	1428	1427
	υ_6	C-D wag (i.p.)	935.1	(53)	941	(8)	934	930
	υ_7	C-C str[g]	1220.1	(8)	1217	(2)	1220	1225
	υ_8	CH_2 rock[g]	882.0	(3)	879	(0.5)	880	872
	υ_9	C=C-C def	496.2	(46)	495	(3)	496	496
A_u	υ_{10}	C-D wag (o.p.)	-		866	(0)	850	855
	υ_{11}	CH_2 wag	-		925	(0)	908	912
	υ_{12}	CH_2 twist	-		488	(0)	480	471
	υ_{13}	C-C tors	303.8 (0-2)[e]		164	(0)	153	150
B_g	υ_{14}	C-D wag (o.p.)	-		819	(0)	820	819
	υ_{15}	CH_2 wag	911 sh	(0.07)	928	(4)	913	910
	υ_{16}	CH_2 twist	743	(0.05)	760	(1)	745	728
B_u	υ_{17}	CH_2 antisym str	-		3104	(0)	3098	3110
	υ_{18}	C-D str	-		2232	(0)	2243	2229
	υ_{19}	CH_2 sym str	-		3020	(0)	3031	3022
	υ_{20}	C=C antisym str	-		1609	(0)	1586	1580
	υ_{21}	CH_2 def	-		1386	(0)	1374	1373
	υ_{22}	C-D wag (i.p.)	-		1124	(0)	1127	1131
	υ_{23}	CH_2 rock	-		844	(0)	852[f]	839
	υ_{24}	C=C-C def	-		282	(0)	287[f]	284

[a] Relative intensities in parenthesis. Observed intensities indicate peak height.
[b] B3LYP/6-311++g(d,p); frequencies scaled with a scaling factor of 0.985 for frequencies less than 1800 cm^{-1} and 0.964 for frequencies greater than 1800 cm^{-1}.
[c] Reference 53. [d] Reference 51.[e] Reference 92. [f] Reference 52.
[g] The C-C stretch and CH_2 rock are strongly coupled.

Table 42: Observed and calculated vibrational frequencies (cm^{-1}) and intensities for *trans* 1,3-butadiene-1,1,4,4-d_4

C_{2h}	Approximate Description	OBS		Calculated[b]		OBS Lit[c]	CALC Lit[d]
A_g	υ_1 CD_2 antisym str	2316	(0.2)	2312	(17)	2316	2318
	υ_2 CD_2 sym str	2224.5	(8)	2207	(13)	2225	2211
	υ_3 CH sym str	3012.1	(5)	3014	(35)	3013	3011
	υ_4 C=C sym str	1613.7	(100)	1640	(100)	1613	1615
	υ_5 CD_2 def	1040.1	(12)	1041	(4)	1040	1040
	υ_6 C-H wag (i.p.)	1296.9	(21)	1304	(9)	1296	1288
	υ_7 C-C str	1168.0	(12)	1172	(11)	1167	1171
	υ_8 CD_2 rock	740.0	(5)	735	(1)	740	732
	υ_9 C=C-C def	452.6	(32)	451	(2)	452	453
A_u	υ_{10} C-H wag (o.p.)[h]	-		979	(0)	955	951
	υ_{11} CD_2 wag	-		740	(0)	728	726
	υ_{12} CD_2 twist[h]	-		399	(0)	396.8[f]	393
	υ_{13} C-C torsion	295.3 (0-2)[e]		158	(0)	149.2[g]	146
B_g	υ_{14} C-H wag (o.p.)	940	(0.1)	952	(2)	930	910
	υ_{15} CD_2 wag (o.p.)	726	(0.4)	739	(3)	728	727
	υ_{16} CD_2 twist	606.1	(0.1)	616	(0.1)	608[f]	614
B_u	υ_{17} CD_2 antisym str	-		2311	(0)	2332	2318
	υ_{18} C-H str	-		3024	(0)	3020	3018
	υ_{19} CD_2 sym str	-		2210	(0)	2226	2212
	υ_{20} C=C antisym str	-		1555	(0)	1533	1519
	υ_{21} CD_2 def	-		1026	(0)	1030	1023
	υ_{22} C-H wag (i.p.)	-		1278	(0)	1275	1264
	υ_{23} CD_2 rock	-		812	(0)	813	820
	υ_{24} C=C-C def	-		253	(0)	257.9[f]	255

[a] Relative intensities in parenthesis. Observed intensities indicate peak height.
[b] B3LYP/6-311++g(d,p); frequencies scaled with a scaling factor of 0.985 for frequencies less than 1800 cm^{-1} and 0.964 for frequencies greater than 1800 cm^{-1}.
[c] Reference 53. [d] Reference 51. [e] Reference 92. [f] Reference 54. [g] Reference 42.
[h] The CD_2 twist and CH wag are strongly coupled.

Table 43: Observed and calculated vibrational frequencies (cm^{-1}) and intensities for *trans* 1,3-butadiene-d_6

C_{2h}		Approximate Description	OBS		Calculated[b]		OBS Lit[c]	CALC Lit[d]
A_g	υ_1	CD_2 antisym str	2343.5	(1)	2313	(14)	2343	2319
	υ_2	CD_2 sym str	2265	(9)	2238	(26)	2266	2244
	υ_3	C-D sym str	2212	(3)	2197	(2)	2212	2198
	υ_4	C=C sym str	1588.8	(100)	1611	(100)	1589	1587
	υ_5	CD_2 def	1047	(2)	1046	(1)	1046	1048
	υ_6	C-D wag (i.p.)	919	(28)	923	(8)	918	913
	υ_7	C-C str	1192	(0.8)	1187	(3)	1192	1180
	υ_8	CD_2 rock	739	(6)	734	(1)	738[f]	730
	υ_9	C=C-C def	440	(14)	440	(2)	439	441
A_u	υ_{10}	C-D wag (o.p.)[g]	-		742	(0)	736[f]	753
	υ_{11}	CD_2 wag	-		731	(0)	719	724
	υ_{12}	CD_2 twist[g]	-		386	(0)	381[f]	379
	υ_{13}	C-C tors	280.9 (0-2)[e]	-	150	(0)	140[f]	138
B_g	υ_{14}	C-D wag (o.p.)	804 br	(0.3)	815	(3)	793	761
	υ_{15}	CD_2 wag	700 br	(0.08)	707	(1)	700	708
	υ_{16}	CD_2 twist	597 br	(0.1)	605	(0.1)	603[f]	606
B_u	υ_{17}	CD_2 antisym str	-		2312	(0)	2350	2318
	υ_{18}	C-D str	-		2240	(0)	2266	2241
	υ_{19}	CD_2 sym str	-		2200	(0)	2220	2198
	υ_{20}	C=C antisym str	-		1540	(0)	1520	1504
	υ_{21}	CD_2 def	-		1047	(0)	1048	1041
	υ_{22}	C-D wag (i.p.)	-		1002	(0)	1005	1000
	υ_{23}	CD_2 rock	-		780	(0)	769[f]	743
	υ_{24}	C=C-C def	-		245	(0)	252[f]	247

[a] Relative intensities in parenthesis. Observed intensities indicate peak height.
[b] B3LYP/6-311++g(d,p); frequencies scaled with a scaling factor of 0.985 for frequencies less than 1800 cm^{-1} and 0.964 for frequencies greater than 1800 cm^{-1}.
[c] Reference 53. [d] Reference 51. [e] Reference 92. [f] Reference 54.
[g] The CD_2 twist and CD wag are strongly coupled.

Table 44: Observed and calculated vibrational frequencies (cm^{-1}) and intensities[a] for *gauche* 1,3-butadiene-d_0

C_2		Approximate Description	OBS		Calculated[b]		OBS Lit[c]	OBS Lit[d]	CALC Lit[e]
A	υ_1	CH_2 antisym str	-		3105	(70)	3103	3070	3105
	υ_2	CH_2 sym str	3023	(117)	3027	(143)	3014	3023	3029
	υ_3	CH sym str	-		3018	(15)	2986	2990	3020
	υ_4	C=C sym str	1614.5	(100)	1643	(100)	1633	1633	1646
	υ_5	CH_2 def	1428	(30)	1440	(18)	1425	1425	1447
	υ_6	C-H wag (i.p.)	-		1322	(15)	-	-	1328
	υ_7	CH_2 rock	1051	(20)	1051	(2)	1087	-	1055
	υ_8	C-H wag (o.p.)	993?	(13)	1000	(12)	983	984	1007
	υ_9	CH_2 wag (o.p.)	-		930	(3)	915	920	938
	υ_{10}	C-C str	869?	(1)	868	(2)	-	-	872
	υ_{11}	CH_2 twist	734	(8)	743	(3)	727	730	748
	υ_{12}	C=C-C angle bend	270.8	(50)	268	(4)	-	-	271
	υ_{13}	torsion	214.9 (0^+-2^+)[f]		154	(1)	-	-	158
B	υ_{14}	CH_2 antisym str	-		3103	(3)	3103	3103	3104
	υ_{15}	CH_2 sym str	-		3021	(11)	3014	3035	3024
	υ_{16}	C-H antisym str	-		3008	(29)	2986	3010	3009
	υ_{17}	C=C antisym str	-		1663	(2)	1612	1602	1668
	υ_{18}	CH_2 def	-		1416	(4)	1403	1403	1423
	υ_{19}	C-H wag (i.p.)	-		1291	(8)	-	-	1296
	υ_{20}	CH_2 rock	-		1088	(5)	-	1087	1094
	υ_{21}	C-H wag (o.p.)	1012?	(12)	1013	(0.2)	996	996	1020
	υ_{22}	CH_2 wag (o.p.)	-		932	(0.5)	914	914	940
	υ_{23}	C=C-C angle bend	589?	(50)	609	(0.2)	596	596	612
	υ_{24}	CH_2 twist	-		465	(0.4)	470	470	468

[a] Relative intensities in parenthesis. Observed intensities indicate peak height.
[b] B3LYP/6-311++g(d,p); frequencies scaled with a scaling factor of 0.985 for frequencies less than 1800 cm^{-1} and 0.964 for frequencies greater than 1800 cm^{-1}.
[c] Reference 55. [d] Reference 44.
[e] Reference 49 (B3LYP/aug-cc-pVTZ; frequencies scaled with a scaling factor of 0.985 for frequencies less than 1800 cm^{-1} and 0.964 for frequencies greater than 1800 cm^{-1}).
[f] Reference 92.

Table 45: Observed and calculated vibrational frequencies (cm^{-1}) and intensities[a] for *gauche* 1,3-butadiene-2,3-d_2

C_2		Approximate Description	OBS		Calculated[b]	
A	υ_1	CH_2 antisym str	3085?	(33)	3104	(67)
	υ_2	CH_2 sym str	3013?	(22)	3022	(78)
	υ_3	CD sym str	-		2233	(31)
	υ_4	C=C antisym str	-		1636	(100)
	υ_5	CH_2 def	1426	(33)	1432	(24)
	υ_6	C-D wag (i.p.)	1174	(6)	1176	(9)
	υ_7	CH_2 rock	873?	(17)	879	(2)
	υ_8	CD wag (o.p.)	830	(4)	840	(3)
	υ_9	CH_2 wag (o.p.)	-		930	(3)
	υ_{10}	C-C str	824	(10)	822	(4)
	υ_{11}	CH_2 twist	-		725	(2)
	υ_{12}	C=C-C angle bend	257.4	(11)	266	(4)
	υ_{13}	torsion	194 (0^+-2^+)[c]		136	(1)
B	υ_{14}	CH_2 antisym str	-		3102	(4)
	υ_{15}	CH_2 sym str	-		3021	(7)
	υ_{16}	C-D str	-		2222	(18)
	υ_{17}	C=C antisym str	-		1633	(2)
	υ_{18}	CH_2 def	1367	(22)	1393	(8)
	υ_{19}	C-D wag (i.p.)	-		939	(3)
	υ_{20}	CH_2 rock	1128?	(3)	1133	(0.03)
	υ_{21}	C-D wag (o.p.)	-		859	(0.5)
	υ_{22}	CH_2 wag (o.p.)	-		930	(2)
	υ_{23}	C=C-C angle bend	-		592	(0.2)
	υ_{24}	CH_2 twist	439	(10)	434	(0.4)

[a] Relative intensities in parenthesis. Observed intensities indicate peak height.
[b] B3LYP/6-311++g(d,p); frequencies scaled with a scaling factor of 0.985 for frequencies less than 1800 cm^{-1} and 0.964 for frequencies greater than 1800 cm^{-1}.
[c] Reference 92.

Table 46: Observed and calculated vibrational frequencies (cm^{-1}) and intensities[a] for *gauche* 1,3-butadiene-1,1,4,4-d_4

C_2	Approximate Description	OBS		Calculated[b]		OBS Lit[c]	CALC Lit[d]
A	υ_1 CD_2 antisym str	2324?	(13)	2312	(25)	2337	2321
	υ_2 CD_2 sym str	2234	(11)	2208	(16)	2228	2213
	υ_3 CH sym str	3026	(14)	3024	(62)	3025	3024
	υ_4 C=C antisym str	1580	(100)	1600	(100)	1592	1575
	υ_5 CD_2 def	1075	(7)	1085	(3)	1084	1077
	υ_6 C-H wag (i.p.)	1307	(9)	1316	(6)	1305	1295
	υ_7 CD_2 rock	-		723	(1)	-	724
	υ_8 CH wag (o.p.)	929	(3)	935	(5)	927	912
	υ_9 CD_2 wag (o.p.)	-		751	(2)	726	741
	υ_{10} C-C str	972	(2)	980	(7)	944	968
	υ_{11} CD_2 twist	595	(6)	601	(2)	594	603
	υ_{12} C=C-C angle bend	249.1	(11)	231	(2)	-	236
	υ_{13} torsion	186 (0^+-2^+)[e]		135	(0.7)	-	163
B	υ_{14} CD_2 antisym str	-		2310	(2)	2337	2319
	υ_{15} CD_2 str	-		2210	(3)	2228	2213
	υ_{16} CH sym str	-		3010	(25)	3013	3013
	υ_{17} C=C antisym str	1596?	(4)	1614	(2)	-	1576
	υ_{18} CD_2 def	-		1035	(2)	1031	1032
	υ_{19} C-H wag (i.p.)	1292	(13)	1296	(3)	1285	1273
	υ_{20} CD_2 rock	-		954	(0.7)	-	945
	υ_{21} C-H wag (o.p.)	-		922	(2)	914	911
	υ_{22} CD_2 wag (o.p)	-		743	(0.4)	727	734
	υ_{23} C=C-C angle bend	-		504	(0.2)	498	512
	υ_{24} CD_2 twist	-		368	(0.2)	373	364

[a] Relative intensities in parenthesis. Observed intensities indicate peak height.
[b] B3LYP/6-311++g(d,p); frequencies scaled with a scaling factor of 0.985 for frequencies less than 1800 cm^{-1} and 0.964 for frequencies greater than 1800 cm^{-1}.
[c] References 44, 55. [d] Reference 51. [e] Reference 92.

Table 47: Observed and calculated vibrational frequencies (cm^{-1}) and intensities[a] for *gauche* 1,3-butadiene-d_6

C_2	Approximate Description	OBS		Calculated[b]		OBS Lit[c]	CALC Lit[d]
A	υ_1 CD_2 antisym str	2318	(4)	2313	(23)	2335	2321
	υ_2 CD_2 sym str	-		2240	(37)	2256	2246
	υ_3 CD sym str	2222	(2)	2199	(3)	2222	2201
	υ_4 C=C sym str	1579	(100)	1592	(100)	1552	1567
	υ_5 CD_2 def	1008	(5)	1007	(5)	-	1003
	υ_6 C-D wag (i.p.)	818?	(3)	840	(1)	-	824
	υ_7 CD_2 rock	-		723	(2)	705	722
	υ_8 C-D wag (o.p.)	-		786	(4)	-	753
	υ_9 CD_2 wag (o.p.)	-		714	(1)	-	717
	υ_{10} C-C str	-		1162	(4)	1165	1154
	υ_{11} CD_2 twist	587?	(2)	593	(1)	587	595
	υ_{12} C=C-C angle bend	238.5	(2)	229	(2)	-	234
	υ_{13} torsion	180 (0^+-2^+)[e]		122	(1)	-	147
B	υ_{14} CD_2 antisym str	-		2311	(1)	2335	2320
	υ_{15} CD_2 sym str	-		2234	(16)	2256	2242
	υ_{16} C-D antisym str	-		2197	(2)	2222	2198
	υ_{17} C=C antisym str	-		1575	(3)	1528	1536
	υ_{18} CD_2 def	-		1061	(0.2)	1056	1052
	υ_{19} C-D wag (i.p.)	881	(1)	880	(3)	877	872
	υ_{20} CD_2 rock	995?	(4)	1002	(1)	-	1002
	υ_{21} C-D wag (o.p.)	-		770	(1)	753	745
	υ_{22} CD_2 wag (o.p.)	-		724	(0.1)	712	725
	υ_{23} C=C-C angle bend	499?	(1)	497	(0.2)	492	504
	υ_{24} CD_2 twist	360	(2)	357	(0.2)	360	351

[a] Relative intensities in parenthesis. Observed intensities indicate peak height.
[b] B3LYP/6-311++g(d,p); frequencies scaled with a scaling factor of 0.985 for frequencies less than 1800 cm^{-1} and 0.964 for frequencies greater than 1800 cm^{-1}.
[c] References 44, 55. [d] Reference 51. [e] Reference 92.

The spectra obtained in the present study of these molecules are the best high quality spectra with the highest signal to noise and highest sensitivity. A large number of figures will be displayed to support that. Figures 60 to 63 present the full gas-phase Raman spectra of the 1,3-butadiene-d_0, and its 2,3-d_2, 1,1,4,4-d_4, and d_6 isotopomers. In each case the computed spectra for the *trans* and *gauche* rotamers are shown for comparison. The observed spectra match the calculated *trans* spectra well, since this rotamer makes up ~98% of the sample. The *gauche* bands are not evident in these figures. As discussed previously, the *trans* A_g bands are generally sharper and more intense than the broad B_g bands. Consequently, the computed spectral bands, all of which are generated with the same band shape, generally match the intensities of the observed A_g bands quite well, but appear too narrow with too much peak height for the B_g bands. These B_g bands are weaker in the first place and the fact that they are broad makes them appear weaker yet.

Figures 64 to 69 show the 1,3-butadiene spectral features in much greater detail. Figures 70 to 76 show the spectral features for the deuterated 2,3-d_2 isotopomer. Figures 77 to 83 show the spectral features for the deuterated 1,1,4,4-d_4 isotopomer. Figures 84 to 89 show the spectral features for the deuterated d_6 isotopomer. Tables 40 to 43 tabulate the assignments for the *trans* rotamers for the four isotopomers and Tables 44 to 47 do the same for the *gauche* rotamers.

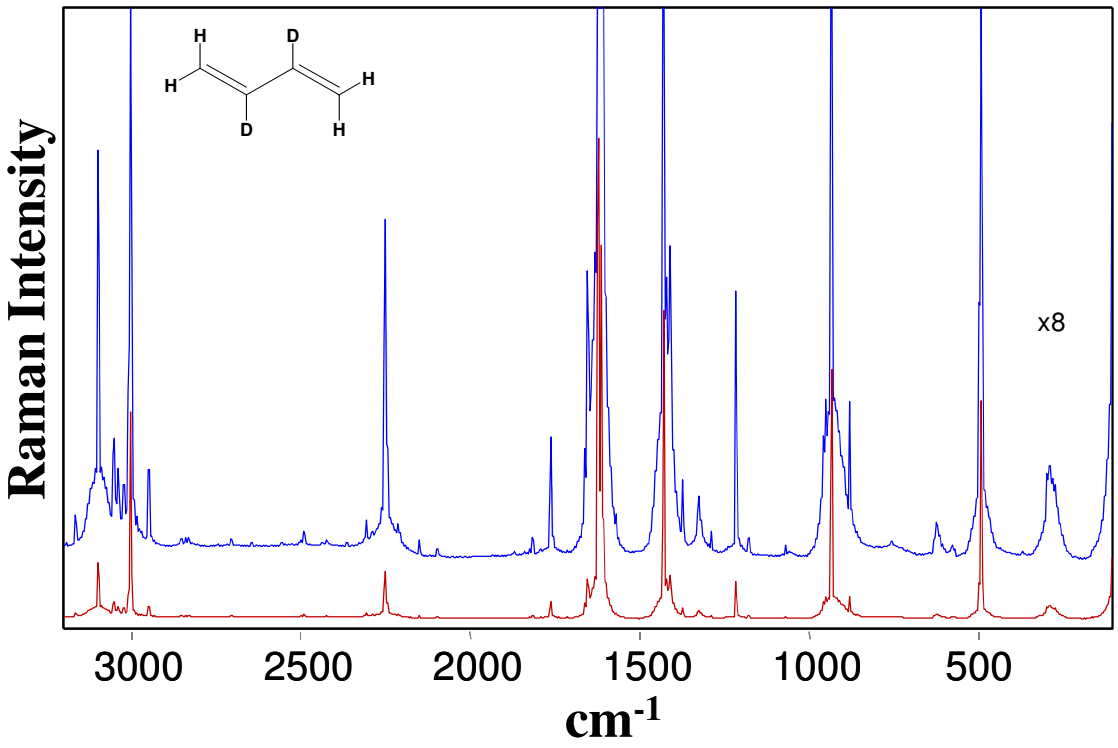

Figure 70. Gas-phase Raman spectrum of 1,3-butadiene-2,3-d_2 in the 200-3200 cm^{-1} region.

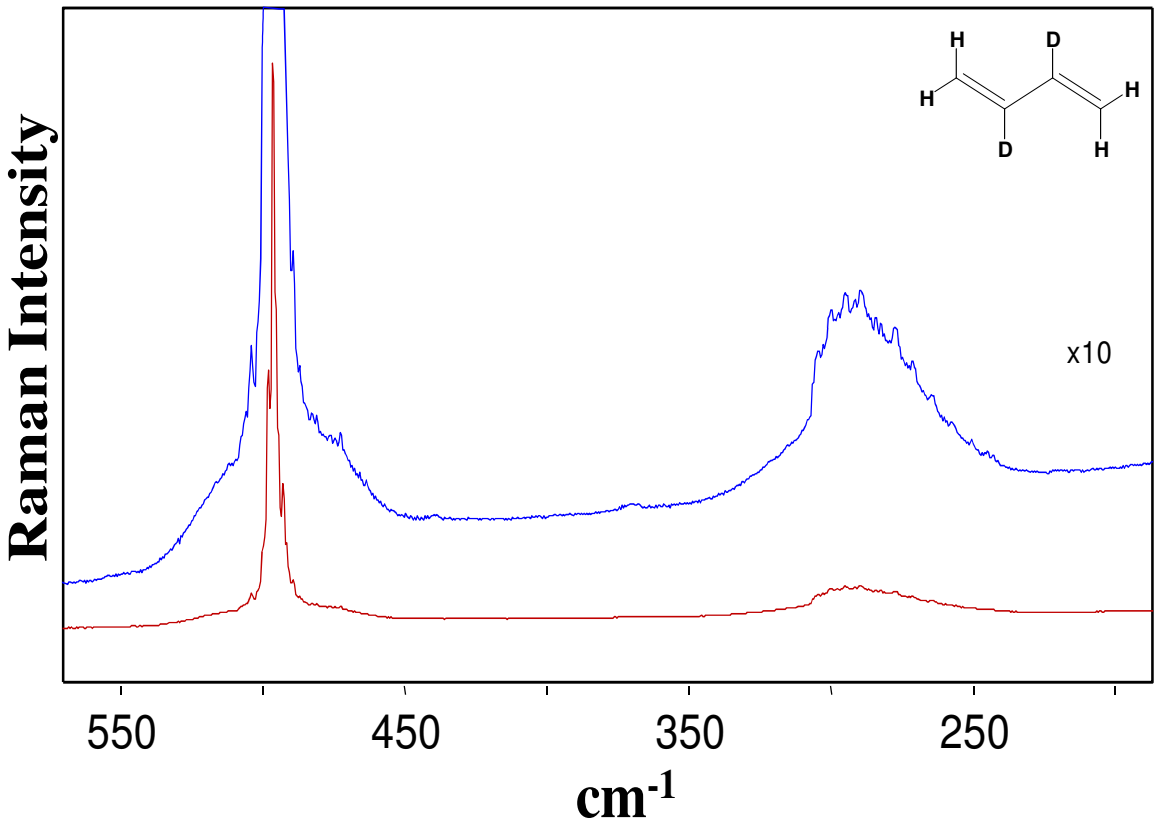

Figure 71. Gas-phase Raman spectrum of 1,3-butadiene-2,3-d_2 in the 200-600 cm^{-1} region.

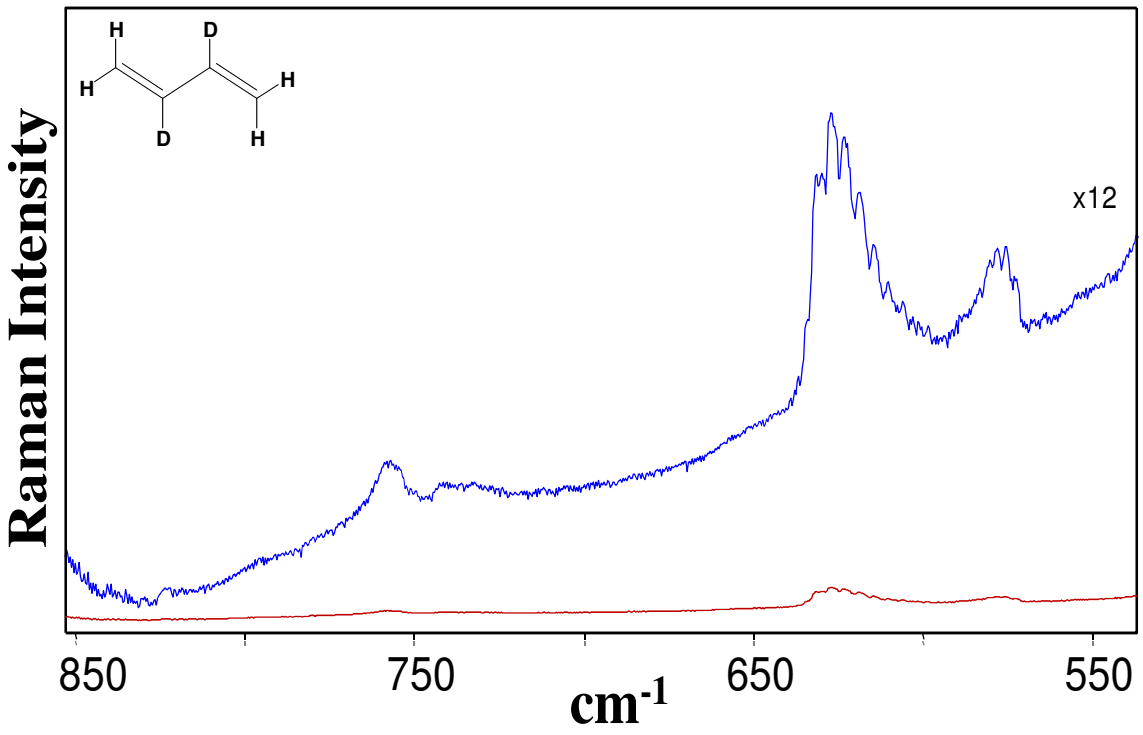

Figure 72. Gas-phase Raman spectrum of 1,3-butadiene-2,3-d_2 in the 550-850 cm^{-1} region.

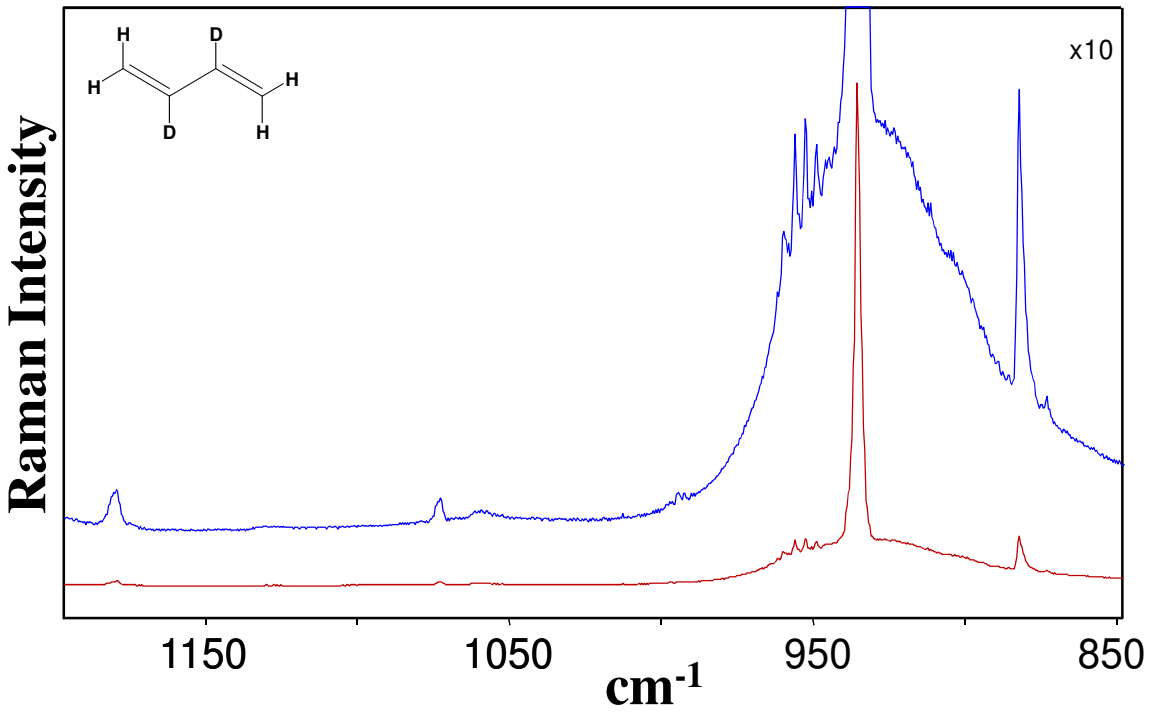

Figure 73. Gas-phase Raman spectrum of 1,3-butadiene-2,3-d_2 in the 850-1200 cm^{-1} region.

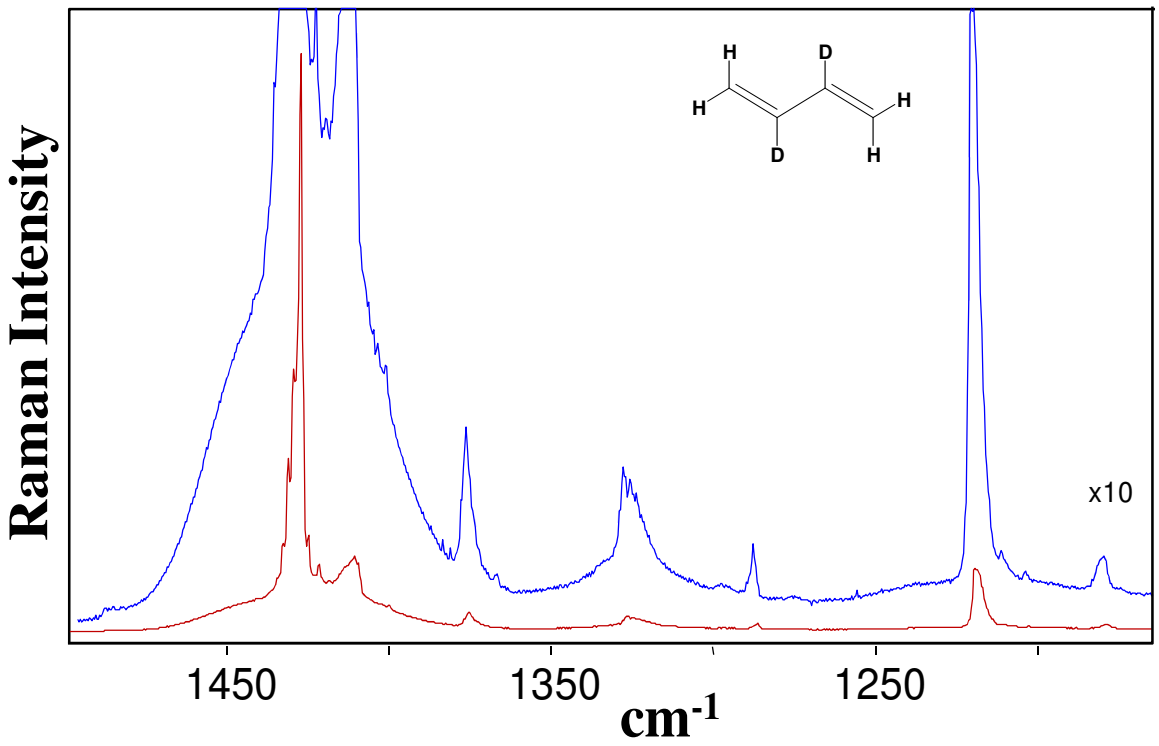

Figure 74. Gas-phase Raman spectrum of 1,3-butadiene-2,3-d_2 in the 1100-1500 cm^{-1} region.

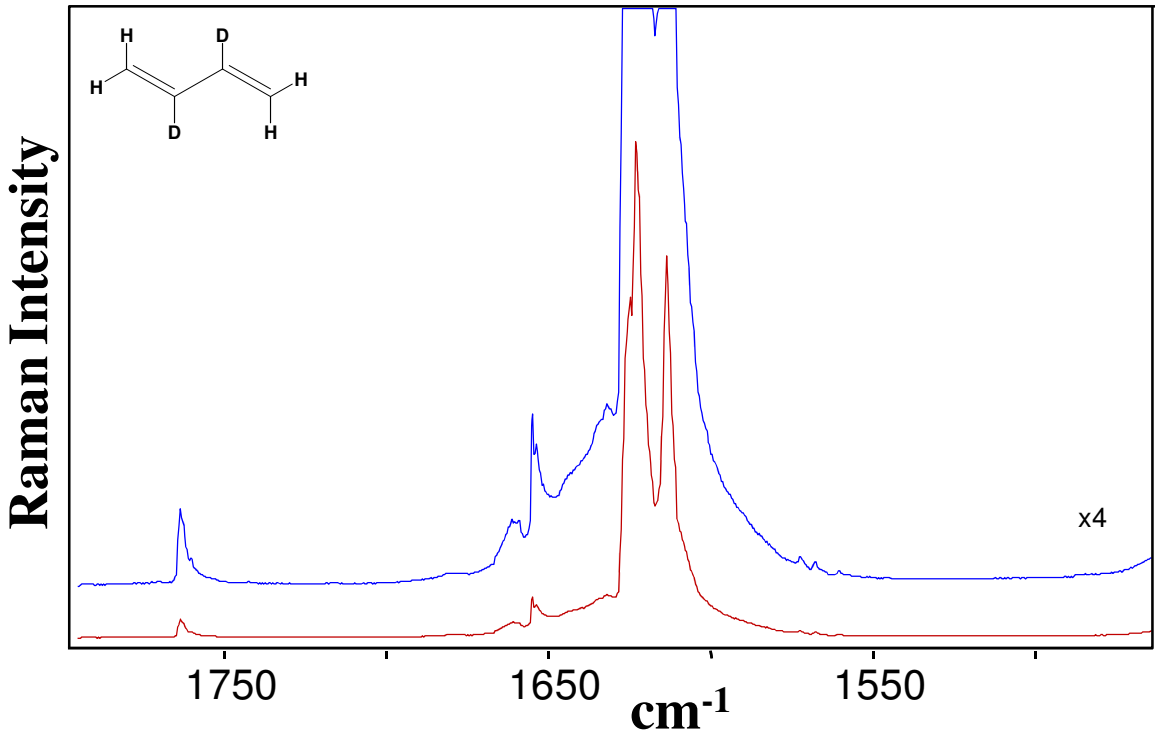

Figure 75. Gas-phase Raman spectrum of 1,3-butadiene-2,3-d_2 in the 1450-1800 cm^{-1} region.

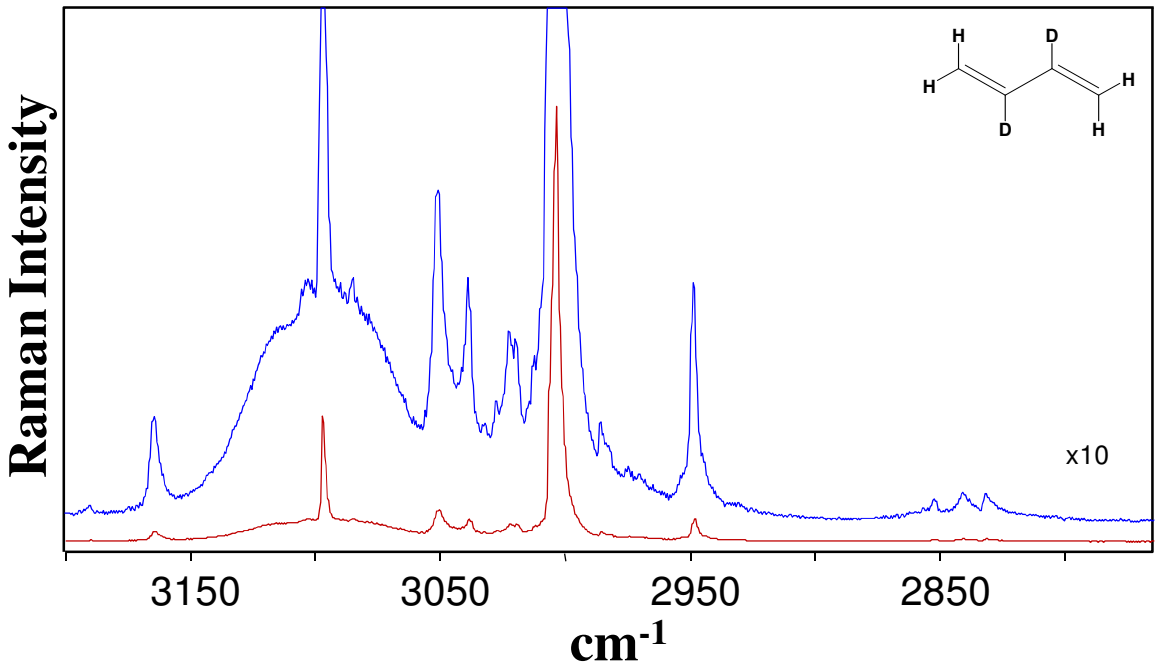

Figure 76. Gas-phase Raman spectrum of 1,3-butadiene-2,3-d_2 in the 2800-3200 cm^{-1} region.

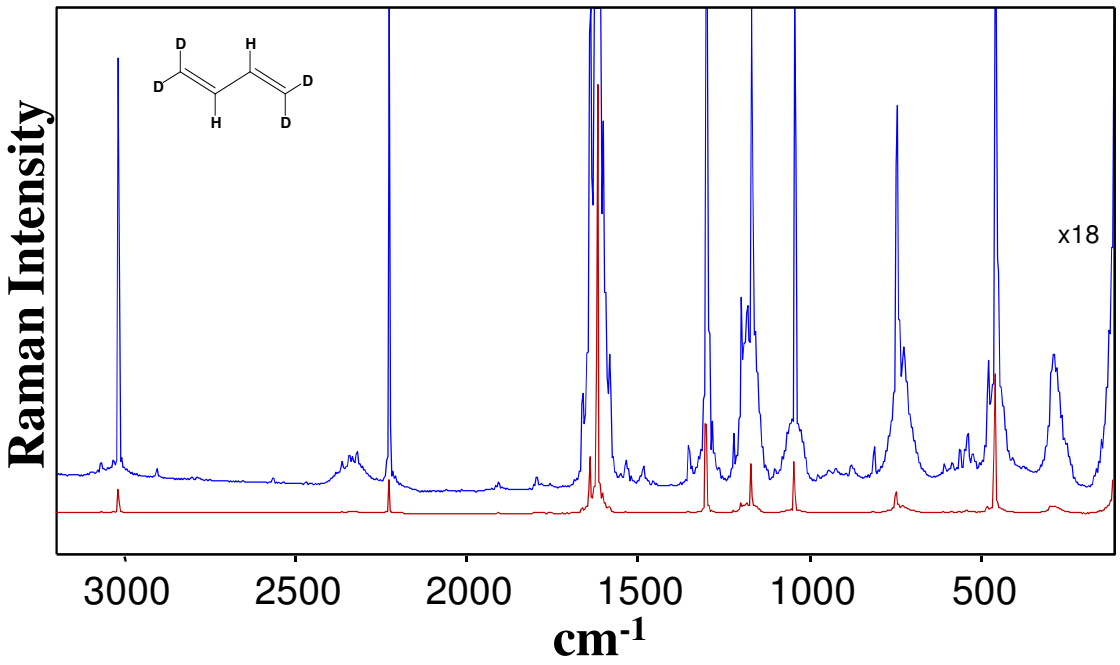

Figure 77. Gas-phase Raman spectrum of 1,3-butadiene-1,1,4,4-d_4 in the 200-3200 cm^{-1} region.

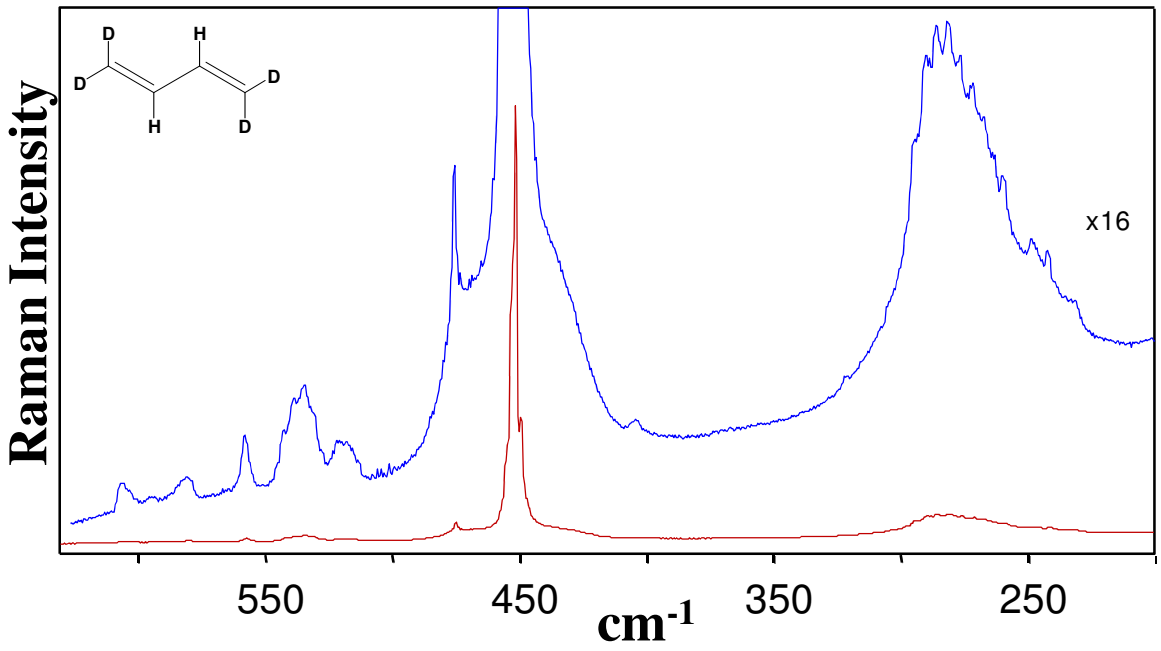

Figure 78. Gas-phase Raman spectrum of 1,3-butadiene-1,1,4,4-d_4 in the 200-600 cm^{-1} region.

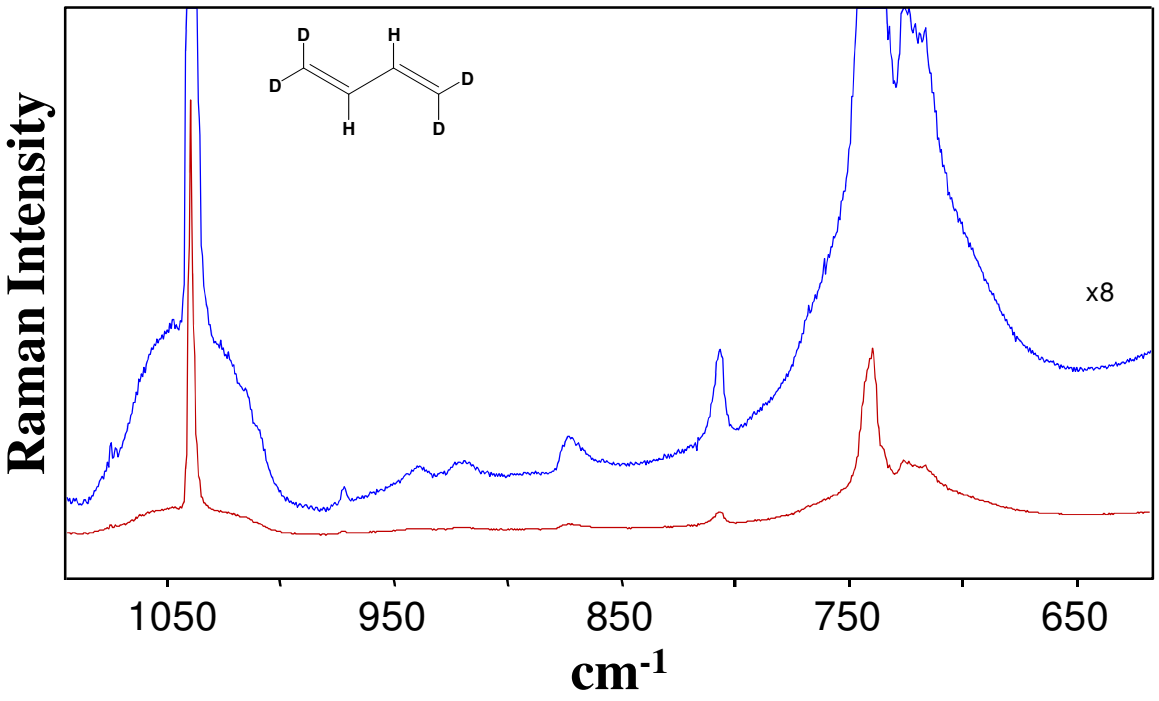

Figure 79. Gas-phase Raman spectrum of 1,3-butadiene-1,1,4,4-d_4 in the 650-1100 cm^{-1} region.

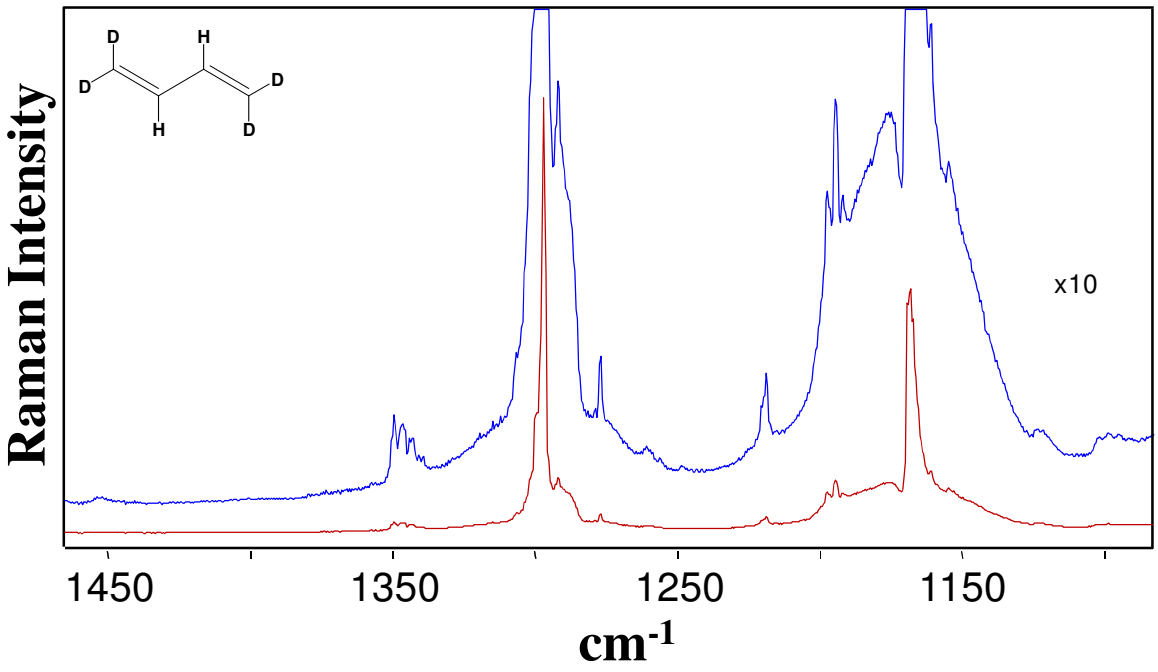

Figure 80. Gas-phase Raman spectrum of 1,3-butadiene-1,1,4,4-d_4 in the 1100-1450 cm^{-1} region.

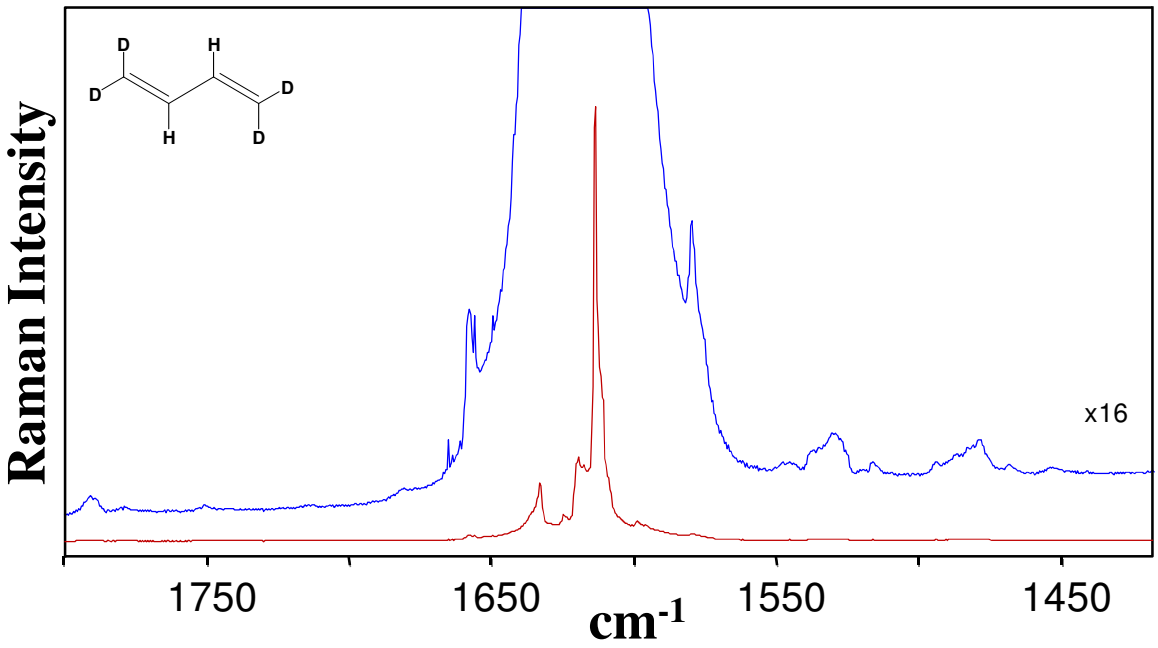

Figure 81. Gas-phase Raman spectrum of 1,3-butadiene-1,1,4,4-d_4 in the 1450-1800 cm^{-1} region.

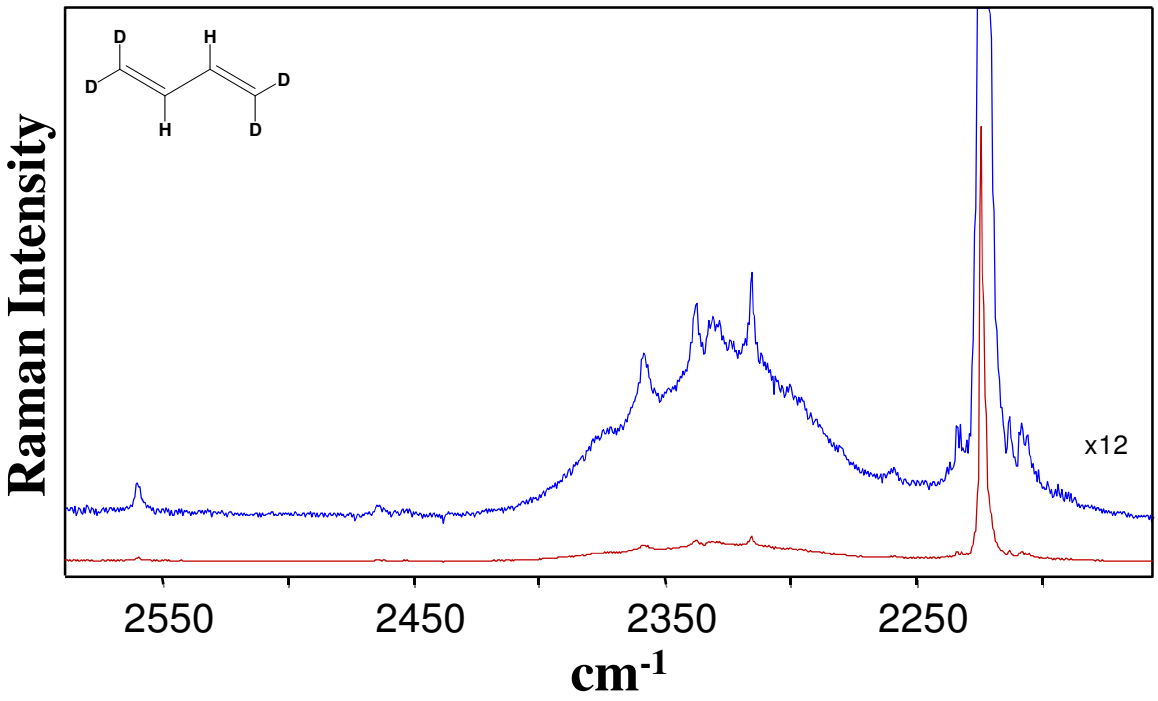

Figure 82. Gas-phase Raman spectrum of 1,3-butadiene-1,1,4,4-d_4 in the 2150-2600 cm^{-1} region.

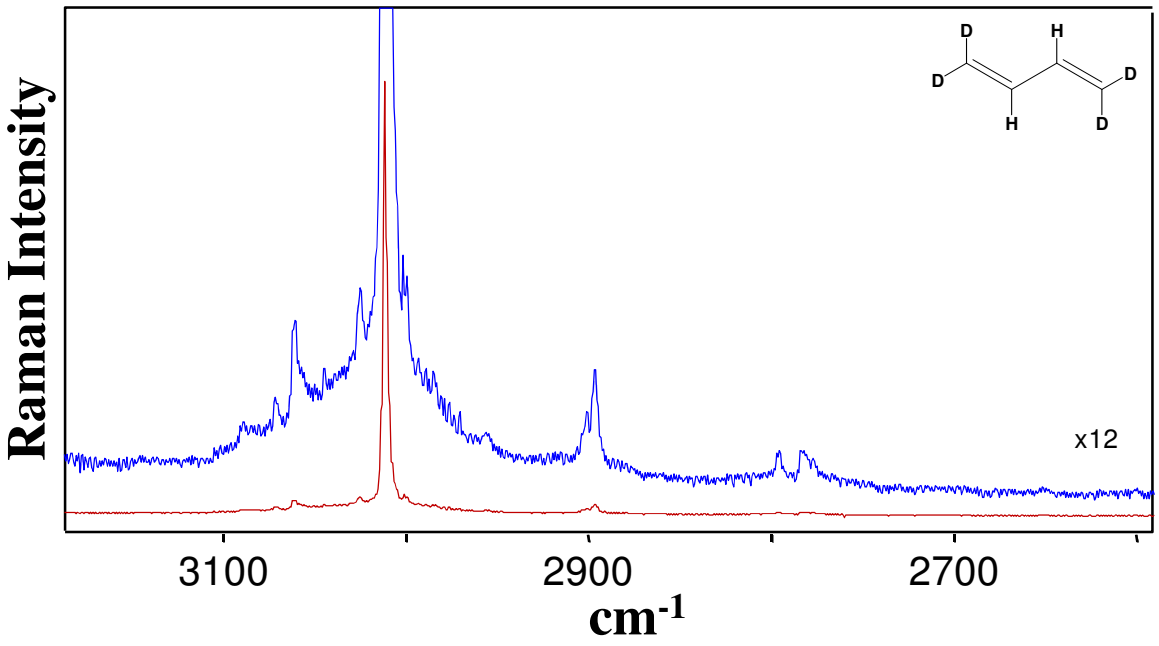

Figure 83. Gas-phase Raman spectrum of 1,3-butadiene-1,1,4,4-d_4 in the 2600-3200 cm^{-1} region.

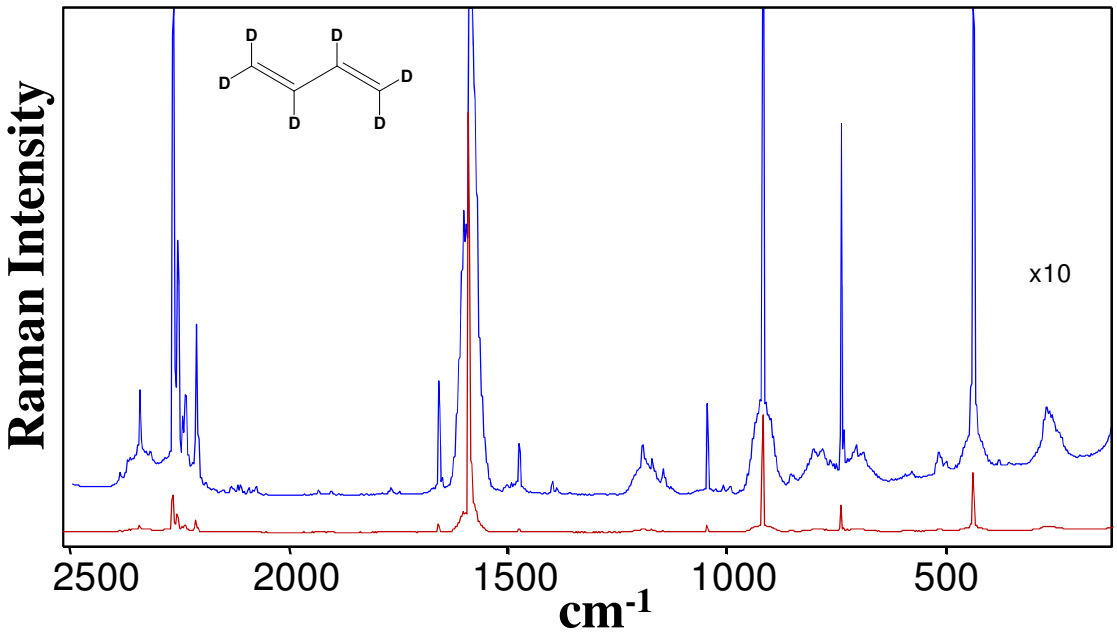

Figure 84. Gas-phase Raman spectrum of 1,3-butadiene-d_6 in the 200-2500 cm^{-1} region.

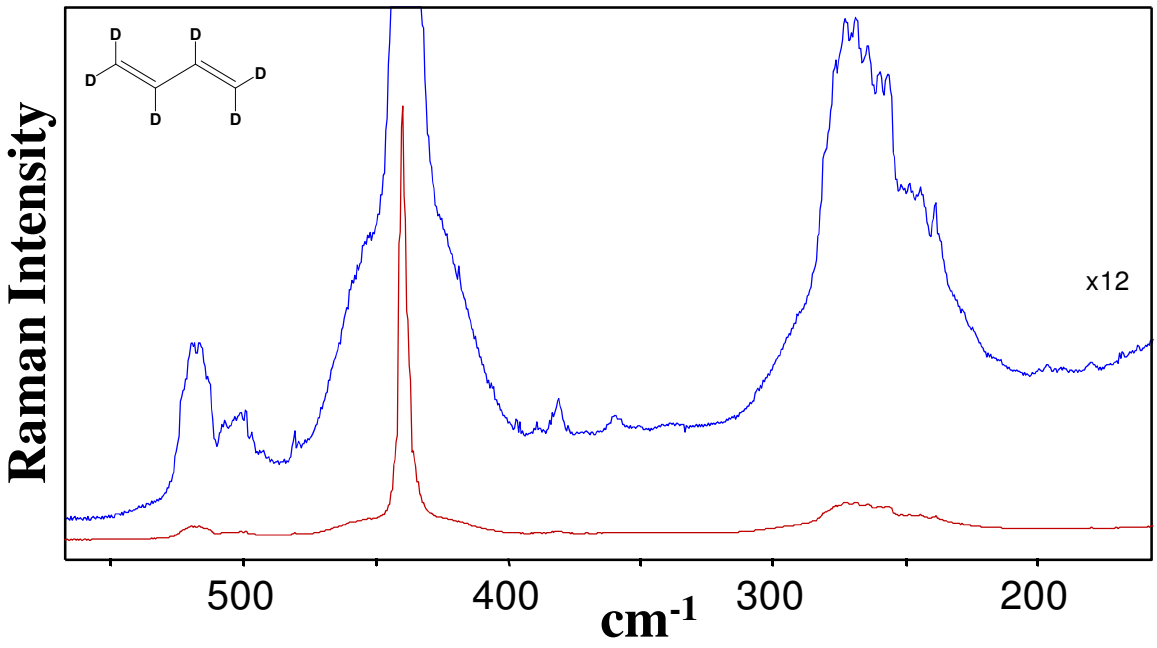

Figure 85. Gas-phase Raman spectrum of 1,3-butadiene-d_6 in the 200-600 cm^{-1} region.

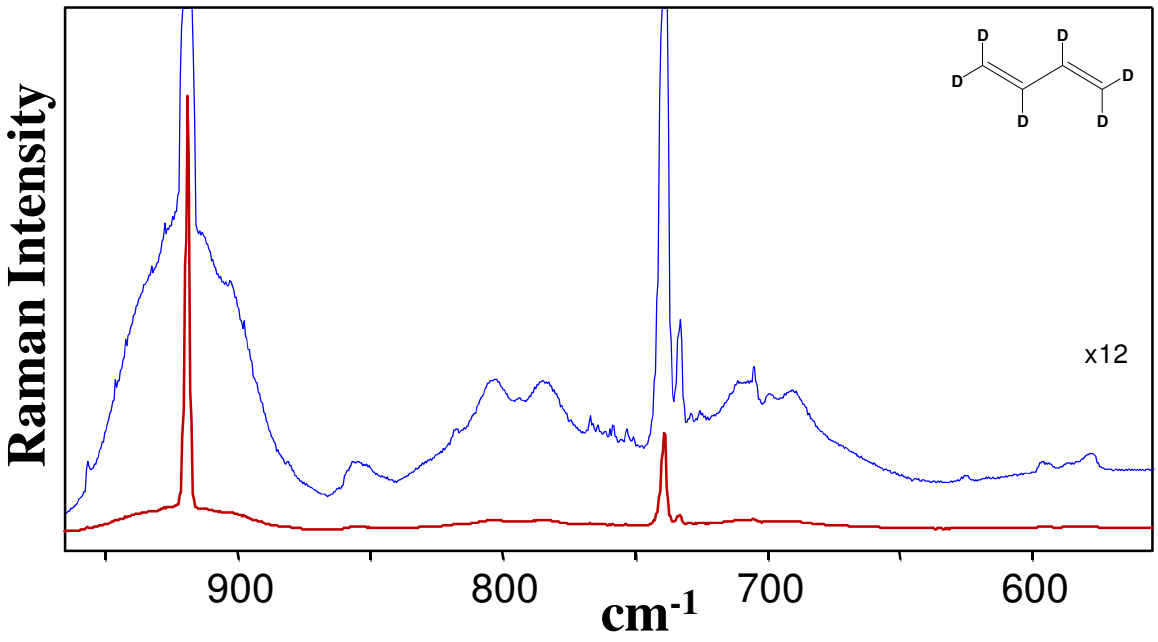

Figure 86. Gas-phase Raman spectrum of 1,3-butadiene-d_6 in the 600-950 cm^{-1} region.

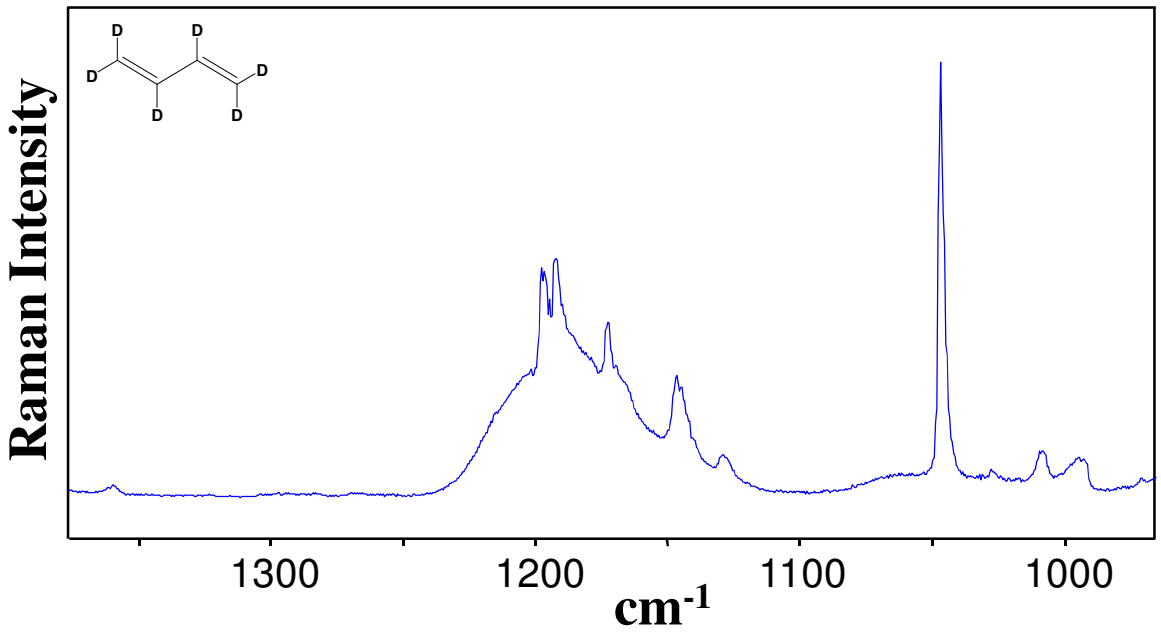

Figure 87. Gas-phase Raman spectrum of 1,3-butadiene-d_6 in the 950-1350 cm^{-1} region.

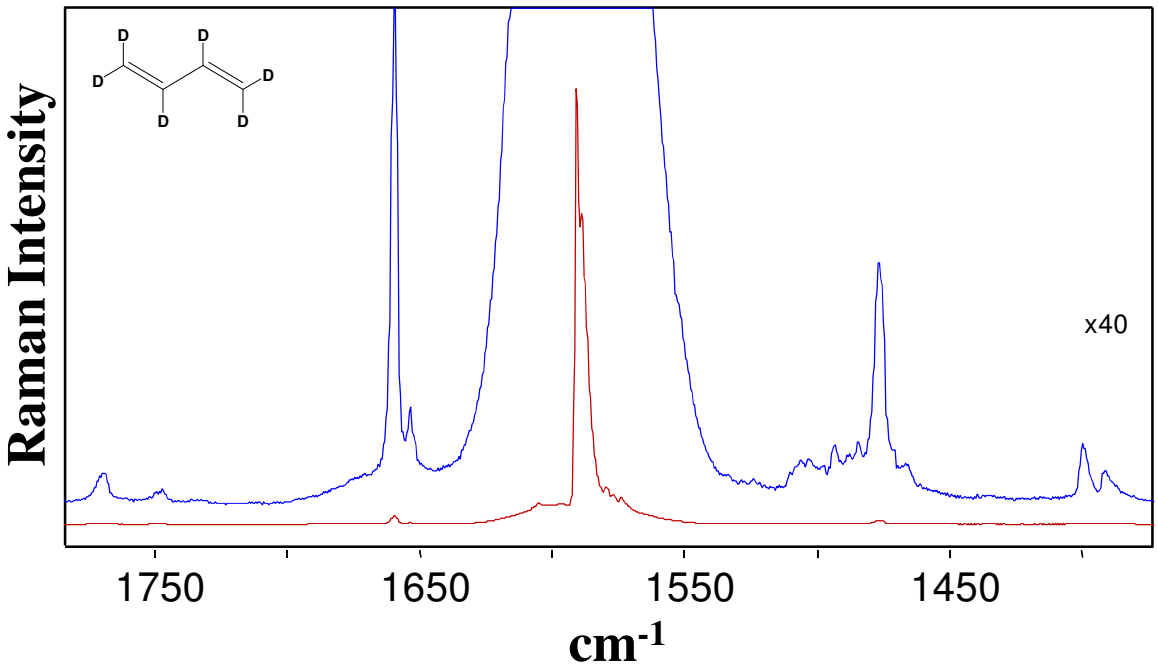

Figure 88. Gas-phase Raman spectrum of 1,3-butadiene-d_6 in the 1400-1800 cm^{-1} region.

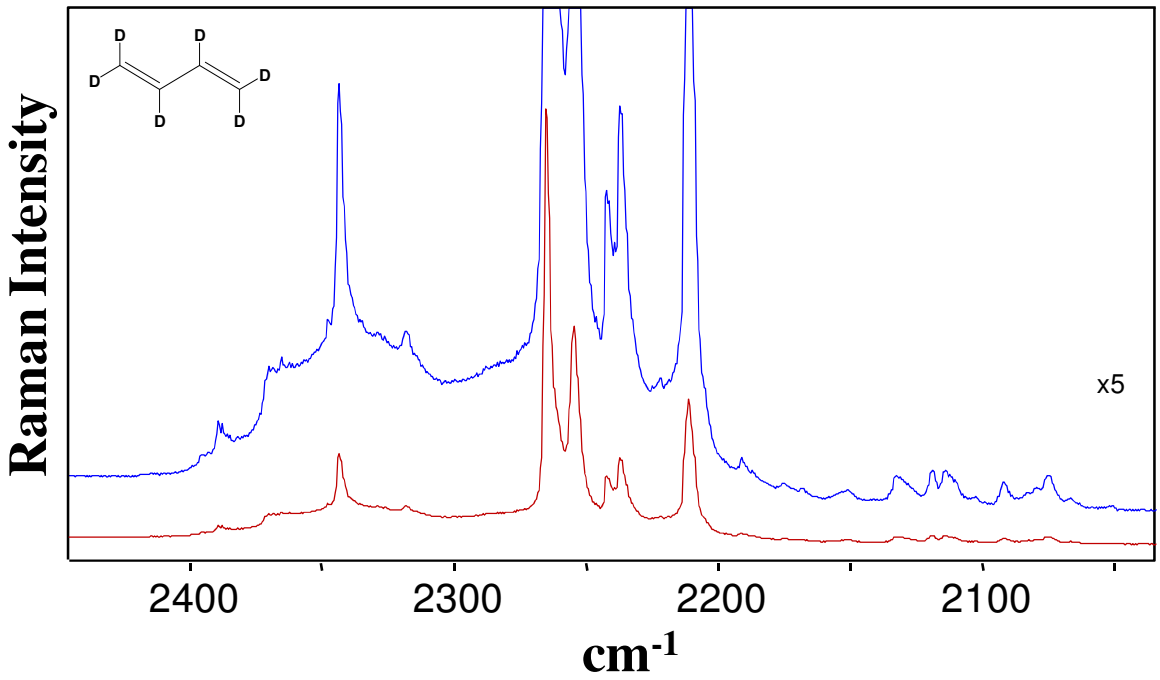

Figure 89. Gas-phase Raman spectrum of 1,3-butadiene-d_6 in the 2050-2450 cm^{-1} region.

Numerous overtones, combination bands, and hot bands were observed for the *trans* rotamers in addition to the bands for the vibrational fundamentals. Tables 48 to 51 tabulate all of the observed Raman bands for the isotopomers.

CONCLUSION

Because of the low abundance (~2%) of the *gauche* rotamer, identification of the *gauche* Raman bands was quite a challenge. In addition to the bands for the *trans* and *gauche* fundamentals, the spectra are rich with overtone and combination bands as well as hot bands from low-lying vibrational states. A number of these have been discussed in previous chapters. The *gauche* bands were assigned on the basis of four criteria. First, their wavenumbers should not differ much from their computed values (generally ±10 cm^{-1}). Second, their computed intensities should be relatively high, and most therefore would correspond to vibrations of A symmetry. Third, the intensity of the bands should increase significantly with temperature. At 260° C the *gauche* conformer should make up about 12% of the sample. Fourth, the current assignments were compared to the published matrix isolation work.[44,55] The heated spectra were only obtained for the d_0 parent sample so the benefit of observing intensity increase upon heating for the deuterated species was precluded. Consequently, the d_0 assignments are most reliable, and six bands to the *gauche* rotamer were attributed with confidence. Four other assignments were more speculative. The d_2 assignments were less reliable for which the spectra were not quite as good, but the spectra and assignments for the d_4 and d_6 isotopomers are quite reliable.

Table 48: Observed vibrational frequencies (cm^{-1}) and assignments for 1,3-butadiene-d_0

ν_{OBS}		Assignment	Inferred
3282.4	mw	$2\upsilon_4$	2x1644.3 = 3288.6
3278.0	mw	$2\upsilon_{21} + \upsilon_9$?	2x1381[a]+512.2 = 3274
3187.7	s	$2\upsilon_{20}$?	2x1597[a] = 3194
3099	s	υ_1	3099
3087.6	vvw	$\upsilon_4 + \upsilon_5$	1644.3+1442.2 = 3086.5
3034.9	m	-	
3023	m	υ_2 (gauche)	3023
3012.5	vvs	υ_2	3012.5
3010 sh	vs	υ_3	3010
2961.5	ms	-	
2933.1	w	$2\upsilon_{16} + \upsilon_5$	2x748+1442.2 = 2938
2923.4	vw	$\upsilon_4 + \upsilon_6$	1644.3+1277.8 = 2922.1
2912.6	vvw	-	
2877.3	m	$2\upsilon_5$?	2x1442.2 = 2884.4
2864.0	vw	$2\upsilon_{23} + \upsilon_8$?	2x990[a]+888.8 = 2869
2842.5	mw	$\upsilon_4 + \upsilon_7$?	1644.3+1204.2 = 2848.5
2757.9	mw	$2\upsilon_{21}$	2x1381[a] = 2762
2688.5	vvvw	$\upsilon_4 + 2\upsilon_{12}$	1644.3+2x525[a] = 2694
2642.6	mw	$\upsilon_5 + \upsilon_7$	1442.2+1204.2 = 2646.4
2524.5	w	-	
2479.6	vvw	-	
2403.8	mw	$2\upsilon_7$	2x1204.2 = 2408.4
2328.6	mw	$\upsilon_5 + \upsilon_8$	1442.2+888.8 = 2331
2306.1	vvw	$2\upsilon_9 + \upsilon_6$	2x512.2+1277.8 = 2302.2
2279.9	vvw	-	-
2152.3	vvw	$\upsilon_4 + \upsilon_9$?	1644.3+512.2 = 2156.5
2092.5	mw	$\upsilon_7 + \upsilon_8$	1204.2+888.8 = 2093
2088.2	m	-	
2009.7	vvw	$2\upsilon_{16} + \upsilon_9$	2x748+512.2 = 2008
1977.1	vvw	$2\upsilon_{23}$	2x990[a] = 1980
1933.1	vvw	-	
1894.7	w	$\upsilon_{20} + \upsilon_{24}$	1597[a]+299[a] = 1896
1873.9	vw	-	
1822.4	w	-	
1798.8	vw	$2\upsilon_{24} + \upsilon_7$	2x299[a]+1204.2 = 1802
1790.7	w	$\upsilon_6 + \upsilon_9$	1277.8+512.2 = 1790
1776.2	ms	$2\upsilon_8$	2x888.8 = 1776.6
1739.4	w	-	
1715.6	mw	$\upsilon_7 + \upsilon_9$	1204.2+512.2 = 1716.4

Table 48: (Continued)

ν_{OBS}		Assignment	Inferred
1679.6	s	$\upsilon_{21} + \upsilon_{24}$	$1381^{a}+299^{a} = 1680$
1661.2	vs	$\upsilon_{15} + \upsilon_{16}$ (0-0)	909.5+748 = 1658
1660.2	vs	(1-1)	1660.2
1658.9	vs	(2-2)	1658.9
1657.7	s	(3-3)	1657.7
1656.4	s	(4-4)	1656.4
1654.6	mw	(5-5)	1654.6
1652.9	mw	(6-6)	1652.9
1650.0	w	(7-7)	1650.0
1644.3	vvs	υ_4	1644.3
1614.5	m	υ_4 (gauche)	1614.5
1583.4	w	-	
1536.5	mw	$\upsilon_{10} + \upsilon_{12}$ (0-0)	$1014^{a}+525^{a} = 1539$
1531.3	mw	(1-1)	1531.3
1524.5	w	(2-2)	1524.5
1518.8	vw	(3-3)	1518.8
1513.9	vw	(4-4)	1513.9
1508.3	vvw	(5-5)	1508.3
1442.2	vs	υ_5	1442.2
1432.4	mw	$\upsilon_{11} + \upsilon_{12}$	$908^{a}+525^{a} = 1433$
1428	w	υ_5 (gauche)	1428
1398.5	m	$\upsilon_8 + \upsilon_9$	888.8+512.2 = 1401
1311	m	$\upsilon_{23} + \upsilon_{24}$ (3-3)	1311
1307	s	$\upsilon_{23} + \upsilon_{24}$ (2-2)	1307
1301	s	$\upsilon_{23} + \upsilon_{24}$ (1-1)	1301
1298	s	$\upsilon_{23} + \upsilon_{24}$ (0-0)	$990^{a}+299^{a} = 1289$
1283.6	m	-	
1277.8	vs	υ_6	1277.8
1204.2	vs	υ_7	1204.2
1193.5	mw	-	
1172.8	mw	$\upsilon_{10} + \upsilon_{13}$ (0-1)	$1014^{a}+162.4^{a} = 1176$
1167.7	mw	(1-2)	1167.7
1162.6	mw	(2-3)	1162.6
1157.9	w	(3-4)	1157.9
1153.5	vw	(4-5)	1153.5
1149.0	vvw	(5-6)	1149.0
1145.2	vvw	(6-7)	1145.2
1069.8	w	$\upsilon_{11} + \upsilon_{13}$	$908^{a}+162.4^{a} = 1070$
1051	vvw	υ_7 (gauche)	1051
1048.9	vvw	$2\upsilon_{12}$	$2x525^{a} = 1050$

Table 48: (Continued)

ν_{OBS}		Assignment	Inferred
1023.2	vvw	$2\upsilon_9$	2x512.2 = 1024.4
1012	vvw	υ_{21} (gauche)?	1012
993	vvw	υ_8 (gauche)?	993
977	vvw	υ_{14}	977
919.5	mw	-	-
909.5	vw	υ_{15}	909.5
888.8	ms	υ_8	888.8
869	w	υ_{10} (gauche)?	869
748	w	υ_{16}	748
734	vvw	υ_{11} (gauche)	734
682.8	m	$\upsilon_{12} + \upsilon_{13}$(0-1)	525[a]+162.4[a] = 687
676.8	m	(1-2)	676.8
670.5	m	(2-3)	670.5
664.3	m	(3-4)	664.3
657.8	mw	(4-5)	657.8
650.7	w	(5-6)	650.7
644.3	vw	(6-7)	644.3
638.8	vw	(7-8)	638.8
632.9	vvw	(8-9)	632.9
589	w	υ_{23} (gauche)?	589
535.3	w	-	-
512.2	vvs	υ_9	512.2
322.4	ms	$2\upsilon_{13}$ (0-2) trans	2x162.4[a] = 324.8
317.3	ms	(1-3)	317.3
311.9	ms	(2-4)	311.9
306.4	ms	(3-5)	306.4
300.4	m	(4-6)	300.4
293.6	m	(5-7)	293.6
286.3	m	(6-8)	286.3
282.0	w	(0^--2^-) gauche	282.0[a]
279.0	w	$2\upsilon_{13}$ (7-9) trans	279.0
275.1	vw	-	
270.8	m	υ_{12} (gauche)	270.8
261.9	vvw	(1^+-3^+) gauche	261.9 [a]
255.3	vvw	-	
226.7	vvw	-	
214.9	vw	(0^+-2^+) gauche	214.9 [a]

[a] References 53, 56, 92.

Table 49: Observed vibrational frequencies (cm^{-1}) and assignments for 1,3-butadiene-2,3-d_2

ν_{OBS}		Assignment	Inferred
3190.1	mw	$2\upsilon_{22} + \upsilon_6$	2x1127[a]+935.1 = 3189
3164.6	ms	-	-
3097.6	s	υ_1	3097.6
3085	m	υ_1 (gauche)?	3085
3050.9	ms	$\upsilon_4 + \upsilon_5$	1623.6+1427.8 = 3051.4
3038.6	m	-	
3013	w	υ_2 (gauche)?	3013
3004.0	vs	υ_2	3004.0
2948.6	m	-	-
2852.1	mw	$2\upsilon_5$	2x1427.8 = 2855.6
2840.8	mw	$\upsilon_4 + \upsilon_7$	1623.6+1220.1 = 2843.7
2831.9	mw	-	
2746.4	w	$2\upsilon_{21}$	2x1374[a] = 2748
2744.1	w	$\upsilon_3 + \upsilon_9$	2248.5+496.2 = 2744.7
2705.3	mw	-	-
2644.5	mw	$\upsilon_5 + \upsilon_7$	1427.8+1220.1 = 2647.9
2556.3	mw	$\upsilon_4 + \upsilon_6$	1623.6+935.1 = 2558.7
2527.9	vw	$\upsilon_{18} + \upsilon_{24}$	2243[a]+287[a] = 2530
2501.4	mw	$\upsilon_4 + \upsilon_8$	1623.6+882.0 = 2505.6
2492.7	m	-	
2437.5	w	$2\upsilon_7$	2x1220.1 = 2440.2
2423.2	mw	-	-
2362.8	mw	$\upsilon_5 + \upsilon_6$	1427.8+935.1 = 2362.9
2308.7	ms	$\upsilon_5 + \upsilon_8$	1427.8+882.0 = 2309.8
2289.6	mw	$2\upsilon_{20} - \upsilon_8$	2x1586[a] - 882.0 = 2290
2252.5	vs	$2\upsilon_{22}$	2x1127[a] = 2254
2248.5	m	υ_3	2248.5
2232	mw	-	
2211.8	m	-	
2153.4	m	$\upsilon_6 + \upsilon_7$	935.1+1220.1 = 2155.2
2118.2	vw	$\upsilon_4 + \upsilon_9$	1623.6+496.2 = 2119.8
2097.5	m	$\upsilon_7 + \upsilon_8$?	1220.1+882.0 = 2102.1
1870.8	mw	$2\upsilon_6$	2x935.1 = 1870.2
1840.9	w	$2\upsilon_{12} + \upsilon_8$(0-1)	2x480[a]+882.0 = 1842
1836.2	w	(1-2)	1836.2
1831.5	vw	(2-3)	1831.5
1824.0	mw	$2\upsilon_{15}$	2x911 = 1822

Table 49: (Continued)

ν_{OBS}		Assignment	Inferred
1817.1	ms	$\upsilon_6 + \upsilon_8$ $2\upsilon_{11}$	935.1+882.0 = 1817 2x908[a] = 1816
1793.3	mw	$2\upsilon_{24} + \upsilon_7$	2x287[a]+1220.1 = 1794
1763.9	vs	$2\upsilon_8$	2x882.0 = 1764
1760.3	ms	$\upsilon_{10} + \upsilon_{11}$	850[a]+908[a] = 1758
1717.4	mw	$\upsilon_7 + \upsilon_9$	1220.1+496.2 = 1716.3
1660.7	s	$\upsilon_{21} + \upsilon_{24}$	1374[a]+287[a] = 1661
1655.3	vs	$\upsilon_{15} + \upsilon_{16}$ (0-0)	911+743 = 1654
1654.1	vs	(1-1)	1654.1
1652.9	s	(2-2)	1652.9
1651.9	s	(3-3)	1651.9
1650.8	ms	(4-4)	1650.8
1649.5	mw	(5-5)	1649.5
1633 br	m	-	
1623.6	vvs	υ_4	1623.6
1613.9	vs	-	
1572.4	s	-	
1567.9	s	-	
1560.7	mw	-	
1487.4	mw	$2\upsilon_{16}$	2x743 = 1486
1431.7	vs	$\upsilon_6 + \upsilon_9$	935.1+496.2 = 1431.3
1427.8	vvvs	υ_5	1427.8
1426	mw	υ_5 (gauche)	1426
1411.4	vs	$\upsilon_{22} + \upsilon_{24}$	1127[a]+287[a] = 1414
1376.1	s	$\upsilon_8 + \upsilon_9$	882.0+496.2 = 1378.2
1367	w	υ_{18} (gauche)	1367
1329.9	w	-	
1327.5	s	$\upsilon_{10} + \upsilon_{12}$(0-0)	850[a]+480[a] = 1330
1325.7	s	(1-1)	1325.7
1323.7	s	(2-2)	1323.7
1321.6	ms	(3-3)	1321.6
1319.6	m	(4-4)	1319.6
1317.9	m	(5-5)	1317.9
1287.2	ms	-	
1128	vvw	υ_{20} (gauche)?	1128
1220.1	vs	υ_7	1220.1
1179.0	s	-	-
1174	vw	υ_6 (gauche)	1174
1072.3	m	-	-
1059.2	mw	$\upsilon_{11} + \upsilon_{13}$	908[a]+153[a] = 1061

Table 49: (Continued)

ν_{OBS}		Assignment	Inferred
1000.8	vvw	$\upsilon_{10} + \upsilon_{13}$(0-1)	850[a]+153[a] = 1003
996.9	w	(1-2)	996.9
994.2	mw	(2-3)	994.2
992.1	w	(3-4)	992.1
989.9	vvw	(4-5)	989.9
986.6	vvw	(5-6)	986.6
984.2	vvw	(6-7)	984.2
982.0	vvw	(7-8)	982.0
959.6	m	$2\upsilon_{12}$(0-0)	2x480[a] = 960
955.8	ms	(1-1)	955.8
952.2	ms	(2-2)	952.2
948.7	ms	(3-3)	948.7
945.5	mw	(4-4)	945.5
942.4	w	(5-5)	942.4
935.1	vvs	υ_6	935.1
911 sh	vw	υ_{15}	911 sh
882.0	s	υ_8	882.0
873	mw	υ_7 (gauche)?	873
824	vvw	υ_{10} (gauche)	824
757.3	mw	-	-
743	vw	υ_{16}	743
633.5	vw	$\upsilon_{12} + \upsilon_{13}$ (0-1)	480[a]+153[a] = 633
631.3	m	(1-2)	631.3
627.4	ms	(2-3)	627.4
622.9	ms	(3-4)	622.9
618.7	m	(4-5)	618.7
614.3	m	(5-6)	614.3
610.1	mw	(6-7)	610.1
605.6	w	(7-8)	605.6
600.7	w	(8-9)	600.7
578.1	m	-	-
575.3	m	$2\upsilon_{24}$	2x287[a] = 574
572.9	mw	-	-
496.2	vvs	υ_9	496.2
439	vw	υ_{24} (gauche)	439
303.8	ms	$2\upsilon_{13}$ (0-2) trans	2x153[a] = 306
302.0	w	(2^--4^-) gauche	302.0[a]
299.1	ms	$2\upsilon_{13}$ (1-3) trans	299.1
294.1	ms	(2-4)	294.1
288.9	ms	(3-5)	288.9

Table 49: (Continued)

ν_{OBS}		Assignment	Inferred
283.4	ms	(4-6)	283.4
281.7	w	(2^+-4^+) gauche	281.7[a]
276.7	ms	$2\upsilon_{13}$ (5-7) trans	276.7
270.4	m	(6-8)	270.4
263.7	m	(7-9)	263.7
257.4	mw	υ_{12} (gauche)	257.4
250.1	mw	(0^--2^-) gauche	250.1[a]
244.4	mw	-	
242.4	w	-	
217.7	vw	(1^+-3^+) gauche	217.7[a]
204	vw	-	
194	vvw	(0^+-2^+) gauche	194[a]
177	vvw	-	

[a] References 52, 53, 92.

Table 50: Observed vibrational frequencies (cm^{-1}) and assignments for 1,3-butadiene-1,1,4,4-d_4

ν_{OBS}		Assignment	Inferred
3071.9	w	$2\upsilon_{11} + \upsilon_4$	2x728[a]+1613.7 = 3070
3061.7	mw	$2\upsilon_{20}$	2x1533[a] = 3066
3026	mw	υ_3 (gauche)	3026
3012.1	s	υ_3	3012.1
2985.2	w	-	
2901.5	mw	$4\upsilon_{15}$	4x726 = 2904
2897.1	m	-	
2796.1	w	$2\upsilon_{23} + \upsilon_7$	2x813[a]+1168.0 = 2794
2783.3	w	$\upsilon_4 + \upsilon_7$	1613.7+1168.0 = 2782
2650.8	vvw	$\upsilon_4 + \upsilon_5$	1613.7+1040.1 = 2653.8
2560.2	mw	$\upsilon_{20} + \upsilon_{21}$	1533[a]+1030[a] = 2563
2464.4	w	$\upsilon_6 + \upsilon_7$	1296.9+1168.0 = 2464.9
2358.8	m	$\upsilon_4 + \upsilon_8$?	1613.7+740.0 = 2353.7
2338.1	m	$\upsilon_5 + \upsilon_6$ $2\upsilon_7$	1040.1+1296.9 = 2337.0 2x1168.0 = 2336
2324	w	υ_1 (gauche)	2324
2316	m	υ_1	2316
2259.2	w	-	
2234	w	υ_2 (gauche)	2234
2224.5	vs	υ_2	2224.5
2208.3	w	$\upsilon_5 + \upsilon_7$	1040.1+1168.0 = 2208.1
2056.9	vw	$2\upsilon_{21}$	2x1030[a] = 2060.0
1904.2	mw	$\upsilon_7 + \upsilon_8$?	1168.0+740.0 = 1908.0
1858.6	vw	-	
1791.1	mw	$\upsilon_{20} + \upsilon_{24}$	1533[a] +257.9[a] = 1791
1779.2	vw	$\upsilon_5 + \upsilon_8$	1040.1 +740.0 = 1780.1
1750.8	w	$\upsilon_6 + \upsilon_9$	1296.9+452.6 = 1749.5
1658.2	ms	-	
1633.1	vs	-	
1619.6	vs	$\upsilon_7 + \upsilon_9$	1168.0+452.6 = 1620.6
1613.7	vvvs	υ_4	1613.7
1598.9	s	$2\upsilon_{13} + \upsilon_6$	2x149.2[a]+1296.9 = 1595.3
1596	m	υ_{17} (gauche)?	1596
1580	s	υ_4 (gauche)	1580
1530.1	ms	$2\upsilon_{12} + \upsilon_8$	2x396.8[a]+740.0 = 1533.6
1516.1	mw	-	-
1493.6	mw	$\upsilon_5 + \upsilon_9$	1040.1+452.6 = 1492.7
1486.9	mw	-	

Table 50: (Continued)

ν_{OBS}		Assignment	Inferred
1478.6	ms	$2\upsilon_8$	2x740.0 = 1480.0
1467.8	mw	$2\upsilon_{13} + \upsilon_7$	2x149.2[a]+1168.0 = 1466.4
1453.1	w	$2\upsilon_{11}$ $2\upsilon_{15}$	2x728[a] = 1456 2x726 = 1452
1349.7	ms	$\upsilon_{10} + \upsilon_{12}$(0-0)	955[a]+396.8[a] = 1352
1346.7	ms	(1-1)	1346.7
1343.3	m	(2-2)	1343.3
1339.9	w	(3-3)	1339.9
1307	w	υ_6 (gauche)	1307
1296.9	vvs	υ_6	1296.9
1292	mw	υ_{19} (gauche)	1292
1276.9	ms	-	
1256.2	w	$2\upsilon_{24} + \upsilon_8$	2x257.9[a]+740.0 = 1255.8
1248.6	vw	$2\upsilon_{12} + \upsilon_9$	2x396.8[a]+452.6 = 1246.2
1218.7	ms	$2\upsilon_{16}$?	2x606.1 = 1212.2
1194.2	ms	$\upsilon_8 + \upsilon_9$	740.0+452.6 = 1192.6
1168.0	vs	υ_7	1168.0
1123.3	mw	$\upsilon_{11} + \upsilon_{12}$	728[a]+396.8[a] = 1125.0
1101.9	mw	$\upsilon_{10} + \upsilon_{13}$(0-1)	955[a]+149.2[a] = 1104
1098.4	mw	(1-2)	1098.4
1094.8	mw	(2-3)	1094.8
1090.8	w	(3-4)	1090.8
1086.5	vw	(4-5)	1086.5
1075	w	υ_5 (gauche)	1075
1040.1	vs	υ_5	1040.1
1016	w	-	
972	vw	υ_{10} (gauche)	972
940	vvw	υ_{14}	940
929.4	vw	υ_8 (gauche)	929.4
873.6	m	$\upsilon_{11} + \upsilon_{13}$	728[a]+149.2[a] = 877
806.9	ms	-	
740.0	ms	υ_8	740.0
726	ms	υ_{15}	726
606.1	m	υ_{16}	606.1
595 br	w	υ_{11} (gauche)	595
580.6	m	$\upsilon_{11} - \upsilon_{13}$	728[a]-149.2[a] = 579
557.9	ms	-	
545.3	mw	$\upsilon_{12} + \upsilon_{13}$(0-1)	396.8[a]+149.2[a] = 546.0
542.8	m	(1-2)	542.8

Table 50: (Continued)

ν_{OBS}		Assignment	Inferred
538.7	m	(2-3)	538.7
534.8	m	(3-4)	534.8
530.9	m	(4-5)	530.9
527.8	mw	(5-6)	527.8
521.2	m	-	
517.9	m	$2\upsilon_{24}$ (0-2)	2x257.9[a] = 515.8
515.8	m	(1-3)	515.8
513.9	m	(2-4)	513.9
475.9	ms	-	
452.6	vs	υ_9	452.6
295.3	mw	$2\upsilon_{13}$ (0-2) trans	2x149.2[a] = 298.4
290.9	m	(1-3)	290.9
289.2	w	(2^--4^-) gauche	289.2[a]
286.6	m	$2\upsilon_{13}$ (2-4) trans	286.6
282.1	m	(3-5)	282.1
277.2	m	(4-6)	277.2
272.2	m	(5-7)	272.2
270.0	w	(2^+-4^+) gauche	270.0[a]
267.5	mw	$2\upsilon_{13}$ (6-8) trans	267.5
263.8	mw	(1^--3^-) gauche	263.8[a]
260.1	m	$2\upsilon_{13}$ (7-9) trans	260.1
249.1	mw	υ_{12} (gauche)	249.1
243.3	m	(0^--2^-) gauche	243.3[a]
240.2	vvw	-	
232.2	mw	-	
207.6	vw	-	
204	vw	(1^+-3^+) gauche	204[a]
198	vw	-	
186	vvw	(0^+-2^+) gauche?	186[a]

[a] References 42, 53, 53,92.

Table 51: Observed vibrational frequencies (cm^{-1}) and assignments for 1,3-butadiene-d_6

ν_{OBS}		Assignment	Inferred
3169.5	m	-	
3127.9	vvw	$\upsilon_3 + \upsilon_6$	2212+919 = 3131
3106.6	vvw	$2\upsilon_{12} + \upsilon_1$	2x381[a]+2343.5 = 3105.5
3045.4	vvw	$2\upsilon_{20}$?	2x1520[a] = 3040
2786.5	mw	-	
2771.8	mw	-	
2753.3	w	$2\upsilon_{22} + \upsilon_8$?	2x1005[a]+739.2 = 2749
2635.6	mw	$\upsilon_4 + \upsilon_5$	1588.8+1047 = 2636
2565.7	vvw	$\upsilon_{20} + \upsilon_{21}$	1520[a]+1048[a] = 2568
2523.0	m	-	
2515.7	mw	$2\upsilon_{10} + \upsilon_5$?	2x736[a]+1047 = 2519
2505.3	mw	$\upsilon_4 + \upsilon_6$	1588.8+919 = 2508
2389.2	m	$2\upsilon_{16} + \upsilon_7$	2x597+1192 = 2386
2387.6	m	$2\upsilon_7$	2x1192 = 2384
2371.3	w	-	
2343.5	s	υ_1	2343.5
2329.5	mw	$\upsilon_4 + \upsilon_8$	1588.8+739 = 2328
2318	m	υ_1 (gauche)	2318
2265	vs	υ_2	2265
2255.6	vs	-	
2242.9	s	$2\upsilon_{16} + \upsilon_5$	2x597[a]+1047 = 2241
2237.5	s	$\upsilon_5 + \upsilon_7$	1047+1192 = 2239
2222	mw	υ_3 (gauche)	2222
2212	vs	υ_3	2212
2191.3	mw	-	
2175.6	w	$2\upsilon_{11} + \upsilon_8$	2x719[a]+739 = 2177
2151.2	mw	-	
2141.5	vvvw	$2\upsilon_{15} + \upsilon_8$	2x700+739 = 2139
2119.6	m	-	
2114.9	m	$\upsilon_6 + \upsilon_7$	919+1192 = 2111
2102.6	w	-	
2092.7	m	$2\upsilon_5$	2x1047 = 2094
2083.6	vw	-	
2075.6	m	-	
2051.7	w	-	
2026.3	w	$\upsilon_4 + \upsilon_9$	1588.8+440 = 2029

Table 51: (Continued)

ν_{OBS}		Assignmen	Inferred
1965.6	w	$\upsilon_5 + \upsilon_6$	1047+919 = 1966
1936.2	mw	$2\upsilon_{16} + \upsilon_8$	2x597+739.2 = 1933
1932.1	mw	$\upsilon_7 + \upsilon_8$	1192+739 = 1931
1836.4	vw	$2\upsilon_6$	2x919 = 1838
1788.3	vw	$\upsilon_5 + \upsilon_8$	1047+739 = 1786
1769.1	m	$\upsilon_{20} + \upsilon_{24}$	1520[a]+252[a] = 1772
1746.8	mw	-	
1659.5	s	$\upsilon_6 + \upsilon_8$	919+739 = 1658
1605.1	ms	$2\upsilon_{14}$	2x804 = 1608
1590.8	vvs	-	
1588.8	vvvs	υ_4	1588.8
1579	s	υ_4 (gauche)	1579
1576.9	s	-	
1573.9	s	-	
1533.4	w	$2\upsilon_{23}$?	2x769[a] = 1538
1505.9	mw	-	
1502.9	mw	$\upsilon_{14} + \upsilon_{15}$	804+700 = 1504
1493.2	m	-	
1484.1	m	$\upsilon_5 + \upsilon_9$	1047+440 = 1487
1476.9	s	$2\upsilon_8$	2x739 = 1478
1470.9	mw	$2\upsilon_{10}$	2x736[a] = 1472
1434.3	vw	$2\upsilon_{11}$	2x719[a] = 1438
1400.2	ms	$2\upsilon_{15}$	2x700 = 1400
1391.9	m	-	
1360.4	mw	$\upsilon_6 + \upsilon_9$	919+440 = 1359
1297.7	vvvw	$\upsilon_{15} + \upsilon_{16}$	700+597 = 1297
1196.4	ms	$2\upsilon_{13} + \upsilon_6$	2x140[a]+919 = 1199
1192	ms	υ_7	1192
1172.9	ms	-	
1147.4	ms	$\upsilon_3 - 2\upsilon_{12}$	2212-2x381[a] = 1450
1047	vs	υ_5	1047
1008	m	υ_5 (gauche)	1008
995	m	υ_{20} (gauche)?	995
919	vvvs	υ_6	919
880	vw	υ_{19} (gauche)	881
855.3	ms	$\upsilon_{11} + \upsilon_{13}$	719[a]+140[a] = 859
818	w	υ_6 (gauche)?	818
804	ms	υ_{14}	804
794.1	w	$\upsilon_2 - 2\upsilon_{10}$	2265-2x736[a] = 793

Table 51: (Continued)

ν_{OBS}		Assignment	Inferred
784.2	ms	-	
766.6	mw	$2\upsilon_{12}$ (0-0)	2x381[b] = 762
763.7	mw	(1-1)	763.7
760.9	w	(2-2)	760.9
757.8	mw	(3-3)	757.8
752.7	mw	(4-4)	752.7
750.4	w	(5-5)	750.4
739	vs	υ_8	739
734.0	ms	-	
700 br	m	υ_{15}	700
597 br	m	υ_{16}	597
587	mw	υ_{11} (gauche)?	587
525.9	w	$\upsilon_{12} + \upsilon_{13}$ (0-1)	381[a]+140[a] = 521
523.5	m	(1-2)	523.5
520.0	ms	(2-3)	520.0
516.7	ms	(3-4)	516.7
513.4	m	(4-5)	513.4
503.6	w	$2\upsilon_{24}$	2x252[a] = 504
499	vw	υ_{23} (gauche)	499
440	vvs	υ_9	440
360	w	υ_{24} (gauche)	360
280.9	m	$2\upsilon_{13}$ (0-2) trans	2x140[a] = 280
276.9	ms	(1-3)	276.9
273.1	ms	(2-4)	273.1
268.9	ms	(3-5)	268.9
264.7	ms	(4-6)	264.7
260.1	m	(5-7)	260.1
257.2	ms	(6-8)	257.2
251.3	vw	(2^+-4^+) gauche	251.3[a]
248.9	m	$2\upsilon_{13}$ (7-9) trans	248.9
244.4	m	$2\upsilon_{13}$ (8-10) trans	244.4
238.5	m	υ_{12} (gauche)	238.5
233.7	vw	-	
228.8	vw	(0^--2^-) gauche	228.8[a]
225.1	w	-	
196.7	w	(1^+-3^+) gauche	196.7[a]
180	vvw	(0^+-2^+) gauche	180[a]

[a] References 42, 52, 53, 92.

CHAPTER XI

PRELIMINARY STUDIES ON THE VIBRATIONAL SPECTRA, STRUCTURE, AND THEORETICAL CALCULATIONS OF 2-CHLORO- AND 3-CHLOROPYRIDINE AND 2-BROMO- AND 3-BROMOPYRIDINE IN THEIR GROUND STATES

INTRODUCTION

In this chapter the investigation of the structure and vibrations of pyridine and substituted pyridines in their ground and excited states has been extended to chloro and bromopyridines. The extensive investigations of the vibrational analyses of pyridine, 2FPy and 3FPy in their electronic ground and excited states were reported in Chapters IV, V, VI and VII. From the previous fluoropyridine studies it was found that the substitution of a fluorine atom on the pyridine ring results in significant π boding interactions within the ring. Therefore, it was of interest to determine whether similar effects would occur with the substitution of chlorine and bromine atoms on the pyridine ring. Green and co-workers[33] have previously reported the infrared and Raman spectra and partial assignments for chloro and bromopyridine molecules in their electronic ground states, but no structural information was reported. In the present study, the infrared spectra were recorded and ground state vibrational frequencies of 2-chloro- and 3-chloropyridine, and 2-bromo- and 3-bromopyridine molecules were assigned.

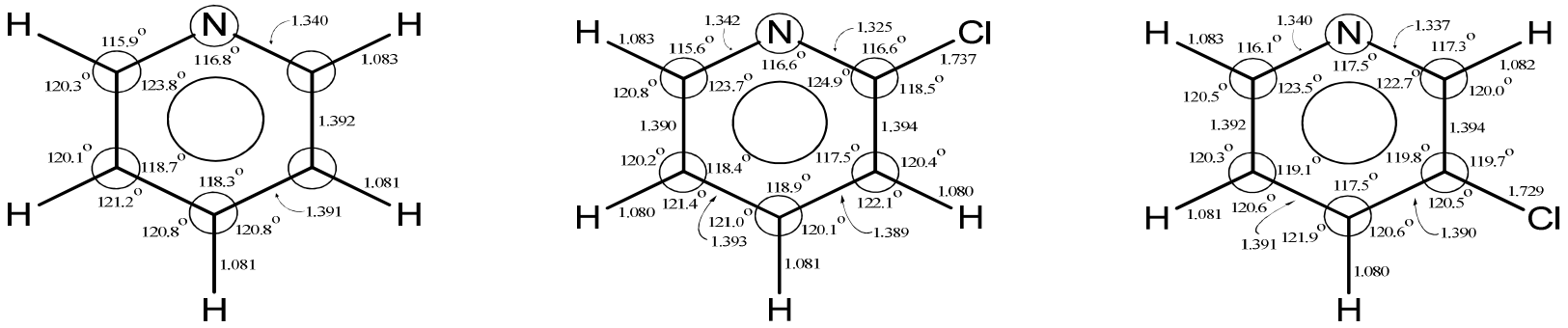

Figure 90. Calculated structures of (a) pyridine-d_0, (b) 2-chloropyridine, and (c) 3-chloropyridine in their S_0 ground electronic state using MP2/cc-pVTZ level of theory.

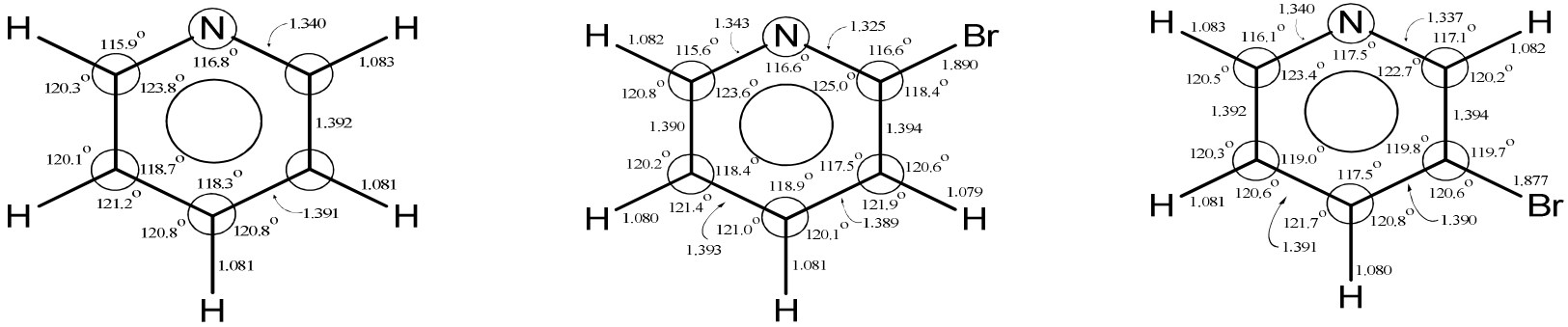

Figure 91. Calculated structures of (a) pyridine-d_0, (b) 2-bromopyridine, and (c) 3-bromopyridine in their S_0 ground electronic state using MP2/cc-pVTZ level of theory.

DFT calculations were used to predict the vibrational frequencies of the twenty-seven fundamentals for each molecule.

EXPERIMENTAL

2-Chloro- and 3-chloropyridine, and 2-bromo- and 3-bromopyridine molecules (99% purity) were purchased from Aldrich and purified by trap to trap distillation. The liquid-phase mid-infrared spectra of these molecules were collected on a Bruker Vertex 70 FT spectrometer equipped with a globar light source, a KBr beamsplitter and deuterated lanthanum triglycine sulfate (DLaTGS) detector. A capillary film of sample between KBr windows was used in each case for mid-infrared experiments. Typically 1024 scans were collected using a resolution of 0.5 cm^{-1}. The liquid-phase far infrared spectra (60-600 cm^{-1}) were also collected on the same instrument equipped with a mylar beamsplitter, and a mercury cadmium telluride (MCT) detector. Liquid films between polyethylene windows were used for far infrared experiments.

THEORETICAL CALCULATIONS

The structures and vibrational frequencies of 2-chloro- and 3-chloropyridine, and 2-bromo- and 3-bromopyridine molecules for the electronic ground state were calculated using the Gaussian 03 program package.[65] *Ab initio* second order Moller-Plesset (MP2) level of theory with the cc-pVTZ basis set was used to find the optimized geometry. Figure 90 shows the optimized geometry of 2-chloro- and 3-chloropyridine, and Figure 91 shows the optimized geometry 2-bromo- and 3-bromopyridine. The DFT-B3LYP

level of theory with the 6-311++G(d,p) basis set was used to calculate the vibrational frequencies and the infrared intensities. Based on previous work,[66-70] a scaling factor of 0.964 was used for the C-H stretching vibrational frequencies and a factor of 0.985 for the lower frequencies.

RESULTS AND DISCUSSION

Structures

Figures 92 and 93 show the liquid-phase and calculated infrared spectra of 2-chloropyridine (2ClPy) and 3-chloropyridine (3ClPy). The substitution of the chlorine atom on the pyridine ring had only a minor effect on the ring bond distances and angles. The notable exception is the N-C(Cl) bond distance for 2ClPy which is only 1.325 Å as compared to 1.340 Å for pyridine and 1.342 Å for the other N-C bond of 2ClPy. Clearly, the substitution of the electronegative chlorine atom resulted in the strengthening of the adjacent N-C bond. There was insignificant effect observed for 3ClPy since the chlorine atom is distant from the nitrogen atom. Here the N-C bond distance of 1.337 Å is similar to the 1.340 Å value for pyridine.

Figures 94 and 95 show the liquid-phase and calculated infrared spectra of 2-bromopyridine (2BrPy) and 3-bromopyridine (3BrPy). The substitution of the bromine atom on the pyridine ring had only a minor effect on the ring bond distances and angles as seen for other halopyridines. The notable exception was the N-C(Br) bond distance for 2BrPy which is only 1.325 Å as compared to 1.340 Å for pyridine and 1.343 Å for the other N-C bond of 2BrPy.

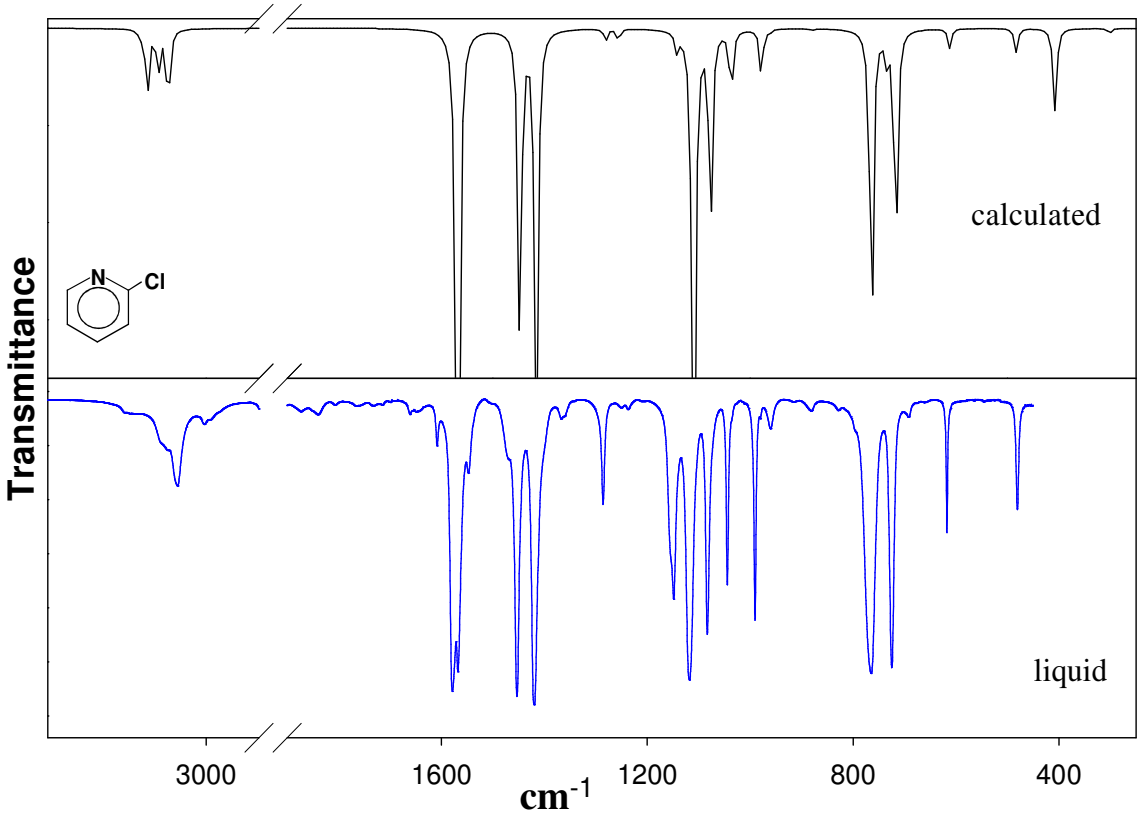

Figure 92. Liquid and calculated IR spectra of 2-chloropyridine.

Table 52: Observed and calculated vibrational frequencies (cm^{-1}) and intensities for 2-chloropyridine

Cs	ν	Approximate Description	Infrared		Calculated[a] ν	Intensity	GKP[b]
A'	1	C-H stretch	3085 sh	mw	3096	(2)	3080
(i.p.)	2	C-H stretch	3073 sh	mw	3085	(15)	3080
	3	C-H stretch	3054	mw	3065	(9)	3057
	4	C-H stretch	3054	mw	3049	(16)	3057
	5	Ring stretch	1579	vs	1588	(61)	1573
	6	Ring stretch	1568	vs	1585	(99)	1565
	7	Ring stretch	1453	vs	1461	(77)	1452
	8	Ring stretch	1420	vs	1427	(100)	1417
	9	C-H wag	1286	m	1295	(3)	1282
	10	Ring stretch	1251	w	1274	(3)	1253
	11	C-H wag	1148	ms	1155	(4)	1146
	12	C-H wag[c]	1118	vs	1121	(123)	1104
	13	C-H wag	1083	m	1088	(49)	1079
	14	Ring stretch[c]	1044	m	1047	(17)	1041
	15	Ring bend	990	m	990	(10)	991
	16	C-Cl stretch[d]	725	s	726	(57)	701
	17	Ring bend	618	m	619	(3)	615
	18	Ring bend[d]	-		413	(14)	404[e]
	19	C-Cl wag	-		307	(2)	315[e]
A''	20	C-H wag	980	w	992	(0.01)	960
(o.p.)	21	C-H wag	960	m	965	(0.4)	934
	22	C-H wag	882	w	880	(0.03)	882
	23	C-H wag	765	vs	765	(84)	761
	24	Ring twist	-		735	(4)	722
	25	Ring bend	481	m	484	(6)	457
	26	Ring bend	-		412	(7)	404
	27	C-Cl wag	-		172	(1)	178

Abbreviations: s, strong; m, medium; w, weak; v, very; sh, shoulder; i.p., in-plane; o.p., out-of-plane.

[a] B3LYP/6-311++g(d,p); frequencies scaled with a scaling factor of 0.985 for frequencies less than 1800 cm^{-1} and 0.964 for frequencies greater than 1800 cm^{-1}. The calculated relative intensities are shown in parentheses.

[b] Reference 33.

[c] The CH wag and ring stretch are strongly coupled.

[d] The C-Cl stretch and ring bend are strongly coupled.

[e] Bands have been reassigned.

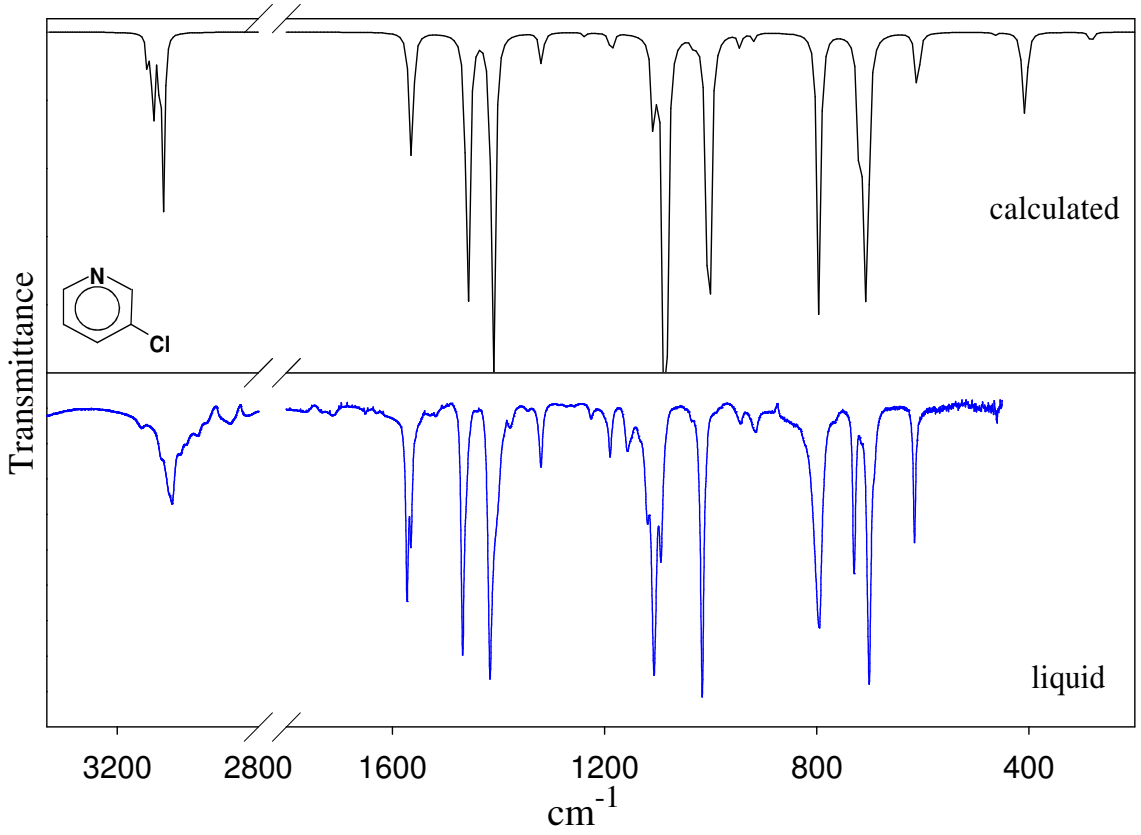

Figure 93. Liquid and calculated IR spectra of 3-chloropyridine.

Table 53: Observed and calculated vibrational frequencies (cm^{-1}) and intensities for 3-chloropyridine

Cs	ν	Approximate Description	Infrared		Calculated[a] ν	Intensity	GKP[b]
A'	1	C-H stretch	3075	mw	3087	(9)	3079
(i.p.)	2	C-H stretch	3075	mw	3071	(24)	3079
	3	C-H stretch	3053 sh	mw	3056	(18)	3052
	4	C-H stretch	3045	m	3045	(35)	3052
	5	Ring stretch	1572	m	1584	(29)	1573
	6	Ring stretch	1565	m	1579	(12)	1569
	7	Ring stretch	1467	vs	1470	(82)	1469
	8	Ring stretch	1416	vs	1425	(100)	1417
	9	C-H wag	1320	mw	1329	(9)	1319
	10	Ring stretch	1226	vw	1255	(1)	1227
	11	C-H wag	1189	mw	1201	(9)	1190
	12	C-H wag	1107	s	1119	(29)	1107
	13	C-H wag	1094	m	1098	(162)	1096
	14	Ring stretch	1036	vw	1041	(6)	1040
	15	Ring bend	1016	vs	1013	(106)	1016
	16	C-Cl stretch[c]	730	m	727	(50)	730
	17	Ring bend	615	m	617	(15)	615
	18	Ring bend[c]	426	w	415	(24)	428
	19	C-Cl wag	292	vw	288	(3)	294
A''	20	C-H wag	-		977	(0.2)	980
(o.p.)	21	C-H wag	944	w	941	(2)	943
	22	C-H wag	915	w	917	(3)	915
	23	C-H wag	795	s	793	(91)	795
	24	Ring twist	701	s	704	(82)	700
	25	Ring bend	461	vw	465	(0.9)	460
	26	Ring bend	402	w	405	(9)	404
	27	C-Cl wag	-		183	(0.06)	199

Abbreviations: s, strong; m, medium; w, weak; v, very; sh, shoulder; i.p., in-plane; o.p., out-of-plane.

[a] B3LYP/6-311++g(d,p); frequencies scaled with a scaling factor of 0.985 for frequencies less than 1800 cm^{-1} and 0.964 for frequencies greater than 1800 cm^{-1}. The calculated relative intensities are shown in parentheses.

[b] Reference 33.

[c] The C-Cl stretch and ring bend are strongly coupled.

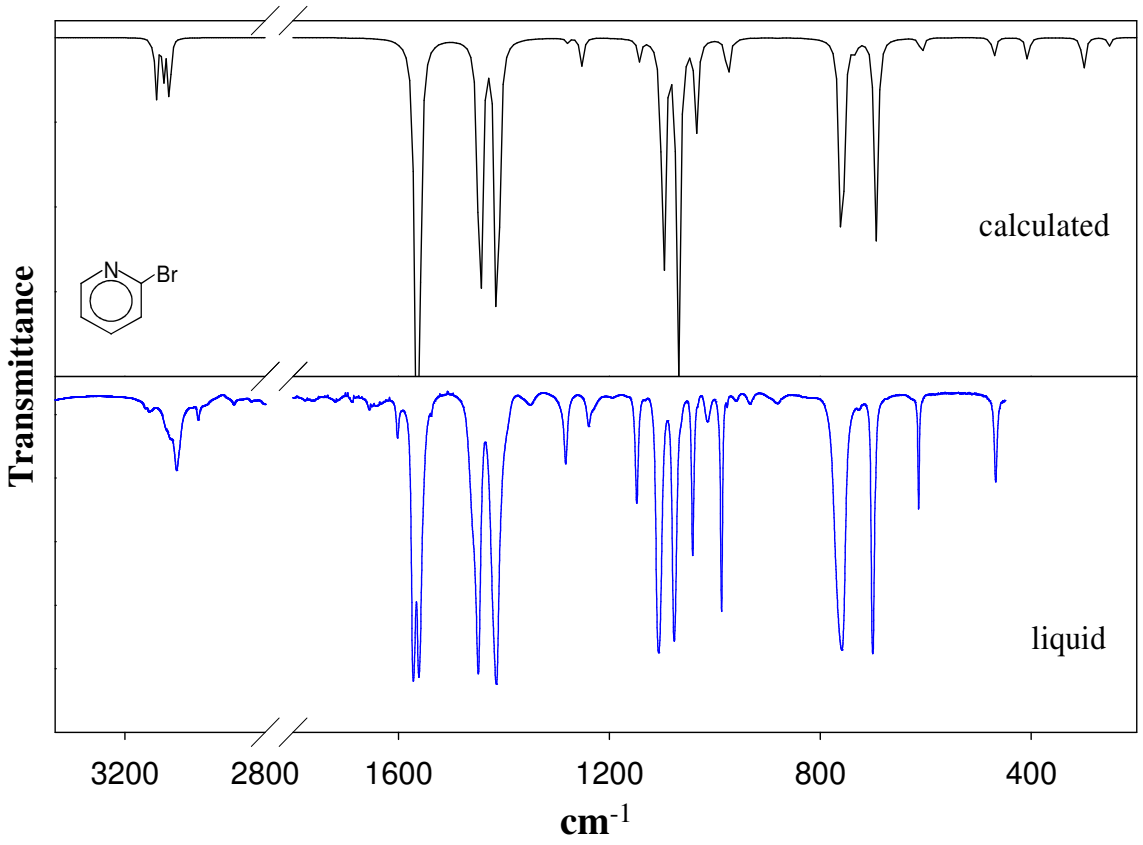

Figure 94. Liquid and calculated IR spectra of 2-bromopyridine.

Table 54: Observed and calculated vibrational frequencies (cm^{-1}) and intensities for 2-bromopyridine

Cs	ν	Approximate Description	Infrared		Calculated[a] ν	Intensity	GKP[b]
A'	1	C-H stretch	3083 sh	mw	3098	(2)	3069
(i.p.)	2	C-H stretch	3070 sh	mw	3084	(15)	3069
	3	C-H stretch	3052	m	3063	(10)	3056
	4	C-H stretch	3052	m	3050	(17)	3056
	5	Ring stretch	1572	vvs	1584	(51)	1573
	6	Ring stretch	1561	vvs	1580	(123)	1565
	7	Ring stretch	1449	vvs	1458	(90)	1452
	8	Ring stretch	1414	vvs	1423	(100)	1417
	9	C-H wag	1283	mw	1294	(2)	1282
	10	Ring stretch	-		1269	(7)	1253
	11	C-H wag	1148	m	1155	(4)	1146
	12	C-H wag[c]	1106	vvs	1108	(67)	1104
	13	C-H wag	1077	vvs	1079	(87)	1079
	14	Ring stretch[c]	1042	m	1044	(28)	1041
	15	Ring bend	987	m	987	(10)	991
	16	C-Br stretch[d]	700	vs	702	(52)	701
	17	Ring bend	614	m	615	(3)	615
	18	Ring bend[d]	312	w	304	(9)	315
	19	C-Br wag	261	vw	256	(3)	265
A''	20	C-H wag	-		991	(0)	960
(o.p.)	21	C-H wag	960	w	964	(0.4)	934
	22	C-H wag	882	w	883	(0.04)	882
	23	C-H wag	759	vvs	762	(83)	761
	24	Ring twist	727	w	731	(2)	722
	25	Ring bend	467	m	472	(6)	457
	26	Ring bend	404	w	409	(7)	404
	27	C-Br wag	-		154	(2)	178

Abbreviations: s, strong; m, medium; w, weak; v, very; sh, shoulder; i.p., in-plane; o.p., out-of-plane.

[a] B3LYP/6-311++g(d,p); frequencies scaled with a scaling factor of 0.985 for frequencies less than 1800 cm^{-1} and 0.964 for frquencies greater than 1800 cm^{-1}. The calculated relative intensities are shown in parentheses.

[b] Reference 33.

[c] The CH wag and ring stretch are strongly coupled.

[d] The C-Br stretch and ring bend are strongly coupled.

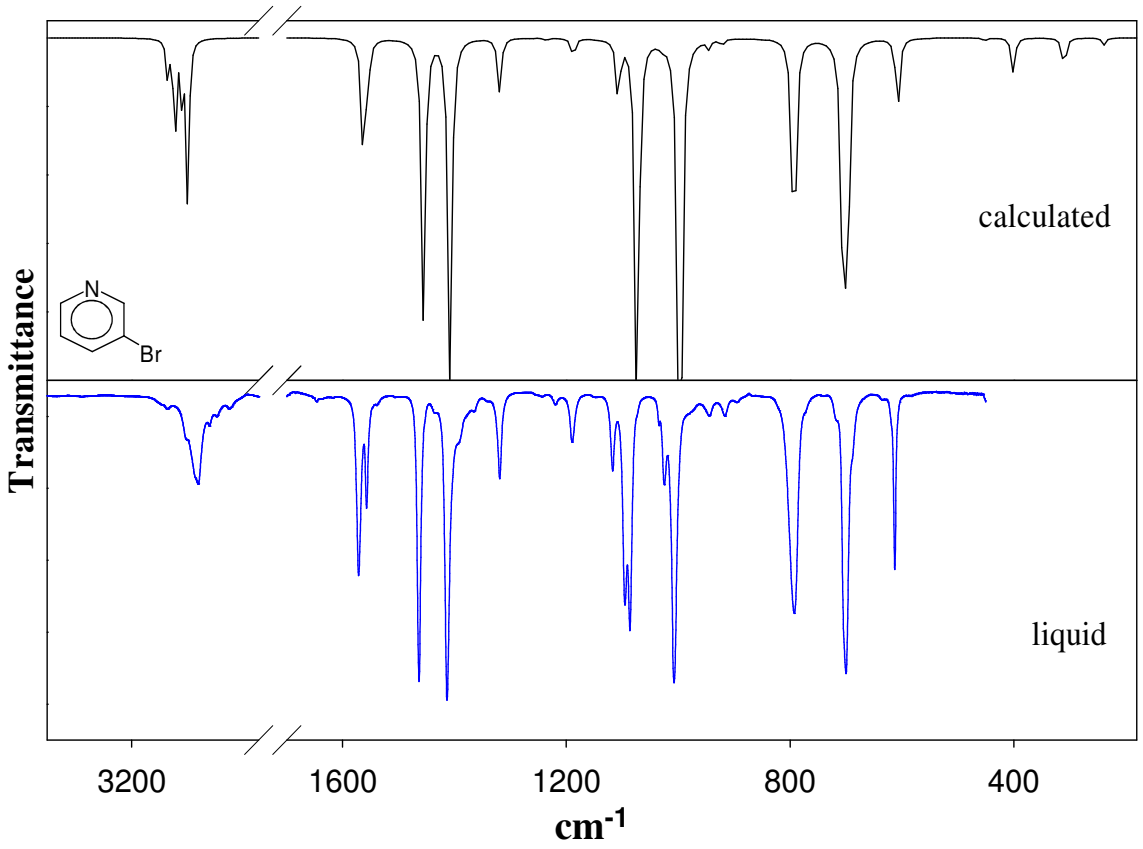

Figure 95. Liquid and calculated IR spectra of 3-bromopyridine.

Table 55: Observed and calculated vibrational frequencies (cm^{-1}) and intensities for 3-bromopyridine

Cs	ν	Approximate Description	Infrared		Calculated[a] ν	Intensity	GKP[b]
A'	1	C-H stretch	3071 sh	mw	3088	(10)	3082
(i.p.)	2	C-H stretch	3071 sh	mw	3071	(27)	3082
	3	C-H stretch	3050 sh	mw	3058	(17)	3052
	4	C-H stretch	3043	m	3045	(40)	3052
	5	Ring stretch	1571	ms	1581	(37)	1573
	6	Ring stretch	1557	m	1573	(14)	1559
	7	Ring stretch	1463	vs	1467	(80)	1467
	8	Ring stretch	1413	vs	1422	(100)	1415
	9	C-H wag	1319	w	1330	(14)	1320
	10	Ring stretch	1244 br	vw	1252	(1)	1221
	11	C-H wag	1190	mw	1202	(10)	1189
	12	C-H wag	1095	m	1119	(20)	1094
	13	C-H wag	1086	m	1084	(117)	1087
	14	Ring stretch	1025	mw	1038	(3)	1024
	15	Ring bend	1007	vs	1007	(173)	1008
	16	C-Br stretch[c]	704 sh	ms	703	(50)	705
	17	Ring bend	613	m	614	(17)	614
	18	Ring bend[c]	319	vw	312	(10)	319
	19	C-Br wag	246?	vvw	242	(2)	246
A''	20	C-H wag	978 sh	vw	978	(0.2)	978
(o.p.)	21	C-H wag	944	w	942	(1)	944
	22	C-H wag	916	w	919	(2)	915
	23	C-H wag	792	vs	790	(103)	792
	24	Ring twist	700	vs	701	(83)	699
	25	Ring bend	448	vw	450	(1)	447
	26	Ring bend	399	w	401	(10)	401
	27	C-Br wag	-		163	(0.1)	182

Abbreviations: s, strong; m, medium; w, weak; v, very; sh, shoulder; br, broad; i.p., in-plane; o.p., out-of-plane.

[a] B3LYP/6-311++g(d,p); frequencies scaled with a scaling factor of 0.985 for frequencies less than 1800 cm^{-1} and 0.964 for frequencies greater than 1800 cm^{-1}. The calculated relative intensities are shown in parentheses.

[b] Reference 33.

[c] The C-Br stretch and ring bend are strongly coupled.

Table 56: Vibrational frequencies (cm^{-1}) of the ring modes of the halopyridines compared to Pyridine

ν[a]	Approximate Description	Pyridine	2FPy	3FPy	2ClPy	3ClPy	2BrPy	3BrPy
5	Ring stretch	1584	1605	1594	1579	1572	1572	1571
6	Ring stretch	1576	1593	1588	1568	1565	1561	1557
7	Ring stretch	1483	1478	1480	1453	1467	1449	1463
8	Ring stretch	1443	1439	1426	1420	1416	1414	1413
10	Ring stretch	1227	1286	1249	1251	1226	1253[b]	1244
11	C-X stretch[d]	-	1266	1227	725	730	700	704
15	Ring stretch	1031	997	1022	1044	1036	1042	1025
16	Ring bend[d] (i.p.)	991	842	816	990	1016	987	1007
17	Ring bend (i.p.)	654	620	613	618	615	614	613
18	Ring bend[d] (i.p.)	601	554	533	404[c]	426	312	319
24	Ring bend (o.p.)	700	733	701	722[b]	701	727	700
25	Ring bend (o.p.)	403	518	507	481	461	467	448
26	Ring bend (o.p.)	375	414	412	404[b]	402	404	399

Abbreviations: i.p., in-plane; o.p., out-of-plane.
[a] Mode number for 2FPy and 3FPy.
[b] From Refrence 33. Not observed in this work.
[c] From Refrence 33. Band has been reassigned.
[d] The C-X stretching vibration is strongly coupled to a ring bending (ν_{16} for 2FPy and 3FPy and ν_{18} for 2ClPy, 3ClPy, 2BrPy and 3BrPy).

Table 57: Ring bond distances (Å) and carbon-halogen bond distances (Å) of halopyridines and pyridine

Bond distances	Pyridine	2FPy	3FPy	2ClPy	3ClPy	2BrPy	3BrPy
N(1) - C(2)	1.340	1.313	1.338	1.325	1.337	1.325	1.337
C(2) - C(3)	1.392	1.391	1.389	1.394	1.394	1.394	1.394
C(3) - C(4)	1.391	1.387	1.384	1.389	1.390	1.389	1.390
C(4) - C(5)	1.391	1.394	1.391	1.393	1.391	1.393	1.391
C(5) - C(6)	1.392	1.388	1.392	1.390	1.392	1.390	1.392
C(6) - N(1)	1.340	1.344	1.340	1.342	1.340	1.343	1.340
C - X	-	1.338	1.340	1.737	1.729	1.890	1.877

The substitution of the electronegative bromine atom results in a slight strengthening of the adjacent N-C bond, but the effect is much less than for 2FPy or 2ClPy. The bromine substitution had an insignificant effect on the ring bond lengths of 3BrPy, as was the case for 3FPy and 3ClPy.

Infrared Spectra

Tables 52 and 53 summarize the observed and calculated vibrational frequencies for 2ClPy and 3ClPy. Tables 54 and 55 summarize the observed and calculated vibrational frequencies for 2BrPy and 3BrPy. Green and coworkers[33] previously made partial assignments for these molecules and these are also shown in Tables 52, 53, 54 and 55. As expected,[66-70] the cc-PVTZ calculation did a remarkably good job of predicting the frequencies. The average difference between experimental and calculated wavenumbers was less than 8 cm^{-1}. From Table 56 it is also clear that most of the pyridine ring vibrational frequencies were not changed much in 2ClPy, 3ClPy, 2BrPy and 3BrPy and the highest four ring stretching modes shifted by less than 18 cm^{-1}. The values of 2FPy and 3FPy are also shown for comparison in the table. The ring bond distances and the C-halogen bond distances of 2FPy, 3FPy, 2ClPy, 3ClPy, 2BrPy and 3BrPy are compared to pyridine in Table 57.

The results for the chloro and bromo pyridines are consistent with those for 2FPy and 3FPy. The motivation for obtaining the data for the ground states of these molecules was to prepare for the spectroscopy of the electronic excited states.

CHAPTER XII

CONCLUSIONS

Several spectroscopic techniques were utilized in this work, including infrared (IR), Raman and ultraviolet (UV) absorption techniques, to study the vibrational energy states of molecules in their electronic ground and excited states. The vibrational potential energy functions (PEFs) for the electronic excited ground and excited states were investigated. *Ab initio* and DFT calculations were carried out to compute the molecular structures and to support the vibrational assignments.

First, the infrared and Raman spectra of liquid and vapor-phase pyridine-d_0 and pyridine-d_5 were used to assign the vibrational frequencies of the electronic ground states. The ultraviolet absorption spectra of pyridine-d_0 and pyridine-d_5 were used to assign the vibrational levels in the $S_1(n,\pi^*)$ electronic excited states. In addition, the PEF for the ring-bending was determined and this showed the molecule to be very floppy and quasi-planar in the excited state with a barrier to planarity of 3 cm^{-1}. Furthermore, *ab initio* and DFT calculations were carried out to compute the molecular structures and to verify the vibrational assignments of the twenty-seven fundamentals.

Second, the infrared, Raman and uv experiments of 2-fluoropyridine (2FPy) and 3-fluoropyridine (3FPy) were carried out. *Ab initio* and DFT calculations were performed to compute the structures of these molecules and were compared to those of pyridine. The ring bond distances differed little from those of pyridine in their electronic ground states. The notable exception was that the N-C(F) bond distance was shortened

in 2FPy due to π interactions but for 3FPy there was considerably less of this effect. The structures and vibronic levels of 2FPy and 3FPy in their electronic excited states were also investigated and compared to those of pyridine. For the S(π,π*) state all of the N-C and C-C bond distances increased due to the decrease in π bond character. The frequencies of the ring modes of the fluoropyridines were also similar to those of pyridine itself. Unlike pyridine, which is very floppy in its electronic excited state, the 2FPy and 3FPy rings remain more rigid. These out-of-plane ring modes were also strongly coupled to the out-of-plane C-F wagging motion. In addition, the investigation of the structure and vibrations of pyridine and substituted pyridines were extended to chloro and bromopyridines. From fluoropyridines, it was found that the substitution of fluorine atoms resulted in significant π boding interactions within the ring. Similar effects were observed with the substitution of chlorine and bromine atoms in the pyridine ring. In the study, the infrared spectra, molecular structure and ground state vibrational assignments of 2-chloro- and 3-chloropyridine, and 2-bromo- and 3-bromopyridine molecules were reported. DFT calculations were used to compute the structures and to predict the vibrational frequencies of the twenty-seven fundamentals.

Furthermore, the full Raman spectra of of 1,3-butadiene and and its 2,3-d_2, 1,1,4,4-d_4, and d_6 isotopomers were investigated. Also, the gas-phase Raman spectra of these isotopomers were recorded with high sensitivity in the region below 350 cm^{-1}, and the internal rotation (torsional) vibration was investigated. The data for all the isotopomers were then fit using a one-dimensional potential energy function of the form $V=½\sum V_n(1-\cos\phi)$. The results from an alternative set of assignments also fit the data

quite well for all of the isotopomers presented. This provided an understanding of the conformational properties of butadiene. In addition, combination and hot band series involving the ν_{13} torsional vibration and other out-of-plane modes of the *trans* rotamer were observed for each of the butadiene isotopomers. Furthermore, the high signal to noise of the Raman spectra made it possible to detect several bands of the more intense *trans* rotor and several bands of the less intense *gauche* rotor, which made up only about 2% of the molecules at ambient temperature.

REFERENCES

1. Henri, V.; Angenot, P. *J. Chim. Phys.* **1936,** *33*, 641.
2. Sponer, H.; Stücklen, H. *J. Chem. Phys.***1946,** *14*, 101.
3. Jesson, J. P.; Kroto, H. W.; Ramsay, D. A. *J. Chem. Phys.***1972,** *56*, 6257.
4. Wilmhurst, J. K.; Bernstein, H. J. *Can. J. Chem.* **1957,** *35*, 1183.
5. Villa, E.; Amirav, A.; Lim, E. C. *J. Chem. Phys.* **1988,** *92*, 5393.
6. Riese, M.; Altug, Z.; Grotemeyer, J. *J. Phys. Chem. Chem. Phys.* **2006¸** *8*, 4441.
7. Wiberg, K. B.; Walters, V. A.; Wong, K. N.; Colson, S. D. *J. Phys. Chem.* **1984,** *88*, 6067.
8. Wong, K. N.; Colson, S. D.; *J. Mol. Spectrosc.* **1984,** *104*, 129.
9. Mochizuki, Y.; Kaya, K.; Ito, M. *J. Chem. Phys.* **1978**, *69*, 935
10. Cai, Z. L.; Reimers, J. R. *J. Phys. Chem. A*. **2000,** *104*, 8389.
11. Fischer, G.; Cai, Z. L.; Reimers, J. R. *J. Phys. Chem. A*. **2003,** *107*, 3093.
12. Becucci, M.; Lakin, N. M.; Pietraperzia, G.; Salvi, P. R.; Castellcui, E.; Kerstel, E. R. *J. Chem. Phys.* **1997**, *107*, 10399.
13. Wilmshurst, J. K.; Bernstein, H. J. *Can. J. Chem.* **1957,** *35*, 1183.
14. Stidham, H. D.; DiLella, D. P. *J. Raman Spectrosc.* **1979,** *83*, 180.
15. Wong, K. N.; Colson, S. D. *J. Phys. Chem.* **1983,** *87*, 2102.
16. Klots, T. D. *Spectrochim. Acta.***1998,** *54A*, 1481.
17. Long, D. A.; Murfin, F. S.; Thomas, E. L. *Trans. Faraday Soc.* **1963,** *59*, 12.
18. Long, D. A.; Thomas, E. L. *Trans. Faraday Soc.* **1963,** *59*, 783.

19. Innes, K. K.; Roos, I. G.; Moomaw, W. R. *J. Mol. Spectrosc.* **1988,** *132*, 492.

20. DiLella, D. P.; Stidham, H. D. *J. Raman Spectrosc.***1980,** *92*, 90.

21. Stidham, H. D.; DiLella, D. P. *J. Raman Spectrosc.* **1980,** *94*, 247.

22. Ozon, Y.; Maehara, M.; Nibu, Y.; Shimada, H.; Shimada. R. *Bull. Chem. Soc. Jpn.* **1986,** *59*, 1617.

23. Chirico, R. D.; Steele, W. V.; Nguyen, A.; Klots, T. D.; Knipmeyer, S. E. *J. Chem. Thermodyn.* **1996,** *28*, 797.

24. Walters, V. A.; Snavely, D. L.; Colson, S. D.; Wiberg, K. B.; Wong, K. N. *J. Phys. Chem.* **1986,** *90*, 592.

25. Partal, F.; Fernández Gómez, M.; López González, J. J.; Navarro, A.; Kearley, G. J. *Chem. Phys.* **2000**, *261*, 239

26. Zerbi, G.; Crawford, B.; Overend, J. *J. Chem. Phys.* **1963,** *381*, 127.

27. Kakiuti, Y.; Akiyama, M.; Saito, N.; Saito, H. *J. Mol. Spectrosc.* **1976,** *61*, 164.

28. Mochizuki, Y.; Kaya, K.; Ito, M. *J. Chem. Phys.* **1976,** *65*, 4163.

29. Wu, D. Y. *Journal of the Chinese Chemical Society*, **2003,** *50*, 735.

30. Olsher, U. *J. Chem. Phys.* **1977,** *66*, 5242.

31. Olsher, U.; Lubart, R.; Brith, M. *Chem. Phys.* **1976,** *17*, 237.

32. Sharma, S. D.; Doraiswamy, S. *J. Mol. Spectrosc.* **1975,** *57*, 377.

33. Green, H. S.; Kynaston, W.; Paisley, H. M. *Spectrochim. Acta.* **1963,** *19*, 549.

34. Medhi, K. C.; Medhi, R. N. *Spectrochim. Acta.* **1990,** *46A*, 1169.

35. Medhi, K. C.; Medhi, R. N. *Spectrochim. Acta.***1990,** *46A*, 1333.

36. Itoh, T. *Chem. Phys. Lett.* **2010,** *491*, 29.

37. Almenningen, A.; Bastiansen, O.; Traetteberg, M. *Acta Chem. Scand.* **1958,** *12,*1221.

38. Kuchitsu, K.; Fukuyama, T.; Morimo, Y. *J. Mol. Struct.* **1968,** *1*, 463.

39. Craig, N. C.; Groner, P.; McKean, D. C. *J. Phys. Chem. A*. **2006**, *110***,** 7461.

40. Aston, J. G.; Szasz, G.; Woolley, H. W.; Brickwedde, F. G. *J. Chem. Phys*. **1946**, *14***,** 67.

41. Lipnick, R. L.; Garbisch, E. W., Jr. *J. Am. Chem. Soc.* **1973**, *95***,** 6370.

42. Cole, A. R. H.; Green, A. A.; Osborne, G. A. *J. Mol. Spectrosc.* **1973**, *48*, 212.

43. Carreira, L. A. *J. Phys. Chem*. **1975**, *62***,** 3851.

44. Arnold, B. R.; Balaji, V.; Michl, J. *J. Am. Chem. Soc.* **1990**, *112***,** 1808.

45. Fisher, J. J.; Michl, J. *J. Am. Chem. Soc.* **1987**, *109***,** 1056.

46. Squillacote, M. E.; Sheridan, R. S.; Chapman, O. L.; F. Anet, F. A. L. *J. Am. Chem. Soc.* **1979**, *101,* 3657.

47. Panchenko, Y. N.; Abramenkov, A. V.; Mochalov, V. I.; Zenkin, A. A. *J. Mol. Spectrosc.* **1983**, *99*, 288.

48. Engeln, R.; Consalvo, D.; Reuss, J. *Chem. Phys.* **1992**, *160***,** 427.

49. Feller, D.; Craig, N. C. *J. Phys. Chem.* **2009**, *113***,** 1601.

50. Craig, N. C.; Sams, R. L. *J. Phys. Chem. A* **2008**, *112*, 12637.

51. Panchenko, Yu. N.; De Maré, G. R. *J. Struct. Chm.* **2008**, *49*, 235.

52. Craig, N. C.; Davis, J. L.; Hanson, K. A.; Moore, M. C.; Weidenbaum, K. J.; Lock, M. *J. Mol. Struct.* **2004**, *695*, 59.

53. Wiberg, K. B.; Rosenberg, R, E. *J.Am. Chem. Soc*. **1990**, *112*, 1509.

54. McKean, D. C.; Craig, N. C.; Panchenko, Y. N.; *J. Phys. Chem. A,* **2006**, *110,* 8044.

55. Furukawa, Y.; Takeuchi, H.; Harada, I.; Tasumi, M. *Bull. Chem. Soc. Jpn.* **1983,** *56,* 392.

56. Craig, N. C.; Moore, M. C.; Patchen, A. K.; Sams, R. L. *J. Mol. Spectrosc.* **2006**, *235,* 181.

57. Haller, K.; Chiang, W.-Y.; del Rosario, A.; Laane, J. *J. Mol. Struct.* **1996**, *379*, 19.

58. Laane, J. *Intl. Rev. in Phys. Chem.* **1999,** *18*, 301.

59. Laane, J. *J. Phys. Chem.* **2000,** *104A*, 7715.

60. Laane, J.; Takahashi, H.; Bandrauk, A. (eds.), Springer, Berlin, Germany **1999,** 3-35.

61. Yang, J.; Wagner, M.; Okuyama, K.; Morris, K.; Arp, Z.; Choo, J.; Meinander, M.; Laane, J. *J. Chem. Phys.* **2006,** *125*, 034308.

62. Yang, J.; Wagner, M.; Laane, J. *J. Phys. Chem. A.* **2006,** *110*, 9805.

63. Yang, J.; Laane, J. *J. Elec. Spectrosc.* **2007,** *45*, 156.

64. Lewis, J. D.; Malloy, T. B., Jr.; Chao, T. H.; Laane, J. *J. Mol. Struct.* **1972**, *12***,** 427.

65. Frisch, M. J.; Trucks, G. W.; Schlegel, H. B.; Scuseria, G. E.; Robb, M. A.; Cheeseman, J. R.; Montgomery, J. A., Jr.; Vreven, T.; Kudin, K. N.; Burant, J. C.; Millam, J. M.; Iyengar, S. S.; Tomasi, J.; Barone, V.; Mennucci, B.; Cossi, M.; Scalmani, G.; Rega, N.; Petersson, G. A.; Nakatsuji, H.; Hada, M.; Ehara,

M.; Toyota, K.; Fukuda, R.; Hasegawa, J.; Ishida, M.; Nakajima, T.; Honda, Y.; Kitao, O.; Nakai, H.; Klene, M.; Li, X.; Knox, J. E.; Hratchian, H. P.; Cross, J. B.; Bakken, V.; Adamo, C.; Jaramillo, J.; Gomperts, R.; Stratmann, R. E.; Yazyev, O.; Austin, A. J.; Cammi, R.; Pomelli, C.; Ochterski, J. W.; Ayala, P.Y.; Morokuma, K.; Voth, G. A.; Salvador, P.; Dannenberg, J. J.; Zakrzewski, V. G.; Dapprich, S.; Daniels, A. D.; Strain, M. C.; Farkas, O.; Malick, D. K.; Rabuck, A. D.; Raghavachari, K.; Foresman, J. B.; Ortiz, J. V.; Cui, Q.; Baboul, A. G.; Clifford, S.; Cioslowski, J.; Stefanov, B. B.; Liu, G.; Liashenko, A.; Piskorz, P.; Komaromi, I.; Martin, R. L.; Fox, D. J.; Keith, T.; Al-Laham, M. A.; Peng, C. Y.; Nanayakkara, A.; Challacombe, M.; Gill, P. M. W.; Johnson, B.; Chen, W.; Wong, M. W.; Gonzalez, C.; Pople, J. A. Gaussian 03, Revision C.02; Gaussian, Inc., Wallingford CT, 2004.

66. Yang, J.; McCann, K.; Laane, J. *J. Mol. Struct.* **2004,** *339*, 695.

67. Yang, J.; Choo, J.; Kwon, O.; Laane, J. *Spectrochim. Acta Part A.* **2007,** *68*, 1170.

68. Autrey, D.; Yang, J.; Laane, J. *J. Mol. Struct.* **2003,** *661*, 23.

69. Al-Saadi, A. A.; Laane, J. *J. Mol. Struct.* **2007,** *830*, 46.

70. Autrey, D.; Choo, J.; Laane, J. *J. Phys. Chem. A*. **2001,** *105*, 10230.

71. Yang, J.; Wagner, M.; Laane, J. *J. Phys. Chem. A*. **2007,** *111*, 8429.

72. Schmidt, M. W.; Baldridge, K. K.; Boatz, J. A.; Elbert, S. T.; Gordon, M. S.; Jensen, J. H.; Koseki, S.; Matsunaga, N.; Nguyen, K. A.; Su, S. J.; Windus, T. L.; Dupuis, M.; Montgomery, J. A. *J. Comput. Chem.* **1993,** *14*, 1347.

73. Bell, R. P. *Proc. R. Soc. London, Ser. A* **1945**, *183*, 328-337.

74. Groner, P.; Johnson, R. D.; Durig, J. *J. Mol. Struct*. **1986**, *142*, 363.

75. Strube, M. M.; Laane, J. *J. Mol. Spectrosc.* **1988,** *129*, 126.

76. Nygaard, L.; Bojesen, I.; Pedersen, T.; Rastrup-Anderson, J. *J. Mol. Struct.* **1968,** *2*, 209.

77. Lipp, E. D.; Seliskar, J. *J. Mol. Spectrosc.* **1978,** *73*, 290.

78. Kondo, S.; Koga, Y.; Nakanaga, T. *J. Phys. Chem.* **1986,** *90*, 1519.

79. Olsher, U. *Spectrochim. Acta.* **1978,** *34A*, 211.

80. Laane, J.; Lord, R. C., *J. Chem. Phys.* **1967**, *47*, 4941.

81. Laane, J. *J. Phys. Chem. A* **2000**, *104*, 7715.

82. Chao, T. H.; Laane, J. *Chem. Phys. Lett.* **1972,** *14*, 595.

83. Lewis, J. D.; Chao, T. H.; Laane, J. *J. Chem. Phys.* **1975**, *62*, 1932.

84. Irwin, R. M.; Laane, J. *J. Mol. Spectrosc.* **1978**, *70*, 307.

85. Laane, J.; Nour, E. M.; Dakkouri, M. *J. Mol. Spectrosc.* **1983**, *102*, 368.

86. Kelly, M. B.; Laane, J.; Dakkouri, M. *J. Mol. Spectrosc.* **1989**, *137*, 82.

87. Blanke, J. F.; Chao, T. H.; Laane, J. *J. Mol. Spectrosc.* **1971**, *38*, 483.

88. Klots, T.; Sakurai, S.; Laane, J. *J. Chem. Phys.* **1998**, *108*, 3531.

89. Rosario, A.; Bitschenauer, R.; Dakkouri, M.; Haller, K.; Laane, J. *J. Phys. Chem. A* 102 **1998**, *102*, 10261.

90. Jagodzinski, P. W.; Irwin, R. M.; Cooke, J. M.; Laane, J. *J. Mol. Spectrosc.* **1980**, *84*, 139.

91. Laane, J.; Haller, K.; Sakurai, S.; Morris, K.; Autrey, D.; Arp, Z.; Chiang, W.-Y.; Combs, A. *J. Mol. Struct.* **2003**, *650*, 57.

92. Boopalachandran, P.; Craig, N.; Groner, P.; Laane, J. *J. Phys. Chem. A* **2011**, accepted.

VITA

Name:	Praveenkumar Boopalachandran
Permanent Address:	Department of Chemistry 3255 TAMU College Station, TX 77843-3255
Email Address:	praveen.tamu@gmail.com
Education:	B.Tech., Chemistry, University of Madras, Chennai, India, 1999 M.S., Chemistry, Texas A&M University-Commerce, Commerce, Texas, USA, 2003 M.S., Chemistry, Texas A&M University, College Station, Texas, USA, 2006 Ph.D., Chemistry, Texas A&M University, College Station, Texas, USA, 2011